1974

The behavior and analysis of two-way simply supported concrete composite floor slabs constructed with cold-formed steel decking

Max Lee Porter
Iowa State University

The behavior and analysis of two-way simply supported concrete composite floor slabs constructed with cold-formed steel decking

by

Max Lee Porter

A Dissertation Submitted to the
Graduate Faculty in Partial Fulfillment of
The Requirements for the Degree of
DOCTOR OF PHILOSOPHY

Department: Civil Engineering
Major: Structural Engineering

Approved:

Signature was redacted for privacy.

In Charge of Major Work

Signature was redacted for privacy.

For the Major Department

Signature was redacted for privacy.

For the Graduate College

Iowa State University
Ames, Iowa
1974

CONTENTS

LIST OF FIGURES

LIST OF TABLES

LIST OF SYMBOLS

a	slab length in x direction, inches
a_{mn}	constants in orthotropic plate theory as expanded by Fourier series and depends on load condition
a_u	depth of rectangular stress block in inches as given by $\frac{A_s f_y}{0.85 f'_c b}$
A_s	area of steel reinforcement, inches squared
A_{s_1}	area of supplementary reinforcing parallel to deck corrugations, square inches
A_{s_2}	area of supplementary reinforcing transverse to deck corrugations, square inches
A_{sd}	cross-sectional area of steel deck per width b, square inches
b	slab length in y direction, inches
b_d	width of cross-section under consideration, usually 12 inches, inches
c	ratio of length to width of slab, a/b, in orthotropic analysis; or depth to extreme tension fiber in flexure formula, inches
$c_1, c_2, \ldots, c_{28}$	coefficients of polynomial series used in curve fitting of deflected surface
C	compressive force on cross-section due to flexure, kips
d	effective slab depth as measured from extreme concrete compression fiber to centroidal axis of steel deck, inches
d_d	depth of steel deck, inches
d_1, d_2	effective depth in each orthogonal direction as measured from top surfaces of slab, inches
d_n	Depth to neutral axis, computed by cracked transformed area concepts, inches
D	Total out-to-out depth of slab or slab element, inches

$D_1 = D_x$ stiffness constant $= \frac{E_1 d_1^3}{12(1 - \nu_1\nu_2)} = \frac{(E_c I_T)_x}{(1 - \nu_c^2)}$, kip-in.^{2}/ft

$D_2 = D_y$ stiffness constant $= \frac{E_2 d_2^3}{12(1 - \nu_1\nu_2)} = \frac{(E_c I_T)_y}{(1 - \nu_c^2)}$, (kip-in.^{2})/ft

D_3 stiffness constant $= \sqrt{D_1 D_2}$, kip-in.^{2}/ft

E external work performed by external loads moving through a virtual displacement

E_c modulus of elasticity of concrete, ksi

E_s modulus of elasticity of steel reinforcement, ksi

E_1, E_2 modulus of elasticity in tension and compression in the principal directions of elasticity, ksi

$(E_c I_T)_x$ flexural stiffness in x direction using transformed moment of inertia per unit width, kip-in.^{2}/ft

$(E_c I_T)_y$ flexural stiffness in y direction using transformed moment of inertia per unit width, kip-in.^{2}/ft

f'_c compressive strength of concrete, psi

f_r modulus of rupture strength in flexure for concrete, psi

f_s stress in supplementary reinforcement to develop ultimate bond stress of splice, psi

F_r rupture tensile strength of steel reinforcement, ksi

F_u ultimate tensile strength of steel reinforcement, ksi

F_y yield stress of steel deck, ksi

i dimensionless coefficient designating ratio of negative moment to the positive moment capacity, m

im negative moment capacity, ft-lb/ft

I internal energy dissipated in the slab to form a mechanism

I_g, I_{g_1}, I_{g_2}, I_{g_3} gross moment of inertia of cross-section neglecting steel reinforcement, inches to the fourth

I_{sf} moment of inertia of steel deck per foot of width based on full cross-sectional deck area, inches to the fourth per foot

I_{sn} moment of inertia for negative bending regions of steel deck per foot of width based on AISI design criteria for reduced cross-sectional deck area according to load deformation, inches to the fourth per foot

I_{sp} moment of inertia for positive bending regions of steel deck per foot of width based on AISI design criteria for reduced cross-sectional deck area according to load deformation, inches to the fourth per foot

I_t transformed moment of inertia, $in.^4$

k_1 intercept of shear-bond regression curve

k_2 slope of shear-bond regression curve

kd distance to neutral axis from top fiber, inches

ℓ length of splice for supplementary reinforcement, inches

L length of yield-line, length of edge of slab, or slab element length, ft.

L' shear span length, inches (assume 1/4 of the span length for uniformly loaded slab elements)

L" effective slab width for four concentrated loads as determined by yield-line mechanism

L.P. load point

m moment capacity of slab on a cross-section perpendicular to steel deck corrugations (longitudinal moment capacity), ft-lb/ft. This moment capacity considers the steel deck in its strong (longitudinal) direction plus considering any additional reinforcement. (Vector direction of m is perpendicular to the reinforcement.)

m, n integer numbers in series expansion of orthotropic plate equations

M, M_u bending moment or ultimate bending moment for flexure formula in slab element analysis, ft-lb/ft

M_x, M_y bending moments per unit width of sections of slab perpendicular to x and y axis respectively, kips

M_{yx}, M_{xy} twisting moments per unit width of sections of slab perpendicular to x and y axis respectively, kips

N_x, N_y transverse shear forces parallel to Z axis for unit width of sections of slab perpendicular to X and Y axis, respectively, kips/ft

p reinforcement ratio, $A_s/b_d d$

P concentrated load force applied at each concentrated load point, kips

P_u ultimate concentrated applied slab load per load point, kips

P_{ue} total ultimate experimental applied load to slab element specimens, kips

q, q_1 applied uniform load (used in orthotropic plate equations), psi

R corner reaction force at each of four corners of slabs, kips

R_f radius for circular fan mechanism, ft

R_s reduced resultant shear strength based upon an elliptical interaction of V_L and V_T, kips/L.P.

s center-to-center spacing of wires for a spot-welded shear transferring device, inches (for cases of embossments where the shear transferring device is a fixed pattern, the value of s is unity)

t_d thickness of steel deck, inches

t_w diameter thickness of wire fabric or deformed wire, inches

T tensile force on cross-section due to flexure, kips

T_B Tensile force located at bottom fiber of steel decking in general strain analysis, kips

T_T Tensile force located at top fiber of steel decking in general strain analysis, kips

T_w Tensile force located at c.g.s. of steel decking in general strain analysis, kips

U_u ultimate bond stress for supplementary reinforcing, psi

V_L ultimate calculated shear force for the longitudinal one-way segment parallel to deck corrugations of the effective load-carrying slab element portion of the collapse mechanism, kips per load point

V_T ultimate calculated shear force based on a one-way slab element transverse to deck corrugations for the effective load-carrying portion of the slab collapse mechanism, kips per load point

V_x, V_y reactive forces per unit width along edge of slab for edges perpendicular to x and y axes, respectively, kips/ft

V_{ue} ultimate experimental shear for a slab element of width b_d, pounds

V_u total ultimate shear including dead load of a slab element of width b_d, pounds

w_z uniform load on slab, psf

w dead load of slab or slab element, psf

W_u uniform ultimate load as found from shear-bond analysis, psf

WWF welded wire fabric

x, y rectangular coordinate locations, inches

X, Y, Z directions of coordinate axis

y_o location of compressive force from the neutral axis, inches

y_{sb} location of steel deck c.g.s. from bottom fiber of deck, inches

z vertical deflection, inches

α dimensionless length parameter of slab designating location of concentrated loads along length of slab

β dimensionless width parameter of slab designating ratio of width of slab to its length

βL width of slab, ft

ξ, η coordinate locations of concentrated load points, inches

$\epsilon_{B_1}, \epsilon_{B_2}, \epsilon_{B_3}, \epsilon_{B_4}$ strain in bottom fiber of steel decking for general strain analysis, microinches/inch

ϵ_c strain in concrete, microinches/inch

$\epsilon_{c_2}, \epsilon_{c_3}, \epsilon_{c_4}$ strain at top fiber of concrete for general strain analysis, microinches/inch

ϵ_s strain in steel, microinches/inch

$\epsilon_{T_1}, \epsilon_{T_2}, \epsilon_{T_3}, \epsilon_{T_4}$ strain in top fiber of steel decking for general strain analysis, microinches/inch

$\epsilon_{T_{c_4}}$ strain in concrete of location at top of steel decking for general strain analysis, microinches/inch

$\epsilon_{w_2}, \epsilon_{w_3}, \epsilon_{w_4}$ strain in web sections of steel decking taken at location of deck c.g.s. for general strain analysis, microinches/inch

$\epsilon_x, \epsilon_y, \epsilon_{45}$ measured strains in the x, y, and 45 degree angle directions, microinches/inch

ϵ_o strain of concrete stress-strain curve at f'_c, taken as 0.002

ϵ_1, ϵ_2 principal strains corresponding to the principal directions 1 and 2, microinches/inch

ϵ_y steel strain corresponding to the yield stress in a uniaxial field, microinches per inch

γ dimensionless width parameter of slab designating location of concentrated loads along width of slab

μ coefficient of orthotropy designating ratio of transverse moment capacity to longitudinal moment capacity

μm moment capacity of slab on a cross-section parallel to steel deck corrugations (transverse moment capacity), ft-lbs/ft (vector direction of μm is parallel to steel deck corrugations)

ν_1, ν_2 Poisson's ratio in each of the principal directions of elasticity (assumed equal to Poisson's ratio of concrete ν_c)

ν_c Poisson's ratio of concrete

$\tau_{xy}, \tau_{zy}, \tau_{zx}, \tau_{yx}$	shearing stress components, ksi
σ_x, σ_y	normal stress components of tension or compression parallel to x and y axes, respectively, ksi
θ	angle that resultant R_s makes with V_L on elliptical interaction plot
σ	flexural stress, psi

CHAPTER 1. INTRODUCTION

General Remarks

There have been rising costs in recent years in the building and general construction industries. This is due to increased wages and material costs which have prompted the increased use of cold-formed steel members as load carrying structural components. One method for cutting costs in labor and materials in multi-story buildings and bridges is by use of cold-rolled steel decking in the concrete floor systems. The cost of conventional construction methods which consist of separate forming operations for installing and removing wooden or steel forms can comprise 35 to 60 percent of the total cost-in-place concreting operation (18). Elimination of this forming operation can be accomplished by using corrugated cold-formed steel decking as a form which remains as a permanent integral part of the floor slab.

A steel deck which has some type of device in the form of rolled embossments, transverse wires, holes, etc., to provide positive interaction between the concrete and the steel can serve as reinforcing for the floor slab. This is usually termed "composite steel-deck reinforced concrete slab construction." This investigation deals with the behavior and analysis of two-way simply-supported concrete composite floor slabs constructed with cold-formed steel decking.

Two typical building floor constructions utilizing cold-formed steel decking are shown in Figures 1 and 2. Both constructions utilize composite decking with concrete topping for the structural load-carrying element. However, other items are oftentimes included such as

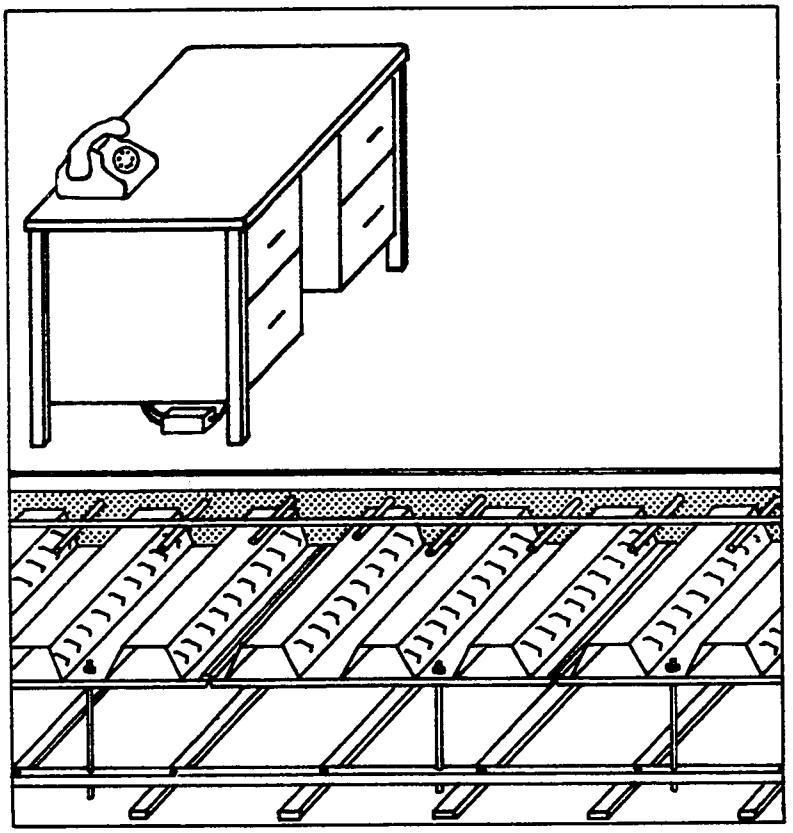

Figure 1. Typical building floor construction utilizing cold-formed steel decking

electrification ducts as shown in Figure 2, or suspended ceilings as shown in Figure 1.

The more important advantages of using cold-formed steel decking as reinforcement for a floor slab system can be summarized by the following statements.

1) The steel deck eliminates the need for installing formwork other than minor division of slab section formwork.

2) The deck eliminates the need for removal of all but minor formwork.

3) The composite deck serves as reinforcing for floor slab and only additional shrinkage, temperature, and negative moment reinforcement is needed where desired.

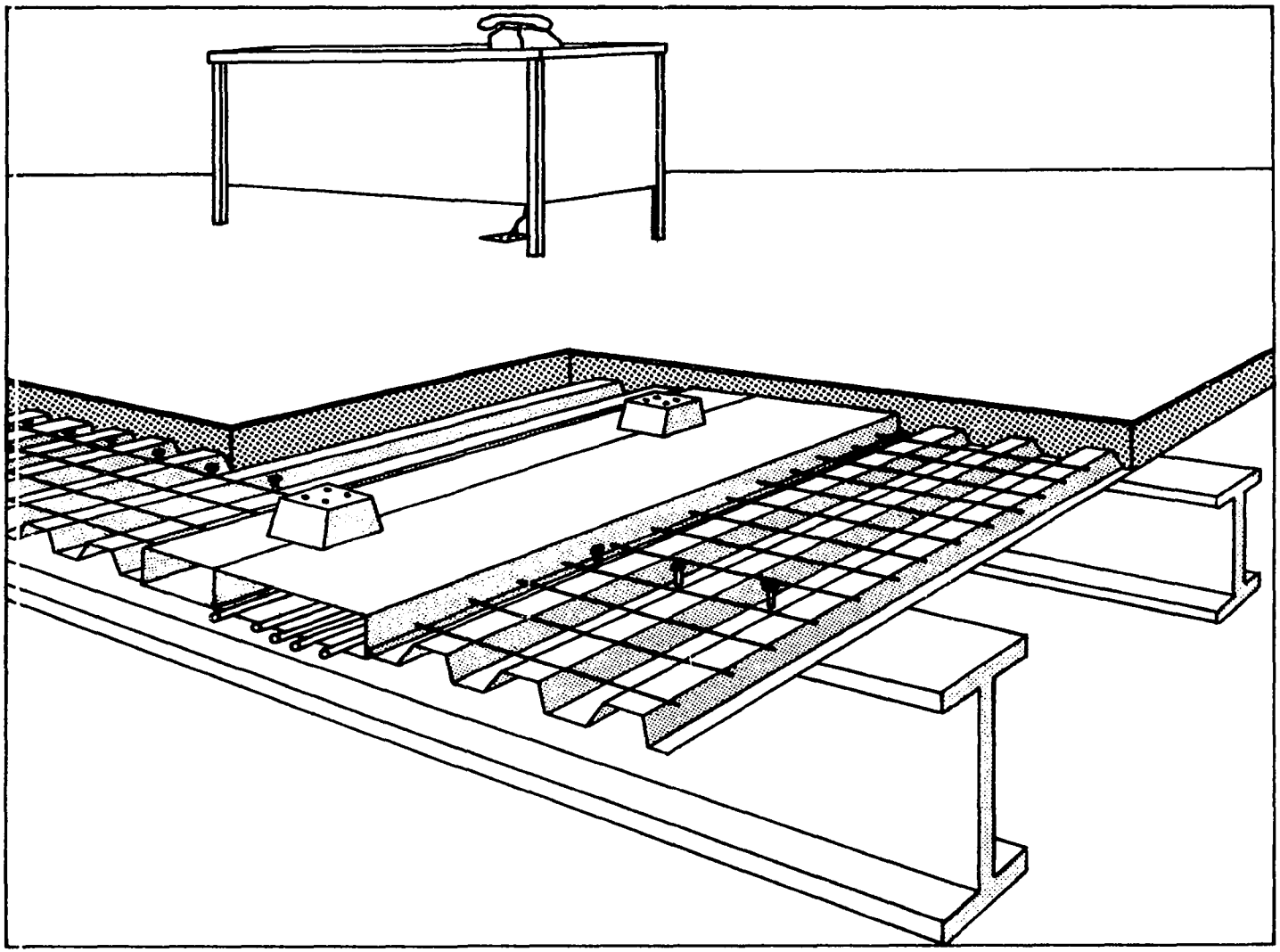

Figure 2. Typical building floor construction utilizing cold-formed steel decking with composite support beams

4) The deck provides a ceiling surface, or in the case of a suspended ceiling, provides easy attachment of support hangers.

5) The deck can be easily placed and handled.

6) The corrugations of the deck contain pre-engineered ducting for electrification, communication, and air distribution.

7) The deck is palletized floor-by-floor for easy shipment and handling and reduces requirements for storage spaces.

8) After placement of the deck panels, the deck surface acts as a safe platform for the workmen, their tools, materials and equipment.

9) The likelihood of construction fires is greatly reduced since most combustible wooden formwork is removed.

10) Time of construction is greatly reduced since casting of additional floors may proceed without having to wait for previously cast floors to gain strength to support shoring.

11) The use of steel decking reduces the dead load of the floor slab with little or no corresponding loss in load-carrying capacity.

The floor is quite often made to act compositely with the steel support beams by attaching protruding studs welded through the decking to the support beams. See Figure 2. This investigation included the behavior and analysis of only the composite floor slab constructed with the steel decking and did not include the aspects of the composite action of the support beams. All reaction conditions in this investigation consisted of simple supports. Other investigations by Fisher (12), Slutter (45), Robinson (37), (38) and others (13), (22), (44), however, have dealt with the composite support beams and slab systems where composite action is insured

by use of welded studs.

The steel deck achieves most of its composite floor integral action by various shear transferring devices. These devices consist of rolled embossments in various plate elements of the decking, transverse wires (T-wires) spot-welded to the top of the corrugations, or holes to allow the concrete to fill the corrugations. In some instances vertical interlocking is provided by the geometry of the deck itself. This investigation utilized deck from only three manufacturers. The deck used has only embossments or transverse wires (T-wires) as shear transferring devices to provide the structural composite interaction.

Object

The primary object of this investigation was to investigate the behavioral characteristics and to analyze full-scale two-way simply supported floor slabs constructed with corrugated cold-formed steel decking which were subjected to concentrated loads. This primary objective was divided into three phases as follows:

1) loading to ultimate failure of full-scale two-way floor slabs reinforced with cold-formed steel decking,
2) compilation of test data to indicate behavioral characteristics, and
3) development of a theoretical approach based upon strength design concepts.

In order to carry out the investigation on two-way slabs, one-way slab element properties, behavioral characteristics, and analyses were needed. These one-way characteristics were obtained by experimental testing to

failure of one-way slab element or beam type specimens, and by appropriate ultimate strength principles of beam analysis including a shear-bond regression analysis for predicting the ultimate load.

The overall intent of this investigation was to provide information to steel deck manufacturers as to possible design criteria for two-way simply supported floor slabs based upon ultimate strength concepts. The effect of concentrated loads due to fork-lift trucks and the transverse distribution of concentrated forces was of primary concern in carrying out the objective of this investigation.

Scope

The laboratory testing consisted of full-scale two-way floor slabs and full-scale one-way slab elements or beams. Full-scale tests were utilized in that model tests involving the scale modeling of the various shear transferring devices on the light gage decking was thought to be almost an impossibility.

Five full-scale two-way simply supported slabs reinforced with three different cold-formed steel decks were constructed and tested to ultimate failure. These full-scale slabs were all 16 feet long by 12 feet wide by 4½ to 5½ inches nominal thickness. All slabs were subjected to the same loading which consisted of four concentrated load points symmetrically centered in a four-foot square in the center of the slab. The four concentrated loads were chosen to approximate the effect of a fork-lift truck, and to ascertain the load distributions encountered with concentrated loads on steel-deck-reinforced floor slabs. Figure 3 shows the position of the load points, the dimensional layout, the types of support reactions, and

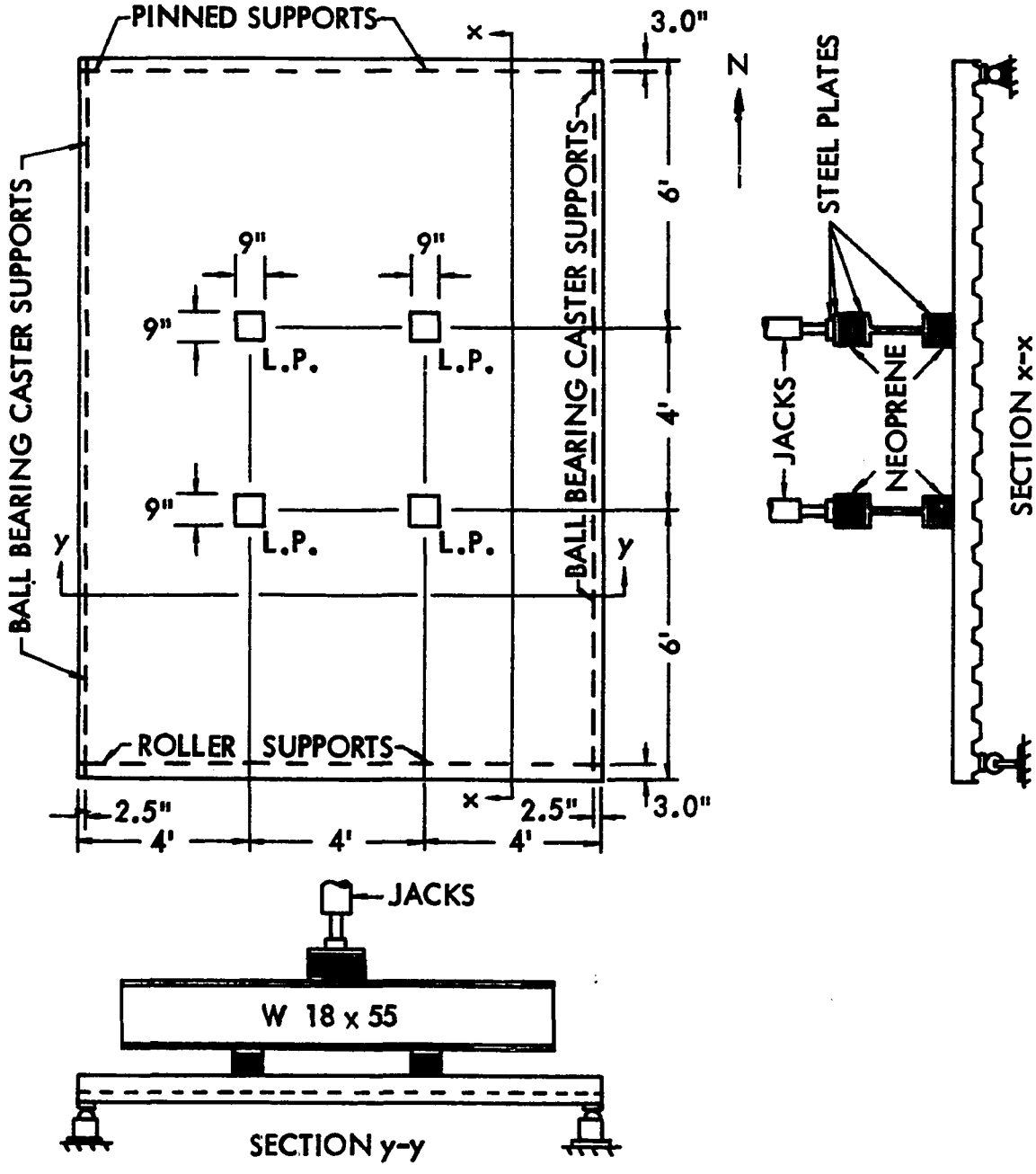

Figure 3. General layout of full-scale slab tests

the orientation of the steel decking used for the five slab tests.

Specimen behavior for the five two-way slabs was observed as evidenced by the following items:

1) crack pattern development and crack width measurements,

2) end slip (horizontal slip between steel deck and concrete) data

along the two opposite edges perpendicular to the corrugations,

3) vertical deflections of the slab at several points,

4) bending strains at several points on the concrete and steel surfaces,

5) vertical reactions as measured by transducers along portions of two edges of the slabs,

6) the ultimate applied load of each slab as measured at the four concentrated load points, and

7) the type of failure at ultimate load.

The first slab had all four corners anchored with instrumented corner restraints to measure vertical uplift reactions at the corners. The other four slabs had no corner restraints, leaving the corners free to displace upward. The upward corner movement was measured by vertical deflection dials. All slabs except the first were cyclic loaded between zero and approximately 60 percent of ultimate ten times to give behavioral data relating to low-cycle repeated loading.

Along with the five full-scale slab tests, 51 full-scale, one-way slab element specimens were constructed and tested. The slab element specimens were reinforced with the same three types of steel decking as employed in the two-way slabs. These tests consisted of one panel width or strip of a steel deck reinforced slab element with a width of two or three feet, a length of 6 to 12 feet and a nominal depth of 4½ to 5½ inches. Their purpose was to determine the one-way strength properties and characteristics to be utilized in comparison to the two-way slab tests. Twelve of the 51 slab element specimens had the steel deck corrugations transverse to the beam length, whereas 39 specimens had the deck corrugations

parallel to the length.

Summary of Research on Composite Deck at Iowa State University

An extensive theoretical and experimental investigation on various aspects of cold-formed steel decking as reinforcement for concrete floor slabs was initiated at Iowa State University in 1967 under the sponsorship of the American Iron and Steel Institute (AISI). Direct guidance from the AISI was provided by the Task Group on Composite Construction under chairmanship of Mr. A. J. Oudheusden. The major portion of the research has involved experimental testing to ultimate. To date 341 specimens of various types have been tested at Iowa State University. A brief description of each study and the number of tests for each is shown in Table 1.

A total of 18 unpublished reports, four published papers, and one oral presentation have resulted from the research at Iowa State University. The unpublished papers are listed as References (9), (7), (11), (10), (23), (24), (26)-(29), (32)-(36), and (40)-(43). The published papers are given by References (8), (30), (31), and (39), and the oral presentation is given by Reference (25).

Table 1. Summary of tests conducted involving cold-formed steel decking as reinforcement for concrete floors

Item No.	Number tested	Type of specimen[a] tested
1	178	One-way slab elements (beams)
2	56	Pushout specimens
3	14	One-way slab elements subjected to repeated loading
4	12	Slab elements with deck corrugations transverse to beam length
5	5	Slab elements continuous over two or three spans
6	6	Slab elements constructed with variable supplementary reinforcement in the form of welded wire fabric
7	31	Slab elements constructed with three-inch-deep steel deck
8	34	Slab elements constructed with non-composite deck with various surface coatings
9	5	Full-size two-way floor slabs simply supported on four edges
Total	341	

[a]All specimens were tested simply supported on a single span with static concentrated loads with 1½-inch decking oriented with corrugations parallel to length unless otherwise indicated.

CHAPTER 2. METHODS OF ANALYSIS AND DESIGN

General Remarks

A simple method of analysis and design for steel-deck reinforced floor slabs is to consider the system as a one-way floor slab. However, design questions arise as to the amount of distribution of forces in the so-called "weak" direction transverse to the deck corrugations, particularly for floor slabs subjected to concentrated loading. There is a further question as to the amount of reactive force carried by those support beams parallel to the deck corrugations. These beams receive those reactive forces from loading which is distributed in the "weak" direction. This chapter contains a description of current design procedures, followed by a presentation of four independent methods of analysis.

Review of Present Design Procedures

Present design procedures for steel-deck reinforced floor slabs treat the system as a one-way conventionally reinforced slab. Thus, such floor slabs are designed basically using working stress methods in accordance with established practices for design of reinforced concrete floors (1, 3). The allowable stresses and the flexural constants for the cold-formed steel decking are calculated based on AISI specifications (5). Additional recommendations for design are contained in each deck manufacturer's catalog.

One of the first significant publications to discuss the design procedures for composite steel-deck reinforced floor slabs was that by B. F. Friberg in 1954 (14). His publication employs working stress principles

of design for the particular steel deck investigated as well as a cost evaluation as compared to a conventionally reinforced concrete slab.

A complete summary of present design procedures employing working stress principles of reinforced concrete construction was given by C. E. Ekberg and R. M. Schuster in 1968 (8).

Various means of analysis were employed in this investigation to study the behavioral characteristics and the predicted ultimate strength of simply supported steel-deck reinforced floor slabs. The methods of analysis include the following:

1) one-way shear-bond regression,
2) yield-line theory,
3) yield-line and shear-bond methods combined,
4) orthotropic plate theory, and
5) curve fitting of deflected surfaces.

Design by One-Way Shear-Bond Regression Analysis

A one-way slab element with steel deck corrugations parallel to the length and with concentrated line loads, such as shown in Figure 4, usually fails by what is termed a shear-bond mode of failure. This type of failure is characterized by the formation of a diagonal shear crack in the concrete at or near one of the load points followed by a loss of bond between the steel decking and the concrete. This results in slippage between steel and concrete at the end of the slab element. Thus, the concrete and steel deck over the shear span, L', in Figure 4 no longer act compositely. This is termed a shear-bond failure and is the primary mode of failure for most steel-deck reinforced slab elements.

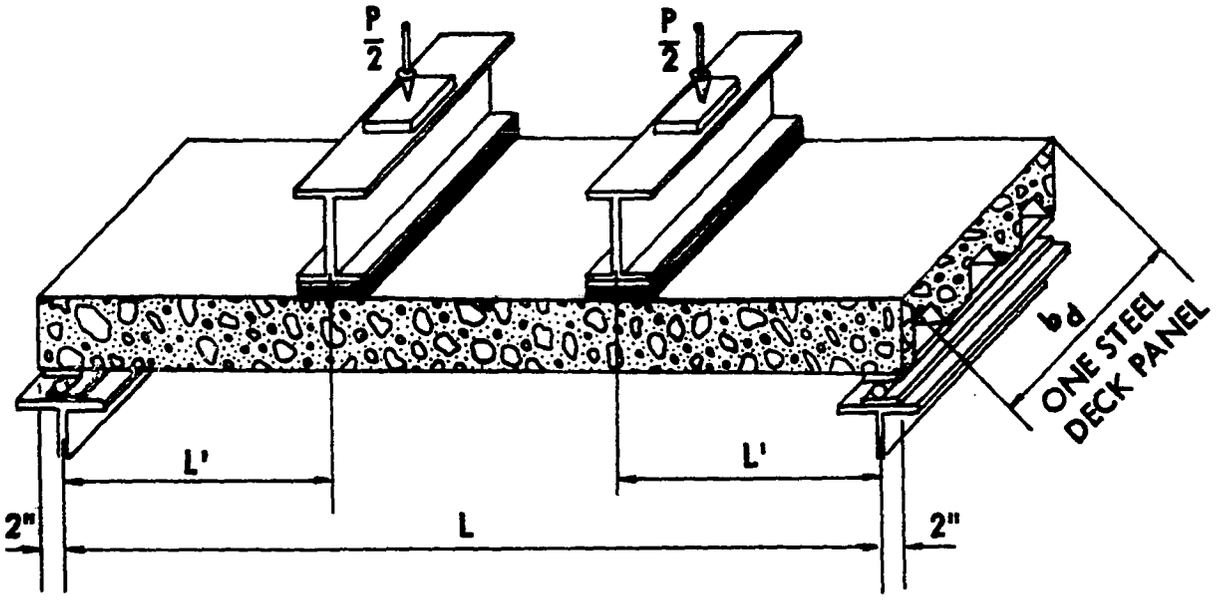

Figure 4. Typical arrangement for testing one-way slab elements

If ultimate failure is by shear-bond, then the shear transferring device (embossments, T-wires, holes, or geometry) would fail to maintain composite action until the full tensile strength of the steel decking could be developed. However, a shear-bond failure may be preceded by partial yielding of the deck cross section in the high moment region. This depends primarily on the strength of the shear transferring device, the percentage of steel, the shear span distance L', and the span length L.

A relationhip has been developed for calculating the ultimate experimental shear capacity of a one-way slab element (40). This is

$$\frac{V_{ue}\, s}{b_d dp} = \frac{k_1 d\sqrt{f'_c}}{pL'} + k_2 \qquad (1)$$

where

f'_c = compressive cylinder strength of concrete, psi

p = reinforcement ratio, $\frac{A_{sd}}{b_d d}$

L' = shear span length, inches (assume ½ of the span length for uniformly loaded elements)

V_{ue} = ultimate experimental shear capacity, pounds

k_1 = slope of regression curve

k_2 = intercept of regression curve

s = center-to-center spacing of a hole or welded shear transferring device, inches (for cases of embossments where shear transferring device is a fixed pattern the value of s is unity)

b_d = width of cross section, inches

d = effective slab depth as measured from extreme concrete compression fiber to centroidal axis of steel deck, inches

A_{sd} = cross-sectional area of steel deck per width b_d, square inches

The use of Equation (1) requires the determination of two constants, k_1 and k_2. These constants are the slope and intercept, respectively, of the regression analysis of the linear relationship between $V_{ue}\, s/(b_d dp)$ and $(d\sqrt{f'_c})/(pL')$. The resulting total ultimate shear, V_u, in pounds for slab elements of span length, L, in feet, and dead load, W in pounds per square foot is given by

$$V_u = \frac{b_d d}{s}\left[\frac{k_1 d}{L'}\sqrt{f'_c} + k_2 p\right] + \frac{wLb_d}{24} \qquad (2)$$

The shear-bond regression analysis was used in this investigation as a means of approximating the ultimate strength of the five two-way slabs used in this investigation. The first four slabs utilized steel decking which had been evaluated previously by slab element tests to determine regression constants k_1 and k_2. Slab 5 utilized steel decking which had not

previously been tested, and thus a series of tests on 29 slab elements were conducted in order to determine k_1 and k_2.

Yield-Line Method of Analysis

General remarks

Steel-deck reinforced floor slabs are designed basically as one-way slabs. However, in certain instances, particularly those involving heavy concentrated loading, two-way action should be given consideration. The yield-line method of analysis provides a means of predicting the two-way flexural behavior of slabs. Not only can the yield-line theory be applied to simply supported slabs, but it can be applied to floor slabs continuous over multiple supports, to floor slabs with interior openings, and to floor slabs of irregular shape.

The yield-line method provides a straight-forward means of estimating the expected ultimate load of a steel-deck reinforced slab for those cases where the moment capacity is the controlling criteria. For slabs containing heavy concentrated loads, some additional reinforcement such as welded wire fabric or heavier may be necessary to prevent the break-up of the slab in the neighborhood of each concentrated load and to provide nominal temperature and shrinkage reinforcement.

For cases where the moment capacity of a particular critical section, as arrived at through the yield-line method, is not attainable and the slab is more critical in shear-bond or deflection, then a combination of the yield-line method and the one-way shear-bond or deflection methods can be utilized. Most simply supported steel-deck reinforced floor slabs fail ultimately by means of shear bond. For such cases involving shear-bond

failure, the yield-line crack pattern mechanism can be utilized in conjunction with the one-way shear-bond analysis. For continuous floor systems where shear-bond may be prevented, the yield-line method affords a very versatile direct approach for the determination of the predicted ultimate load.

A detailed review covering the yield-line methodology is contained in Reference (29) by Porter and Ekberg. This referenced report presents a literature review, general concepts, basic assumptions, methods of use, and application of the yield-line theory. A complete coverage of the development of the yield-line theory and general application to slab systems is given in a text by Jones and Wood (17).

Report Reference (29) also discusses and derives some basic mechanisms as applied to steel-deck reinforced slabs. The next two sections present the yield-line mechanisms considered in this investigation.

Application of yield-line theory to steel-deck reinforced slabs

Application of the principles of yield-line theory involves the computation of the flexural moment capacities in the longitudinal and transverse directions, respectively. Ultimate strength procedures for flexural computations were utilized for the determination of moments m and μm for the longitudinal and transverse directions, respectively. A detailed discussion of methods for the strength computation of m and μm is given in Chapters 6 and 7.

In accordance with yield-line principles, several collapse mechanisms were investigated. The derivation of the work equations for two such mechanisms are presented. Figure 5 indicates one of the collapse mechanisms

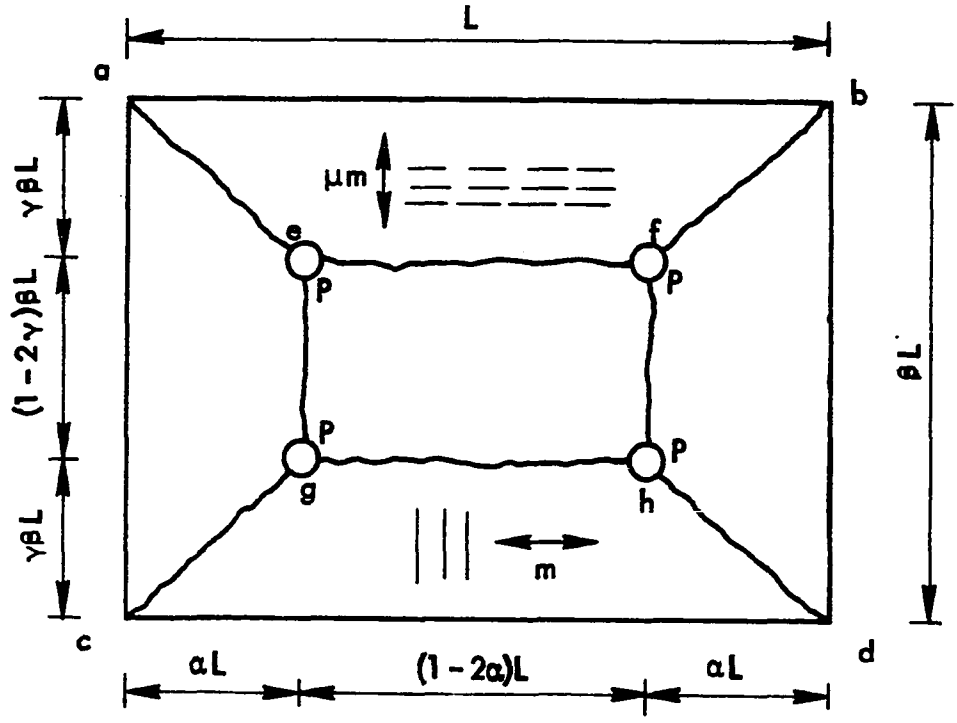

Figure 5. First collapse mechanism for simply supported slab under combined uniform and concentrated loading

considered.

First, the internal energy, I, for the mechanism in Figure 5, may be arrived at as follows: (using the vector summation of moments for each segment)

$$I = 2\left[\mu m(\beta L)\left(\frac{1}{\alpha L}\right) + m\, L\left(\frac{1}{\beta\gamma L}\right)\right]$$

which may be reduced to

$$I = \frac{2m}{\alpha\beta\gamma}\left[\mu\beta^2\gamma + \alpha\right] \qquad (3)$$

Next, the external energy is arrived at by considering the displacement of the loads by giving the segment efgh a unit displacement. The external energy is as follows:

$$E = 2\left[(1 - 2\gamma)(\beta L)(\alpha L)w(1/2) + 2(1/2)(\beta\gamma L)(\alpha L)w(1/3)\right.$$
$$\left. + (1 - 2\alpha)L(\beta\gamma L)w(1/2) + 2(1/2)(\alpha L)(\beta\gamma L)w(1/3)\right]$$
$$+ w(1 - 2\alpha)L(1 - 2\gamma)\beta L(1) + 4P(1)$$

which reduces to

$$E = \frac{w\beta L^2}{3}\left[-3\alpha + 4\alpha\gamma - 3\gamma + 3\right] + 4P \qquad (4)$$

Applying the principle of internal dissipation of energy equalling the external work, then Equations (3) and (4) are set equal, and solving for the required moment capacity gives:

$$m = \frac{w\alpha\beta^2\gamma L^2(-3\alpha + 4\alpha\gamma - 3\gamma + 3)}{6(\mu\beta^2\gamma + \alpha)} + \frac{2P\alpha\beta\gamma}{\mu\beta^2\gamma + \alpha} \qquad (5)$$

Equation (5) applies to the yield mechanism shown in Figure (5) and gives the correct design, m, only if this mechanism is the correct one. The most important parameter for the determination of the correct mechanism is the position of concentrated loads and the relative magnitude between the concentrated and uniform loads.

The second general yield-line mechanism is shown in Figure 6. The vector summation of the moments for the internal energy is

$$I = 2\left[\mu m(\beta L)\left(\frac{1}{\alpha L''}\right) + im(\beta L)\left(\frac{1}{\alpha L''}\right) + mL''\left(\frac{1}{\beta\gamma L}\right)\right]$$

which may be reduced to

$$I = \frac{2mL}{\alpha\beta L''}\left[\mu\beta^2 + i\beta^2 + \left(\frac{L''}{L}\right)^2\left(\frac{\alpha}{\gamma}\right)\right] \qquad (6)$$

Next the external energy is found by considering the displacement of the loads by giving segment abcd in Figure 6 a unit displacement. The

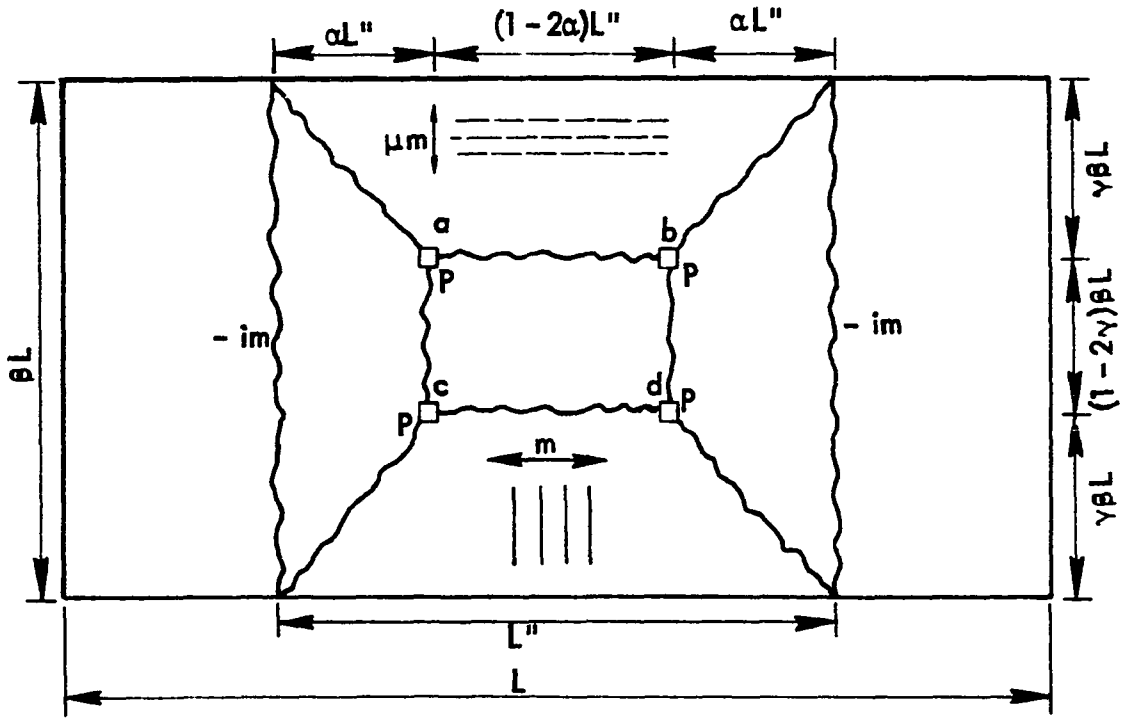

Figure 6. Second collapse mechanism for simply supported slab under combined uniform and concentrated loading

external energy is as follows:

$$E = 2\Big[(1 - 2\gamma)(\beta L)(\alpha L'')w(1/2) + 2(1/2)(\beta\gamma L)(\alpha L'')w(1/3) + (1 - 2\alpha)L''(\beta\gamma L)w(1/2) + 2(1/2)(\alpha L'')(\gamma\beta L)w(1/3)\Big] + w(1 - 2\alpha)(L'')(1 - 2\gamma)(\beta L)(1) + 4P(1)$$

which reduces to

$$E = \frac{w\beta L'' L}{3}\left[-3\alpha + 4\alpha\gamma - 3\gamma + 3\right] + 4P \qquad (7)$$

Equating (6) and (7) and solving for m gives

$$m = \frac{w\alpha\beta^2(L'')^2(-3\alpha + 4\alpha\gamma - 3\gamma + 3)}{6\left[\mu\beta^2 + i\beta^2 + \left(\frac{L''}{L}\right)^2\left(\frac{\alpha}{\gamma}\right)\right]} + \frac{2P\alpha\beta L''}{L\left[\mu\beta^2 + i\beta^2 + \left(\frac{L''}{L}\right)^2\left(\frac{\alpha}{\gamma}\right)\right]} \qquad (8)$$

The designer must always assure himself, when using the yield-line approach, that he has reached a mechanism very close to the true case, since the predicted collapse load will be greater or at best equal to the true value. Such items as membrane action and torsional restraints in the slab will help the designer compensate for not finding the true collapse mechanism.

Formation of fans

Heavy concentrated loads can oftentimes cause a fan type of formation of yield lines such as that shown in Figure 7. The fan formations do not change the results significantly in the cases involving distributed loads only, but for cases involving heavy concentrated loads the fans will be centered on the load points and the value of the collapse load will be significantly affected.

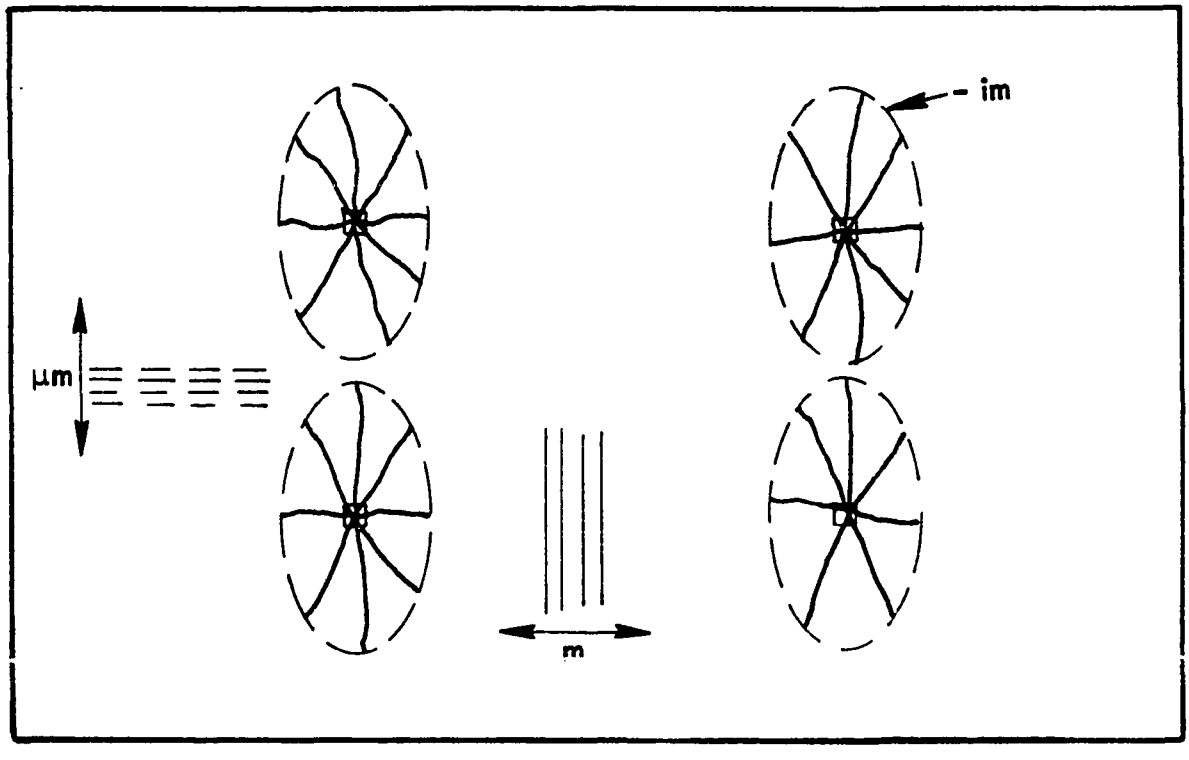

Figure 7. Formation of fans under concentrated loads

For orthotropically reinforced slabs, advantage may be taken of the affine transformation to arrive at a solution by considering the slab as isotropically reinforced and the resulting fan as being circular in shape rather than elliptical as would be the case for the orthotropic slab. Development of a full circle will not always result in that the boundaries may dictate that a partial circular fan is more critical. Development of an expression for the collapse load for a circular fan is given by Jones and Wood (17). Thus, for the circular fan shown in Figure 8, the moment capacity, m, due to a concentrated load, P, and uniform load, w, is

$$m = \frac{P + (1/3)\pi R_f^2 w}{2\pi(1 + i)} \tag{9}$$

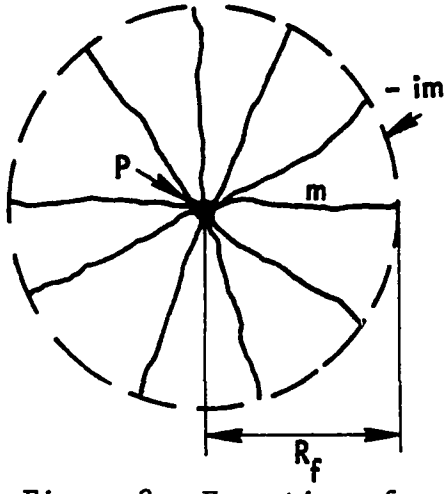

Figure 8. Formation of circular fan

If the uniform load is negligible, then the required isotropic reinforcement, m, is given by

$$m = \frac{P}{2\pi(1 + i)} \tag{10}$$

If no top reinforcement is provided then i = 0 and the collapse load is then $P = 2\pi = 6.28m$.

Using the rules of affine transformation, then the collapse load for the elliptical fan for the orthotropically reinforced steel-deck slab is

$$P = 2\pi m\sqrt{\mu}(1 + i) \tag{11}$$

This is quite an interesting result, for if no reinforcement is counted on in the transverse direction, then P = 0. Of course, this is unsatisfactory and the need is obvious for transverse reinforcement of some kind to be

present or counted on to prevent the breakup of the slab in a fan pattern of failure. Thus, if heavy concentrated loads are expected, then serious consideration must be given to the problem of transverse reinforcing.

The yield-line theory was used in two approaches in this investigation. The first approach involved computation of the ultimate collapse load to predict the flexural capacity of steel-deck slab systems. Mechanism equations such as Equations (5), (8), and (11) were utilized to give the ultimate flexural capacity. The second approach involved the use of the yield-line theory to establish a mechanism for a controlling shear-bond mode of failure. Applications of these approaches and computational results are given in Chapter 7.

Two-Way Slab Behavior as Predicted by Orthotropic Plate Theory

Behavioral characteristics of deflection, bending moment distributions, and shear distributions of the full-size two-way floor slabs were analyzed by use of orthotropic plate theory. The basic analysis by orthotropic plate theory considered the steel-deck reinforced slabs as rectangular plates with simply supported edges. Orthotropic plate theory was selected for analysis of behavioral characteristics since the nature of the steel-deck reinforcement provided much greater stiffness in the direction parallel to the corrugations, whereas the stiffness at right angles to the corrugations was relatively small. Load tests on slab elements with deck corrugations parallel to length and transverse to length were performed to give numerical values for the stiffness in each orthogonal direction.

The general differential equation governing the deflection of an orthotropic plate is given in References (19) and (48). Using the notation

given in Reference (19), the general differential equation is

$$D_1 \frac{\partial^4 z}{\partial x^4} + 2D_3 \frac{\partial^4 z}{\partial x^2 \partial y^2} + D_2 \frac{\partial^4 z}{\partial y^4} = q \qquad (12)$$

where

q = uniform load

z = vertical deflection

x, y = rectangular coordinate locations

D_1 = stiffness constant = $\frac{E_1 d_1^3}{12(1 - \nu_1 \nu_2)} = \frac{(E_c I_T)_x}{(1 - \nu_c^2)}$

D_2 = stiffness constant = $\frac{E_2 d_2^3}{12(1 - \nu_1 \nu_2)} = \frac{(E_c I_T)_y}{(1 - \nu_c^2)}$

D_3 = stiffness constant = $\sqrt{D_1 D_2}$

E_1, E_2 = modulus of elasticity in tension and compression in the principal direction

ν_1, ν_2 = Poisson's ratio in each of the principal directions of elasticity (assumed equal to Poisson's ratio of concrete, ν_c)

d_1, d_2 = effective depth in each orthogonal direction as measured from the top surface

E_c = modulus of elasticity for concrete

$(E_c I_T)_x$ = flexural stiffness in x direction using transformed moment of inertia

$(E_c I_T)_y$ = flexural stiffness in y direction using transformed moment of inertia

For the steel-deck reinforced slabs in this investigation, the y- and x-directions of elasticity were considered as parallel and transverse to the corrugations, respectively. Thus, D_1 is really D_x and is the stiffness transverse to the corrugations, whereas D_2 is really D_y and is the

stiffness parallel to the corrugations. The sign convention used for Equation (12) is shown in Figure 9.

The use of d_1 and d_2 for computing the orthogonal stiffness is not included in References (19) and (48) but is included here as a means of approximating the stiffness in each orthogonal direction. The effective depth, d_1, is considered only to the top of the corrugations, whereas d_2

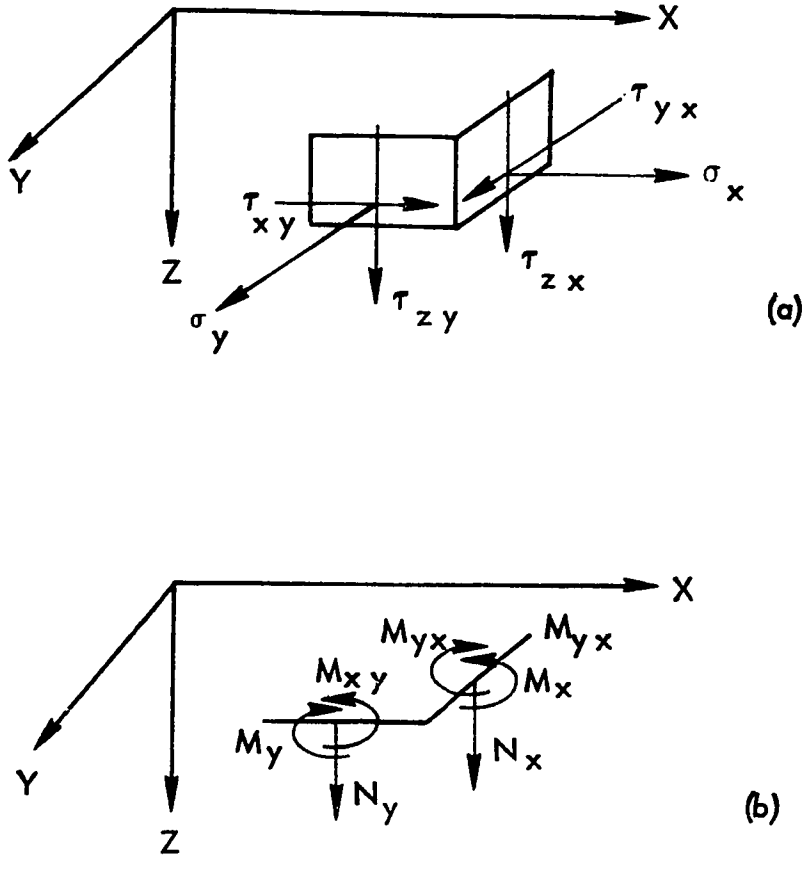

Figure 9. Sign convention for orthotropic plate equations

is considered to the centroidal axis of the steel decking. Thus, the constants D_1 and D_2 use the EI stiffness of a transformed section for each orthogonal direction.

The solution of Equation (12) is subject to the following boundary conditions of a simply supported plate:

1) for $x = 0$ and $x = a$, $z = M_x = 0$, and

2) for $y = 0$ and $y = b$, $z = M_y = 0$

where a is the length along the x direction and b the length along the y direction. As given in Reference (19), the solution to Equation (12) is of the form of the series

$$z = \sum_{m=1}^{\infty} \sum_{n=1}^{\infty} A_{mn} \sin \frac{m\pi x}{a} \sin \frac{n\pi y}{b} \tag{13}$$

The coefficients A_{mn} are found by the expansion of q into a double Fourier series

$$q = \sum_{m=1}^{\infty} \sum_{n=1}^{\infty} a_{mn} \sin \frac{m\pi x}{a} \sin \frac{n\pi y}{b} \tag{14}$$

where

$$a_{mn} = \frac{4}{ab} \int_0^a \int_0^b q \sin \frac{m\pi x}{a} \sin \frac{n\pi y}{b} \, dx dy \tag{15}$$

Substitution of Equations (13) and (14) into Equation (12) and comparing coefficients of identical terms gives the following expression contained in Reference (19) for the deflection:

$$z = \frac{b^4}{\pi^4} \sum_{m=1}^{\infty} \sum_{n=1}^{\infty} a_{mn} \frac{\sin \frac{m\pi x}{a} \sin \frac{n\pi y}{b}}{D_1 \left(\frac{m}{c}\right)^4 + 2D_3 n^2 \left(\frac{m}{c}\right)^2 + D_2 n^4} \tag{16}$$

where c = a/b. The coefficients a_{mn} depend upon the load distribution. For a uniformly loaded slab

$$a_{mn} = \frac{16q_1}{\pi^2}\left(\frac{1}{mn}\right) \text{ for m and n = 1, 3, 5, etc.,} \tag{17}$$

and $a_{mn} = 0$ for all other m and n, where q_1 is the uniform load per unit area. For a concentrated load, P, at the point (ξ, k), such as was applied to four locations of the slabs in this investigation, the coefficients are

$$a_{mn} = \frac{4P}{ab} \sin \frac{m\pi\xi}{a} \sin \frac{n\pi k}{b} \tag{18}$$

for all m and n.

The differential equations for the various forces as given in References (19) and (48) are as follows for

Moment:

$$\left.\begin{aligned} M_x &= -D_1\left(\frac{\partial^2 z}{\partial x^2} + \nu_2 \frac{\partial^2 z}{\partial y^2}\right) \\ M_y &= -D_2\left(\frac{\partial^2 z}{\partial y^2} + \nu_1 \frac{\partial^2 z}{\partial x^2}\right) \\ M_{xy} &= -(1 - \nu_c)\sqrt{D_x D_y}\,\frac{\partial^2 z}{\partial x \partial y} \end{aligned}\right\} \tag{19}$$

Shears:

$$\left.\begin{aligned} N_x &= -\frac{\partial}{\partial x}\left(D_1 \frac{\partial^2 z}{\partial x^2} + D_3 \frac{\partial^2 z}{\partial y^2}\right) \\ N_y &= -\frac{\partial}{\partial y}\left(D_3 \frac{\partial^2 z}{\partial x^2} + D_2 \frac{\partial^2 z}{\partial y^2}\right) \end{aligned}\right\} \tag{20}$$

Reactive Forces:

$$\left.\begin{aligned} &\text{for edge } x = a, \\ &V_x = \left(N_x - \frac{\partial M_{xy}}{\partial y}\right) x = a \\ &\text{for edge } x = b, \\ &V_y = \left(N_y - \frac{\partial M_{xy}}{\partial x}\right) y = b \\ &\text{for the corners,} \\ &R = 2(M_{xy})\ x=a,\ y = b \end{aligned}\right\} \qquad (21)$$

Using Equation (16) and substituting into Equations (19), (20), and (21), the following equations are obtained for the various forces:

$$M_x = \frac{D_1 b^4}{\pi^2} \sum_{m=1}^{\infty} \sum_{n=1}^{\infty} a_{mn} \left[\frac{\left(\frac{m^2}{a^2} + \frac{\nu_2 n^2}{b^2} \right) \sin \frac{m\pi x}{a} \sin \frac{n\pi y}{b}}{D_1 \left(\frac{m}{c}\right)^4 + 2D_3 n^2 \left(\frac{m}{c}\right)^2 + D_2 n^4} \right] \qquad (22)$$

$$M_y = \frac{D_1 b^4}{\pi^2} \sum_{m=1}^{\infty} \sum_{n=1}^{\infty} a_{mn} \left[\frac{\left(\frac{n^2}{b^2} + \frac{\nu_1 m^2}{a} \right) \sin \frac{m\pi x}{a} \sin \frac{n\pi y}{b}}{D_1 \left(\frac{m}{c}\right)^4 + 2D_3 n^2 \left(\frac{m}{c}\right)^2 + D_2 n^4} \right] \qquad (23)$$

$$M_{xy} = - \frac{(1 - \nu_c)\sqrt{D_1 D_2}(b)^3}{a\pi^2} \sum_{m=1}^{\infty} \sum_{n=1}^{\infty} mn \frac{a_{mn} \cos \frac{m\pi x}{a} \cos \frac{n\pi y}{b}}{D_1 \left(\frac{m}{c}\right)^4 + 2D_3 n^2 \left(\frac{m}{c}\right)^2 + D_2 n^4} \qquad (24)$$

$$N_x = \frac{D_1 b^4}{a^3 \pi} \sum_{m=1}^{\infty} \sum_{n=1}^{\infty} a_{mn} \frac{m^3 \cos \frac{m\pi x}{a} \cos \frac{n\pi y}{b}}{D_1 \left(\frac{m}{c}\right)^4 + 2D_3 n^2 \left(\frac{m}{c}\right)^2 + D_2 n^4}$$

$$+ \frac{D_3 b^2}{a\pi} \sum_{m=1}^{\infty} \sum_{n=1}^{\infty} a_{mn} \frac{mn^2 \cos \frac{m\pi x}{a} \sin \frac{n\pi y}{b}}{D_1 \left(\frac{m}{c}\right)^4 + 2D_3 n^2 \left(\frac{m}{c}\right)^2 + D_2 n^4} \tag{25}$$

$$N_y = \frac{D_3 b^3}{\pi a^2} \sum_{m=1}^{\infty} \sum_{n=1}^{\infty} a_{mn} \frac{nm^2 \sin \frac{m\pi x}{a} \sin \frac{n\pi y}{b}}{D_1 \left(\frac{m}{c}\right)^4 + 2D_3 n^2 \left(\frac{m}{c}\right)^2 + D_2 n^4}$$

$$+ \frac{D_2 b}{\pi} \sum_{m=1}^{\infty} \sum_{n=1}^{\infty} a_{mn} \frac{n^3 \sin \frac{m\pi x}{a} \cos \frac{n\pi y}{b}}{D_1 \left(\frac{m}{c}\right)^4 + 2D_3 n^2 \left(\frac{m}{c}\right)^2 + D_2 n^4} \tag{26}$$

$$V_x = \frac{D_1 b^4}{a^3 \pi} \sum_{m=1}^{\infty} \sum_{n=1}^{\infty} a_{mn} \frac{m^3 (-1)^m \sin \frac{n\pi y}{b}}{D_1 \left(\frac{m}{c}\right)^4 + 2D_3 n^2 \left(\frac{m}{c}\right)^2 + D_2 n^4}$$

$$+ \frac{b^2}{a\pi} (\nu_c D_1) \sum_{m=1}^{\infty} \sum_{n=1}^{\infty} a_{mn} \frac{mn^2 (-1)^m \sin \frac{n\pi y}{b}}{D_1 \left(\frac{m}{c}\right)^4 + 2D_3 n^2 + D_2 n^4} \tag{27}$$

$$V_y = \frac{b^3}{\pi a^2} (\nu_c D_1) \sum_{m=1}^{\infty} \sum_{n=1}^{\infty} \frac{a_{mn} m^2 n (-1)^n \sin \frac{m\pi x}{a}}{D_1 \left(\frac{m}{c}\right)^4 + 2D_3 n^2 \left(\frac{m}{c}\right)^2 + D_2 n^4}$$

$$+ \frac{D_2 b}{\pi} \sum_{m=1}^{\infty} \sum_{n=1}^{\infty} \frac{a_{mn} n^3 (-1)^n \sin \frac{m\pi x}{a}}{D_1 \left(\frac{m}{c}\right)^4 + 2D_3 n^2 \left(\frac{m}{c}\right)^2 + D_2 n^4} \tag{28}$$

$$R = \frac{-(2)(1-\nu_c)(\sqrt{D_1 D_2})(b^3)}{a\pi^2} \sum_{m=1}^{\infty} \sum_{n=1}^{\infty} \frac{a_{mn} mn(-1)^m(-1)^n}{D_1\left(\frac{m}{c}\right)^4 + 2D_3 n^2\left(\frac{m}{c}\right)^2 + D_2 n^4} \tag{29}$$

The corner reaction shown by Equation (29) was computed for all five slabs tested. However, only Slab 1 physically had corner tie-down reactions during testing. The other four slabs were free to lift off their supports at each of the four corners and continued to lift inwardly as loading increased. Thus, the boundary conditions and resulting series equations employed using the orthotropic plate equations are only approximate for the last four slabs.

The orthotropic plate equations were programmed on an IBM 360 model 70 computer. The number of terms of the series were all combinations of m and n each equal to nine making a total of 81 terms of each series solution.

Three types of EI stiffness calculations were performed to establish D_1, D_2, and D_3. All three were based on a transformed section by transforming the steel to an equivalent area of concrete by multiplying by the modular ratio. The first type of stiffness was based upon an uncracked section and was used for analysis involving fairly low loads where the stresses in tension were less than the modulus of rupture stress of the concrete, f_r. The second type of stiffness neglected the concrete in tension and considered the section completely cracked to the neutral axis. This second stiffness was used for analyzing a cracked slab at higher loads.

The third type of stiffness involved an approximation by considering an average of those sections which were uncracked and those sections that

were cracked. This was done by iteration in the orthotropic plate theory computer programs by comparing the stress at the bottom fiber to the modulus of rupture, f_r. If the f_r was less than the computed fiber stress at the location in question, the stiffness was based upon a cracked section, whereas if the f_r was greater than the computed fiber stress the stiffness was based upon an uncracked section. After each of the stiffnesses were computed, an average approximate stiffness to be used in the orthotropic plate computer program was formed by simply averaging all stiffnesses for all locations.

Slab Behavior Based on Curve Fitting of Deflected Surfaces

Since there were a significant number of vertical deflection measurements made throughout the slab, most of which were located in one quadrant of the slab, curve fitting equations were established for various loads for each of the slabs. The curve fitting was based upon writing sixth order polynomial equations of the form

$$\begin{aligned} z = {} & c_1 + c_2x + c_3y + c_4x^2 + c_5y^2 + c_6xy + c_7x^3 + c_8y^3 \\ & + c_9x^2y + c_{10}xy^2 + c_{11}x^4 + c_{12}y^4 + c_{13}x^2y^2 + c_{14}x^3y \\ & + c_{15}xy^3 + c_{16}x^5 + c_{17}y^5 + c_{18}x^4y + c_{19}x^3y^2 + c_{20}x^2y^3 \\ & + c_{21}xy^4 + c_{22}x^6 + c_{23}y^6 + c_{24}x^2y^4 + c_{25}x^3y^3 + c_{26}x^4y^2 \\ & + c_{27}x^5y + c_{28}xy^5 \end{aligned} \tag{30}$$

The coefficients c_1, c_2, ..., c_{28} were solved by a least squares computer program designated as "ULSQ" which is a Fortran subroutine for curve fittings. This computer program was available through the Iowa State University Computation Center Library (16).

One Equation (30) was determined for each load desired for each slab, then behavior characteristics in the form of force distributions were studied. This was done by employing the differential equilibrium Equations (19), (20), and (21) as was done with the orthotropic theory study. Thus, based on a given deflected surface the moments, shears, and reactive forces were found. The resulting polynomial expressions for moments are

$$\begin{aligned} M_x = - D_1 \big[& 2c_4 + 2\nu_c c_5 + 2x(3c_7 + \nu_c c_{10}) + 2y(c_9 + 3\nu_c c_8) \\ & + 12c_{11}x^2 + 6xy(c_{14} + \nu_c c_{15}) + 12\nu_c c_{12}y^2 + 20c_{16}x^3 \\ & + 20\nu_c c_{17}y^3 + 12c_{18}x^2y + 12\nu_c c_{21}xy^2 + 30c_{22}x^4 \\ & + 30\nu_c c_{23}y^4 + 20c_{23}x^3y + 20\nu_c c_{23}xy^3 + 2c_{19}x(3y^2 + \nu_c x^2) \\ & + 2c_{20}y(y^2 + 3\nu_c x^2) + 2c_{24}y^2(y + 6\nu_c x^2) + (2c_{13} \\ & + 6c_{25}xy)(y^2 + \nu_c x^2) + 2c_{26}x^2(6y^2 + \nu_c x^2) \big] \end{aligned} \tag{31}$$

$$\begin{aligned} M_y = - D_2 \big[& 2c_5 + 6c_8y + 2c_{10}x + 12c_{12}y^2 + 2c_{13}x^2 + 6c_{15}xy \\ & + 20c_{17}y^3 + 2c_{19}x^3 + 6c_{20}x^2y + 12c_{21}xy^2 + 30c_{23}y^4 \\ & + 12c_{24}x^2y^2 + 6c_{25}x^3y + 2c_{26}x^4 + 20c_{28}xy^3 + \nu_c(2c_4 + 6c_7x \\ & + 2c_9y + 12c_{11}x^2 + 2c_{13}y^2 + 6c_{14}xy + 20c_{16}x^3 + 12c_{18}x^2y \\ & + 6c_{19}xy^2 + 2c_{20}y^3 + 30c_{22}x^4 + 2c_{24}y^4 + 6c_{26}xy^3 \\ & + 12c_{26}x^2y^2 + 20c_{27}x^3y) \big] \end{aligned} \tag{32}$$

$$M_{xy} = -(1 - \nu_c)\left[c_6 + 2c_9x + 2c_{10}y + 4c_{13}xy + 3c_{14}x^2 + 3c_{15}y^2 + 4c_{18}x^3 + 6c_{19}x^2y + 6c_{20}xy^2 + 4c_{21}y^3 + 8c_{24}xy^3 + 9c_{25}x^2y^2 + 8c_{26}x^3y + 5c_{27}x^4 + 5c_{28}y^4\right] \quad (33)$$

The resulting polynomial expressions for the shear forces are

$$N_x = -D_1\left[6c_7 + 24c_{11}x + 6c_{14}y + 60c_{16}x^2 + 24c_{18}xy + 6c_{19}y^2 + 120c_{22}x^3 + 6c_{25}y^3 + 24c_{26}xy^2 + 60c_{27}x^2y\right] - D_3\left[2c_{10} + 4c_{13}x6c_{15}y + 6c_{19}x^2 + 12c_{20}xy + 12c_{21}y^2 + 24c_{24}xy^2 + 18c_{25}x^2y + 8c_{26}x^3 + 20c_{28}y^3\right] \quad (34)$$

$$N_y = -D_3\left[2c_9 + 4c_{13}y + 6c_{14}x + 12c_{18}x^2 + 12c_{19}xy + 6c_{20}y^2 + 8c_{24}y^3 + 18c_{25}xy^2 + 24c_{26}x^2y + 20c_{27}x^3\right] - D_2\left[6c_8 + 24c_{12}y + 6c_{15}x + 60c_{17}y^2 + 6c_{20}x^2 + 24c_{21}xy + 120c_{23}y^3 + 24c_{24}x^2y + 6c_{25}x^3 + 60c_{28}xy^2\right] \quad (35)$$

The resulting polynomial expressions for the reactive forces are

$$V_x = -D_1\left[6c_9 + 24c_{11}x + 6c_{14}y + 60c_{16}x^2 + 24c_{18}xy + 6c_{19}y^2 + 120c_{22}x^3 + 6c_{25}y^3 + 24c_{26}xy^2 + 60c_{27}x^2y\right] + (-D_3 + 1 - \nu_c)\left[2c_{10} + 4c_{13}x + 6c_{15}y + 6c_{19}x^2 + 12c_{20}xy + 12c_{21}y^2 + 24c_{24}xy^2 + 18c_{25}x^2y + 8c_{26}x^3 + 20c_{28}y^3\right] \quad (36)$$

$$V_y = (- D_3 + 1 - \nu_c)\left[2c_9 + 4c_{13}y + 6c_{14}x12c_{18}x^2 + 12c_{19}xy + 6c_{20}y^2 + 8c_{24}y^3 + 18c_{25}xy^2 + 24c_{26}x^2y + 20c_{27}x^3\right] - D_2\left[6c_8 + 24c_{12}y + 6c_{15}x + 60c_{17}y^2 + 6c_{20}x^2 + 24c_{21}xy + 120c_{23}y^3 + 24c_{24}x^2y + 6c_{25}x^3 + 60c_{28}xy^2\right] \quad (37)$$

The coordinate points for which vertical deflections were selected for the least squares curve fitting included boundary deflections for corner uplift and zero displacement as well as interior coordinate locations. The number of selected points ranged from 80 to 157. Symmetry of measured deflection points was utilized to reach this number of points to obtain the proper surface equations for the deflected shape of the experimental slab specimens. The results of moment, shear, and reaction force computations were compared to those obtained by ordinary orthotropic plate theory and to those obtained by reduction of measured strain and reaction data.

CHAPTER 3. DESCRIPTION OF TEST SPECIMENS AND EQUIPMENT

Description of Slab Specimens

General remarks

All five of the steel-deck reinforced full-scale slabs were supported and tested as shown in Figure 10. All slabs were simply supported with roller and pin bearing supports on the south and north sides, respectively, as shown and with ball-bearing-ball caster bearing supports on the west and east sides.

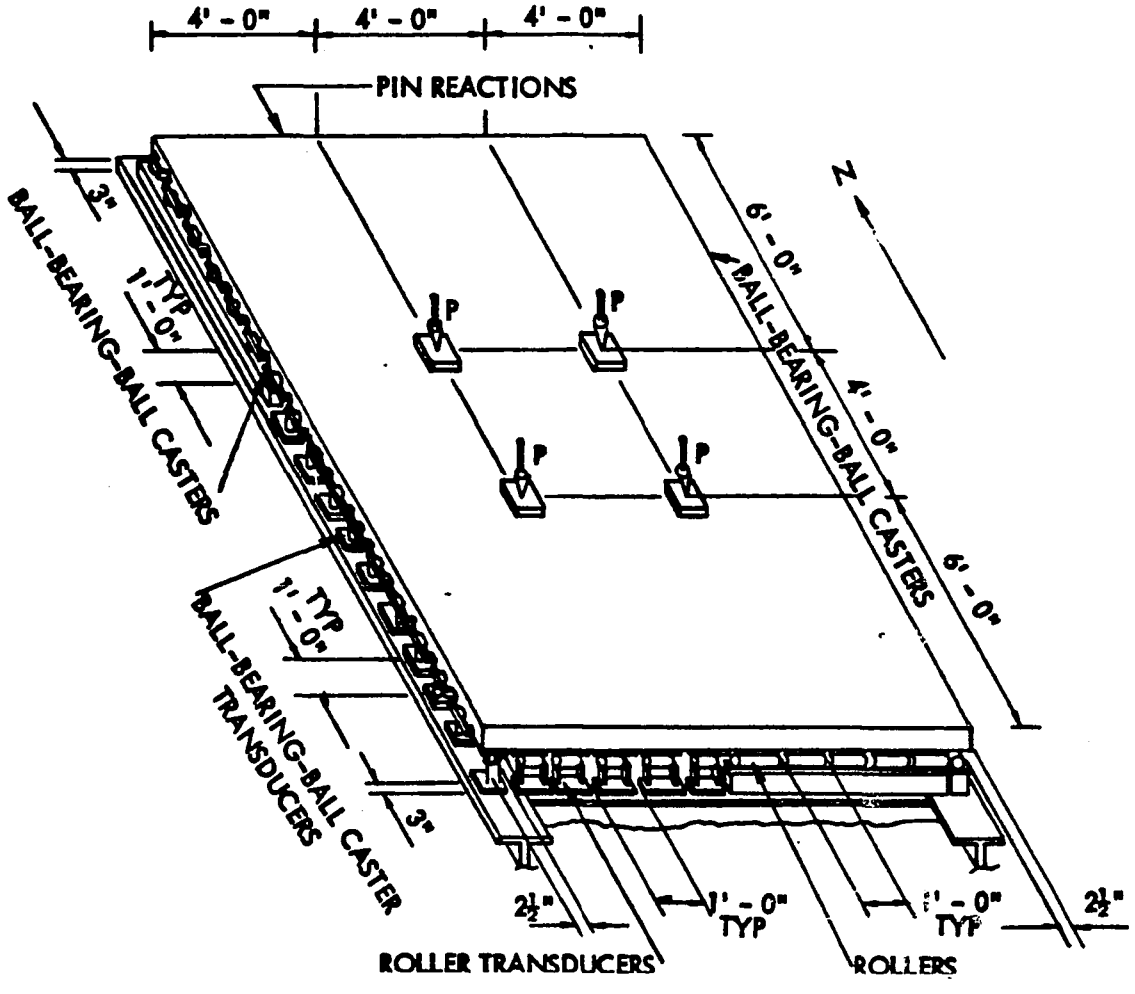

Figure 10. General layout of full-scale slab tests

The design thickness for the first four slabs was established at 4.5 inches and for the fifth slab was 5.5 inches. However, the thickness of each slab deviated somewhat due to variations in deflection under the weight of the wet concrete. The actual thickness was measured at various points throughout the slab and these values were utilized in the analysis.

The primary reinforcement for the slabs was corrugated cold-formed steel decking furnished by the manufacturer. The first three slabs contained nominal 20-gage steel decking with 1½-inch corrugations as supplied by Company I.* The fourth slab contained nominal 24-gage decking with 1 5/16-inch deep corrugations as supplied by Company G. The fifth slab contained nominal 20-gage decking with 3-inch deep corrugations as supplied by Company O.

Supplementary reinforcement in the form of welded wire fabric (WWF) was utilized in three of the five slabs. Slab 1 contained fabric commonly designated 6 X 6 X 6/6, i.e. number six gage wires on six-inch center-to-center spacing in both longitudinal and transverse directions. Slab 2 contained 6 X 12 X 0/4 WWF with the zero-gage wire on six-inch centers spanning the 16-foot direction and the four-gage wire on 12-inch centers spanning the 12-foot direction. The welded wire fabric in Slabs 1 and 2 was placed directly on top of the steel decking. Slabs 3 and 4 did not contain any reinforcement in addition to the steel decking; however, the decking used in Slab 4 is manufactured with deformed wire no. D-4 spot-welded to the top of decking with the wire transverse to the direction of the corrugations. Slab 5 had only 6 X 6 X 10/10 WWF which was placed

*Each steel deck is identified by a letter, omitting the name of the supplying company, to avoid direct comparison.

approximately 1 to 1½ inches from the top surface of the slab.

Materials

The materials used in the construction of the test slabs consisted of corrugated cold-formed steel decking, supplementary reinforcement steel, and Portland Cement Concrete. No effort was made to alter the characteristics of those materials from what would be expected in a normal construction job. For example, the steel decking was used in an "as received" condition from the manufacturer except care was taken to insure that the reinforcement was free of grease and oil.

Steel decking and supplementary steel The nominal 20-gage steel decking used in Slabs 1, 2, and 3 was manufactured from sheets of steel conforming to American Society for Testing and Materials specification designation ASTM A611-70 (formerly ASTM A245-64) having a minimum yield point of 33,000 psi. The surface coating consisted of an iron phosphate treatment applied prior to forming. The configuration of this 20-gage steel decking for a one-foot wide typical section is shown in Figure 11.

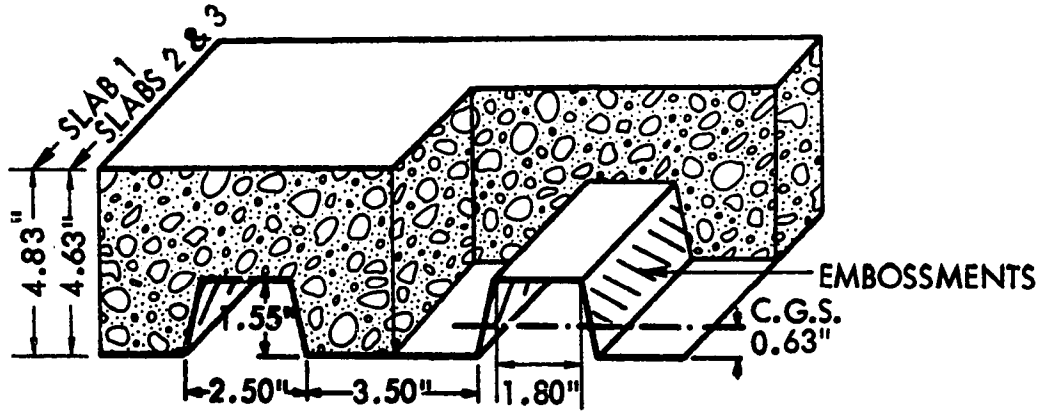

Figure 11. Typical view of steel decking utilized in Slabs 1, 2, and 3

The nominal 24-gage steel decking used in Slab 4 was manufactured from sheets of steel conforming to ASTM A446-71 specification for grade E steel having a minimum yield strength (0.5 percent offset method) of 80,000 psi. The deck units were galvanized under the 1.25 oz. per square foot coating class conforming to ASTM A525-71. The decking had transverse deformed no. D-4 wires (commonly called T-wires) spaced on three-inch centers attached by spot welds to the top corrugations. The configuration of the 24-gage steel decking for a one-foot wide typical section is shown in Figure 12.

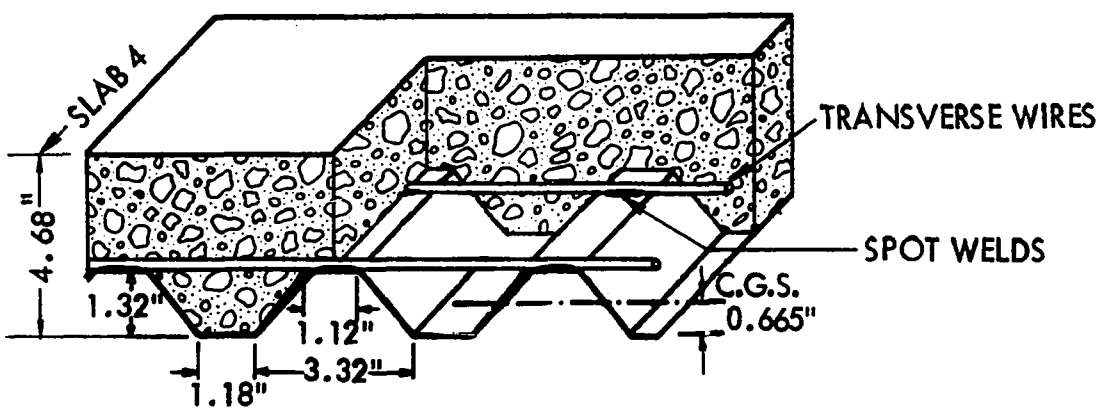

Figure 12. Typical view of steel decking utilized in Slab 4

The three-inch-deep steel decking utilized in Slab 5 was manufactured from sheets of nominal 20-gage steel conforming to ASTM A611-70 specification having a minimum yield point of 33,000 psi. The steel had a wiped coating of zinc conforming to ASTM A525-71 and to Federal Specification QQ-S-775d Type 1, class e. The configuration of this decking for a typical repeating section is shown in Figure 13.

Tensile tests were run on selected coupons cut from the steel decking, welded wire fabric, and T-wires to determine the modulus of elasticity, yield strength, and tensile strength. The tensile tests for the steel

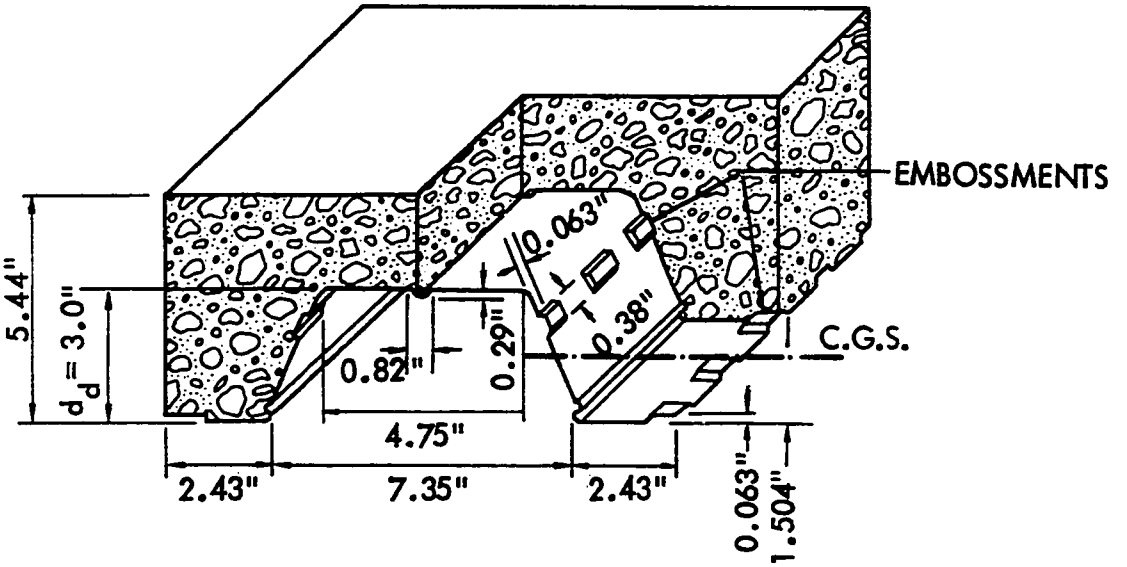

Figure 13. Typical view of steel decking used in Slab 5

decking conform to ASTM designation A370-71b. The tensile tests for the welded wire fabric and the deformed T-wires conform to ASTM A82-70 and A496-70, respectively. The typical properties and average results of at least three such tensile tests for the steel decking, the various gage sizes of WWF, and the deformed T-wires are contained in Table 2.

The steel deck moment of inertias for positive bending and for negative bending were calculated by utilizing a computer program based on procedures outlined in the American Iron and Steel Institute's design specification entitled "Specification for the Design of Cold-Formed Steel Structural Members" (5).

Two of the tensile specimens for the steel decking were instrumented with strain gages in the longitudinal and transverse directions as a means of determining Poisson's Ratio and a check on the stress-strain relationship. The average Poisson's Ratio is shown in Table 2. Typical stress vs. strain curves for the steel deckings, welded wire fabrics, and T-wires are shown in Figure 14.

Table 2. Material properties of steel decking, welded wire fabric, and deformed wire

Property	20-gage Type I Decking	24-gage Type G Decking	20-gage Type O Decking
Steel thickness or diameter (inches), t_d or t_w	0.0369	0.0252	0.0347
Area of steel, A_s, A_{s_1}, or A_{s_2} ($in.^2/ft$)	0.625	0.376	0.575
Deck moment of inertia, I_{sf}($in.^4/ft$)	0.267	0.0998	0.875
Deck moment of inertia, I_{sn}($in.^4/ft$)	0.227	0.0854	0.683
Deck moment of inertia, I_{sp}($in.^4/ft$)	0.240	0.0854	0.842
Modulus of elasticity, E_s (ksi)	29,400	30,500	31,000
Yield point or strength, F_y (ksi)	42.2	101.6(.5%)	49.4
Ultimate strength, F_u (ksi)	59.6	103.8	56.0
Rupture Strength, F_r (ksi)	50.0	92.7	48.3
Percent elongation (8 in. length)	19.5	0.6	21.0
Percent elongation (2 in. length)	35.3	2.5	32.0
Poisson's Ratio	0.282	0.217	0.278

6-gage WWF wire	No. D-4 Deformed wire	4-gage WWF wire	0-gage WWF wire	10-gage WWF wire
0.191	0.212 (Avg. Dia.)	0.222	0.304	0.134
0.057	0.1504	.039	0.145	0.0282
–	–	–	–	–
–	–	–	–	–
–	–	–	–	–
27,800	35,200	27,900	27,800	26,500
79.0(.5%)	92.1(.5%)	84.6(.5%)	82.6(.5%)	119.4(.5%)
84.5	105.4	95.8	88.2	122.0
53.0	77.3	76.6	65.3	93.5
–	3.7	–	–	–
5.5	–	5.8	7.0	5.4
–	–	–	–	–

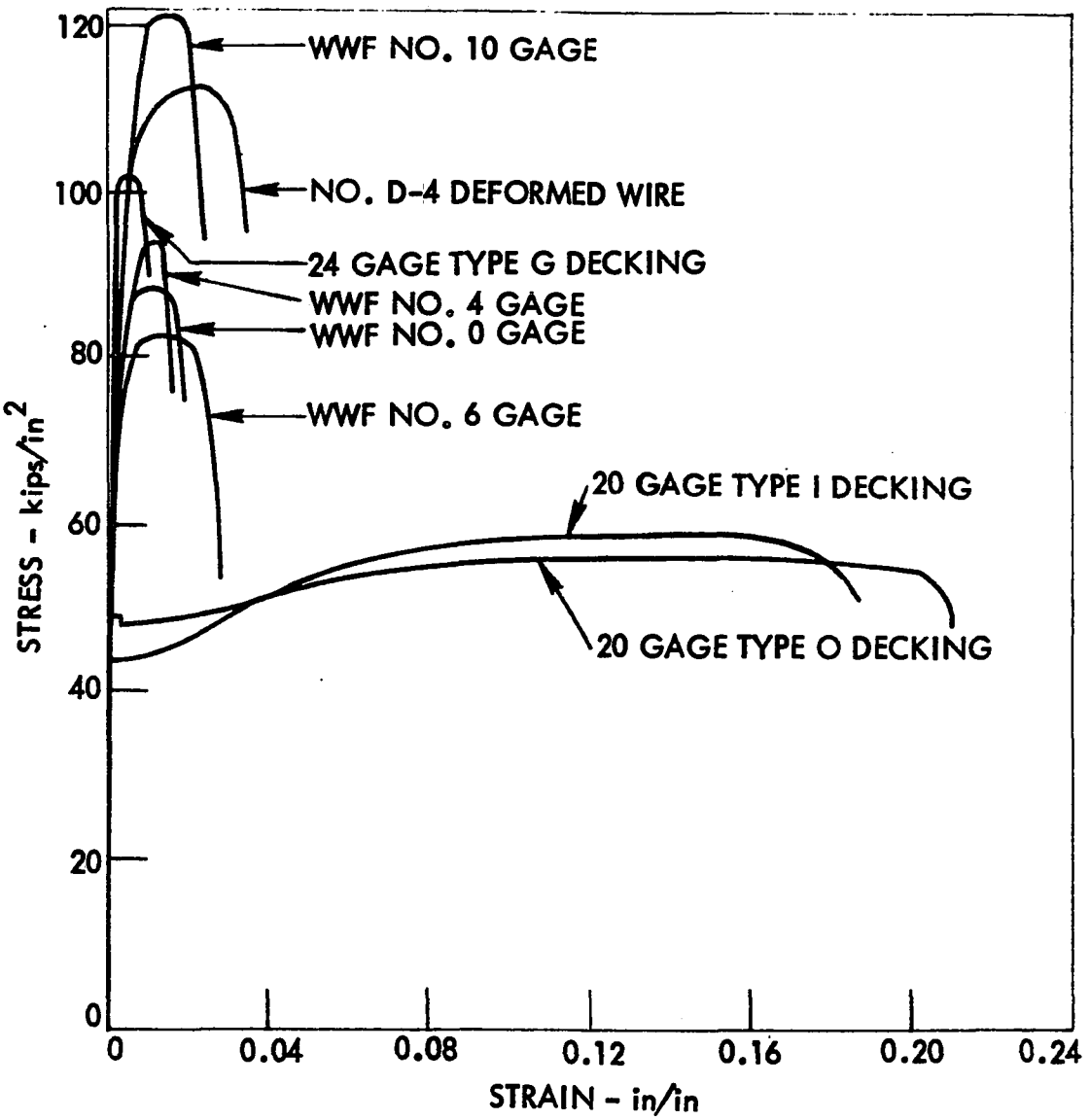

Figure 14. Typical stress vs. strain curves for tensile tests of coupons for the steel decking, welded wire fabric, and deformed wire

Concrete The concrete used in this investigation was purchased from a local ready-mix plant. The concrete was ordered to meet the following specifications:

1. minimum of 3,000 psi ultimate compressive strength in seven days,
2. 3/4-inch maximum size crushed rock aggregate,
3. 2½- to 3½-inch slump, and
4. no reducing agents or admixtures.

The concrete mix consisted of approximately 1466 lb /cu. yd. of fine aggregate, 1868 lb /cu. yd. of coarse aggregate, and 470 lb /cu. yd. of cement. The ultimate compressive strength, f'_c, was determined from an average of 6 X 12-inch control cylinders tested in accordance with ASTM C39-71. Testing of the cylinders occurred within one day of testing of slab specimens. Modulus of rupture and split cyclinder strengths were determined by ASTM C78-64 and ASTM C496-71 standards, respectively. The actual resulting measured values of the concrete properties for each pour and for each set of specimens within a pour are contained in Table 3.

Stress-strain properties of the concrete used in the slab tests were determined by placing strain gages axially on the surface of four of the 6 X 12-inch cylinders. A Poisson's Ratio of 0.17 for this concrete mix was determined by placing strain gages transverse to the vertical ones on two of the same four cylinder tests. The experimental stress-strain results gave a value of the modulus of elasticity of concrete quite close to that as computed by the method in the ACI Code (2). Thus, the modulus of elasticity used in this investigation was computed from the ACI Code's recommended method.

Fabrication, casting, curing, and shore removal of slab specimens

Fabrication Fabrication, along with subsequent casting and curing of the full-scale test slabs, was accomplished in place directly on the slab reactions. Fabrication of each of the slab specimens was accomplished in the following steps:

1. construction of formwork directly on the frame supports,
2. construction of shoring,
3. attachment of strain gages to the steel decking,

Table 3. Summary of concrete properties

Date of Casting	Concrete Pour Number	Specimens Formed From Casting	Average Compressive Strength f_c, psi
10/4/69	26	transverse slab elements Nos. 1 and 2	4300(5)
11/30/70	28	Slab 1	4157(7)
5/21/71	29a	Slab 2	3538(12)
5/21/71	29b	longitudinal slab elements Nos. 1 and 2	3931(2)
5/21/71	29b	longitudinal slab elements Nos. 3-6	4036(3)
7/16/71	30	Slab 3	3951(10)
9/30/71	31	transverse slab elements Nos. 3-7	3479(2)
10/14/71	32a	Slab 4	3835(10)
10/14/71	32b	longitudinal slab elements No. 7	3947(2)
10/14/71	32b	longitudinal slab elements No. 8	4117(2)
10/14/71	32c	transverse slab elements Nos. 8-10	4142(2)
2/15/72	33	longitudinal slab elements Nos. 9-18	4451(3), 4453(3) 4622(3), 4542(3)
2/28/72	34a	Slab 5	4300(8)
2/28/72	34b	longitudinal slab elements Nos. 19-20	4419(4)
4/5/72	35	longitudinal slab elements Nos. 21-30	3631(3), 3701(3) 3924(3)
4/10/72	36	longitudinal slab elements Nos. 31-39	3590(3), 3500(4) 3530(4)
8/4/72	37	transverse slab elements Nos. 11 and 12	3717(6)

Average Slump, inches	Age of f_c', days	Modulus of Rupture, f_r, psi	Age of Modulus of Rupture, days	Split Cylinder Tensile Modulus, psi	Age of Split Cylinder Test, Days
2 3/4(3)	33	466(4)	33	529(6)	33
2 1/2(5)	15	485(3)	21	456(5)	22
5 1/2(3)	17	470(2)	17	482(5)	27
5 1/2(3)	21	–	–	–	–
5 1/2(3)	25	–	–	–	–
3 (3)	17	–	–	422(4)	17
3 1/4(4)	18	455(4)	19	451(3)	19
3 1/4(4)	16	521(4)	16	454(4)	16
3 1/4(4)	19	–	–	–	–
3 1/4(4)	22	–	–	–	–
3 1/4(4)	21	–	–	501(2)	21
2 (3)	14, 15 17, 18	–	–	–	–
2 (3)	17	554(2)	17	504(4)	17
2 (3)	18	–	–	–	–
3 1/4(2)	14, 15 16	–	–	–	–
3 1/2(3)	14, 15 16	–	–	–	–
2 (7)	21	483(9)	21	438(5)	21

4. placement of the steel decking on the supports,
5. placement of the welded wire fabric (Slabs 1, 2, and 5 only),
6. installation of deflection dials direction underneath the steel decking,
7. placement of lifting anchors,
8. attachment of wooden dowels to steel forms to provide holes for later attachment of end-slip measuring dials (except Slab 1), and
9. placement of the concrete.

The slab specimens were made with the aid of prefabricated, adjustable steel forms supplied by the Economy Form Company of Des Moines, Iowa. Prior to placement of the concrete, these forms were coated with a non-staining, paraffin form oil to insure easier stripping. Figure 15 shows an overall view of the assembled side forms with the steel decking in place prior to placement of the welded wire fabric (Slabs 1, 2, and 5) and of the

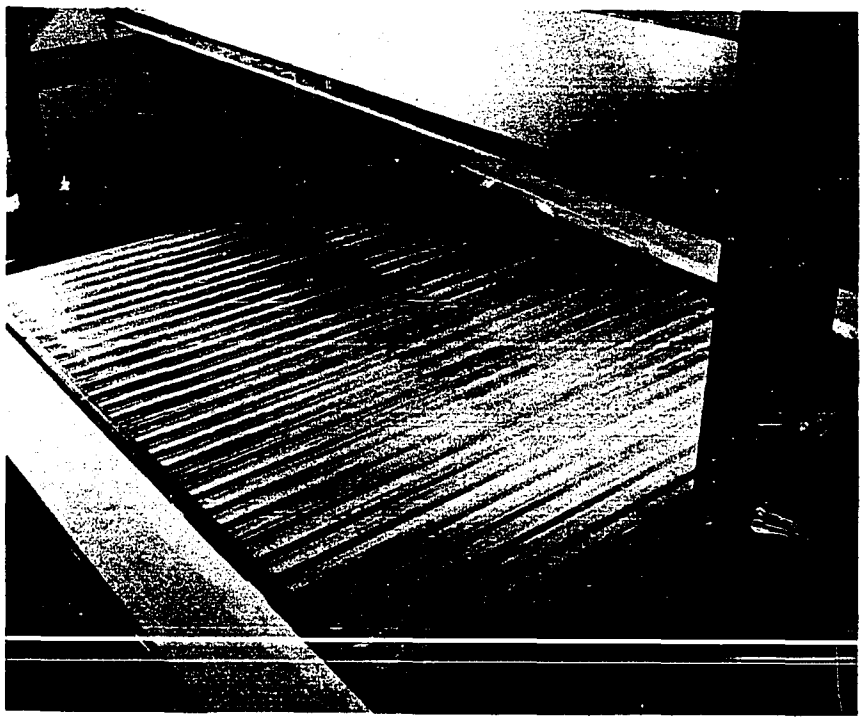

Figure 15. Overall view prior to placement of the concrete

concrete. The view in Figure 15 is from the northeast corner looking towards the southwest corner. Included in this figure are wooden walkways on the east and west sides of the slab. These walkways along with three additional walkways, which span between those shown in Figure 15, were constructed to aid in placement of the concrete and also to provide a walkway during testing.

A more detailed view of how the steel forms were supported is shown in Figure 16. The steel forms were bolted through an approximately one-inch-high wooden spacer to a ½-inch-thick steel plate which in turn was bolted over a nominal 4 X 4-inch piece of timber to the steel wide-flange support beams. The pin, roller, and ball-bearing-ball caster reactions were placed on or attached to the ½-inch steel plate. An inside view

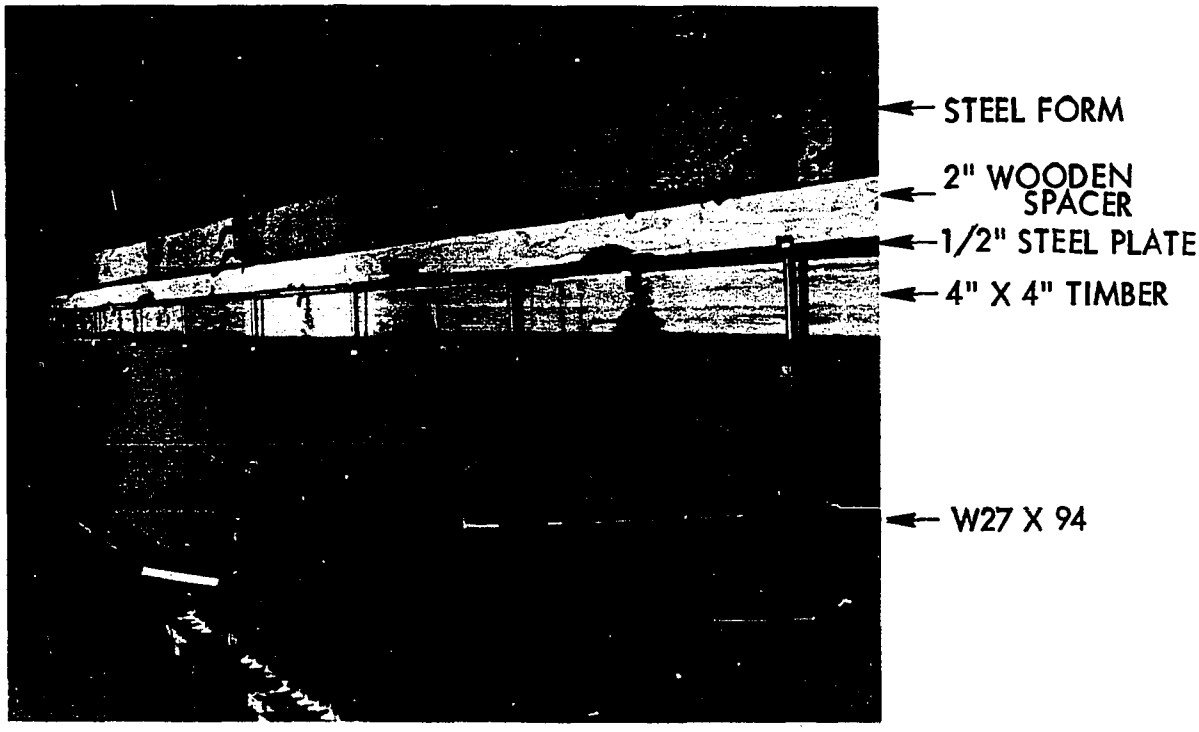

Figure 16. East support beam showing form fabrication for slabs

of the pinned and ball-bearing-ball caster supports and of the steel forms prior to placement of the steel decking is shown in Figure 17. In Figure 17, the pinned reactions consisting of steel plates welded to rollers are seen on the left side (north side of slab), and the ball-bearing-ball caster reactions are those on the right side (east side of slab). Short segments of steel plates were placed between the ball-caster reactions on the right and the steel decking for the purpose of transmitting the load down from the slab to the reaction at every one-foot interval (except Slab 4 where the interval was approximately 14 inches).

One line of shoring was provided for all slabs at midspan of the 12-foot length and placed transverse to the direction of the corrugations of the steel decking. This shoring was constructed from pieces of timber

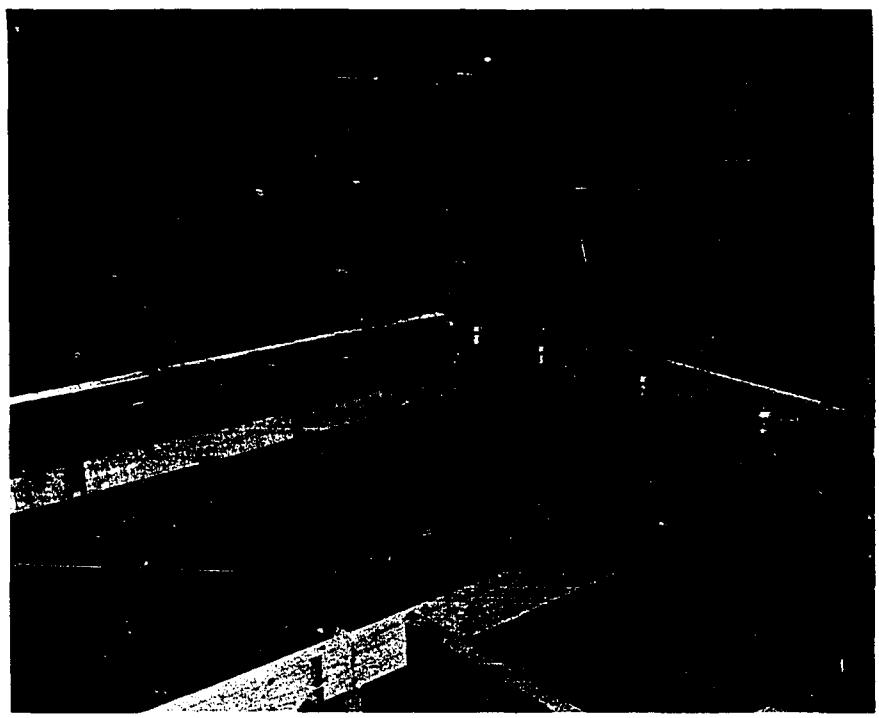

Figure 17. Northeast corner of slab support frame showing support reactions and form assembly prior to casting

4 X 4 inches in nominal size. Two pieces with a total length of approximately 16 feet were positioned horizontally with the top side at the predetermined level of the bottom of the steel decking. The horizontal members of the shoring for Slab 1 were supported at midspan of the 16-foot direction by a 4 X 4 timber post and at the ends by the reaction support steel wide-flange beams. Due to the deflection of the shoring which occurred for the first slab, the remainder of the slabs had the 4 X 4 timber posts at approximately the 1/6 points of the 16-foot span to provide for a minimal amount of shoring deflection due to the wet concrete.

Before placement of the steel decking, strain gages were attached to the bottom side of the steel decking. These gages were wired and connected to indicator units prior to placement of the concrete.

After placement of the shoring and strain gages, the steel decking was put in place by simply laying it in place so that it rested on the plates over the ball-bearing-ball caster supports along the east and west sides and along the shoring in the center. The width of each steel deck panel was 24 inches in the first three slabs, 32 inches in the fourth slab, and 36 inches in the fifth slab. The side-laps of the decking in Slab 5 were fastened by spot welds at 4-foot intervals in preformed holes as per manufacturer's recommendations. After placement of the deck panels in the first three slabs, a space of approximately 3/8 of an inch existed along the south edge where the panels did not completely cover the 16-foot direction. This space was filled with a plywood strip. Caulking compound was then used between the prefabricated forms and the decking to prevent the concrete from seeping through.

Once the decking had been placed, the welded wire fabric was placed.

The 6 X 6 X 6/6 fabric in Slab 1 and the 6 X 6 X 10/10 fabric in Slab 5 came in rolls six feet wide, and, therefore, it was necessary to lap this fabric to obtain the 12-feet X 16-foot slab dimensions. The lapping was accomplished by laying these pieces of the 6-foot wide sections 12 feet in length side by side to form the 16-foot length giving a one-foot side overlap between each section.

The fabric in Slabs 1 and 2 was placed directly on top of the steel decking. The fabric in Slab 5 was placed on 1-inch-high slab bolsters which in turn rested on the top fibers of the decking; however, the flexibility of the 6 X 6 X 10/10 fabric in Slab 5 did not lend itself to a uniform placement of the fabric at this level.

The 6 X 12 X 0/4 welded wire fabric in Slab 2 came in sheets 6'-6" X 11'-0", again necessitating lapping. The lapping was accomplished by placing one sheet in each quadrant of the slab and cutting (with a torch) until the lap consisted of one space each way. Thus, the laps were symmetrical about each centerline of Slabs 1, 2, and 5.

Special-purpose slab lifting anchors with a working tensile load capacity of 2,000 pounds each were purchased. These anchors were placed on top of the steel decking along the east and west edges in approximately the center part of each two-foot wide section and spaced about 10 inches inward from the east and west edges of the slab. Thus, a total of 16 slab anchors (8 on each side) were placed prior to pouring of the concrete.

One-half-inch-diameter wooden dowels about 4 inches long were attached to the steel forms at various locations along the east and west sides of the Slabs 2, 3, 4, and 5 prior to placement of the concrete. After curing of the concrete, these dowels were drilled out and one-half-inch-diameter

steel rods were inserted in the holes for attachment of mechanical dials.

Casting Placing of the concrete for the five slabs occurred on November 30, 1970, May 21, 1971, August 2, 1971, October 14, 1971, and February 28, 1972. The concrete was delivered by a conventional ready-mix truck and was conveyed to the slab forms by means of a bucket supported from an overhead crane. The concrete was ordered to be delivered with a minimum amount of added water. Upon delivery, slump tests meeting ASTM C143-71 specifications were taken to determine the amount of water needed to bring the slump up to the 2½- to 3½-inch specified range. In the case of Slab 2, the slump was already over the specified range so no added water was needed. Periodically, during casting, additional slump tests were taken as a check on the consistency and a small amount of water was added if needed, to insure workability of the mix during the remaining period of concrete placement. The average slump for each slab was given previously in Table 2.

Control specimens consisting of plain concrete cylinders and beams were prepared in accordance with ASTM C31-69 specifications. The cylinders were made using 6 X 12-inch waxed cardboard cylinder molds and cast at intervals during the concrete pouring of the slabs so as to obtain a representative average of the concrete strength. The plain concrete beams of dimensions 6 X 6 X 30 inches were cast in order to obtain the modulus of rupture. No modulus of rupture beams were made for Slab 3 due to lack of concrete.

Placing of the concrete in the slabs began at the south end and progressed across the slab to the north end. A concrete finisher, who is normally employed by a local building construction contractor, was engaged

to help handle the placing and finishing operations on all slabs except Slab 5. An internal vibrator normally employed in field operations and supplied by the contractor was used by the concrete finisher to obtain satisfactory compaction and placement of the concrete.

Just prior to placement of the concrete, weights were laid on top of the decking and welded wire fabric along the east and west reactions to help prevent movement of the decking and fabric on the supports and to prevent movement of reaction plates between the bearing supports and the decking. As pouring of the concrete progressed, these weights were removed. The total concrete placing time for each slab was approximately one hour and ten minutes.

After final screeding and after a short time lapse, the concrete finisher proceeded to trowel the final finish surface on the slabs. The surface was finished to a very smooth texture to aid in placing strain gages on the concrete surface. During final finishing the lifting anchors were located and the concrete removed over them sufficiently to allow later insertion of the screw lift hooks.

Curing and shore removal Six hours after placement of concrete, the slab, the test slab control cylinders, and modulus of rupture specimens were covered with wet burlap over which were placed sheets of plastic. Three days later the prefabricated steel forms were removed from the sides of the slabs along with the molds for the flexure beams and control cylinders. After the seven days of curing, the wet burlap and plastic were removed and all concrete was exposed to normal room conditions until tested.

Throughout the curing from the time the slabs were cast until the time of testing, the laboratory temperature and humidity were continuously

recorded on a hygro-thermograph. These recordings are summarized in Table 4.

Table 4. Average values of recorded temperature and humidity for slab tests

Slab No.	Wet Curing		Room Curing	
	Temperature (°F)	Humidity (%)	Temperature (°F)	Humidity (%)
1	71	43	74	32
2	85	65	75	40
3	80	68	74	62
4	75	76	75	67
5	–	–	71	26

Shore removal for Slabs 1 and 3 took place during the wet curing of the concrete after which time the concrete had obtained a maximum strength of 2500 psi. The approximate concrete cylinder strengths at the time of shore removal for each slab are summarized in Table 5.

Table 5. Summary of shore removal for full-scale slabs

Slab No.	Days after casting until shore removal	Approximate concrete strength at time of shore removal (psi)
1	5	2800
2	10	3519
3	5	2635
4	9	3307
5	7	3590

Description of Slab Element Specimens

Slab elements with deck corrugations transverse to their length

The flexural capacity of 12 slab elements constructed with transverse steel decking was obtained in order to ascertain the amount of two-way action which may be expected in the companion slabs. The transverse specimens consisted of two-foot wide slab strips, six feet in length as indicated in Figure 18.

The primary reinforcement for seven of these transverse specimens was the 1½-inch-deep steel decking corresponding to Slabs 1, 2, and 3; the primary reinforcement for three slab elements was the nominal 24-gage 1 5/16-inch-deep decking like that in Slab 4, and the primary reinforcement for two specimens was the nominal 20-gage 3-inch-deep steel decking like that in Slab 5. Of the seven elements containing the 20-gage 1½-inch-deep decking, two had 6 X 6 X 6/6 welded wire fabric placed directly on top of the decking, two had 6 X 12 X 0/4 wire fabric placed directly

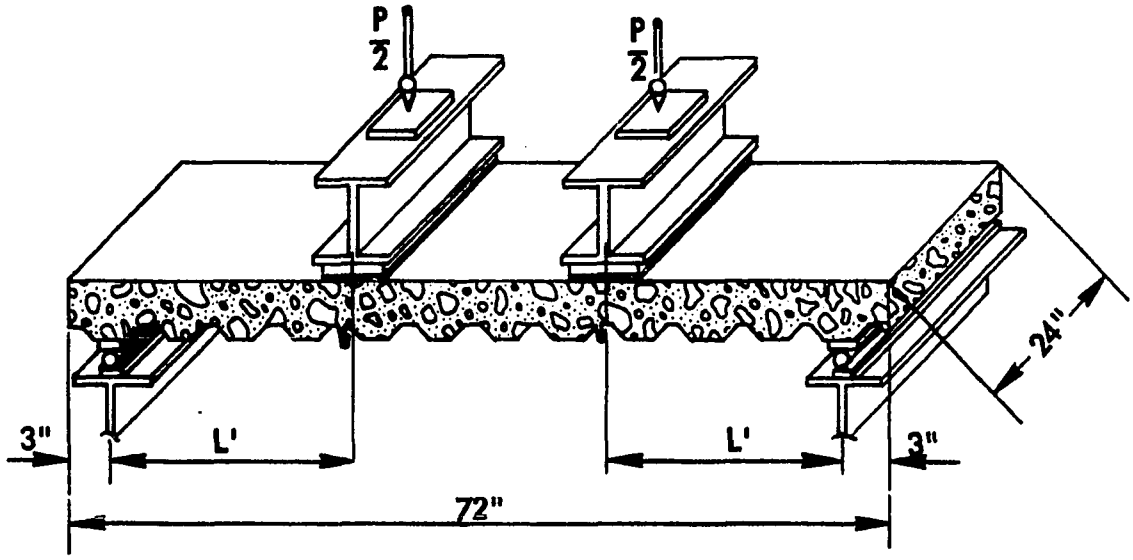

Figure 18. Typical test on slab element with transverse decking

on top of the decking oriented like in Slab 2 with the zero-gage wire transversing across the corrugations, and the remaining three of the seven contained no welded wire fabric.

The only additional reinforcement utilized in those transverse specimens containing the 24-gage steel decking is that of the deformed T-wires which were attached to the top of the decking. Since the deformed wire transverses the corrugations, the wire is in a position to help reinforce the slab element and to help distribute forces transverse to the corrugations. Like in Slab 5, the two transverse specimens containing the 20-gage 3-inch deep steel decking also contained 6 x 6 x 10/10 welded wire fabric. However, this fabric was located approximately 1½ inches from the top fiber of concrete.

Table 6 summarizes the basic characteristics of these transverse specimens. Included in Table 6 are the specimen depths, primary and supplementary reinforcing, the concrete pour number and the age of the specimen, the concrete compressive strength, modulus of rupture, and split cylinder strength for each concrete pour may be found by looking at Table 3 for each pour number. The typical steel stress vs. strain diagrams for each type of decking and supplementary reinforcing contained in the transverse specimens were shown in Figure 14.

Slab elements with deck corrugations parallel to their length

In addition to the many one-way slab element specimens tested prior to the full-scale slab testing program, 39 one-way elements were tested in conjunction with the two-way slab tests. These slab elements had the steel decking oriented in a direction parallel to the specimen length (longitudinal specimens). An indication of the typical longitudinal slab element

Table 6. Summary description of 6' X 2' slab elements with steel decking oriented transverse to specimen length (See Figure 18)

Transverse Specimen No.	Concrete Pour No.[a]	Specimen Reinforced Similar to Slab No.	Out-to-out Depth, Inches
1	26	3	5
2	26	3	5
3	31	2	4½
4	31	1	4½
5	31	2	4½
6	31	1	4½
7	31	3	4½
8	32c	4	4½
9	32c	4	4½
10	32c	4	4½
11	37	5	5½
12	37	5	5½

[a]Refer to Table 3 for concrete strengths.

[b]Material properties for steel reinforcing are given in Table 2.

[c]This gage thickness is not the same as that of the decking used in Slab 1.

[d]The 6 X 12 X 0/4 WWF was oriented with zero gage wire transverse to deck corrugations.

[e]The 6 X 6 X 10/10 WWF was located approximately one-inch from the top surface of the concrete.

Steel Deck Reinforcement[b]				
Nominal Gage Thickness	Nominal Depth of Decking, Inches	Typical Cross Section of Decking Shown in Figure	Supplementary Reinforcing[b]	Number of Days from Casting to Testing
22[c]	1 1/2	11[c]	none	33
16[c]	1 1/2	11[c]	none	33
20	1 1/2	11	6 x 12 x 0/4[d]	18
20	1 1/2	11	6 x 6 x 6/6	18
20	1 1/2	11	6 x 12 x 0/4[d]	19
20	1 1/2	11	6 x 6 x 6/6	19
20	1 1/2	11	none	19
24	1 5/16	12	No. 4 deformed wire	19
24	1 5/16	12	No. 4 deformed wire	21
24	1 5/16	12	No. 4 deformed wire	21
20	3	13	6 x 6 x 10/10[e]	21
20	3	13	6 x 6 x 10/10[e]	21

test is shown in Figure 19.

Six of the 39 longitudinal slab elements were constructed as a preliminary check on the determination of the effect of welded wire fabric resisting the shear-bond failure characteristics. These six were reinforced with nominal 20-gage steel decking like that used in Slabs 1, 2, and 3. Two of the six contained no welded wire fabric, two contained 6 X 6 X 6/6 fabric, and two contained 6 X 12 X 0/4 fabric. The welded wire fabric was placed directly on top of the decking and oriented to correspond with the full-size companion slabs containing the same reinforcement. The overall size of these six one-way slab elements was 6 ft by 2 ft by 4½ in.

Two longitudinal specimens were constructed with 24-gage decking as a

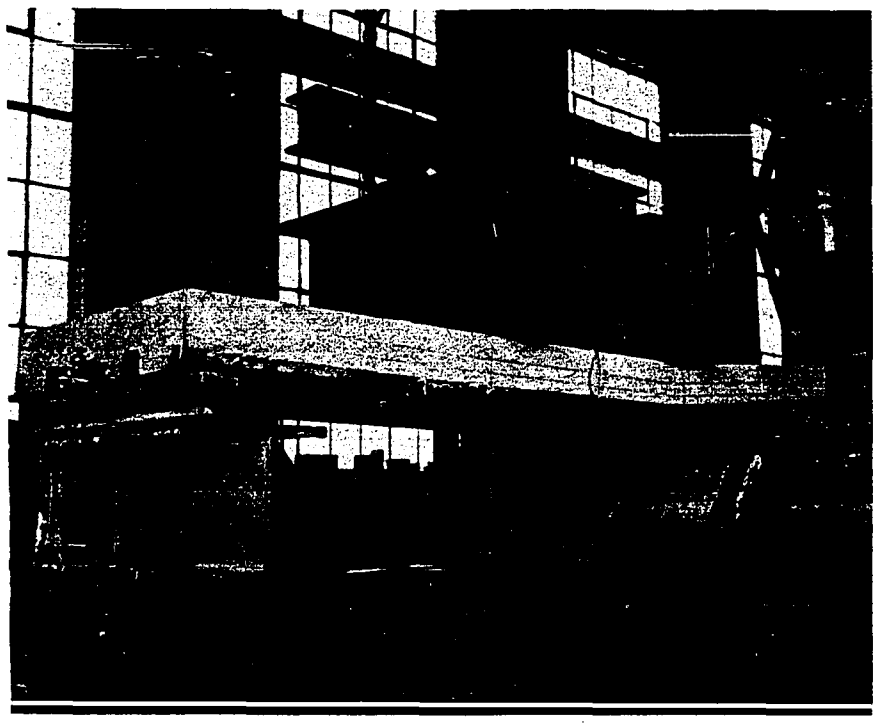

Figure 19. Typical test arrangement with steel deck corrugations parallel to specimen length

check on the one-way capacity of Slab 4. This decking contained deformed wires spot welded to the tops of the corrugations at 3-inch intervals. The overall size of these two specimens was 12 feet in length by 34 inches in width by 4½ inches in depth, and the loading was applied so as to conform with Slab 4.

Two other longitudinal slab elements were constructed as a check on the one-way capacity of an element of Slab 5. These two specimens were 12 feet in length, 36 inches in width, and 5½ inches in depth, and loaded with a line loading placed at the same distance from the reactions as that of the load points in Slab 5. Like Slab 5, these two specimens were reinforced with nominal 20-gage 3-inch deep decking and 6 X 6 X 10/10 welded wire fabric placed approximately 1½ inches from the top fiber of concrete.

The remaining 29 longitudinal slab elements were constructed to obtain one-way shear-bond regression coefficients for the 3-inch deep decking that was used in Slab 5. All of these specimens had nominal dimensions of 36 inches in width and 5½ inches in depth. Table 7 gives the number of slab elements constructed of each gage thickness for each length and shear span. No additional reinforcing other than the steel decking was used in these 29 slab elements. The material properties of the steel decking for each gage thickness for the 3-inch deep steel decking is given in Table 8.

A complete summary of all longitudinal one-way slab element tests is contained in Table 9. The specimen type given in Table 9 refers to the main purpose for which the longitudinal specimen was tested. For example, if the specimen was constructed as a check on the one-way capacity of an element of a particular slab, it is listed as a companion type specimen giving the particular slab by which the one-way specimen was identically

Table 7. Number of slab elements constructed with each gage thickness of deck for 29 specimens using 3-inch deep decking

Shear Span, L' inches	Total Length, L feet	Number of Slab Elements Tested			
		16 gage	18 gage	20 gage	22 gage
86	16	1[a]	1[a]	1[a]	1[a]
70	12	2[a]	2[a]	3[a]	0
48	12	0	0	3[a]	0
48	10	3	3	0	0
24	6	3	3	3	0
	Totals:	9	9	10	1

[a]Denotes that a central support (simulating shoring) was used. All other specimens were supported at ends only.

Table 8. Material properties for 3-inch steel decking used in 29 slab element tests

	Thickness of Steel Deck			
	16 gage	18 gage	20 gage	22 gage
Modulus of Elasticity, ksi x 10^3	31.2	30.6	31.0	27.5
Yield Point, ksi	42.9	42.1	49.4	43.6
Ultimate Strength, ksi	52.5	51.9	56.0	54.4
Rupture Strength, ksi	41.2	41.6	48.3	48.4
Percent Elongation, 2 in. gage length	28	29	21	44
Percent Elongation, 8 in. gage length	49	41	32	27
Thickness, in.	0.0595	0.0453	0.0347	0.029

Table 9. Summary description of slab elements with steel decking oriented parallel to specimen length (See Figure 19.)

Longitudinal Specimen No.	Specimen size, length x width x depth (ft x ft x in.)	Concrete Pour No.[a]	Number of Days from Casting to Testing
Purpose: Test effect of WWF			
1	6 x 2 x 4½	29b	21
2	6 x 2 x 4½	29b	21
3	6 x 2 x 4½	29b	24
4	6 x 2 x 4½	29b	25
5	6 x 2 x 4½	29b	24
6	6 x 2 x 4½	29b	25
Purpose: Companion to Slab 4			
7-8	12 x 2 5/6 x 4½	32b	19-22
Purpose: 3-inch deck, shear-bond			
9-12	12 x 3 x 5½	33	14-15
13-15	6 x 3 x 5½	33	15-17
16-18	12 x 3 x 5½	33	17-18
Purpose: Companion to Slab 5			
19-20	12 x 3 x 5½	34b	17
Purpose: 3-inch deck, shear-bond			
21	16 x 3 x 5½	35	14
22	12 x 3 x 5½	35	14
23-24	12 x 3 x 5½	35	15
25-27	10 x 3 x 5½	35	15
28-30	6 x 3 x 5½	35	16
31-33	6 x 3 x 5½	36	14-15
34-36	10 x 3 x 5½	36	15
37-38	12 x 3 x 5½	36	15-16
39	16 x 3 x 5½	36	16

[a] Refer to Table 3 for concrete strengths.

[b] The number 4-gage wire was placed parallel to the corrugations.

Steel Deck Reinforcement				Material Properties of Steel Reinforcement Given in Table No.
Nominal Gage Thickness	Nominal Depth of Decking, in.	Typical cross Section shown in Figure	Supplementary Reinforcing	
Purpose: Test effect of WWF				
20	1 1/2	11	6 x 12 x 0/4 WWF[b]	2
20	1 1/2	11	none	2
20	1 1/2	11	6 x 6 x 6/6 WWF	2
20	1 1/2	11	none	2
20	1 1/2	11	6 x 12 x 0/4 WWF[b]	2
20	1 1/2	11	6 x 6 x 6/6 WWF	2
Purpose: Companion to Slab 4				
24	1 5/16	12	no. 4 deformed wire trans. to corrugations	2
Purpose: 3-inch deck, shear-bond				
20	3	13	none	8
20	3	13	none	8
20	3	13	none	8
Purpose: Companion to Slab 5				
20	3	13	6 x 6 x 10/10 WWF	2
Purpose: 3 inch-deck, shear-bond				
22	3	13	none	8
16	3	13	none	8
16	3	13	none	8
16	3	13	none	8
16	3	13	none	8
18	3	13	none	8
18	3	13	none	8
18	3	13	none	8
18	3	13	none	8

constructed. Other items included in Table 8 include specimen size, primary and supplementary reinforcing, concrete pour number, and the age of the specimen at the time of testing. The concrete compressive strength, modulus of rupture, and split cylinder strength for each concrete pour may be found by looking at Table 3. The material properties of the steel reinforcing is given either in Table 8 or in Table 2, as indicated in Table 9. The typical stress vs. strain diagrams for each type of steel decking and supplementary reinforcing used for each longitudinal slab element are shown in Figure 14.

Test Equipment For Slab Specimens

Test frame and loading apparatus

All five two-way full-scale slab tests were conducted utilizing a self-contained loading frame comprising various structural steel wide-flange shapes. Figure 20 indicates the framework used. The slab specimens rested on pin, roller, and ball-bearing-ball caster reactions which in turn rested on the W27 X 94 and W24 X 68 support beams (see Figure 20). During testing, strains and deflections were taken on these beams. The resulting stiffness of the support beams and frame was considered as infinite in comparison to that of the slab specimens, and thus, the small deflections of the support beams were neglected in the analysis of the slab specimens.

The pin, roller, and ball-bearing-ball caster reactions rested on a ½-inch steel plate which in turn was bolted over a nominal 4 X 4-inch piece of timber to the W27 X 94 or W24 X 68 support beams. The placement of these reactions was described earlier during the casting phase. The pin supports were located along the north edge, the roller supports along the

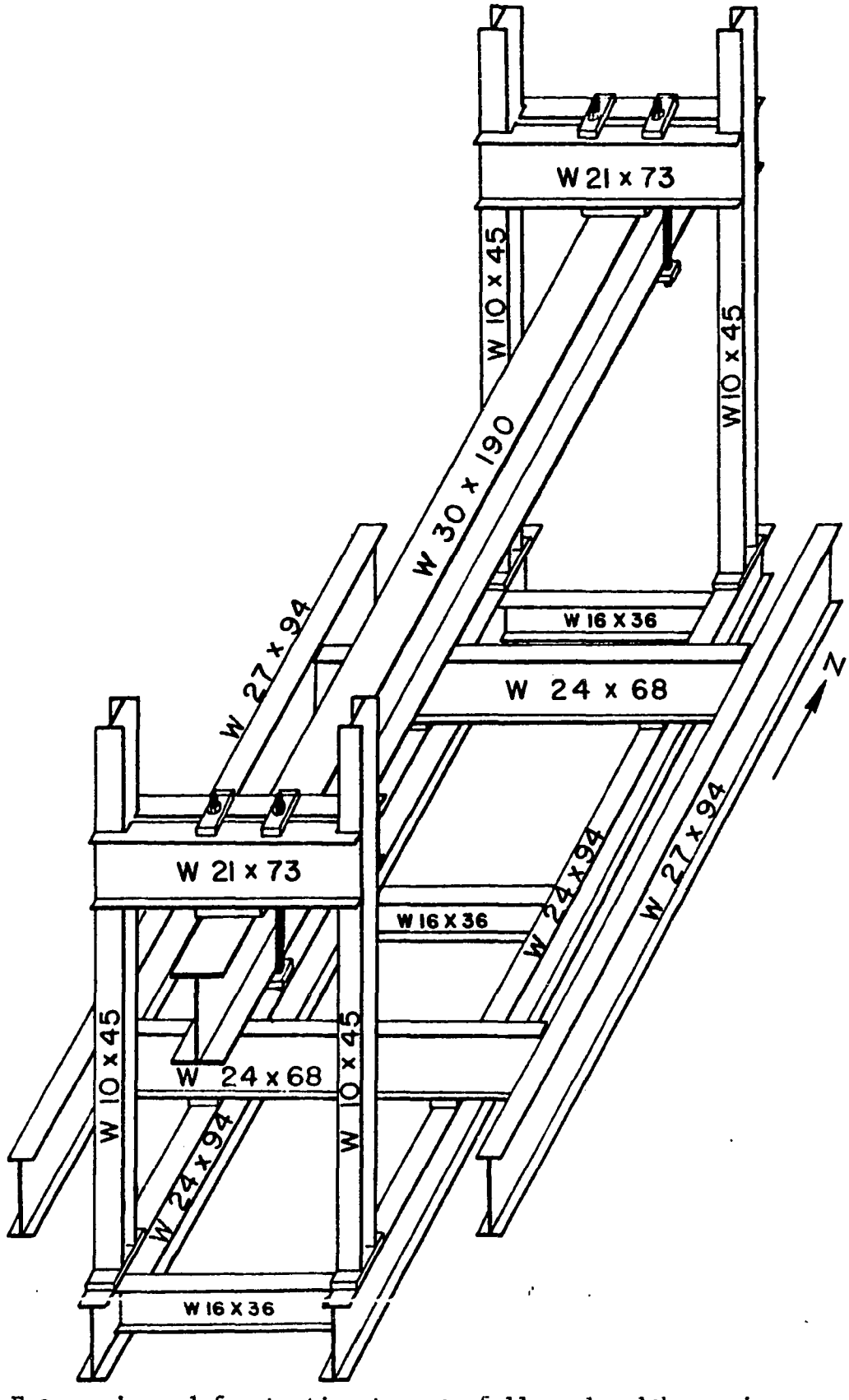

Figure 20. Framework used for testing two-way full-scale slab specimens

south edge, and the ball-bearing-ball caster supports along the east and west edges. The locations of these supports were indicated in Figure 3. Figure 21 shows the five types of reactions used. From left to right they are as follows:

1. roller transducer, used along most of south reaction to measure vertical forces at one-foot intervals;
2. ball-bearing-ball caster transducer, used along most of west reaction to measure vertical forces;
3. ball-bearing-ball caster attached to steel plate resting on nominal 4 X 4 timber, used along remaining west reaction and all of east reaction;
4. pin reactions one-foot in length (two-inch-diamter steel rod with a steel plate welded on top), used along all of north reaction; and

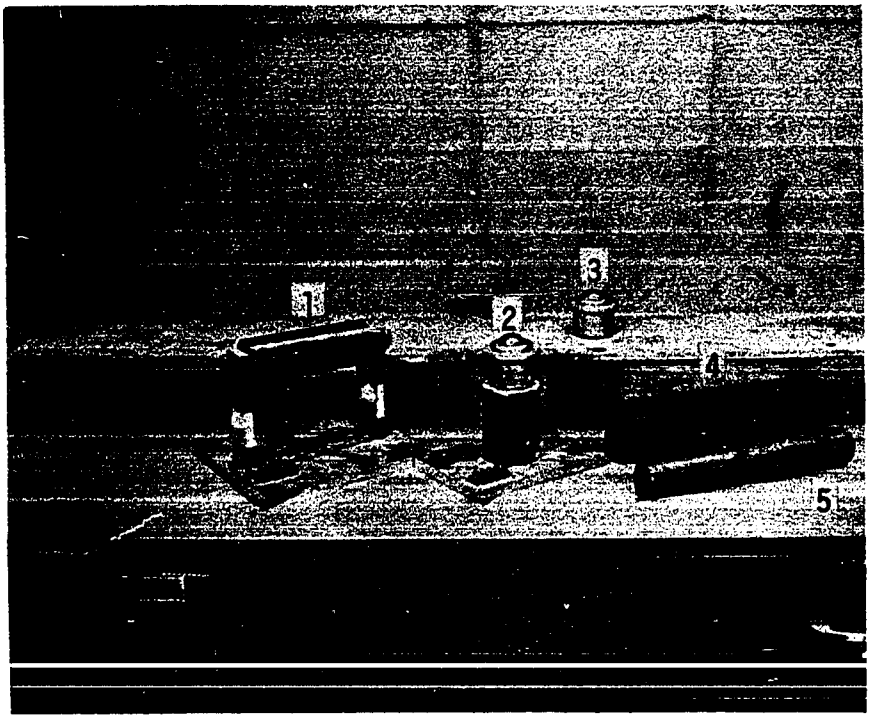

Figure 21. View showing slab reactions

5. roller reactions one-foot in length (two-inch-diameter steel rod), used along remaining south reaction.

Loading of the test slabs was accomplished by two Enerpac 50-ton hand-operated hydraulic cylinders (model RC-5013T). These cylinders are shown in Figure 22 attached to the W30 X 190 beam by a roller assembly to facilitate movement. The clamps were used to prevent movement during testing. The load from each cylinder was divided into two concentrated loads by a W18 X 55 spreader beam. Elastomeric bridge bearing pads are visible in Figure 22 between each hydraulic cylinder and the top of the spreader beam. These pads had dimensions of 9 X 14 X 1 3/4 inches and were of medium expansion quality. Similar pads of dimensions 9 X 9 X 2 7/8 inches were located at the four load points between the bottom of spreader beams and top surface of slab.

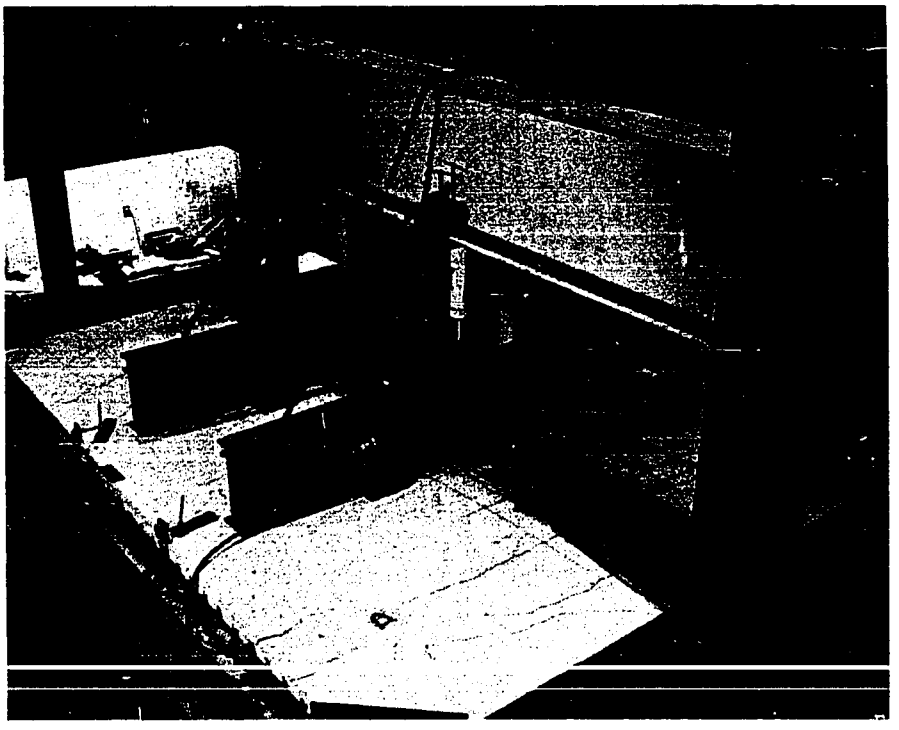

Figure 22. Overall view of test arrangement

Instrumentation

The items of instrumentation used for the five two-way slab tests consisted of the following:

1. electrical strain gage rosettes and single strain gages placed on the top surface of the concrete,
2. electrical strain gage rosettes and single strain gages placed on the steel decking corresponding in location to those on the concrete,
3. vertical load transducers (roller and ball-bearing-ball caster types) to determine the reaction distributions,
4. corner tie-down transducers on Slab 1 only to measure uplift force at the corners of Slab 1,
5. static strain indicators and switching units for monitoring strain gage and transducer readings,
6. mechanical deflection gages, and a theodolite for determining deflections,
7. pressure gages for reading calibrated jack loads,
8. deflectometer readings and/or mechanical deflection indicators to measure end slip along east and west edge of each slab,
9. single strain gages at midspan of four of the support beams of test frame,
10. mechanical deflection dials at midspan of two of the reaction support beams and at one or more corners of the reaction support beam frame,
11. an illuminated six-power magnified comparator with graduated scale for measuring crack widths, and

12. a hygro-thermograph recorder to record temperature and humidity continuously throughout wet and dry curing of slab specimens.

Table 10 indicates a summary of the number of deflection and electrical strain gage measurements made for each slab test. The locations of the strain gages, vertical deflection gages, end slip gages, and deflectometers are given in Figures 23, 24, 25, 26, and 27 for Slabs 1, 2, 3, 4, and 5, respectively. As can be seen, the more highly instrumented portion of the slabs was the southwest quadrant.

The electrical strain gage measurements for all slab tests were made by use of various models of SR-4 portable strain indicators each connected to a switching unit. Various types of strain gages were employed in the slab tests. These consisted of foil gages of ½-inch gage length for the steel and transducer applications and paper-backed wire gages of 0.8-inch gage length for the concrete surface applications. Those strain gages applied to the top surface of the concrete were affixed to a previously-made epoxy patch approximately two inches square. This type of concrete strain application is described in Reference 15. Those strain gages used for transducer and steel deck applications were applied with epoxy and coated with commercial gage coatings. Those strain gages embedded internally in Slab 5 were also coated in wax to prevent damage and moisture leakage. All rosette strain gages indicated in Table 10 were rectangular rosettes except for five locations along the centerline of Slab 2 where advantage was taken of symmetry.

The roller and ball-bearing-ball caster transducers each had their main load carrying members fabricated from structural aluminum to achieve the desired sensitivity for the expected load. Each ball-bearing

Table 10. Summary of number of deflection and strain gage measurements made for each slab test

Slab No.	No. of Deflection Gages Including 4 corners	No. of Deflecto-meters	No. of End Slip Gages	No. of Strain Gages on Test Frame	No. of Strain Gage Rosettes		No. of Single Strain Gages		No. of Deflection Gages Under Test Frame
					Conc.	Steel	Conc.	Steel	
1	39[a]	4	0	4	26	28	0	0	4
2	32	4	8	3	13	16	1	1	4
3	32	0	12	0	14	14	0	1	3
4	32	0	12	4	14	14	0	1	4
5	30	0	12	4	14	20	1	1 + 3[b]	3

[a]No corner uplift displacement gages were utilized on Slab 1 since corner tie-downs were used.

[b]Three strain gages were placed on steel rods embedded in concrete for Slab 5.

Figure 23. Plan view of Slab 1 indicating locations of strain gages, reaction transducers, vertical deflection dials, end slip dials, and deflectometers

Scale

1" = 3' - 0"

Notes

(1) All strain gages on steel decking were mounted on bottom corrugation except as indicated by a T signifying that gage was mounted on the top corrugation

(2) All deflectometers measured end slip at the bottom corrugations of steel decking

Key

L.P. load points

+ strain gage rosettes on concrete and steel deck surfaces

□ vertical deflection dials

○ ball-bearing-ball caster reactions

● ball-bearing-ball caster transducers

▭ roller reactions

▬ pin reactions

▬ roller transducers

⊠ deflectometers

⊗ vertical deflection dials under support reaction beams

⊖ single strain gage on support beams

* strain gage rosette only on steel decking

⊞ strain gage rosettes on concrete and steel deck surfaces and deflection dial

○ single strain gage on test frame

▭ corner tie-down transducer assemblies

▭ corner tie-down assemblies

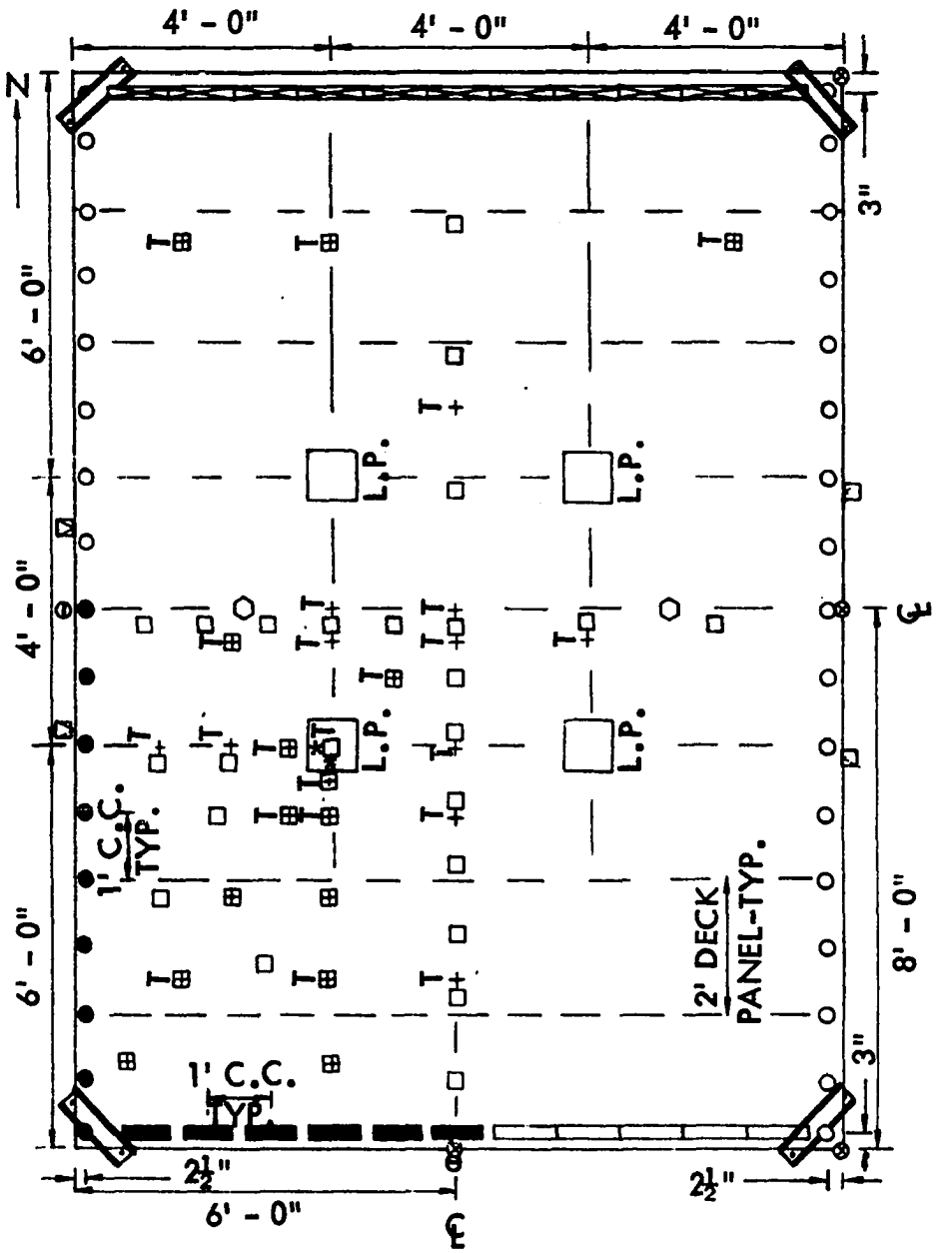
4' - 0"
4' - 0"
4' - 0"
N
3"
6' - 0"
4' - 0"
6' - 0"
L.P.
L.P.
L.P.
L.P.
1' C.C. TYP.
2' DECK PANEL-TYP.
8' - 0"
1' C.C. TYP.
3"
2½"
2½"
6' - 0"
℄
℄

Figure 24. Plan view of Slab 2 indicating locations of strain gages, reaction transducers, vertical deflection dials, end slip dials, and deflectometers

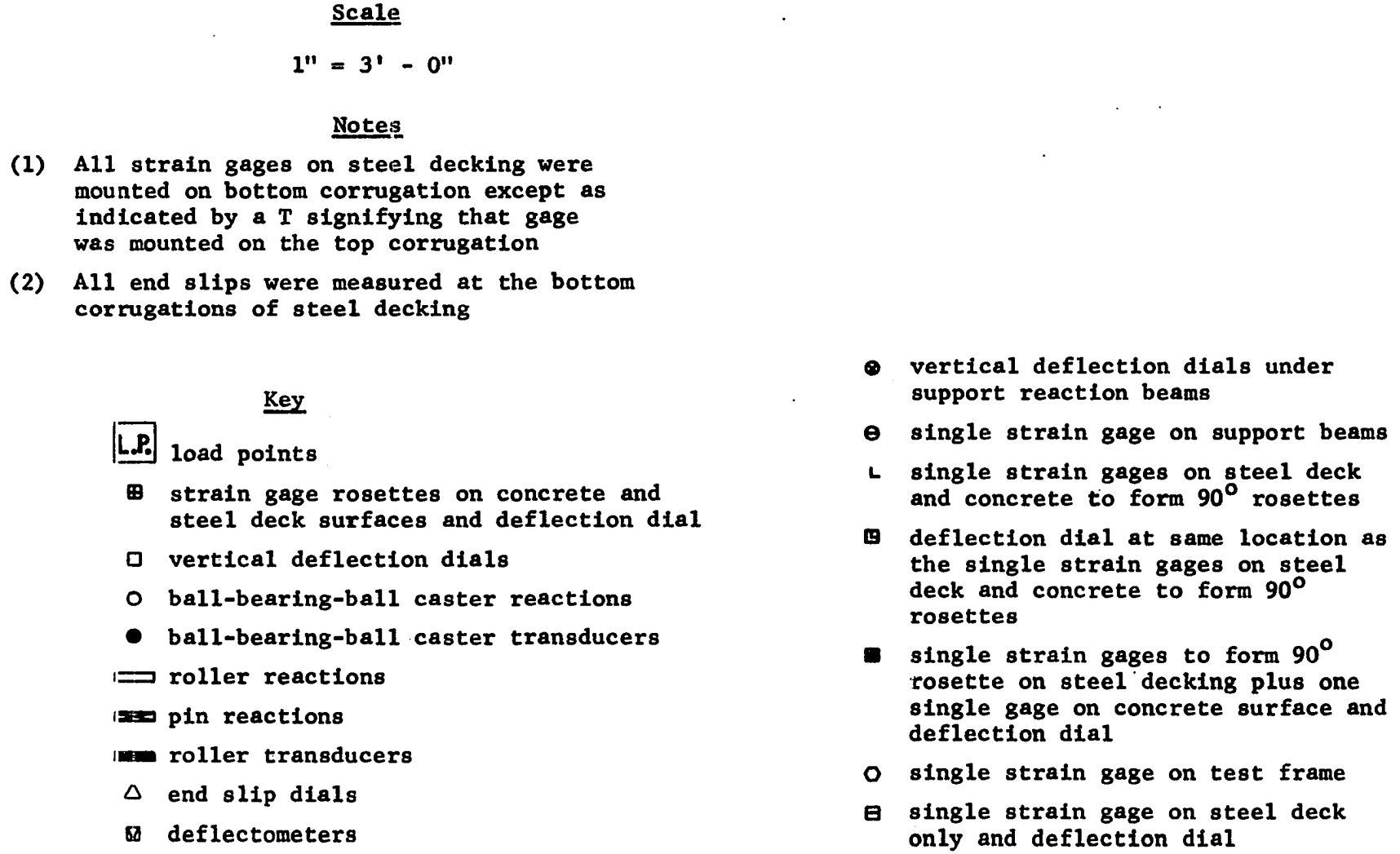

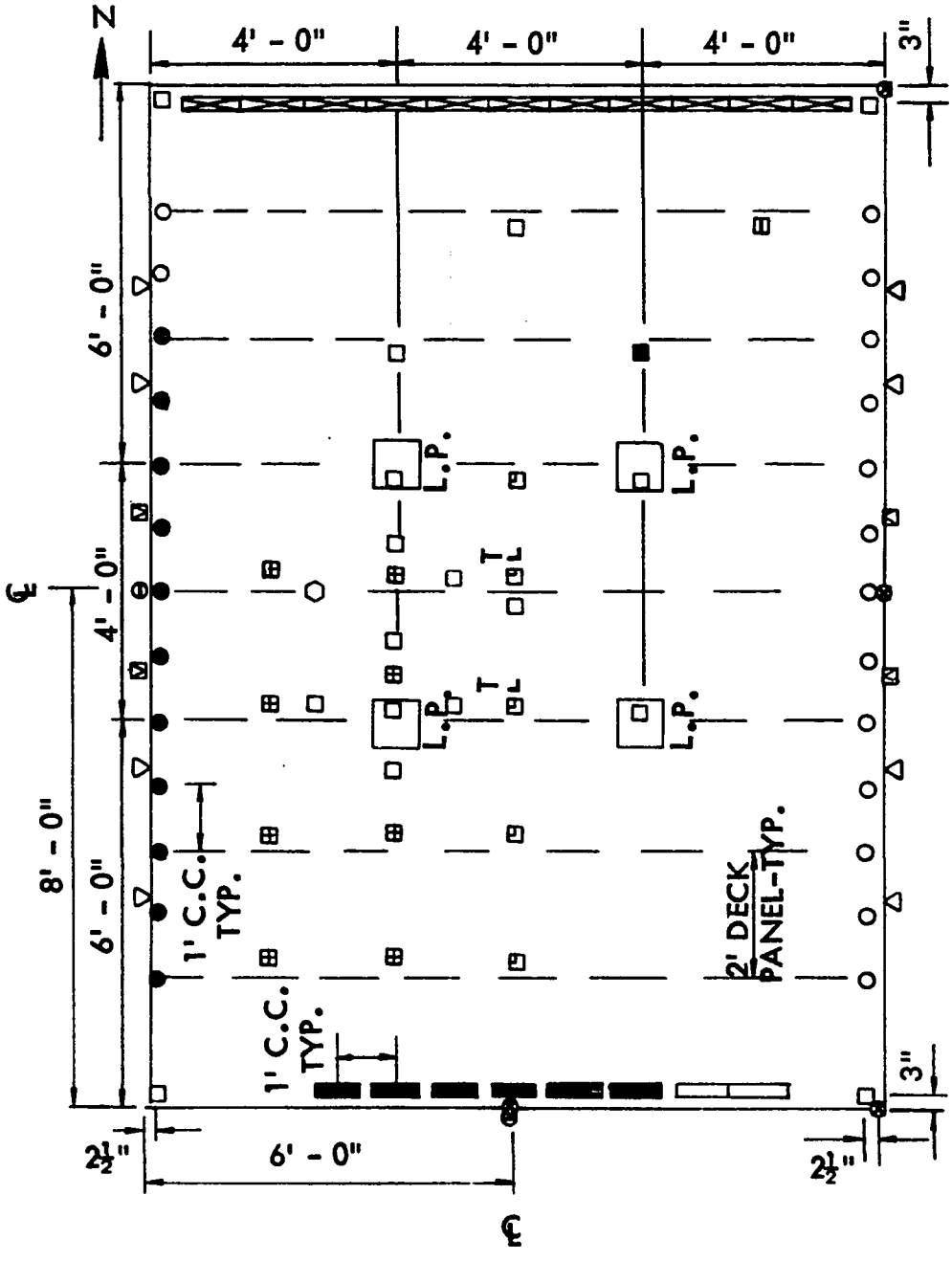
N
4' - 0"
4' - 0"
4' - 0"
3"
6' - 0"
4' - 0"
8' - 0"
6' - 0"
L.P.
L.P.
L.P.
L.P.
T
L
T
L
1' C.C. TYP.
1' C.C. TYP.
2' DECK PANEL-TYP.
3"
2½"
6' - 0"
2½"
℄
℄

Figure 25. Plan view of Slab 3 indicating locations of strain gages, reaction transducers, vertical deflection dials, and end slip dials

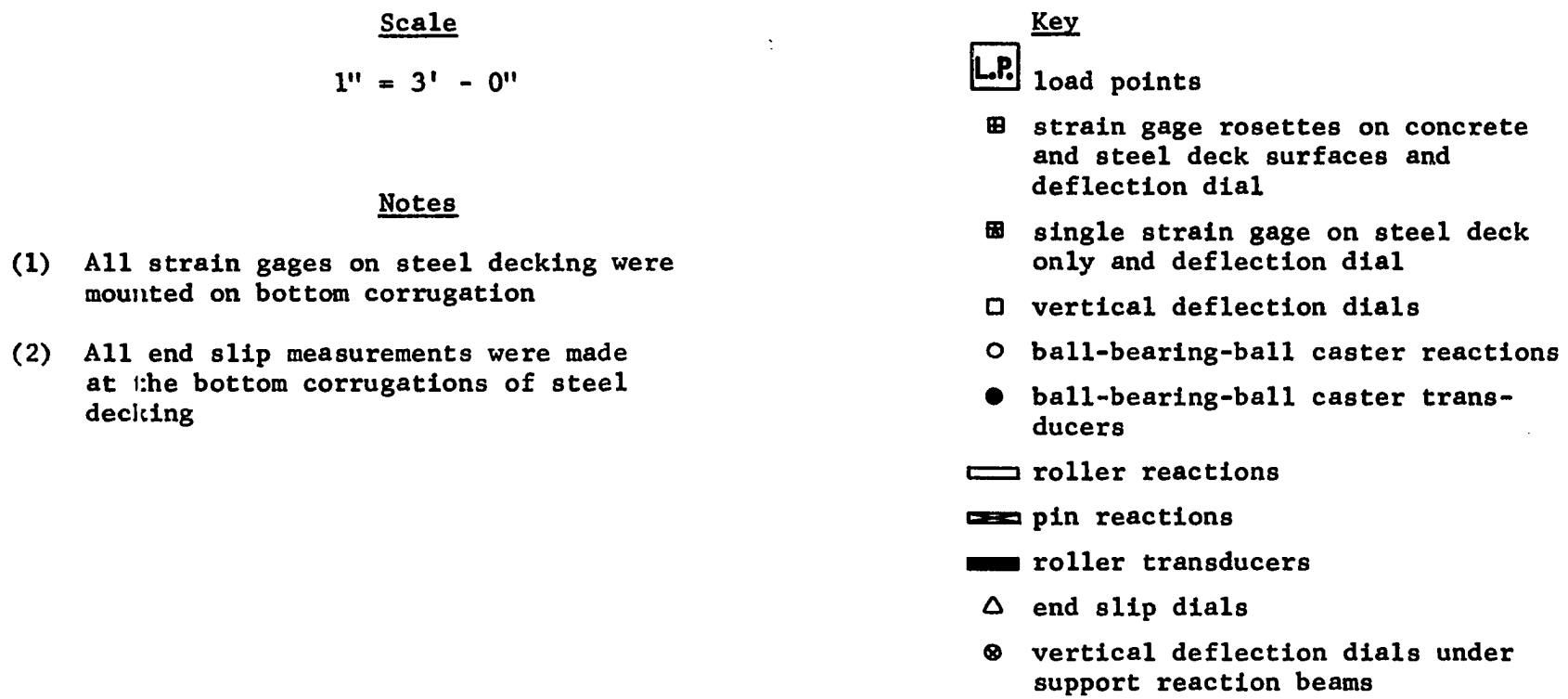

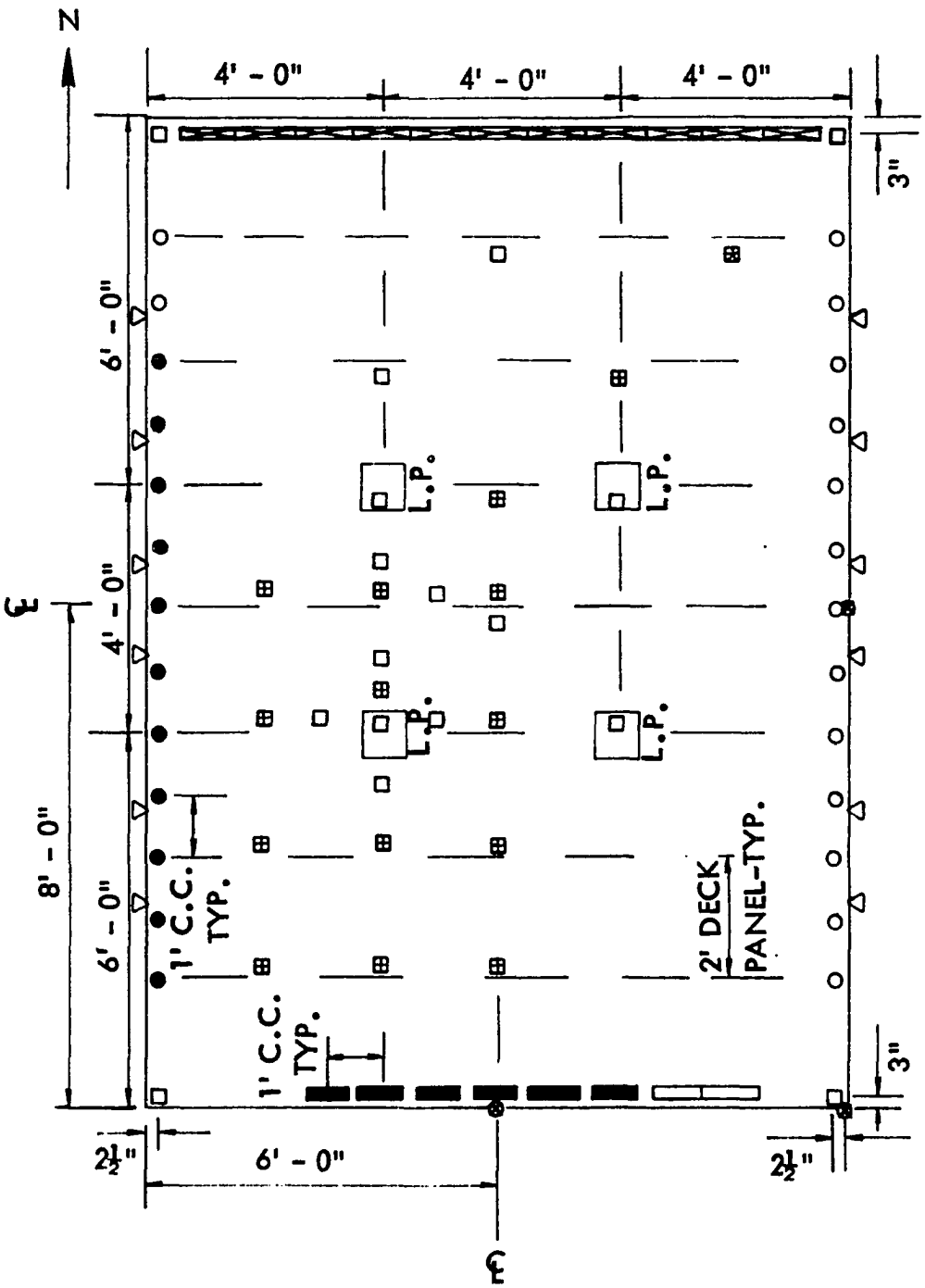
N
4' - 0"
4' - 0"
4' - 0"
3"
6' - 0"
4' - 0"
8' - 0"
6' - 0"
L.P.
L.P.
L.P.
L.P.
1" C.C. TYP.
1" C.C. TYP.
2' DECK PANEL-TYP.
3"
2½"
6' - 0"
2½"

Figure 26. Plan view of Slab 4 indicating locations of strain gages, reaction transducers, vertical deflection dials, and end slip dials

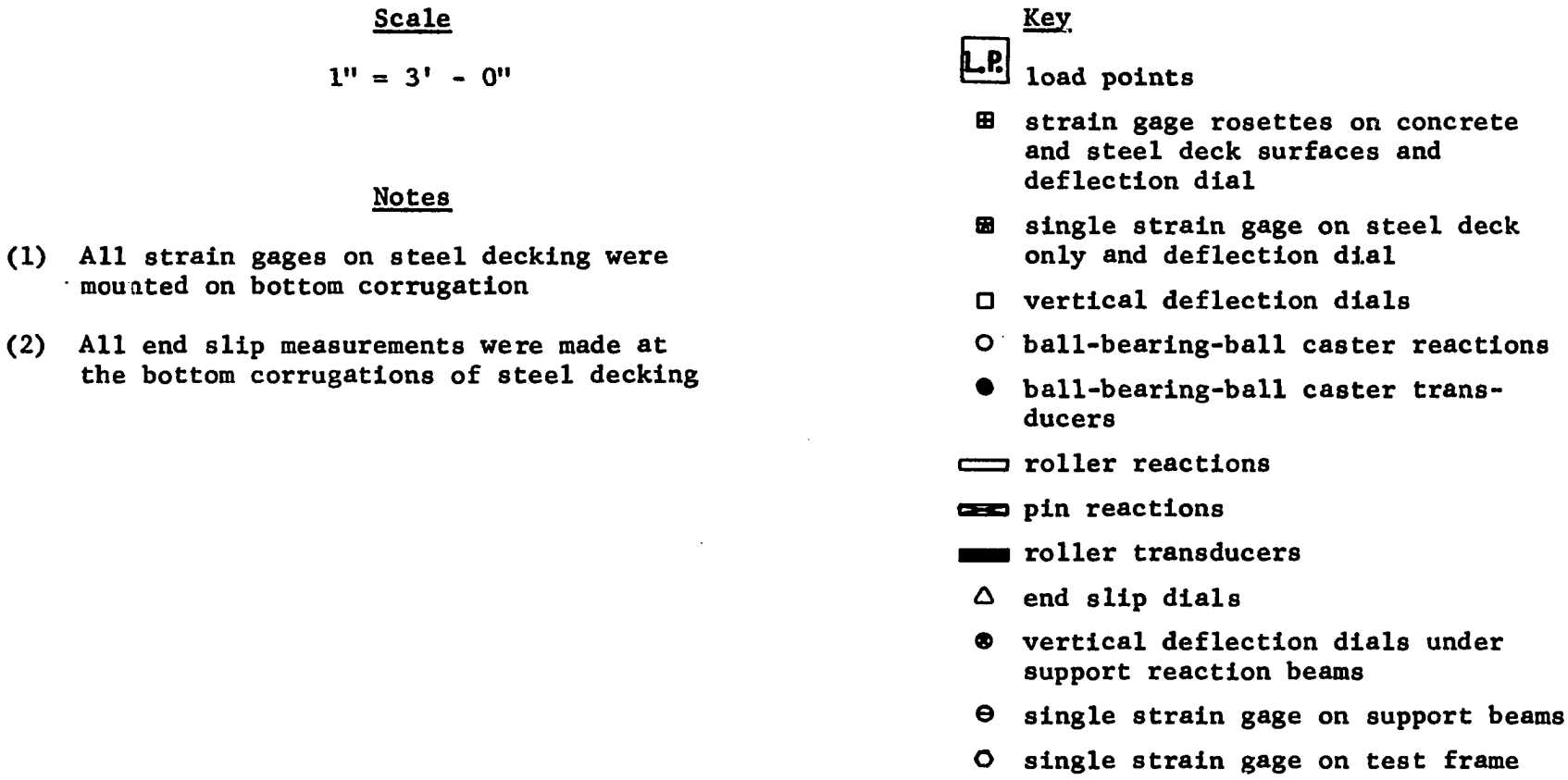

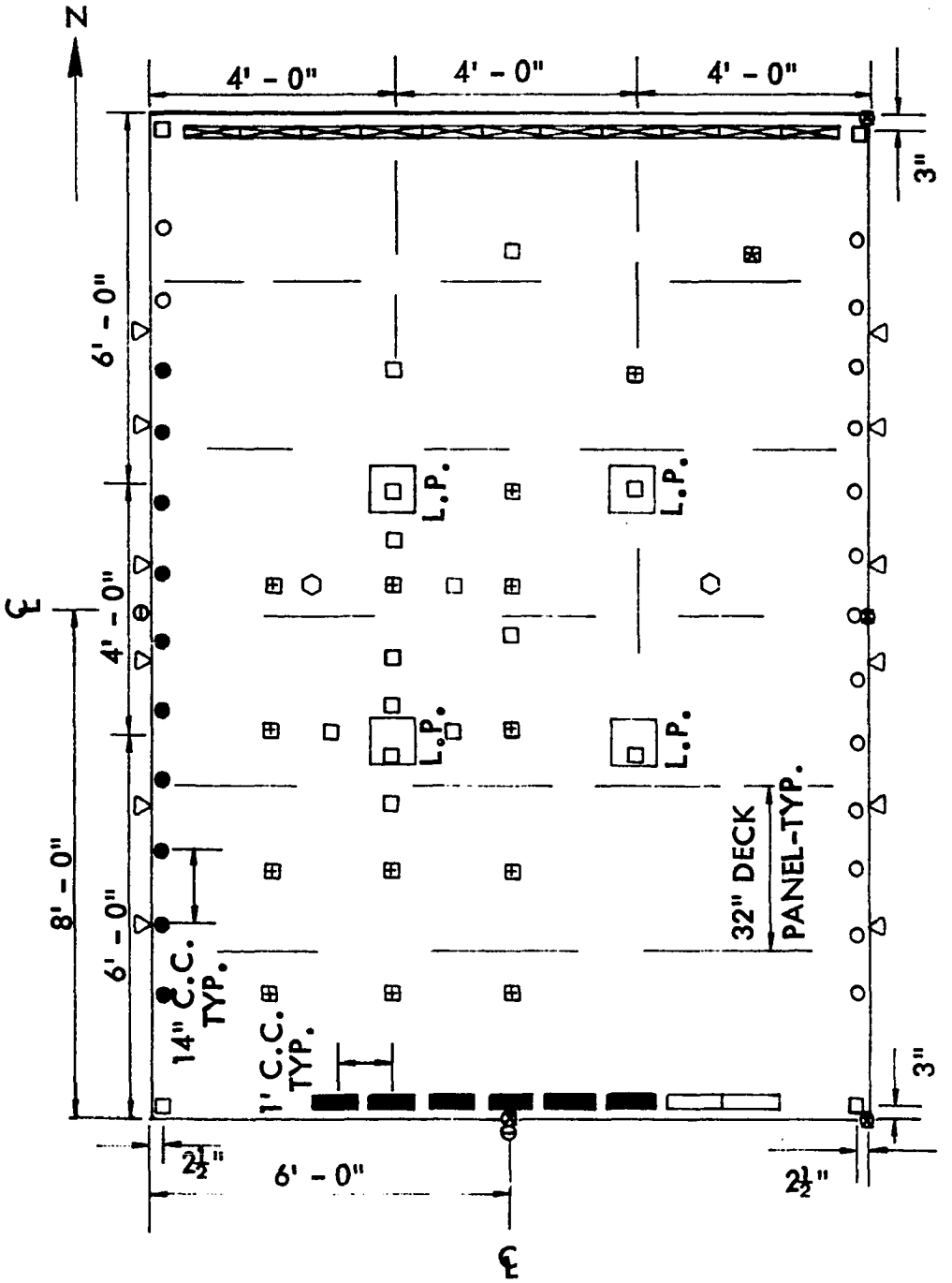
N
4' - 0"
4' - 0"
4' - 0"
3"
6' - 0"
4' - 0"
8' - 0"
6' - 0"
L.P.
L.P.
L.P.
L.P.
32" DECK PANEL-TYP.
14" C.C. TYP.
1' C.C. TYP.
3"
2½"
6' - 0"
2½"

Figure 27. Plan view of Slab 5 indicating locations of strain gages, reaction transducers, vertical deflection dials, and end slip dials

Scale

1" = 3' - 0"

Notes

(1) All strain gages on steel decking were mounted on bottom corrugation except as indicated by a T signifying that gage was mounted on the top corrugation

(2) All end slip measurments were made at the bottom corrugations of steel decking

Key

L.P. load points

⊞ strain gage rosettes on concrete and steel deck surfaces and deflection dial

◫ single strain gage on concrete and steel deck surfaces and deflection dial

□ vertical deflection dials

○ ball-bearing-ball caster reactions

● ball-bearing-ball caster transducers

▭ roller reactions

▬ pin reactions

▮ roller transducers

△ end slip dials

⊗ vertical deflection dials under support reaction beams

⊖ single strain gage on support beams

○ single strain gage on test frame

★ rosette on top corrugation of steel deck

⧫ rosette placed on inclined (web) portion of steel decking

—•— embedded single strain gage located approximately 3 5/8" from bottom of slab

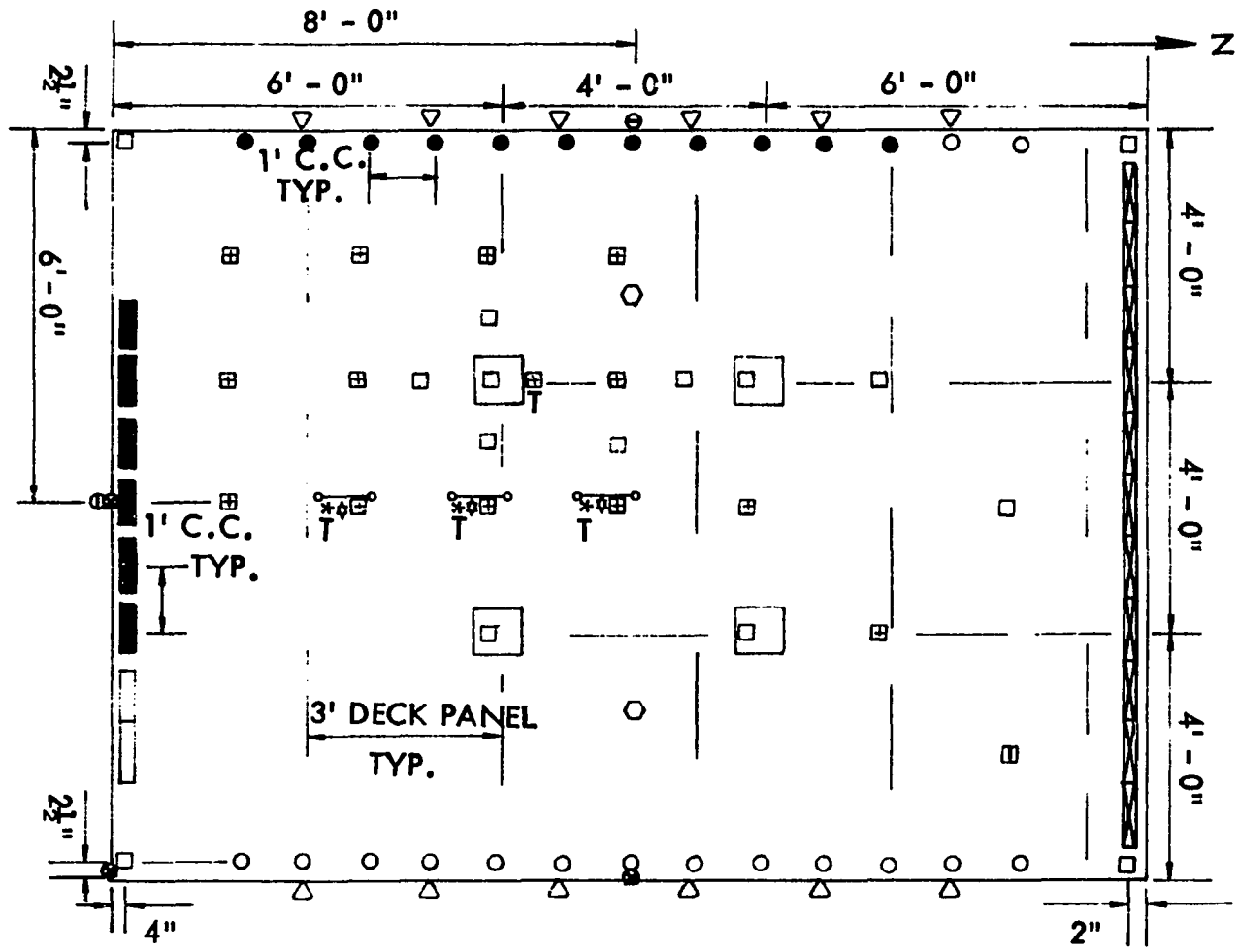
8' - 0"
Z
6' - 0"
4' - 0"
6' - 0"
2½"
1' C.C.
TYP.
6' - 0"
4' - 0"
4' - 0"
4' - 0"
1' C.C.
TYP.
3' DECK PANEL
TYP.
2½"
4"
2"

transducer had two strain gages on opposite sides diametrically mounted vertically and two on opposite sides mounted horizontally to form a complete four-arm bridge wired to measure only vertical loads and to eliminate bending effects. The roller transducers had a total of eight strain gages with four mounted on each leg consisting of two vertical (on opposite sides) and two horizontal (on opposite sides). The eight gages were wired so as to be one complete four-arm bridge to measure only vertical loads and to eliminate bending effects. The final conversion of strains into loads for these transducers was accomplished by calibration and subsequent linear regression analysis of load-strain data taken from loading the transducers in a screw action balanced weight testing machine. An additional calibration check of the transducers was performed in a 60-kip Southwark-Emery hydraulic testing machine.

Three of the four corner tie-down assemblies used in the testing of Slab 1 were instrumented with strain gages. The use of one of the tie-down assemblies during testing is shown in Figure 28. The instrumented assemblies had a total of eight strain gages with four mounted as a complete bridge on each rod. Each bridge had two opposite gages positioned vertically and two horizontally to measure only vertical loads. As was done with the other transducers, the strain to load conversion was made by calibration. The calibration was performed on a 60-kip Southwark-Emery hydraulic testing machine with a subsequent linear regression analysis performed on the data using a Hewlett-Packard electronic desk-top computer with a plotter.

On Slabs 1 and 2, four deflectometers were attached to the top surface of concrete. These deflectometers consisted of small aluminum, strain-

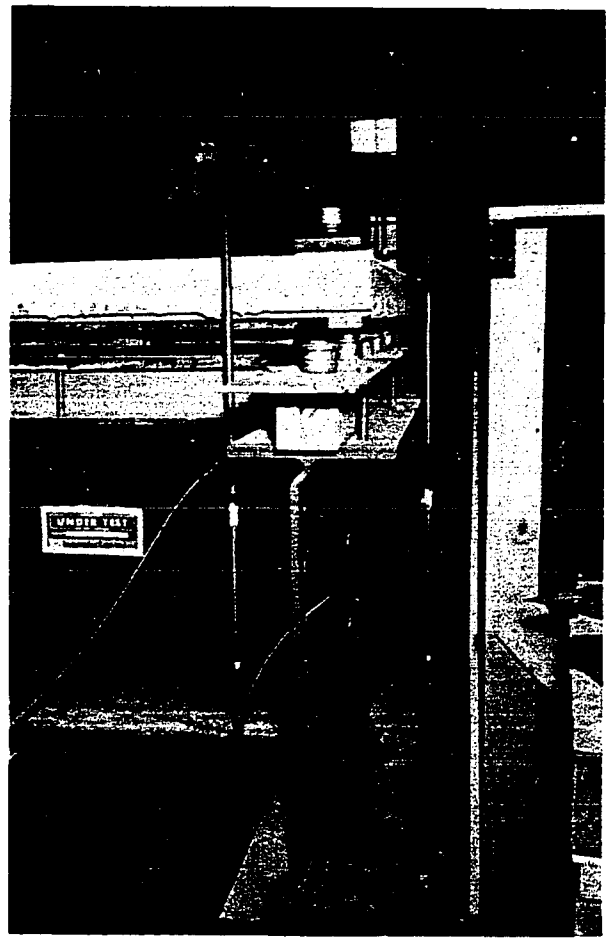

Figure 28. View of corner tie-down assembly to restrain uplift of the corners of Slab 1

gaged cantilever beams with the free end attached to the steel decking as shown in Figure 29. The deflectometers were used to measure slippage between the steel deck and the concrete as were the mechanical end-slip dials on Slabs 2, 3, 4, and 5. The deflectometers were continuously monitored by a BL-274 Brush amplifier and recorded by an oscillograph. The mechanical dial-gages to measure end-slip were mounted on rods which were firmly embedded in the concrete. The dial stem then rested on small tabs affixed to the steel decking.

Vertical deflections were measured by mechanical deflection dial

Figure 29. View of a deflectometer assembly on Slabs 1 and 2 to measure slip between steel deck and concrete

indicators until displacements exceeded the stem travel (approximately one inch), at which time deformations were taken by a surveyor's T-16 theodolite. A wooden grillage frame was constructed beneath the level of the slabs for the purpose of supporting the mechanical deflection gages. This framework and a general view of the reactions for Slab 1 is shown in Figure 30. The dial support grillage was constructed so as to rest only on the bottom frame which rested on the laboratory floor in order to be completely independent of the slab reaction beam system. The corner uplift measurements for Slabs 2, 3, 4, and 5 were also made by mechanical gages

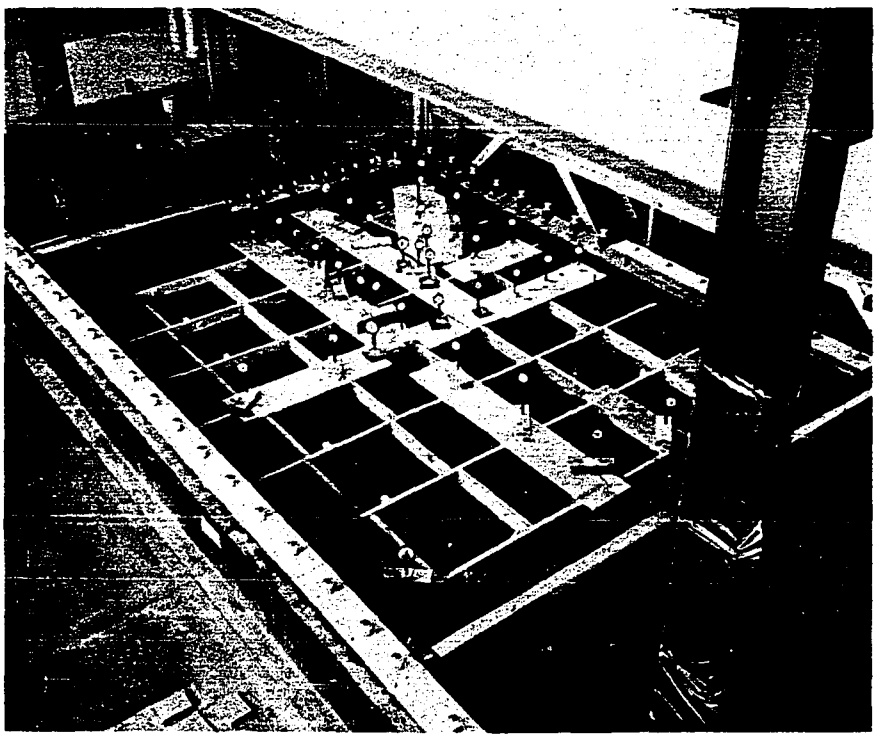

Figure 30. Grillage frame for supporting dials and general view of reaction framework

until stem travel was exceeded at which time the theodolite was used. The corner uplift gages were mounted on stands which in turn were mounted on the reaction beams. The deflections measured by the theodolite were accomplished with the aid of an engineer's scale to which a bull's-eye bubble was attached for leveling purposes. The smallest division on the engineers scale was 0.02 inches.

Test Equipment For Slab Element Specimens

Loading apparatus

The loading of the one-way longitudinal slab element specimens numbered 1 through 20 in Table 9 was applied by a 400,000-pound capacity Baldwin-Southwark hydraulic testing machine. However, the loading of

longitudinal specimens numbered 21 through 39 in Table 9 was applied by the same framework and 50-ton hydraulic cylinders as used in two-way slab tests. This change was due to the availability of a new structural laboratory following testing of the first 20 specimens.

The loading apparatus used for the one-way transverse slab element specimens numbered 1 through 10 in Table 6 was a 400,000-pound capacity Baldwin-Southwark hydraulic testing machine. Upon availability of the new structural laboratory, the same framework used in the slab tests was employed for specimen Numbers 11 and 12 in Table 6. The loading of these two specimens was accomplished by two 10-ton capacity Enerpac hydraulic cylinders (model number RC-1010) connected to a hand-operated hydraulic pump. These 10-ton cylinders were calibrated using a 60-kip capacity Southwark-Emery hydraulic universal testing machine. The cylinder calibration took place after first performing a calibration check of the testing machine using a recently calibrated 15-kip proving ring. The calibrations for final pressure conversion to equivalent load values were determined from a best fit linear regression of the data.

Instrumentation

Instrumentation for the one-way slab elements was not the same for all specimens, but consisted of the following types:

1. electrical strain gages placed parallel to specimen length on the top surface of the concrete at centerline of specimen,
2. electrical strain gages parallel to specimen length on the top, side, and bottom of the corrugations of the steel decking for a cross-section at centerline of specimen,

3. static strain indicators for monitoring strain gage readings,
4. pressure dials for reading calibrated jack loads for those specimens tested using hydraulic cylinders,
5. mechanical deflection dial indicators to measure vertical deflections,
6. mechanical deflection dial indicators to measure end-slip,
7. curvature over a 10-inch gage length as measured by a Whittemore mechanical strain gage at centerline of specimen, and
8. visual observation of crack patterns on all specimens with use of a six-power comparator for measuring crack widths on some specimens.

Dial displacement gages were used on all the one-way slab element specimens to measure vertical deflections under the load points and at midspan. Dial displacement gages to measure slippage between the concrete and the steel decking (end-slip) were used on 24 or the 39 longitudinal specimens. No end-slip dials were used on the transverse specimens since no slippage could take place due to the corrugations. A detailed summary of the various types of instrumentation in addition to the vertical deflection dials for each of the one-way slab elements containing decking with corrugations parallel to length is given in Table 11. A similar summary of instrumentation employed for those one-way specimens with the corrugations transverse to the length is given in Table 12.

Table 11. Summary of instrumentation in addition to vertical deflection dials employed on one-way slab element longitudinal specimens

Specimen No.	Purpose of Specimen	End-slip Measured?	Crack Widths Measured?
1-3	Test effect of WWF	yes	yes
4-6	" " " "	yes	yes
7-8	Companion to Slab 4	no	no
9-11	3-inch deck, shear-bond	yes	no
12	" " " "	yes	no
13	" " " "	yes	yes
14	" " " "	yes	no
15	" " " "	yes	no
16	" " " "	yes	yes
17-18	" " " "	yes	yes
19	Companion to Slab 5	yes	no

Strain gages? If so, number and description as to placement	Special Instrumentation?
no	curvature at midspan by Whittemore 10-inch gage length
yes - 4 strain gages: top surface of concrete, internal embedded at 1 3/4 inches from top surface, at levels of top steel deck corrugation on concrete (cut opening), and bottom fiber of bottom corrugation of steel decking; all at midspan	curvature at midspan by Whittemore 10-inch gage length
yes - 4 strain gages: top surface of concrete and top and bottom corrugations of steel decking at midspan and bottom corrugation under one load point	no
no	no
yes - 2 strain gages: top and bottom corrugations of steel deck at midspan	used Whittemore strain gage on top fiber of concrete at midspan, 10-inch gage length
no	no
no	no
yes - 5 strain gages: top surface of concrete; top, bottom, and side corrugations of steel decking at midspan; and bottom corrugation of steel decking at one load point	no
yes - 5 strain gages: top surface of concrete; top, bottom, and side corrugations of steel decking at midspan; and bottom corrugation of steel decking at one load point	no
yes - 4 strain gages: top surface of concrete; top, bottom, and side corrugations of steel d decking at midspan	no
yes - 6 strain gages: top surface of concrete; top, bottom, and side corrugations of steel decking; and internal embedded at 2½ inches from top surface at midspan; and bottom corrugation of steel decking under one load point	no

Table 11. Continued

Specimen No.	Purpose of Specimen	End Slip Measured?	Crack Widths Measured?
20	Companion to Slab 5	yes	no
21-23	3-inch deck, shear-bond	yes	no
24	" " " "	no	no
25	" " " "	yes	no
26-28	" " " "	no	no
29	" " " "	yes	no
30-31	" " " "	no	no
32	" " " "	no	yes
33	" " " "	yes	yes
34-35	" " " "	no	yes
36	" " " "	yes	yes
37	" " " "	no	yes
38-39	" " " "	yes	yes

Strain gages? If so, number and description as to placement	Special Instrumentation?
no	no
yes - 5 strain gages: top surface of concrete; top and bottom corrugations and 90° rosette on side corrugation of steel decking at midspan	no
no	no
yes - 5 strain gages: top surface of concrete; top and bottom corrugations and 90° rosette on side corrugation of steel decking at midspan	no
no	no
yes - 5 strain gages: top surface of concrete; top and bottom corrugations and 90° rosette on side corrugation of steel decking at midspan	no
no	no
no	Whittemore - 2 inch gage length used to measure crack widths at 4 3/4 inches from top fiber
yes - 5 strain gages: top surface of concrete; top and bottom corrugations and 90° rosette on side corrugation of steel decking at midspan	same as No. 32
no	same as No. 32
yes - 5 strain gages: top surface of concrete; top and bottom corrugations and 90° rosette on side corrugation of steel decking at midspan	same as No. 32
no	same as No. 32
yes - 5 strain gages: top surface of concrete; top and bottom corrugations and 90° rosette on side corrugation of steel decking at midspan	same as No. 32

Table 12. Summary of instrumentation employed on one-way slab element transverse specimens (See Table 6 for specimen descriptions)

Specimen No.	Number and Location of Vertical Deflection Dials	Number and Location Of Strain Gages
1	5: located at 2' (joint), 2' - 3", 3' ($\mathbb{Q}$), 3' - 9", and 4' (joint) from end of specimen	none
2	3: located at 2' (joint), 3' ($\mathbb{Q}$), and 4' (joint) from end of specimen	none
3	3: same as No. 2	none
4	3: same as No. 2	none
5	3: same as No. 2	3: top surface of concrete and top corrugation of decking at midspan and bottom corrugation of decking immediately north of midspan
6	3: same as No. 2	3: same as No. 5
7	3: same as No. 2	none
8	1: located at $\mathbb{Q}$ only	none
9	1: located at $\mathbb{Q}$ only	3: top surface of concrete and bottom corrugation of decking at midspan and top corrugation of decking immediately south of midspan
10	1: located at $\mathbb{Q}$ only	3: same as No. 9
11	3: located at 2' - 3", 3' ($\mathbb{Q}$), and 3' - 10" from end of specimen	3: same as No. 5
12	3: same as No. 11	3: same as No. 5

CHAPTER 4. TEST PROCEDURES

Test Procedure for Two-Way Slabs

General remarks

The gathering of the test data for all the two-way slab tests actually started at the time of casting when deflections, reaction transducer loads, and strains were measured on the steel decking due to the weight of concrete placed. Deflection, transducer, and strain readings on the steel decking were read every two or three days throughout curing of the slabs to obtain behavioral information regarding curing effects. These deflections, reactions, and strains were also recorded prior to and following shore removal to ascertain the effects of shore removal.

All five two-way slab tests were performed on the specimens as cast on their supports and were not moved prior to testing. Prior to the application of any load on the slabs, the remaining items of instrumentation were installed. These items included strain gages on the concrete surface, deflection gages under the support frame, end slip instrumentation in the form of dial-gages and/or deflectometers, and, for Slab 1 only, corner tie-down assemblies. All instrumentation readings were taken before and after placement of load beams. The application of load began with the placement of the load beams under each hydraulic cylinder. Prior to load beam placement, the standard neoprene bridge bearing pads were placed on the concrete (to insure a more uniform load distribution) and positioned at the four symmetrical concentrated load points indicated in Figure 10. Steel bearing plates were placed over the neoprene pads before load beam placement. After load beam placement, positioning of an additional bridge bearing pad and bearing plates (on top and underneath the pad) occurred

under each cylinder prior to application of the hydraulic loading. The weight of the pads, plates, and load beams amounted to 0.4 kips of applied load at each of the four concentrated load points. Upon completion of load beam placement, hydraulic loading of the slabs began as discussed later in this chapter.

Throughout the loading sequence at each load increment a complete set of instrumentation readings were taken including strains, reactions, deflections, observation and recording of crack patterns, crack widths (except Slab 1), progression of corner uplifts (except Slab 1), and general description of slab behavior and progress of testing. The loading throughout testing generally consisted of increments of 1 or 2 kips per load point. A time elapse of about two minutes occurred while each increment of loading was applied followed by a time elapse of about 10 to 15 minutes for reading of instrumentation. All load levels subsequently mentioned include the 0.4 kips of weight at each of the four load points due to the loading beams, but not the dead weight of the slab itself, except as noted.

After ultimate slab failure and completion of final instrumentation readings, the slabs were removed from their support frame by an overhead crane making use of cast-in-place lifting anchors. Upon placement of each slab on the laboratory floor, the slab was sawed into sections with a power concrete cutting saw. After sawing, each section was turned over and the steel decking removed to allow for observing and recording of crack patterns on the underside of each slab. Sawing the slabs also allowed the checking of the measured thickness of each slab. After recording the thicknesses along the saw cuts, the slabs were discarded.

The control cylinder and modulus of rupture specimen accompanying each slab test were tested according to ASTM specifications as given previously. These control specimens were tested on the same day as the corresponding slab test. A tabulation of the compressive and tensile concrete strengths was given in Table 3.

Slab 1

Prior to placement of the load beams for Slab 1, the corner reaction tie-down assemblies were positioned so that the corner force was applied at a location equal to the intersection of the underneath reactions in each direction. A slight uplift at all four corners was observed when the shoring was removed. The magnitude of this uplift varied from 1/16 inches to 1/8 inches, but did not extend inward along the reactions more than a few inches. The installation of the corner tie-downs did not occur until just prior to load application and after the slight uplift had already occurred. The slight uplift may be considered insignificant, depending on the actual construction procedures that would exist in a true building situation.

Test loading of Slab 1 occurred on December 15, 1970, 15 days after casting. The first load increment was 1.4 kips at each load point including the 0.4 kips of weight of the load beams, pads, and plates. Loading then progressed in increments of 2 kips at each load point with instrumentation readings taken at each load step. This 2-kip increment loading progressed uniformly until 13.4 kips per load point. At this point popping occurred and the load suddenly dropped to 11.4 kips. At this point the mechanical deflection dials were removed and deflections were taken by use of a

Theodolite. The popping was attributed to sudden rupturing of some of the welded wire fabric.

Upon attempting to reload, additional popping noise occurred accompanied by a further reduction in load to 10.6 kips. Reloading was again attempted. The load was uniformly increased from 10.6 to 13.4 kips per load point with instrumentation readings taken at each of these loading stages. Loading was further increased to 13.7 kips at which time additional popping noise occurred and load fell to 12.0 kips. An attempt to apply additional load resulted in a decrease of load to 10.7 kips. Instrumentation readings were taken at the 12.0 and 10.7 kips-load level even though complete failure was considered imminent.

Additional jacking operations only resulted in numerous popping sounds with greatly increased deflections and a further reduction of the load. The test was then terminated and the load removed to permit a recording of final deflections and strains. The time of testing from zero load on the hydraulic cylinders until the test was terminated was approximately 4½ hours.

Slab 2

Testing of Slab 2 occurred on June 7, 1971, 17 days after casting. No corner tie-down assemblies were employed on Slab 2. The first load level was 1.4 kips per load point. Then the loading was increased in successive increments of 2.0 kips per load point until 9.4 kips was reached. At this stage, loading was reduced to only that of the weight of the load beams and plates (0.4 kips per point) and then reloaded to 9.4 kips per point load and subsequently removed to 0.4 kips. This cycling of the load took place a total of 10 times between 0.4 kips and 9.4 kips per load point.

During cycling, the loading was not increased in increments of 2.0 kips per load point, but was applied either as a full increment or a half increment to the 9.4 kip cycling load.

After the 10 cycles, Slab 2 was once again loaded in increments of 2 kips per load point after the first increment of 1.0 kip until a load of 9.4 kips was reached. At this point the deflection dials were removed and deflections were taken by use of a Theodolite. Then further loading occurred until 11.0 kips was reached. At this level a popping noise was heard, and the load fell to 10.7 kips per point. Loading was resumed until a load of 11.4 kips per load point was reached when two successive "pops" occurred accompanied by a drop in load to 10.4 kips and then to 9.4 kips per point. Readings were taken and loading was resumed until reaching 10.4 kips when crack propagation occurred accompanied by a drop back to 9.4 kips per load point.

Loading then continued to 11.4 kips and successively to 15.4 kips per point with instrumentation readings being taken at 11.4, 11.9, 12.4, 13.4, 14.4, and 15.4 kips. At this stage, the slab had been severly distorted. An attempt to load above this point produced a maximum load of 15.5 kips per point, but then deflection was increasing quite rapidly and load could not be maintained at that level. Also enough distortion had been reached so as to allow the ends of the load beams to touch the slab. Testing was terminated at this point. The time of testing from zero load on the hydraulic cylinders until the test was terminated was approximately 12 hours.

Slab 3

Testing of Slab 3 occurred on August 2, 1971, 17 days after casting.

No corner tie-down assemblies were used on Slab 3. The first load level was 1.4 kips per load point. Then loading was increased in successive increments of 2.0, 2.0, and 1.0 kips per load point with all instrumentation readings being taken at each increment until 6.4 kips per load point was reached. At this stage, loading was reduced to only that of the weight of the load beams and plates (0.4 kips per point) and then reloaded to the 6.4 kips-per-point load and subsequently removed to 0.4 kips per point. This cycling of the load took place a total of 10 times between 0.4 kips and 6.4 kips per load point. During cycling, the loading was not increased in increments of 2.0 kips per load point, but was applied either as a full increment or a half increment to the 6.4-kip cycling load.

After the 10 cycles, the slab was loaded in successive increments of 3.0, 2.0, and 2.0 kips per load point until a load of 8.2 kips was reached. At this level two small popping sounds were heard accompanied by a reduction in load to 7.9 kips per load point. All instrumentation readings were taken at 7.9 kips per point and loading was resumed to 8.4 kips per load point. At this point the deflection dials were removed and a Theodolite was used. During the recording of the instrumentation readings, a popping noise was heard and load reduced only slightly. The slab was reloaded to the 8.4 kips level and instrumentation readings were retaken. Loading was then increased to 8.8 kips per load point when two successive loud pops occurred accompanied by a drop to 7.7 kips per point. All readings were taken at this point. Reloading took place until 8.4 kips per point was reached when two more successive loud pops occurred while the load was being held for recording of instrumentation readings. Load fell at this point to 5.5 kips. Attempting to reload resulted in another loud

pop and subsequent drop in load to 4.5 kips per point. Further reloading was attempted; however, the slab was unable to sustain a load above 5.2 kips per point. Testing was terminated at this point. The total time of testing for Slab 3 was approximately 10 hours.

Slab 4

Testing of Slab 4 occurred on October 30, 1971, 16 days after casting. No corner tie-down assemblies were used on Slab 4. After placement of the load beam and plates, the applied load was increased in successive increments to loads of 1.4, 2.4, 3.4, 5.4, 6.4, 7.4, 8.4, and 9.4 kips per load point. Instrumentation readings were taken at each of these increments. After the 9.4 kips level, loading was reduced to only that of the weight of the load beams and plates (0.4 kips per point) and then reloaded to the 9.4-kip level and subsequently removed to 0.4 kips per point. This cycling of the load between 0.4 and 9.4 kips took place a total of ten times. During cycling, the loading was continuous up to the 9.4-kip level, except for the first unloading and reloading when readings were taken with the load held at 5.4 kips per load point.

After the ten cycles, the slab was reloaded in successive increments to failure. During the first phase of this reloading, a total of 1.4 kips per load point was applied, followed by six increments of 2.0 kips per point to a level of 13.4 kips. During this final loading run to ultimate, the mechanical deflection gages were removed after the 9.4 kips readings and a Theodolite was used to measure deflections for the remaining load stages. Upon loading to 14.4 kips, two fairly loud pops occurred. While this 14.4-kip load was being maintained to take instrumentation readings,

a loud "bang" occurred accompanied by a falling of applied load to 6.2 kips per load point. An attempt to reload resulted in a load of 6.6 kips per load point when more popping occurred and the load fell to 5.7 kips. Further loading resulted in more popping with the load falling to 5.2 kips. Testing terminated when the load had fallen to 4.6 kips per load point. The total time of testing for Slab 4 was approximately 11½ hours.

Slab 5

Testing of Slab 5 occurred on March 16, 1972, 17 days after casting. No corner tie-downs were used on Slab 5. After placement of the load beams and plates, the applied load was increased in successive 1.0 kip increments from 1.4 to 5.4 kips per load point. At this stage, loading was then reduced to only that of the weight of the load beams and plates (0.4 kips per point), after which the slab was reloaded to the 5.4 kip-level. The jack load was removed again to 0.4 kips per point to complete the second cycle. This cycling of the load between 0.4 kips and 5.4 kips per load point took place a total of 10 times.

During cycling, the load was applied continuously up to the 5.4 kips level with instrumentation readings taken only at 0.4 and 5.4 kips per load point. After ten cycles, Slab 5 was loaded in successive increments to failure. The first increment of this reloading was 1.4 kips per load point. At this point the load was left on the slab for approximately 40 minutes with instrumentation readings taken at the beginning and end of this period to give an indication of short-time creep under load. The next successive increments brought the load level to 6.4, 7.4, 8.4, and 9.4 kips per point. The mechanical deflection gages were removed after the 8.4 kips readings and a Theodolite was used for the remaining load levels. Just

prior to reaching 9.4 kips, a fairly loud popping noise was heard at 8.7 kips. Instrumentation readings were not taken at this point, but loading continued until the increment was completed at 9.4 kips. In the midst of securing readings, while the load was maintained at 9.4 kips, another pop was heard accompanied by a drop in load to 8.7 kips per load point. Instrumentation readings were taken at this stage. Continued attempts to apply load resulted in a falling off of load with a large increase in top surface cracking. Testing was terminated at an applied load of approximately 6.5 kips. Load was then removed and final zero readings were taken. The total time of testing for Slab 5 was approximately 9½ hours.

Slab Element Specimens

All slab element specimens were tested on simple span supports, consisting of a pinned reaction at one end and a roller reaction at the other, each with a 2-inch wide bearing plate between support and specimen. All longitudinal specimens except Numbers 9, 11, 17, 23, 24, 37, and 38 (see Table 9) were subjected to a symmetrical loading of two concentrated line loads as depicted in Figure 4. The excepted specimens so indicated were subjected to a single concentrated line load applied at the center of the length of the specimen. Neoprene bearing pads 5" wide by ½" thick by the specimen width, b_d, were applied on the concrete along the lines of load application to ensure a more uniform line load distribution. Steel bearing plates 5" wide by ½" thick were placed between the neoprene pads and the transverse load beams.

After the slab element specimens had been supported and before the placement of the load beams, deflection dials were positioned, strain gages

(when employed) were hooked to strain recorders, Whittemore tabs (when employed) were attached, and end-slip dial gages (when employed) were mounted. In the case of those specimens containing strain gages, those gages located on the steel decking were mounted prior to casting, whereas those gages on the concrete were mounted approximately two or three days prior to testing.

Prior to testing or immediately following testing, the actual widths and depths of the slab elements were measured at various locations. In addition to the instrumentation readings taken for each test, the cracking characteristics and the mode of failure was observed and recorded. All slab element specimens were loaded continuously in loading increments from zero load (plus weight of load beams) to ultimate failure. No cycling of load occurred for the slab elements in this investigation. However, repeated loading of slab element specimens was previously done prior to this investigation (23).

Loading increments for the slab element specimens varied depending on the expected ultimate load. Generally, the increments used for the longitudinal specimens were 1.0 or 0.5 kips with instrumentation readings taken at each load level. In some cases, load increments were larger at the start of the test and decreased by about one-half after about one-half of the expected ultimate load was reached. The time elapsed for loading of each specimen was about one minute per increment and, for instrumented specimens, the time elapsed for reading of instrumentation was only long enough to take the readings, that being about one minute or less.

The control cylinders and, when made, the modulus of rupture specimens accompanying each slab element test were tested within a period of one day

of the corresponding slab element test. Most control specimens were tested the same day as the corresponding slab element test. A tabulation of the compressive and tensile concrete strengths was given in Table 3.

CHAPTER 5. TEST RESULTS AND ANALYSIS OF DATA FOR FULL-SCALE TWO-WAY SLABS

General Remarks

The five two-way full-scale slab tests conducted in this investigation were all of the same basic sizes and were all subjected to the same type of loading as described previously. However, several important variables existed which influenced the results. These variables included the following:

1. type of steel decking employed as primary reinforcement and its corresponding cross-sectional area;
2. amount (size and cross-sectional area) of supplementary reinforcing, both parallel and transverse to the steel deck corrugations;
3. yield strengths of both primary and supplementary reinforcing;
4. corner restraints;
5. average out-to-out thickness and depth of concrete over top corrugation of steel decking; and
6. concrete strength at time of testing.

Variables other than those listed were considered as minimal. The difference in the concrete strength was utilized in the analysis of the data; but since all slabs were constructed with the same basic mix proportions and were tested within a two-day age span, the concrete variation was small.

A complete summary of the above-mentioned variables together with the ultimate load sustained by each slab is given in Table 13. Another important variable affecting the slab test results is the amount of the cycling

Table 13. Summary of important slab variables and ultimate and cycling loads for each slab test

	Slab 1
Applied Load	
Ultimate load, P_u-kips/load point	13.7
Cycling load - kips/load point	none
Thickness and Supports	
Average out-to-out thickness, inches	4.83
Average depth of concrete over top corrugation, inches	3.28
Corner support condition	restrained
Steel Deck Reinforcement	
Type of steel decking	I
Cross section of deck shown in Figure	11
Cross-sectional area, A_{sd} - $in.^2/ft$	0.625
Yield point or strength, F_y - ksi	42.2
Supplementary Reinforcing (welded wire fabric, WWF; or T-wires)	
Type of WWF	6 x 6 x 6/6
Position of WWF	on decking
Area of WWF parallel to deck corrugations, A_{s_1} - $in.^2/ft$	0.057
Area of WWF or T-wire transverse to deck corrugations, A_{s_2} - $in.^2/ft$	0.057
Yield strength (@ 0.005 strain), ksi	79.0
Concrete	
Average compressive strength, ksi	4160

Slab 2	Slab 3	Slab 4	Slab 5
15.5	8.8	14.4	9.4
9.4	6.4	9.4	5.4
4.62	4.63	4.68	5.44
3.07	3.08	3.37	2.44
free	free	free	free
I	I	G	O
11	11	12	13
0.625	0.625	0.376	0.575
42.2	42.2	101.6	49.4
6 X 12 X 0/4 on decking	none ----	T-wires attached to decking	6 x 6 x 10/10 one inch from top of slab
0.034	none	none	0.0282
0.144	none	0.150	0.0282
82.6 (#0 gage) 84.6 (#4 gage)	none	92.1	119.4
3538	3951	3835	4300

load to which each slab, except the first, was subjected. The amount of the cycling load is contained in Table 13. When cycling occurred, however, all slabs (except Slab 1) were subjected to the same number of cycles, that being 10.

Note in Table 13 that Slabs 2 and 4, with the greater amount of additional supplementary reinforcing transverse to the corrugations, sustained the greater ultimate loads. This result is as expected since the additional reinforcing transverse to the corrugations and below the neutral axis allows a better distribution of the positive (compression on top fibers) moments transverse to the deck corrugations in the critical areas in the central region of the slab. Thus, Slab 3, which had no supplementary reinforcing transverse to the corrugations, sustained the lowest ultimate load.

The ultimate load of Slab 1 was considered as higher than what it would have been if subjected to the same conditions as Slabs 2 and 3. That is Slab 1 was not cycled 10 times, thus allowing a higher ultimate load to be applied. In addition, Slab 1 had its corners restrained from uplift by corner tie-downs which were not present on the other slabs. The presence of the corner restraints provided an increased stiffness to Slab 1.

A direct comparison of Slabs 1 and 3 to determine the percentage increase of the no-cycling and corner restraint effects is modified by another variable, that being the amount of supplementary reinforcing in these two slabs. As noted in Table 13, Slab 1 had the 6 X 6 X 6/6 WWF as supplementary reinforcing, whereas Slab 3 had no supplementary steel. The presence of the supplementary WWF in Slab 5 was not considered as effective

in contributing to the distribution of the bending moments transverse to the corrugations as the supplementary reinforcing of Slabs 1, 2, and 4. This ineffectiveness was due to the depth location of the WWF in Slab 5. The vertical location of the WWF was not below the neutral axis to sufficiently aid in distributing the positive moments in the central region of the slab.

The thickness of Slabs 1-4 was nominally set at 4½ inches; however, the deflection of the steel decking caused a greater thickness to occur. The thickness of Slab 5 was set at slightly less than 5½ inches and the increased stiffness of the 3-inch-deep steel decking provided very little increase in thickness to occur due to deck deflection. The actual thickness of each slab was determined at each location where a mechanical deflection gage was positioned. The deflection reading together with the difference in elevations measured by a surveyor's Theodolite gave the actual slab thickness at each location.

The actual thicknesses of the slabs were also determined after each slab had been sawed into strips. These actual thicknesses were determined by simply measuring the thickness at one-foot intervals along the saw-cut edges and external edges of the slabs. The two means of measuring the thicknesses checked very closely. The average thickness shown in Table 13 for each slab is an average of interior and exterior thicknesses. This average thickness was used in the general analyses involving orthotropic plate theory, yield-line ultimate strength theory, and shear-bond regression analysis. However, for the reduction of the strain data into a corresponding bending moment at each particular location, the slab thickness as measured at that location was used to determine the experimental force

distributions.

In observing the ultimate load in Table 13, it is important to note the type of failure that occurred for the five slab tests. None of the five slabs tested failed by extensive yielding of the steel-deck reinforcement. However, the steel deck did yield in some local areas in the central regions or around the concentrated load points. None of the slabs failed by a concrete compressive type of failure. In addition, no punching shear failure occurred, although there were some signs of punching failure near the end of some of the tests. All five slabs failed ultimately by a shear-bond type of failure. That is, slippage parallel to the deck corrugations between the steel decking and the concrete occurred over the central regions of each slab. Details of this end slippage are presented later in this chapter along with the behavioral results of failure progression, observed crack propagation, load-deflection characteristics, strain distributions, and support reaction distribution.

Behavioral Characteristics During Curing and Shore Removal

As indicated in Chapter 3, vertical slab deflections and strain measurements were taken during the time of the concrete curing prior to applied load testing. These measurements commenced at the time of casting and extended for about 15 days until the day of ultimate testing, including measurements before and after shore removal. All deflections and steel-deck strains indicated in Figures 23-27 for the five slabs were recorded periodically during the curing period. Concrete strains were not recorded since these strain gages were not applied until near the time of testing.

Even though the deflections and steel strains were measured and recorded at all the instrumented locations, only a very brief description of these results is presented. These results give an indication of each slab's behavior during the curing and shore removal stages.

The deflection behavior of the five slabs during curing and shore removal stages is given in Figure 31 for four key locations. These four point locations are the following:

1. centerpoint of slabs,
2. center between the two western-most load points,
3. center between the two southern-most load points, and
4. at a location near the southwest load point.

The plotted values of deflections for each of these points is shown in Figure 31. The exact location of each of the points plotted is noted.

The left-hand ordinate of zero days for each slab represents the deflection of the deck at that location due to weight of the wet concrete. This initial value of deflection for Slab 1 is misleading in that the shoring was not as strongly supported allowing more deflection of two of the four points away from the center point shore post support location. The other four slabs show a more realistic initial deflection. The initial deflection near the north-south centerline shoring was, of course, less for Slabs 2-5.

The deflection of the slabs during curing prior to shore removal was very small with the shoring carrying a large portion of the slab dead weight. Thus, not much deflection due to creep occurred prior to shore removal.

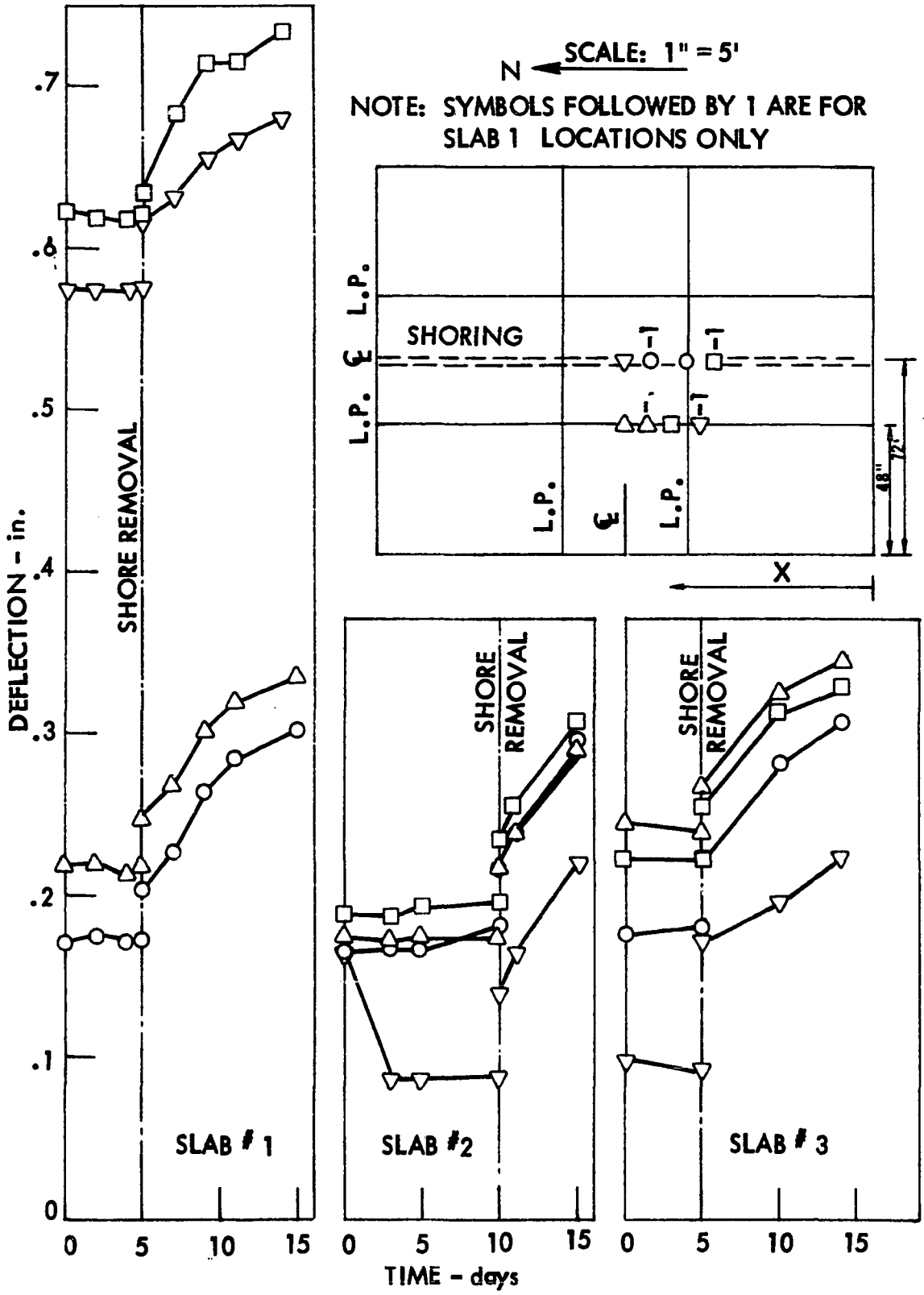

Figure 31. Deflection behavior of full-scale slabs during curing and shore removal

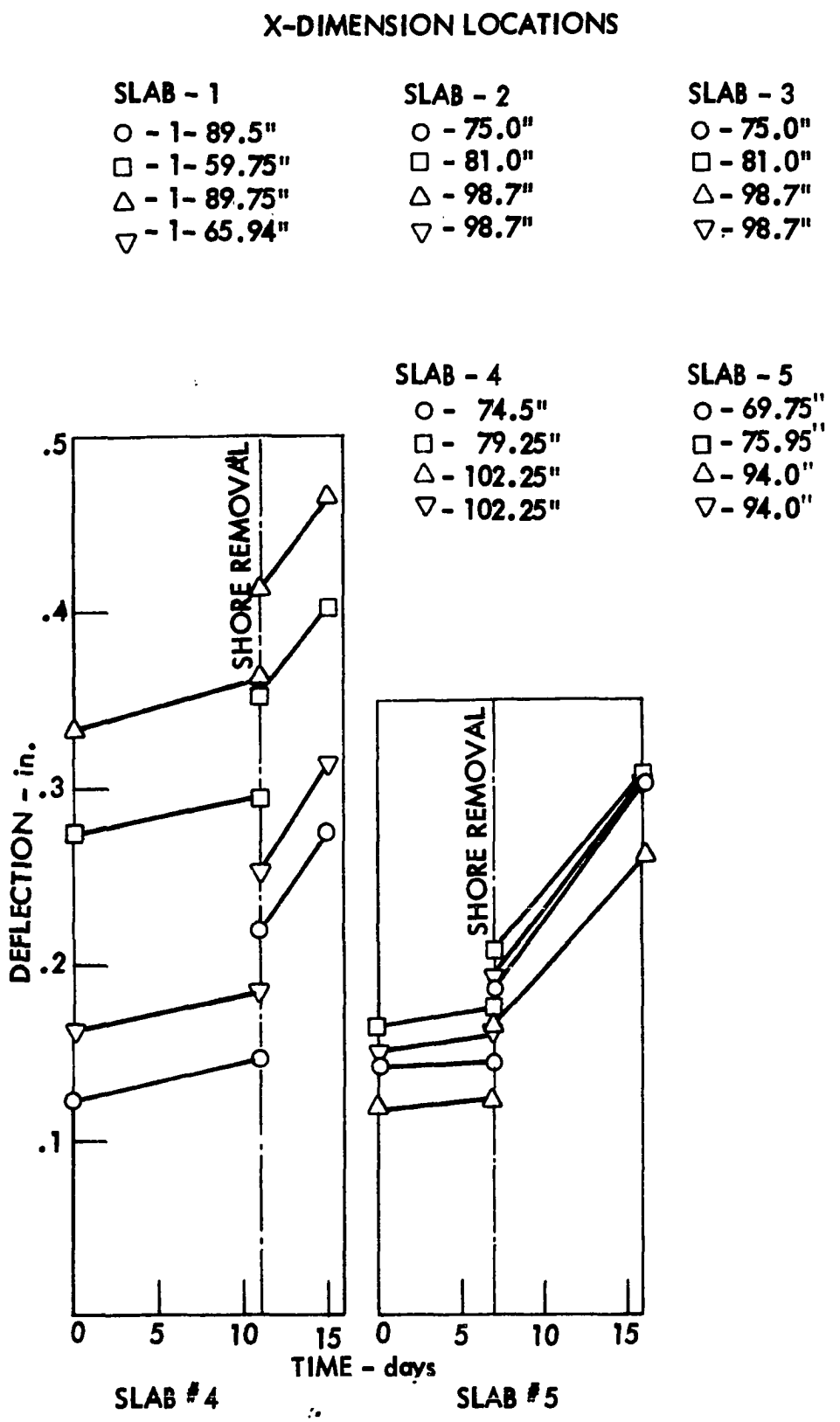

Figure 31. Continued

The deflections due to shore removal are represented as a vertical jump in deflection at the time of shore removal as indicated on Figure 31 for each slab. The amount of shore removal deflection for Slab 1 was partially negated by the shore deflection during casting. However, Slabs 2-5 demonstrated significant jump in deflection of around 0.05 inches at shore removal. The shore removal deflection is, of course, due to the weight of the slab that was on the shore being transferred to the composite, reinforced floor slab system. This slab weight on the shore can be approximated by considering the center reaction from a continuous two-span beam strip parallel to the deck corrugations.

A significant aspect of Figure 31 is the amount of creep deflection which occurred during the time after shore removal. As can be seen, the deflection for the days after shore removal is higher than the amount of instantaneous shore removal deflection. This shows that a significant amount of creep may occur for such systems. However, these measurements are insufficient to reach any general conclusions regarding creep effects for the design of steel-deck reinforced slabs.

Failure Progression and Observed Crack Patterns

An indication of the behavior of the two-way slabs subjected to a symmetrical pattern of four concentrated loads can be seen by looking at the sequence of events leading to failure and to the progression of cracking along the edges and across the surface of the slabs. Table 14 contains a detailed compilation of the sequence of events leading to failure at each important stage in loading for each slab. The tabulated loads, deflections, and strains in Table 14 are for applied jack load plus weight of load beams

Table 14. Summary of occurrences during loading to failure of each two-way slab test

Event
Slab 1
Loaded uniformly in increments of loading
While loading from 9.4 to 11.4 kips, four top surface cracks occurred - one diagonally across each of the four corners; see Crack Numbers 1, 2, 3 and 4 in Figure 32; these cracks also occurred on east and west edges. See Figure 33, Numbers 1 and 2 on each side.
Diagonal corner cracks opened; held load at 13.4 for about 5 minutes while instrumentation readings taken; at this time a pop occurred (attributed to possible sudden rupture of a section of WWF); load fell to 11.4 kips; deflection dials were removed.
Took deflection readings with Theodolite and took other instrumentation readings; then reloaded to 12.6 kips.
Pop of WWF occurred accompanied by end slip of about 1/16 inch on west side along central region between load points; load fell to 11.2 kips, Crack Numbers 5 and 6 appeared across surface - see Figure 32. Readings taken at 11.2 kips, then reloaded to 13.4 kips.
Readings taken at 13.4 kips; top surface Crack Numbers 7, 8, 9, 10, 11, 12, and 13 occurred - See Figure 32. Additional end slip occurred; loaded to 13.7 kips.
Loud pop occurred at 13.7 kips; load fell to 12.1 kips with readings taken at 12.0 kips. Top surface Crack Number 14 occurred - See Figure 32. Then reloaded.
Three pops in succession occurred accompanied by additional end slip on east side and a drop in load to 11.2 kips; reloaded to 11.7 kips with 4 successive pops occurring; Crack Numbers 15, 16, 17, 18, 19, 20, 21, 22, and 23 occurred in Figure 32; load fell to 10.7 kips. Attempt to reload resulted in 6 more pops; readings were taken at 10.7 kips; north load beam contacted concrete surface due to slab deflection; test terminated.
Test terminated; final permanent set readings taken.

[a] Strains were measured on top corrugation for Slab 1; strains for all other slabs were measured on bottom configurations. Extrapolated strains for the bottom corrugation of Slab 1 are shown in parenthesis.

Load - kips/load point	Centerpoint Deflection - inches	Centerpoint steel strain parallel to corrugations - microinches (+ = tension)
0.0 to 9.4	0.0 to 0.421	0 to 295[a] (0 to 594)
9.4 to 11.4	0.421 to 0.695	295 to 407 (594 to 978)
13.4	0.945	749 (1387)
11.4	1.397	696 (1282)
12.6 to 11.2	1.517	672 (1226)
13.4	2.817	462 (974)
13.7 to 12.1	3.197	94 (441)
12.9 to 11.2 to 10.7	3.817	24 (437)
0.0	2.917	-563 (---)

Table 14. Continued

Event
Slab 2
Loaded uniformly in increments of loading; at 7.4 kips, first crack on west edge of Slab 2 located 4' - 3" from north edge - see Crack Number 1 in Figure 33. Also Cracks 1 and 2 on east edge in Figure 33 occurred.
No readings taken; Crack Number 2 on west edge of Figure 33 occurred. Cracks 1 and 2 in Figure 32 started progressing on top surface from previous edge cracking of Crack Numbers 1 in Figure 33.
Four more diagonal edge cracks occurred on east edge shown as Numbers 3, 4, 5, and 6 in Figure 33. Also Cracks 3, 4, and 5 developed on west edge. End of first cycle of loading - started unloading, took readings at 5.4 and 0.4 kips.
Crack Number 6 on west edge in Figure 33 developed; unloaded and took readings at 5.4 and 0.4 kips.
Crack Numbers 7 and 8 on east edge occurred; during unloading to 5.4 kips, Crack Number 7 on west edge was discovered; took readings at 5.4 and 0.4 kips.
Cracking same as before; slab had gradually lifted off north and south supports so that at this stage only about 15" of length of pinned reaction was providing bearing. Unloaded, took readings at 5.4 and 0.4 kips. Crack 8 developed on west edge as shown in Figure 33.
No apparent changes occurred.
Distribution of bearing length of support appeared to be about 15 inches along center of north support and 26" along center of south support. Crack 2 on top surface in Figure 32 showed a vertical shearing separation from one side to the other side. This continued as loading increased.
No changes noted.
Top surface Crack Number 3 in Figure 32 appeared. Unlike other top surface cracks, this one did not originate from a previous edge crack.

[b]Number after dash indicates loading cycle; 11 indicates final loading cycle to ultimate.

Load - kips/load point	Centerpoint Deflection - inches	Centerpoint steel strain parallel to corrugations - microinches (+ = tension)
0.0 to 7.4	0.0 to 0.451	0 to 523
8.4	---	---
9.4 - 1[b]	0.711	808
9.4 - 2	0.746	842
9.4 - 3	0.766	863
9.4 - 4	0.797	873
9.4 - 5	0.826	895
9.4 - 6	0.838	906
9.4 - 7	0.846	916
9.4 - 8	0.854	916

Table 14. Continued

Event
Slab 2 - continued
Crack 4 on top surface appeared as shown in Figure 32.
No changes noted.
Final loading to ultimate; deflection dials removed, deflections taken by Theodolite.
During attempted loading to next increment of 11.4 kips, a pop occurred at 11.0 kips with loss in load to 10.7 kips; resulted in small end slip on wet edge; Cracks 5 and 6 appeared on top surface as shown in Figure 32. Only end slip readings taken.
Upon reaching 11.4 level, two successive pops occurred, load fell to 10.4 and then to 9.6 kips; sounded as if WWF or some kind of failure occurred in southwest quadrant; more end slip occurred. Crack 9 on west edge developed; surface Crack Numbers 7, 8, 9, 10, 11, and 12 shown in Figure 32 appeared; readings taken at 9.4 kips and not at 11.4.
Attempt to load to next increment resulted in drop in load back to 9.4 kips as surface Cracks 13, 14, and 15 developed. Readings taken at 9.4 kips.
Surface Cracks 16, 17, 18, and 19 developed. See Figure 32. East edge Crack Number 9 also appeared - See Figure 33.
Surface Cracks 20, 21, 22, and 23 appeared along with east edge Crack 10 and west edge Crack 10.
East edge Crack 11 appeared; west edge Crack 11 appeared. See Figure 33. Top surface Cracks 24, 25, and 26 appeared. See Figure 32.
Top surface Cracks 27, 28, 29 appeared and east edge Crack 12 developed. Approximately 1/8 inch of end slip had been developed on both east and west edges at this stage.
Top surface Crack 30 appeared.
About ½ inch of end slip existed on both sides; slab greatly distorted; difficult to maintain load; some slight signs of peripheral cracks near load points as top surface Cracks 31, 32, 33, 34, 35, and 36 appeared.

Load - kips/load point	Centerpoint Deflection - inches	Centerpoint steel strain parallel to corrugations - microinches (+ = tension)
9.4 - 9	0.871	924
9.4 - 10	0.873	924
9.4 - 11[b]	0.876	926
11.0 - 11	---	---
11.4 - 11 to 9.4 - 11	1.230	772
10.5 to 9.4 - 11	1.510	739
11.4 - 11	2.310	877
11.9 - 11	2.550	900
12.4 - 11	2.710	910
13.4 - 11	3.110	932
14.4 - 11	3.750	907
15.4 - 11	4.750	886

Table 14. Continued

Event
Slab 2 - continued
Difficult to maintain load as load was gradually falling; deflections increasing even more until load beams touched top surface of concrete; no readings were able to be taken at this stage; surface Cracks 38, 39, and 40 occurred after ultimate load. Loading was removed.
Permanent distortion readings taken.
After placement of additional plates for clearance under load beams, slab was reloaded; as load reached 12.9 kips, a succession of six pops occurred accompanied by a dropping in load. Readings were not taken and testing terminated.
Slab 3
Loaded uniformly in increments of loading; at 5.4 kips, 3 hairline diagonal shear cracks developed along east and west edges - see Crack Numbers 1 and 2 on west edge and Crack 1 on east edge in Figure 33.
Two small popping noises heard; Crack 2 appeared on east edge - See Figure 33; Cracks 1-4 appeared on top surface as propagated from previous edge cracks - See Figure 32. End of first cycle; started unloading to 3.4 when Crack 5 on top surface had developed; then loaded to 0.4 kips.
Upon reloading on second cycle, Crack 3 on east and west edges in Figure 33 developed.
Crack 6 on top surface in Figure 32 appeared.
No apparent changes.
At start of fourth cycle, Crack 7 on top surface in Figure 32 appeared.
At start of fifth cycle, Crack 8 on top surface appeared.
Completion of cycling loads with no more apparent changes.
Loaded uniformly in increments on final run to ultimate. Attempt to load to 8.4 kips could not be achieved, got to 8.2 when two pops occurred along east edge, load fell to 7.9 kips, small end slip (0.004 inches) occurred on east side.

Load - kips/load point	Centerpoint Deflection - inches	Centerpoint steel strain parallel to corrugations - microinches (+ = tension)
15.5 - 11	---	---
0.4	3.850	-114
0.4 to failure - 12	---	---
0.0 to 5.4	0.0 to 0.258	0 to 320
6.4 - 1[b]	0.403	525
3.4 - 2	0.250	335
6.4 - 2	0.437	563
6.4 - 3	0.448	600
0.4 - 4	0.107	180
0.4 - 5	0.113	185
6.4 - 5 to 6.4 - 10	0.460 to 0.483	600 to 626
0.4 - 11 to 7.4 - 11	0.124 to 0.570	200 to 745

Table 14. Continued

Event
Slab 3 - continued
Crack 4 on the east edge in Figure 33 occurred; top surface Cracks 9 and 10 in Figure 32 occurred; deflection dials removed after readings taken.
While taking readings, a pop noise was heard towards southwest corner resulting in end slip near southwest load point. Surface Cracks 11, 12, and 13 in Figure 32 occurred. Slab at this stage had completely lifted (minimum of about ½ inch) off entire north and south support reactions for a distance inward of approximately four feet on each side. Thus, only the central eight feet of slab were carrying the load at this stage. After pop occurred load fell slightly; slab was reloaded to 8.4 where a complete set of readings was taken as load fell gradually to 8.2 kips, then reloaded to 8.4 again where another complete set of readings was taken. Deflections and strains on right indicate change from second 8.4 to third 8.4 kip readings.
Upon continued loading the load reached 8.8 kips when a loud pop occurred and load fell to 7.9 kips followed by another loud pop and load fell to 7.7 kips when readings were taken (as shown to right). Significant visual end slip now occurred measuring about 0.02 inches.
Reloading occurred, reached 8.4 kips level again, started to take readings when consecutive pops resulted in a load falling to 7.7, 7.0, and 5.7 kips each. Cracks 14, 15, and 16 on Figure 32 occurred. The south section of the slab suddenly came down on its supports with a loud bang at the 7.0-kip level. Attempting to reload from 5.5 kips resulted in Cracks 17, 18, 19, 20, and 21 at 6.3 kips with a loud bang resulting in the north portion of slab causing it to rest on its supports. Further attempts to reload from 4.5 kips resulted in some increase in load with increased end slip on both east and west edges. Continued loading resulted in more end slip and a falling of load. Test was terminated.
Permanent set readings.
Slab 4
Loaded uniformly in increments to 5.4 kips when several small cracking sounds were heard, possibly due to chemical bond breaking between deck and concrete. Corner uplift had occurred so that slab was free of supports for a distance of four feet each direction from each corner.

Load - kips/load point	Centerpoint Deflection - inches	Centerpoint steel strain parallel to corrugations - microinches (+ = tension)
7.9 - 11[b]	0.704	930
8.4 - 11	0.920 to 1.020	1104 to 1234
8.8 to 11 to 7.7 to 11	1.120	1200
8.4 - 11	1.420	not taken
0.0	1.900	not taken
0.0 to 5.4	0.0 to 0.313	0 to 487

Table 14. Continued

Event
Slab 4 - continued
First edge cracking occurred with Cracks 1, 2, and 3 developed on both east and west edges. See Figure 33. Note cracking fairly symmetrical.
Edge Cracks 4 and 5 on both east and west sides developed. See Figure 33. Several small distressing sounds heard during loading increment.
Some distressing sounds as loading increased, edge Crack 6 in Figure 33 developed.
End of first cycle of loading. Edge Crack 6 on west edge and edge Crack 7 on east edge in Figure 33 developed. Based on uniaxial stress field the stress in bottom fiber of steel was about 46,800 psi. The deflection at this stage at center was approximately 2¼ times the L/360 deflection criteria. After readings taken at 9.4, then unloading began.
Top surface Cracks 1, 2, and 3 in Figure 32 appeared upon unloading in first cycle.
No apparent changes in crack patterns occurred during all cycles of loading except for some changes in measured crack widths and part of Crack 4 (one inch long) of Figure 32 appeared at tenth cycle.
No changes in crack patterns; deflections taken by Theodolite.
Crack 5 in Figure 32 appeared. Edge Cracks 7, 8 and 9 on west edge in Figure 33 appeared.
Two fairly loud pops occurred upon loading to 14.4 kips surface Cracks 5, 6, 7, 8, and 9 occurred. All readings taken except for completion of deflection readings, when, while taking these readings, a loud bang occurred which resulted in surface Cracks 10, 11, 12, 13, 14, 15 and 16 in Figure 32. Loud bang resulted in considerable end slip on east edge of about ½ inch, but only about 0.02 inches on west edge. T-wires were torn from decking as observed from underneath side of slab. The general locations of torn T-wires were recorded. Load fell after the bang to 6.2 kips.
Readings taken at 6.2 kips after fall from 14.4; attempt to reload reached 6.6 kips with two pops occurring accompanied by a drop to 5.7 kips with top surface Cracks 17 through 22 appearing. Further attempts to reload resulted in more popping and further drop in load.

Load - kips/load point	Centerpoint Deflection - inches	Centerpoint steel strain parallel to corrugations - microinches (+ = tenstion)
6.4	0.466	743
7.4	0.639	1039
8.4	0.804	1318
9.4 - 1[b]	0.950	1534
5.4 - 1	0.731	1144
9.4 - 2 to 9.4 - 11	0.995 to 1.094	1584 to 1668
11.4 - 11	1.334	2020
13.4 - 11	1.634	2485
14.4 - 11	not taken	2895
6.2 - 11	2.074	1455

Table 14. Continued

Event
Slab 4 - continued
Readings at test termination; top surface Cracks 23 and 24 appeared.
Readings taken for permanent set in Slab 4.
Slab 5
Loaded uniformly in increments of loading to end of first cycle. Crack Numbers 1 and 2 on both east and west edges in Figure 33 occurred. The slab unloaded to 0.4 kips and reloaded. Loading and unloading continued 10 times.
Cracks 3 and 4 on the east edge in Figure 33 appeared.
Cracks 3 and 4 on the west edge and Crack 5 on the east edge as shown in Figure 33 developed.
Crack 6 on east edge in Figure 33 appeared and first crack on top surface in Figure 32 appeared.
No apparent changes.
Crack 1 on top surface elongated inward about one inch.
No apparent changes.
Crack 7 on east edge in Figure 33 appeared.
No noticeable changes.
Crack 5 on west edge shown in Figure 33 developed. End of cycling. Starting from 0.4 kips, the final eleventh cycle was to failure.
No apparent changes from 10 - 10 kips but load was held at this stage for 31 minutes to determine short-time creep characteristics.
No apparent changes after holding for 31 minutes except for slight increases in deflection and strain.
Crack 8 on east edge and Crack 6 on west edge in Figure 33 appeared as well as top surface Cracks 2, 3, and 4 in Figure 32 developed from previous edge cracks.

Load - kips/load point	Centerpoint Deflection - inches	Centerpoint steel strain parallel to corrugations - microinches (+ = tension)
4.6 - 11	2.834	1184
0.4	not taken	635
0.0 to 5.4 - 1[b]	0.0 to 0.282	0 to 479
5.4 -2	0.300	499
5.4 - 3	0.308	507
5.4 - 4	0.312	516
5.4 - 5	0.320	519
5.4 - 6	0.323	525
5.4 - 7	0.324	529
5.4 - 8	0.327	531
5.4 - 9	0.327	531
5.4 - 10	0.330	539
10 - 11	0.333	538
10 - 11	0.343	549
6.4 - 11	0.466	699

Table 14. Continued

Event
Slab 5 - continued
Top surface Crack 5 in Figure 32 developed.
Top surface Cracks 6, 7, 8, 9, and 10 shown in Figure 32 appeared as well as Crack 7 on west edge in Figure 33. Elevations taken with both dials and Theodolite at this level, then dials removed and remaining elevations taken with Theodolite.
While loading to 9.4 kips some end slip was observed on both east and west sides at 8.8 kips, accompanied by a loud popping noise on southeast quadrant of slab. Upon reading 9.4 kips, load was held for about 2 minutes when continued pumping could not hold load at the 9.4 level; load fell to 8.8 kips; most readings at the 9.4-kip level were actually taken at the 8.8-kip level. The two deflections at right indicate both the 9.4 and 8.8-kip levels. During those stages of loading, top surface Cracks 11 through 23 in Figure 32 developed. As can be seen from cracks in Figure 32, some signs of punching shear cracking developed around the northeast load point.
Readings taken again at this level as load had fallen from the previous 8.8 kips. As attempted loading continued beyond this stage, the load continued to fall and the test was terminated after load fell to 6.8 kips.
Final permanent set readings taken.

Load - kips/load point	Centerpoint Deflection - inches	Centerpoint steel strain parallel to corrugations - microinches (+ = tension)
7.4 - 11	0.551	905
8.4 - 11	0.800	1191
9.4 - 11 to 8.8 - 11	1.240 to 1.480	1609
7.9 - 11	2.100	1635
0.0	1.360	254

at each load point and do not have any amount added for slab dead weight.

Included in Table 14 with each event is the corresponding vertical deflection and steel deck strain at the center of the slab. The strains and deflections are included only for those loads at which these instrumentation readings were read. Additional strain information indicating the maximum strain and its location and strain distribution behavior is given in a later section on strain behavior. The strains given are those recorded in the direction parallel to the steel-deck corrugations since this is the larger strain direction developed and is an indication of the one-way steel stress in the strong direction of the slab. The strain at the center of the slab was not necessarily the maximum strain, since the concentrated load points produced somewhat larger strains in the vicinity of the load points.

The strain given in Table 14 is for the bottom corrugation of steel decking except for Slab 1 where the gage was located on the top corrugation. Extrapolation of the strain, assuming linear strain across the section, to the bottom corrugation for Slab 1 was made by simply extending the distribution of the known concrete strain on top surface and the strain on top corrugation of steel decking using the actual measured thickness at that point. This extrapolated strain is shown in parenthesis for Slab 1 in Table 14.

In looking at the strains and deflections, a few interesting observations can be made. One important observation concerns the comparison of the uniaxial strain to cause yielding (i.e. F_y/E_s) compared to the actual strain of the center of the slab. The yield strain for Slabs 1, 2, and 3 is 1435; for Slab 4, 3331; and for Slab 5, 1594 microinches per inch. As

can be seen, Slabs 1, 3, and 4 came fairly close to yielding at the center, whereas Slab 2 only reached 65 percent of the yield strain.

The lower strain at the center of Slab 2 is significant since this slab had a much greater amount of supplementary reinforcing transverse to the deck corrugations. Thus, the additional reinforcing allowed a better distribution of forces to take place. The higher strains of Slab 4 were due to a different type decking.

Slab 5 was the only one that did reach the yield strain, but this occurred after the ultimate load had been reached. This slab was also the only one that had an increase in strain after ultimate load. This increase can be explained by the fact that Slab 5 contained the 3-inch deck making the deck a greater percentage of the total thickness. Thus, after the loss of total composite action had occurred, the deck, with its greater capacity by itself, then withstood more load and consequently had its steel fibers strained more immediately after ultimate load.

Along with reduced strain at center for Slab 2, Slab 2 also could sustain a much greater deflection (4.75 inches) before failure. This again was due to the greater supplementary steel. On the other hand, Slab 3, with no supplementary steel, could not withstand near as much deflection (1.02 inches) at ultimate as Slab 2 could.

Contained in Table 14 are referrals to Figures 32 and 33 which show specified crack information. Figure 32 indicates the cracking that occurred on the top surface of the five slab specimens, whereas Figure 33 indicates the diagonal type of cracking that occurred on both the east and west edges of each slab. The crack numbers in each of these two figures indicate the order of occurrence of the cracks.

Accompanying Figures 32 and 33 are two tables giving the measured crack widths at certain stages of loading. Table 15 gives crack widths for the top surface cracking and Table 16 gives crack widths for the edge cracking. Slab 1 is omitted from Tables 15 and 16 since crack width measurements were not taken on this slab. The crack widths were made with a six-power comparator with a least devision of 0.1 mm. For those measurements given in inches, the measurement was made simply with an engineer's scale. The inch measurements were used only for those cracks of considerable size.

As can be seen from Tables 15 and 16, most cracks that developed were in the 0.1 mm range and some of these cracks remained small even after ultimate loading. Those cracks with the greatest width at final measurement after testing signify the major failure cracks. Note that the major failure crack widths were much larger for Slab 2 than for the other slabs. This was attributed to the increased ductility of this slab due to the benefit of the better distribution of forces from the additional supplementary reinforcing steel. Thus, larger crack widths could occur before final failure.

It is particularly important to note the type of edge cracking that took place. The major edge cracks were all diagonal in nature (roughly at a 45 degree angle) and propagated diagonally up and towards the nearest north or south edge. The development of the diagonal shear cracks propagated from a corner of a top corrugation of the steel decking. As loading progressed these cracks proceeded to the top fibers of the slab and then propagated inward along the top surface. The widths of the diagonal cracks were greatest at their starting point and diminished to about 0.1 mm at their uppermost point. The major failure cracks began to open up along the

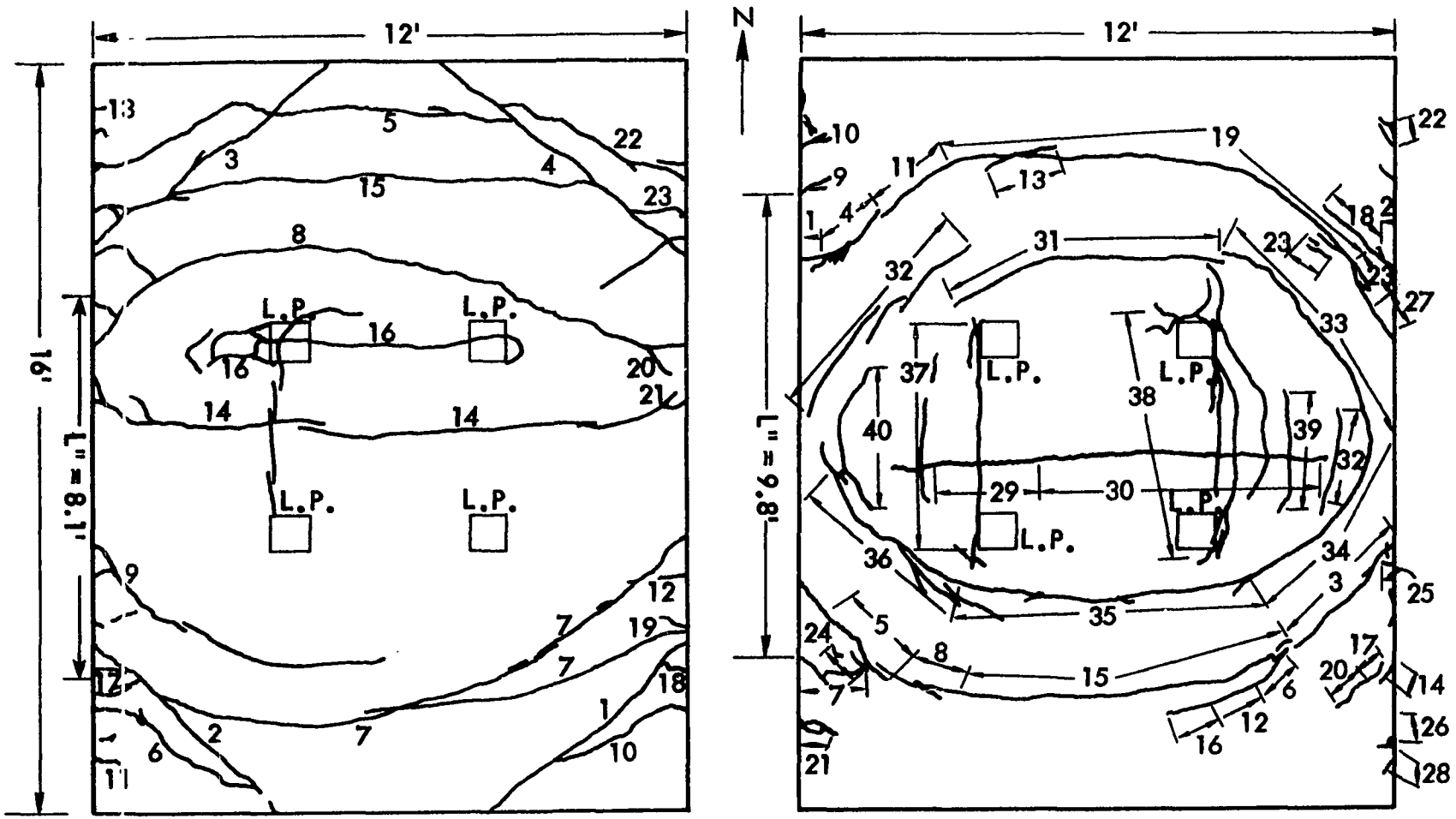

Figure 32. Crack patterns on top surface of each slab test

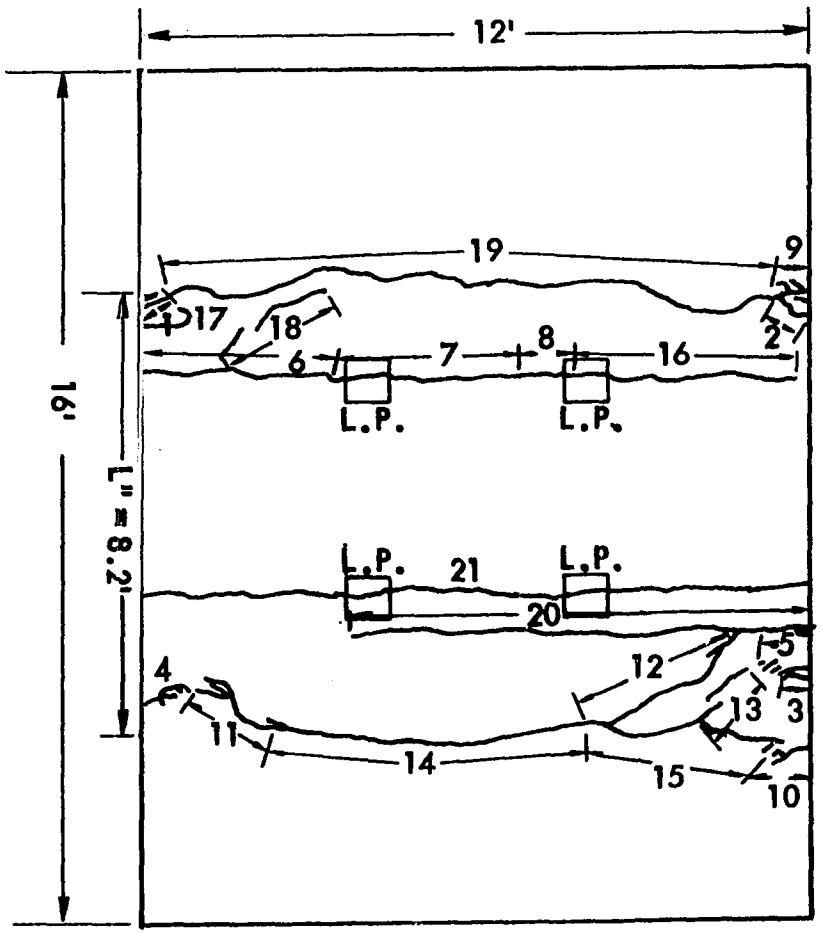

SLAB 3

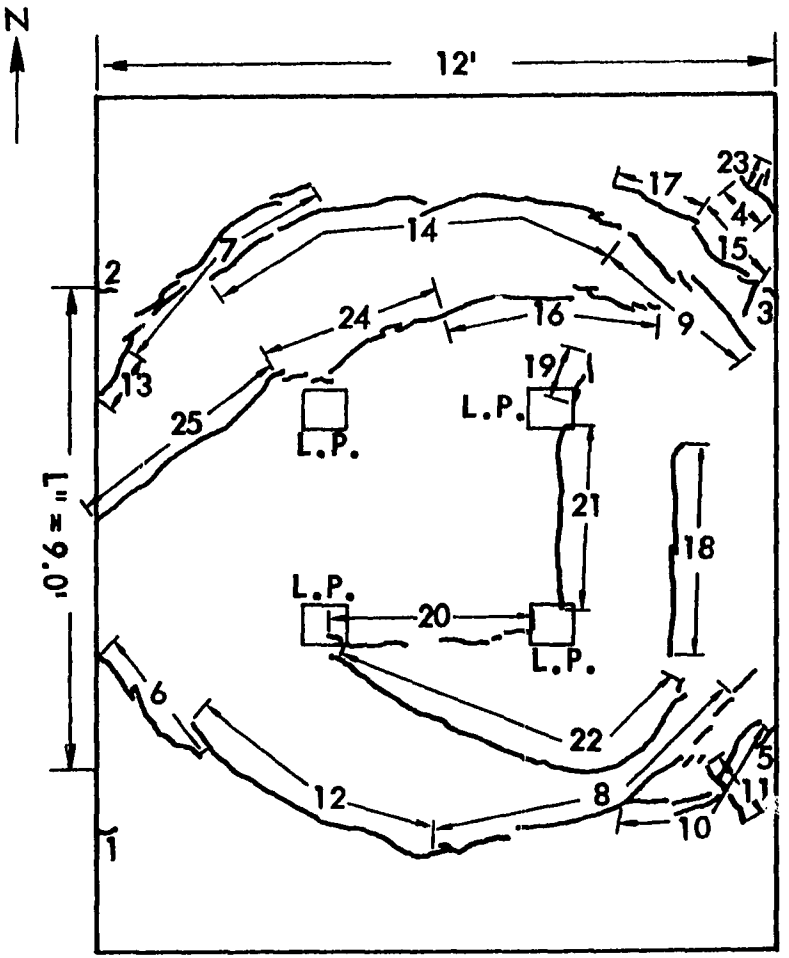

SLAB 4

Figure 32. Continued

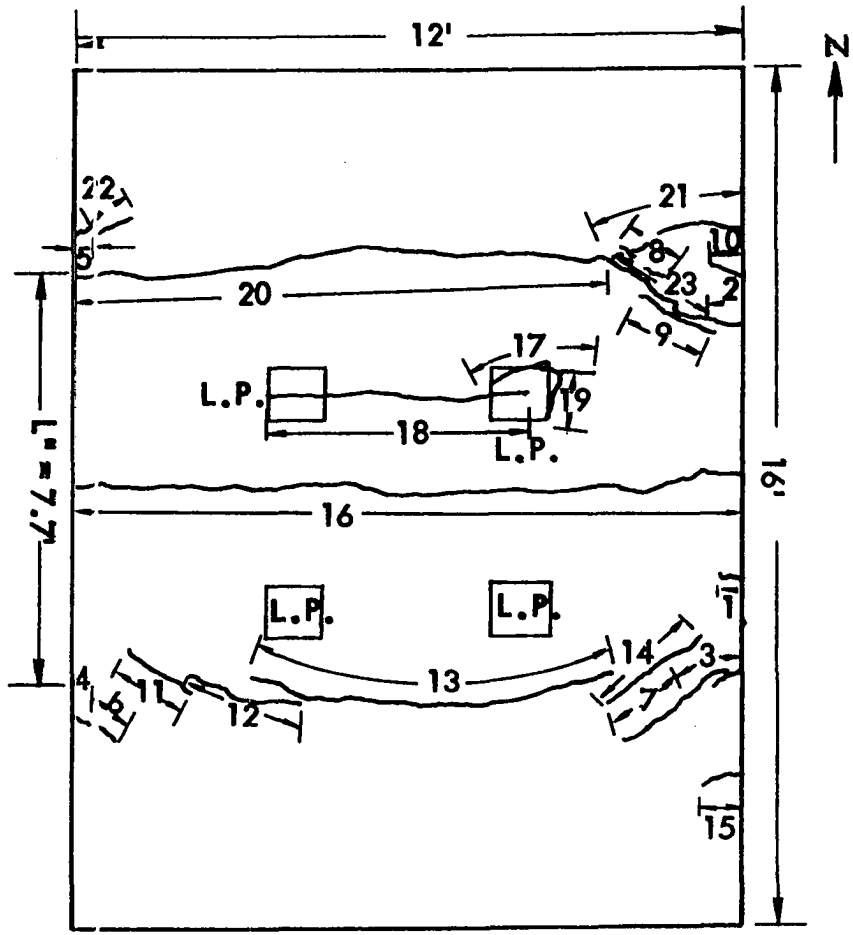

SLAB 5

NOTES:

1. NUMBERS INDICATE APPROXIMATE ORDER OF CRACK OCCURRENCE. SEE TABLE 14 FOR LOAD AT WHICH EACH CRACK OCCURRED.
2. DIAGONAL CORNER CRACKS EXIST ONLY FOR SLAB 1 DUE TO PRESENCE OF CORNER TIE DOWNS.
3. SEE TABLE 15 FOR APPROXIMATE CRACK WIDTHS AT EACH LOAD.
4. THE L" LENGTHS SHOWN ARE AVERAGE MEASURED VALUES FOR THE CRACK MECHANISM OF EACH SLAB.

Figure 32. Continued

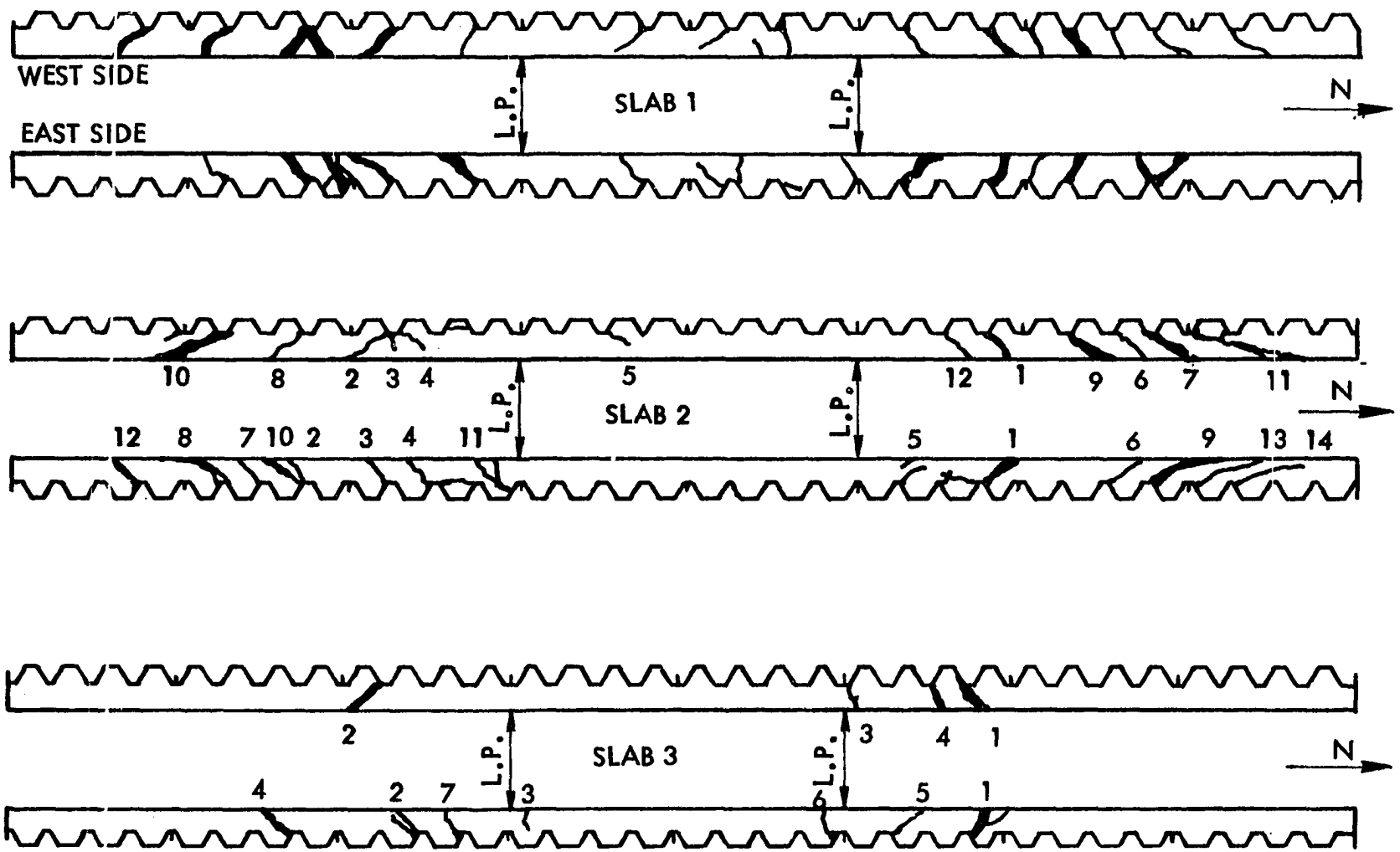

Figure 33. Crack patterns on east and west edges of each slab test

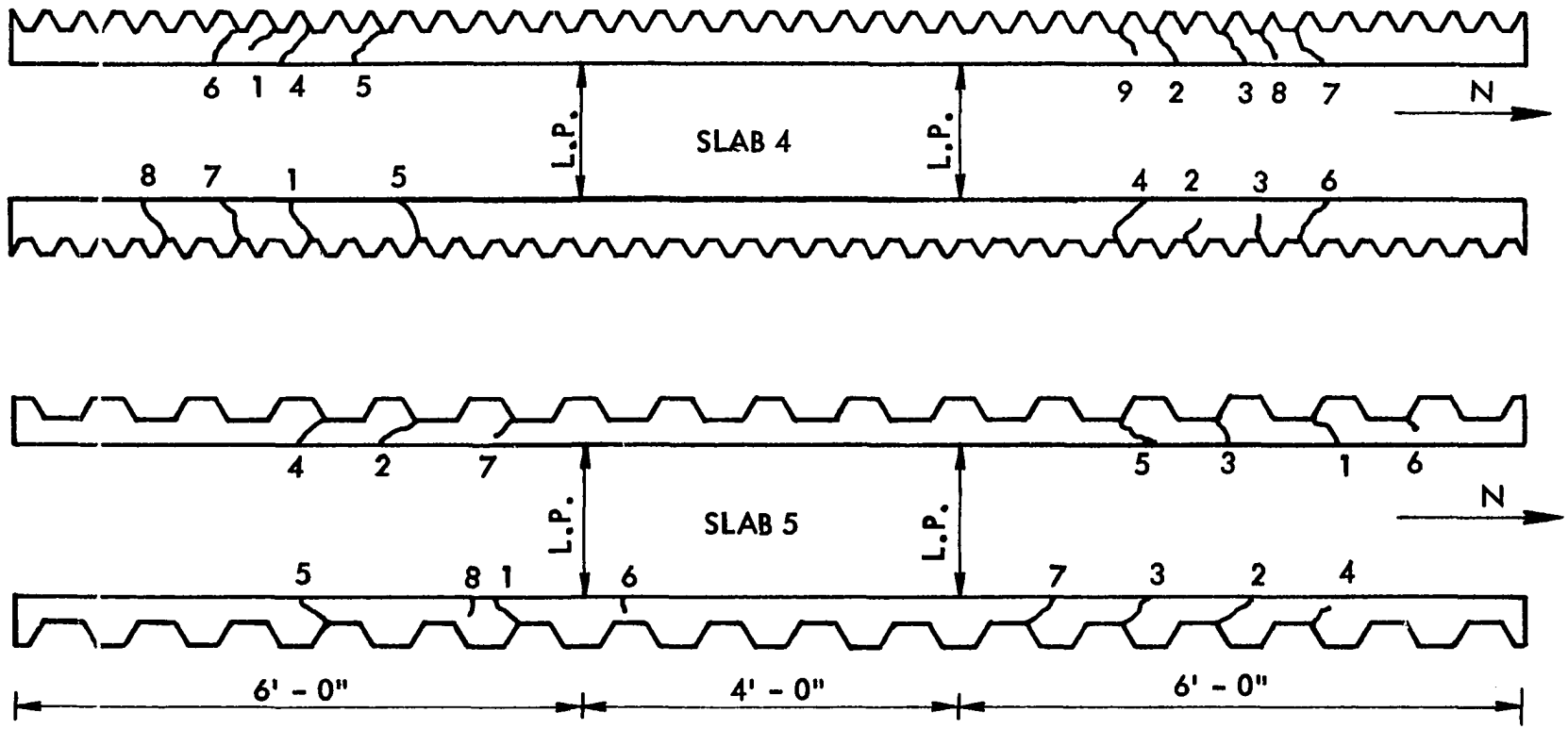

SCALE: 1"= 2' - 0" HORIZONTAL

NOTES: 1. NUMBERS INDICATE APPROXIMATE ORDER OF CRACK OCCURRENCE.
2. SEE TABLE 14 FOR LOAD AT WHICH PARTICULAR CRACK OCCURRED.
3. SEE TABLE 16 FOR CRACK WIDTHS AT EACH LOAD.

Figure 33. Continued

Table 15. Measured crack widths of top surface cracking for slab specimens

Load (kips)	Cycle	Crack number[a] and average widths (mm)[b]									
		1	2	3	4	5	6	7	8	9	10
Slab 2[c]											
8.4[d]	1	.1	.1								
9.4	1	.3	.1								
9.4	2	.4*[e]	.2								
9.4	6	-[f]	.3*								
9.4	8			.1							
9.4	9				.1						
11.4 to 9.4	11[g]				.1	.1	.1	1.5*	.1	.1	.1
11.4	11						.2				
11.9	11				.2						
12.4	11										
13.4	11										
14.4	11										
15.4	11										
Final		2.0*	2.0*	2.0	.8	.5	.5	2.5*	1.8	.7*	3.0*

[a]See Figure 32 for crack number locations.

[b]An engineer's scale was used on only those cracks given in inches; otherwise all measurements are given in millimeters.

[c]Crack widths are not given for Slab 1 since they were not measured.

[d]No cracking was observed below first listed load for each slab.

[e]An * indicates that there was a vertical (shear) separation of the crack as well as the horizontally measured value.

[f]Blank spaces after initial cracking merely indicate no crack measurement obtained for that load level.

[g]Eleven indicates the final cycle to ultimate.

Table 15. Continued

Load (kips)	Cycle	Crack number[a] and average widths (mm)[b]									
		11	12	13	14	15	16	17	18	19	20
Slab 2[c]											
8.4	1										
9.4	1										
9.4	2										
9.4	6										
9.4	8										
9.4	9										
11.4 to 9.4	11[g]	.1	.1	.1	.5	.1					
11.4	11					.3	.1	.1	.2	.2	
11.9	11									.4	.1
12.4	11										
13.4	11										
14.4	11										
15.4	11										
Final		1.7	.2	.1	1.0*	3.0	.1	.2	.5	2.2	.1

Table 15. Continued

Load (kips)	Cycle	Crack number[a] and average widths (mm)[b]									
		21	22	23	24	25	26	27	28	29	30
Slab 2[c]											
8.4	1										
9.4	1										
9.4	2										
9.4	6										
9.4	8										
9.4	9										
11.4 to 9.4	11[g]										
11.4	11										
11.9	11	1.1	.1	.1							
12.4	11				.1	.1	.1				
13.4	11						.7	.1	.2	.1	
14.4	11	0.2"*								.2	.1
15.4	11						.22"				.1
Final		2.5*	1.0*	.1	.1	0.1	.22"*	.3	.2*	.1	.1

Table 15. Continued

Load (kips)	Cycle	Crack number[a] and average widths (mm)[b]									
		31	32	33	34	35	36	37	38	39	40
Slab 2[c]											
8.4	1										
9.4	1										
9.4	2										
9.4	6										
9.4	8										
9.4	9										
11.4 to 9.4	11[g]										
11.4	11										
11.9	11										
12.4	11										
13.4	11										
14.4	11										
15.4	11	.2	.1	.1	.2	.2	.1				
Final		1.4	.3	.4	.3	.7	.4	0.5	2.0	0.3	0.2

Table 15. Continued

Load (kips)	Cycle	Crack number[a] and average widths (mm)[b]								
		1	2	3	4	5	6	7	8	9
Slab 3										
6.4[d]	1	.1	.1	.1	.1					
3.4	1					.1				
6.4	2			.1			.1			
0.4	3						.1			
6.4	3	.1			.1		.2			
0.4	4							.1		
0.4	5								.1	
6.4	5						.2			
6.4	8	.2				.1	.2			
5.4	11	.2			.2		.2			
7.9	11	.4	.1		.6		.2	.2		.3
8.4	11	.1	.1	.8	.07"		.2	.2	.2	.1
Final		.36"*	.50"*	.11"*	.12"*	.08"*	0.1"	0.1"	.05"	.50*

Table 15. Continued

Load (kips)	Cycle	Crack number[a] and average widths (mm)[b]											
		10	11	12	13	14	15	16	17	18	19	20	21
Slab 3													
6.4	1												
3.4	1												
6.4	1												
0.4	3												
6.4	3												
0.4	4												
0.4	5												
6.4	5												
6.4	8												
5.4	11												
7.9	11	1.2											
8.4	11		.1	.1	.1								
Final		.30"*	0.1"	.06"	.1	.1	.06"	.2	.1"*	.3	.2"	.06"	.04"

Table 15. Continued

Load (kips)	Cycle	Crack number[a] and average widths (mm)[b]											
		1	2	3	4	5	6	7	8	9	10	11	12
Slab 4													
5.4[d] (unloading)	1	.1	.1	.1									
13.4	11				.1								
14.4	11					.2	.1	.1	.1	.2			
6.2	11					.5		.3		.2	.1	.7	.5
5.7	11												
4.6	11	.1	.1	.1	.1	.5	.1	.3	.1	.2	.1	.7	.5
Slab 5													
5.4[d]	4	.1											
6.4	11		.1	.1	.1								
7.4	11					.1							
8.4	11						.1	.1	.1	.1	.1		
9.4	11											.1	.1
Final							.2	.2				.3	

Table 15. Continued

Load (kips)	Cycle	Crack number[a] and average widths (mm)[b]											
		13	14	15	16	17	18	19	20	21	22	23	24
Slab 4													
5.4	1												
13.4	11												
14.4	11												
6.2	11	.5	.2	.2	.2								
5.7	11					.2	.1	.2	.2	.2	.1		
4.6	11	.5	.2	.2	.2	.2	.1	.2	.2	.2	.1	.2	.2
Slab 5													
5.4	4												
6.4	11												
7.4	11												
8.4	11												
9.4	11	.1	.1	.1	.1	.1	.1	.1	.1	.1	.1	.1	
Final		.9	.4		1.2	.2	1.3		3.2	1.2		.9	

Table 16. Measured crack widths of edge cracking for slab specimens

Load (kips)	Cycle	West edge crack no.[a] and average crack widths (mm. except inches where noted)[b]					
		1	2	3	4	5	6
Slab 2[c]							
7.4[d]	1	0.4	0	0	0	0	0
9.4	1	0.5	0.3	0.2	0.2	0.1	0
9.4	3	0.5	0.3	-[e]			0.1
9.4	4	0.5	0.3				0.1
9.4	11[f]	0.5	0.3				0.1
11.4 to 9.4	11	0.5	0.3				0.1
11.4	11	0.5	0.3				0.1
11.9	11	0.5	0.3				0.1
12.4	11	0.5	0.3				0.1
13.4	11	0.5	0.3				0.1
15.4	11	0.5	0.3				0.1
Final		1.6	1.2	0.2	0.2	0.1	0.1

[a]See Figure 33 for crack number locations.

[b]An engineer's scale was used on only those cracks given in inches; otherwise all measurements are given in millimeters.

[c]Crack widths are not given for Slab 1, since they were not measured.

[d]No cracking was observed below first listed load for each slab.

[e]Blank spaces after initial cracking merely indicate no crack measurement obtained for that load level.

[f]Eleven indicates the final cycle to ultimate.

Table 16. Continued

Load (kips)	Cycle	West edge crack no.[a] and average crack widths (mm. except inches where noted)[b]					
		7	8	9	10	11	12
Slab 2[c]							
7.4[d]	1	0	0	0	0	0	0
9.4	1	0	0	0	0	0	0
9.4	3	0.1	0	0	0	0	0
9.4	4	0.1	0.1	0	0	0	0
9.4	11[f]	0.1	0.1	0	0	0	0
11.4 to 9.4	11	0.3	0.1	0.5	0	0	0
11.4	11	0.3	0.1	0.5	0	0	0
11.9	11	0.15"	0.1	0.5	1.5	0	0
12.4	11	0.15"	0.1	0.5	1.5	0.6	0
13.4	11	0.2"	0.1	0.5	1.5	0.6	0
15.4	11	0.3"	0.18"	0.5	0.28"	0.6	0
Final		0.2"	0.18"	0.15"	0.30"		0.1

Table 16. Continued

Load (kips)	Cycle	East edge crack number[a] and average crack widths (mm except inches where noted)[b]						
		1	2	3	4	5	6	7
Slab 2								
7.4[d]		0.3	0.2	0	0	0	0	0
9.4	1	0.7	0.2	0.2	0.1	0.2	0.1	0
9.4	3	0.7	0.2	0.2	0.1	0.2	0.1	0.1
9.4	4	0.7	0.2	0.2	0.1	0.2	0.1	0.1
9.4	11[f]	0.7	0.2	0.2	0.1	0.2	0.1	0.1
11.4 to 9.4	11	0.7	0.2	0.2	0.1	0.2	0.1	0.1
11.4	11	0.7	0.2	0.2	0.1	0.2	0.1	0.1
11.9	11	0.7	0.2	0.2	0.1	0.2	0.1	0.1
12.4	11	0.7	0.2	0.2	0.1	0.2	0.1	0.1
13.4	11	0.07"	0.2	0.2	0.1	0.2	0.1	0.1
15.4	11	0.11"	0.2	0.2	0.1	0.2	0.1	0.1
Final		0.20"	1.0	0.3	1.0	0.3	0.2	0.2

Table 16. Continued

Load (kips)	Cycle	East edge crack number[a] and average crack widths (mm except inches where noted)[b]						
		8	9	10	11	12	13	14
Slab 2								
7.4[d]	1	0	0	0	0	0	0	0
9.4	1	0	0	0	0	0	0	0
9.4	3	0.1	0	0	0	0	0	0
9.4	4	0.1	0	0	0	0	0	0
9.4	11[f]	0.1	0	0	0	0	0	0
11.4 to 9.4	11	0.1	0	0	0	0	0	0
11.4	11	0.1	0.1	0	0	0	0	0
11.9	11	0.2	0.1	0.2	0	0	0	0
12.4	11	0.2	0.1	0.2	0.1	0	0	0
13.4	11	0.2	0.16"	0.2	0.1	0.2	0	0
15.4	11	0.2"	0.32"	0.2	0.1	0.2	0	0
Final		0.25"	0.36"	0.4	0.6	0.5	0.6	0.4

Table 16. Continued

Load (kips)	Cycle	West end crack no.[a] and average crack widths (mm)[b]				East end crack no.[a] and average crack widths (mm)[b]						
		1	2	3	4	1	2	3	4	5	6	7
Slab 3												
5.4	1	.1	.1			.1						
6.4	1	.1	.3			.4	.2					
3.4	1	.2										
3.4	2			.1				.1				
6.4	3	.3	.4	.2		.3	.3					
6.4	4	.4	.4	.3		.3	.4					
6.4	8	.4	.4	.2		.4	.4					
5.4	11	.4	.4	.4		.4	.4					
7.9	11	.9	.9	.3		.9	.5		.04"			
8.4	11	.9	.1"	.2		.1"	.8		.1"			
7.7	11	.1"	.12"									
Final		.36"	.12"	.2	.12"	.45"	.15"	.1	.23"	.1"	.05"	.05"

Table 16. Continued

Load (kips)	Cycle	West edge crack no.[a] and average crack widths (mm)[b]								
		1	2	3	4	5	6	7	8	9
Slab 4										
6.4	1	.05	.05	.05						
7.4	1	.1		.1	.1	.1				
8.4	1		.1			.1				
9.4	1						.1			
9.4	2						.15			
9.4	3									
9.4	6		.2	.2			.2			
13.4	11					.5	.5	.3	.1	.1
14.4	11					.8				
5.7	11	.1	.2	.2	.1	.8	.5	.3	.1	.1
Slab 5										
5.4	1	.1	.1							
5.4	2									
5.4	3			.1	.1					
5.4	4		.1							
5.4	8									
5.4	10			.1		.1				
6.4	11		1.1				.1			
8.4	11				.2			.1		
Final		.1	.13"	2.0	.2"	.15"	.1	.3		

Table 16. Continued

Load (kips)	Cycle	East edge crack no.[a] and average crack widths (mm)[b]							
		1	2	3	4	5	6	7	8
Slab 4									
6.4	1	.05	.05	.05					
7.4	1	.1			.15	.1			
8.4	1						.1		
9.4	1							.1	
9.4	2				.25		.3		
9.4	3					.2			
9.4	6								
13.4	11					.6			
14.4	11							.2	
5.7	11	.1	.05	.05	5.1	.6	.3	6.4	.1
Slab 5									
5.4	1	.1	.1						
5.4	2			.1	.1				
5.4	3					.1			
5.4	4						.1		
5.4	8	.1						.1	
5.4	10								
6.4	11	.25	.1	.1	.1	.1		.1	.1
8.4	11		2.0			2.0			
Final		.2	.3"	.3	.3"	.25"	.1	1.5	.1

edge when the top surface cracking occurred. Along with the diagonal shear type cracking, it is important to note that the major diagonal edge cracks were accompanied by a relative vertical displacement.

The direction of the diagonal cracks in Figure 33 is of interest when compared to the corresponding direction for a diagonal shear crack in an ordinary reinforced concrete beam type specimen. For an ordinary reinforced concrete beam specimen subjected to a symmetrical pattern of two concentrated loads, the diagonal shear crack would propagate towards the load points. However, the diagonal shear cracks in the slabs tested propagated away from the load points. This is due to a difference in the shear distribution of the two types of structures. In a beam, the shear is zero between the load points and maximum between the load points and the end reactions. However, for these slabs, the reactions were greater between the load points creating more shear in this region and hence the diagonal crack propagating away from the load points, as dictated by the direction of the principal tensile stresses on a vertical plane at the slab edge.

The cracking of the slabs on the top surface in Figure 32 was commenserate with the type of loading applied. That is, the areas included by the four concentrated loads displaced downward and eventually broke away from the outer regions of the longer direction of the slabs, leaving a central region of each slab as the effective load-carrying element. This effective load-carrying section of each slab was approximately 8 feet wide spanning the 12-foot width of the slab. This effective load-carrying width, based on an average distance between major crack lines near the ultimate load, is shown in Figure 32. This effective width crack pattern

substantiates the yield-line distance, L", shown in Figure 6. The only difference between the theoretical crack pattern and the actual one is that the actual one is slightly curved. This curvature can be taken into account by integrating the work equations in yield line theory over the curved surface. However, for design, this is rather laborious and does not appreciably affect the answer.

Additional information regarding the crack patterns, substantiating the yield-line pattern concept, was gained by examining the crack pattern on the underneath side of each slab. After completion of each slab test, the steel decking was removed so that the complete crack patterns for the bottom fibers of concrete could be observed. See Figure 34.

Some cracks shown in Figure 34 were due to high stresses caused by moving the slabs after testing and thus must be discounted. The crack pattern of the underside of Slab 3, for example, must be discounted because the slab completely broke up when it was being handled after testing. However, the major cracks of Slab 3, as shown in Figure 34, were recorded as they propagated through the top as the slab was placed on the laboratory floor following testing. The crack pattern shown in Figure 34 for Slab 4 covers only one-half the slab because the steel decking was only removed for one-half the slab. The decking was difficult to remove because of the necessity to first separate the welded T-wires from the decking.

The basic underside crack patterns of the slabs seemed to substantiate the yield-line mechanism of Figure 6. It is observed that the cracking in Figure 34 generally propagates outward from the load points to the edges at about the location where the top cracking intersects the edge. This intersection occurs at ends of the effective width, L", (discussed above)

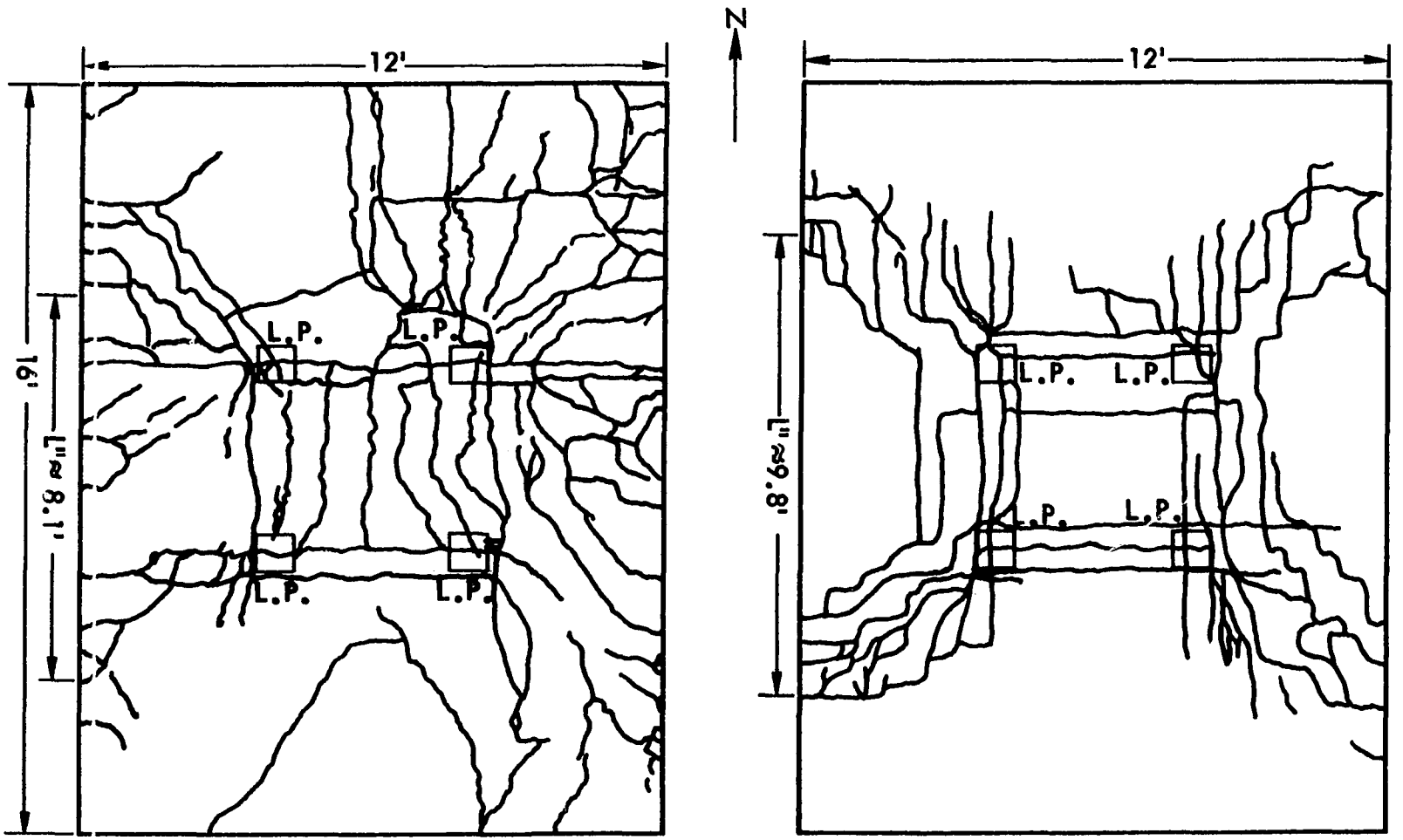

SLAB 1 SLAB 2

Figure 34. Crack patterns on bottom surface of concrete after removal of steel decking

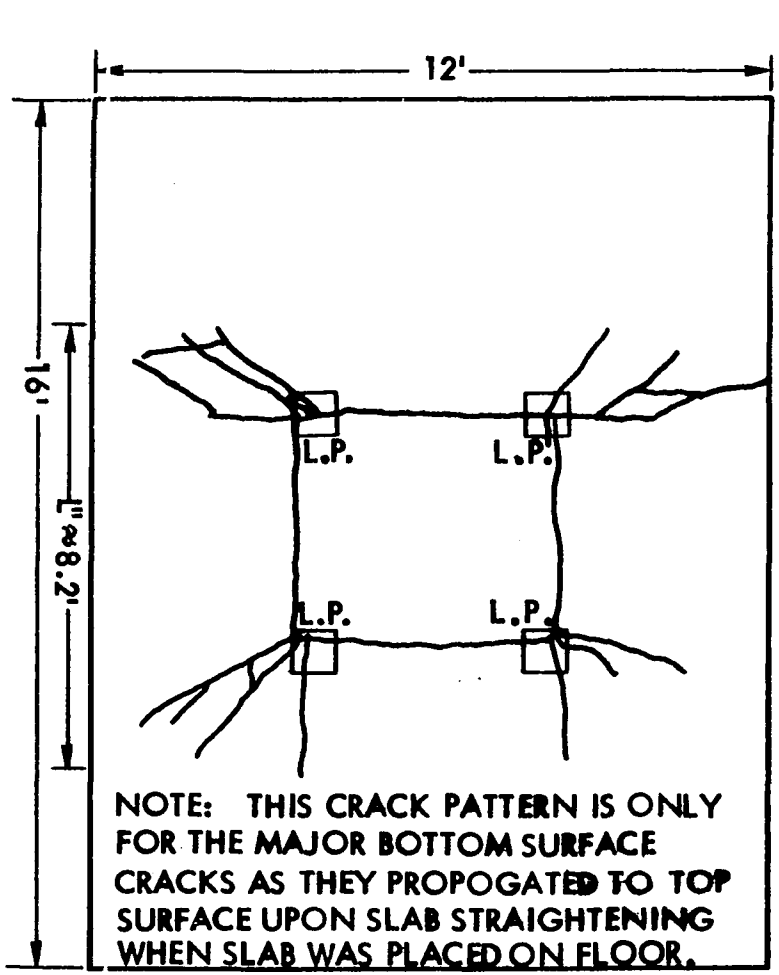

SLAB 3

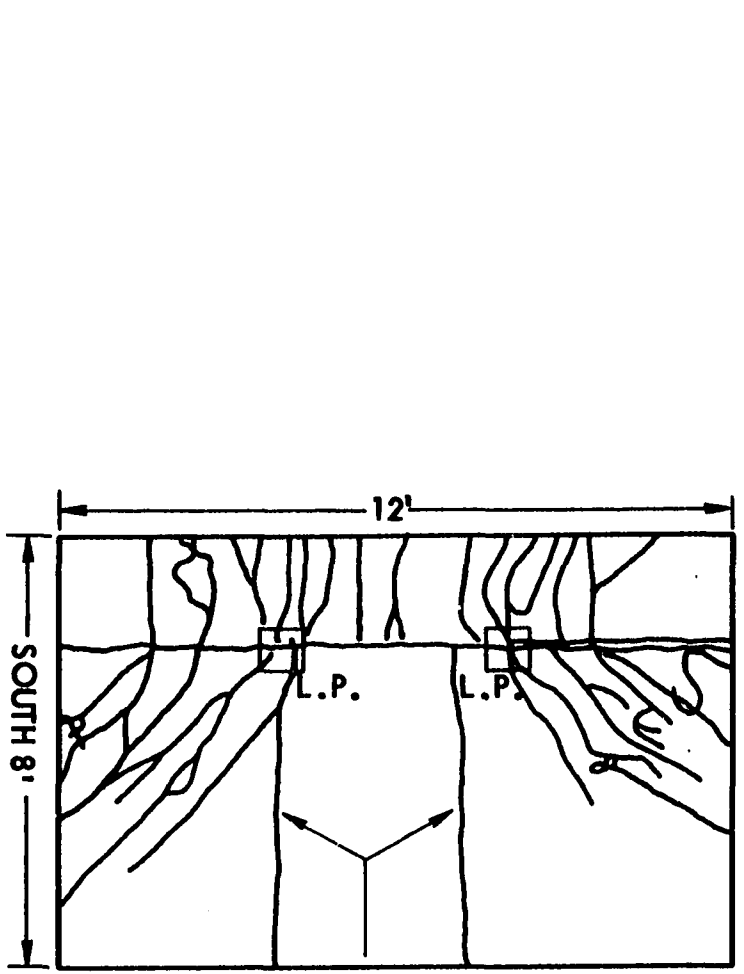

SLAB 4

NOTE: THESE TWO CRACKS WERE ATTRIBUTED TO SLAB OVERTURNING.

Figure 34. Continued

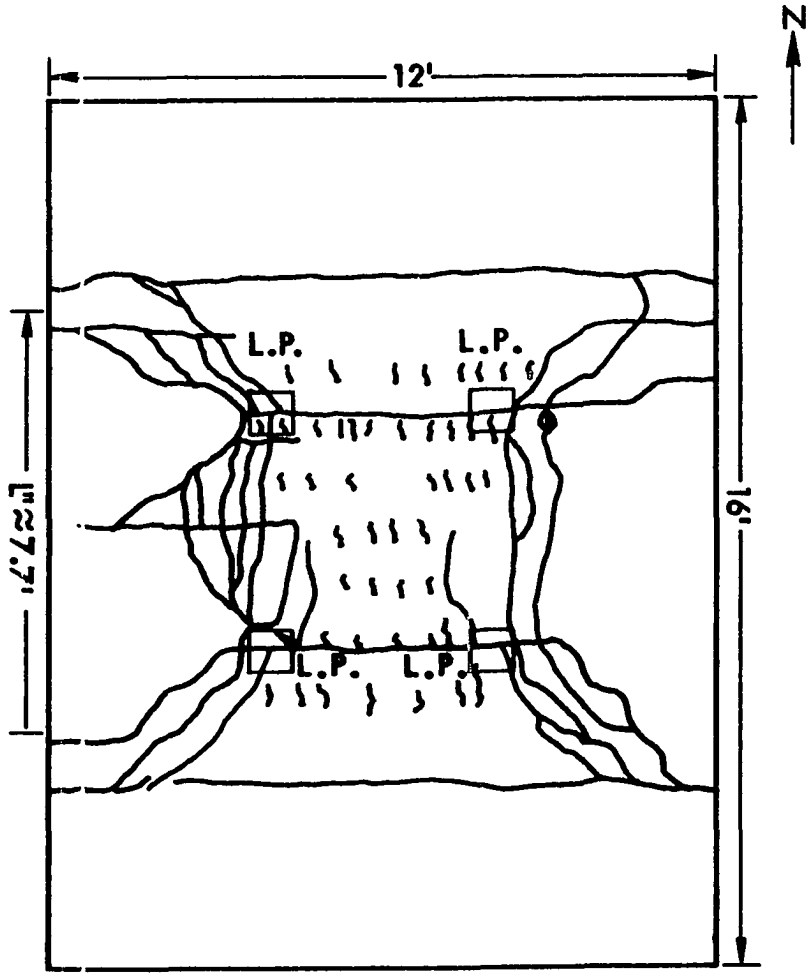

SLAB 5

NOTES:

1. THE DIMENSION TO EFFECTIVE LENGTH, L", IS SAME AS THAT GIVEN FOR TOP SURFACE CRACKING IN FIGURE 32.
2. CRACK PATTERN FOR SLAB 3 IS INCOMPLETE, CRACKS SHOWN ARE AS PENETRATED TOP FIBER AFTER SLAB REMOVAL.

Figure 34. Continued

for the top surface cracking. The same effective length, L", given in Figure 32 is indicated on each of the diagrams in Figure 34 for a comparison. The crack patterns of both the underneath and top surfaces indicate the mechanism of failure for these slabs. Thus, the mechanism in Figure 6 can be taken as the collapse mechanism for these slabs subjected to the four centrally-located concentrated loads.

Photographs of Failed Full-Scale Slab Specimens

Photographs showing the top surface cracking for each full-scale slab and example photographs of the edge cracking are shown in this section. All photographs were taken after testing of the slab was completed.

Figure 35 shows the test setup and the cracked top surface of Slab 1.

Figure 35. Test arrangement and overall view of Slab 1 after testing

Slab 1 was the only slab with corner tie-downs and consequently is the only slab with diagonal cracking across the corners. A more detailed close-up view of the top surface cracking for Slab 1 is shown in Figure 36. The figure is made of four photographs, each comprising approximately one-fourth of the top surface area. This explains the uneven matchup of the slab edges. The markings adjacent to each crack indicate the load on each jack in kips or the line pressure of the hydraulic system in ksi. The grid lines are at one foot intervals measured from the slab edges. The slight space in the center of Figure 36 is due to the overhead beam from which the photographs were taken. The 9-in. x 9-in. loading pads remain on the slab indicating the points of load application. The strain gage locations are quite visible in Figure 36. The cracks in the figure have been highlighted to help distinguish them from the strain gage wires.

The edge cracking of Slab 1 is shown in Figure 37. The tie-down assemblies at two corners are visible in the photograph. As can be seen, the diagonal shear cracking generally progresses upward and to the left for cracks to the left of centerline and upward and to the right for cracks to the right of centerline. The shear-bond end slip that occurred at ultimate failure of the slab occurred over the central eight and one-half feet between the major diagonal cracks.

Overall views of the top surface cracking that occurred for Slabs 2, 3, and 4 are shown, respectively, in Figures 38-40. Figure 40 combines two photographs showing the east and west halves of the top surface. It is observed that, the predominate top surface cracking is perpherial to the central four-foot area outlined by the four concentrated load points. Figure 39 clearly shows how the predominate negative moment cracks extend

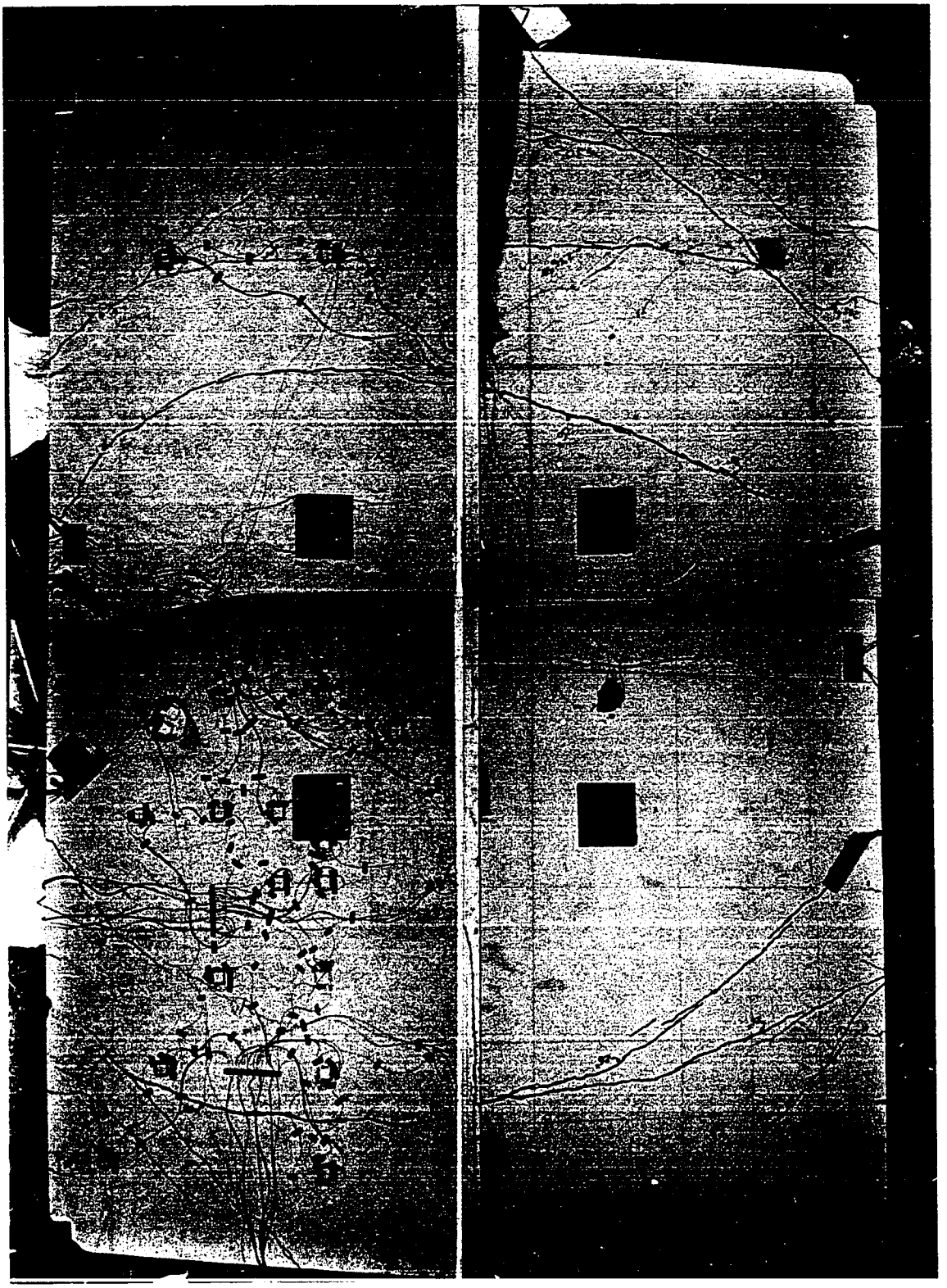

Figure 36. Composite photograph of top surface of Slab 1 after completion of test

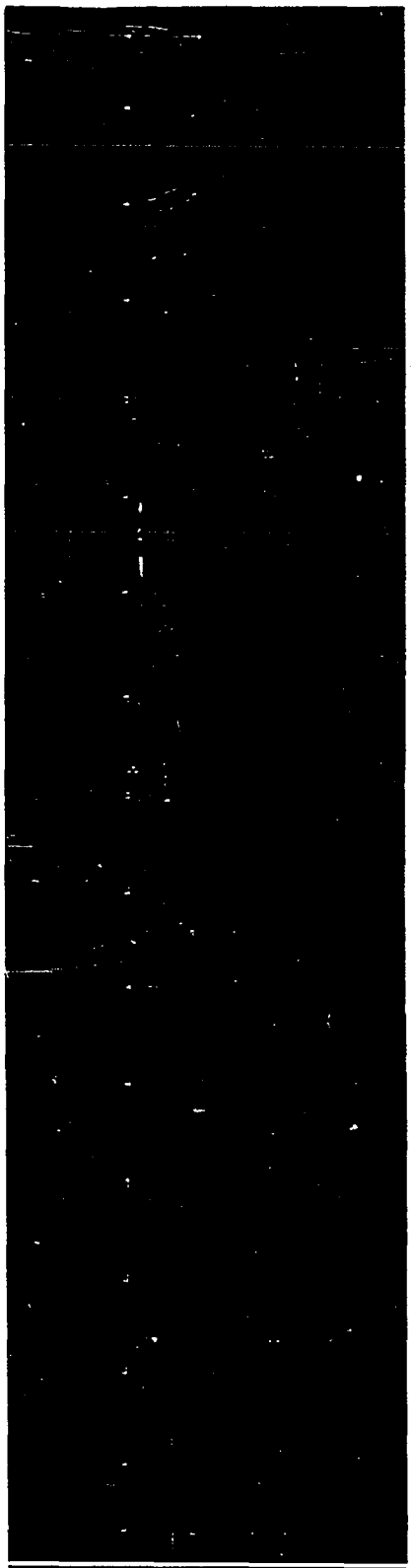

Figure 37. Composite photograph of east edge cracking of Slab 1

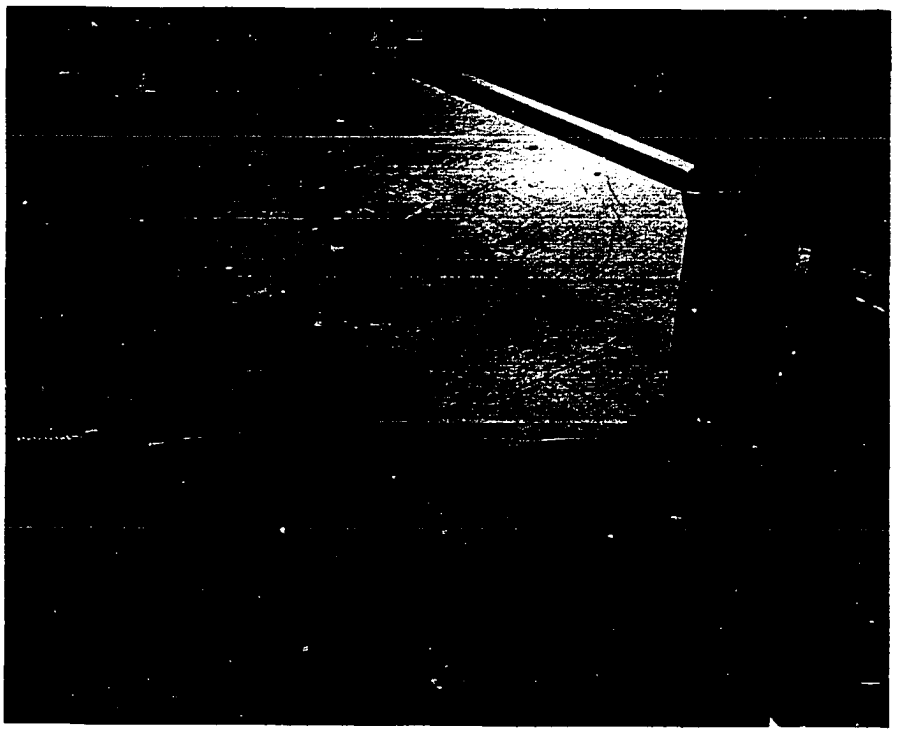

Figure 38. Overall view of top surface of Slab 2

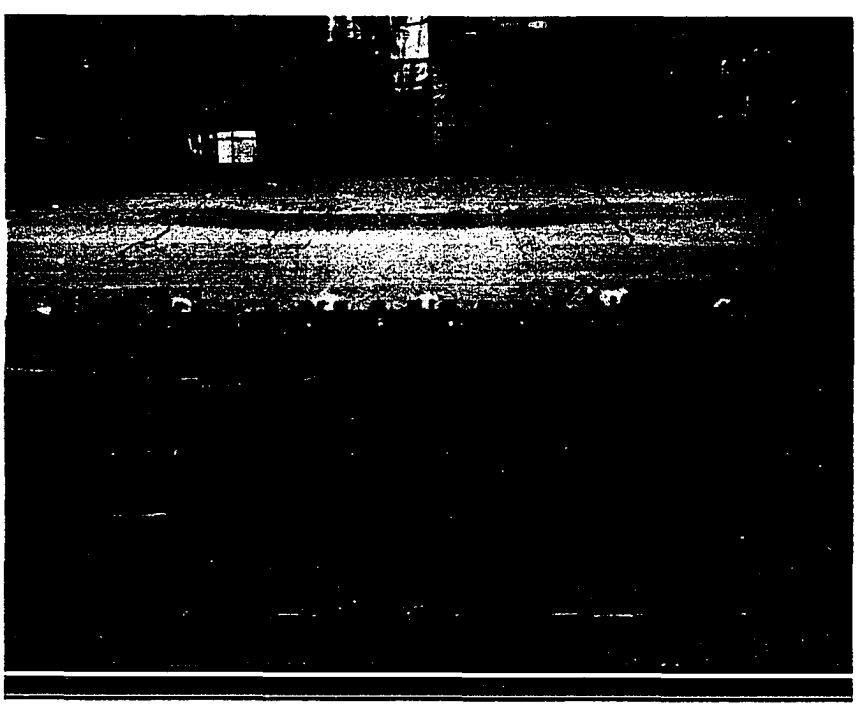

Figure 39. Top surface cracking of Slab 3 after testing

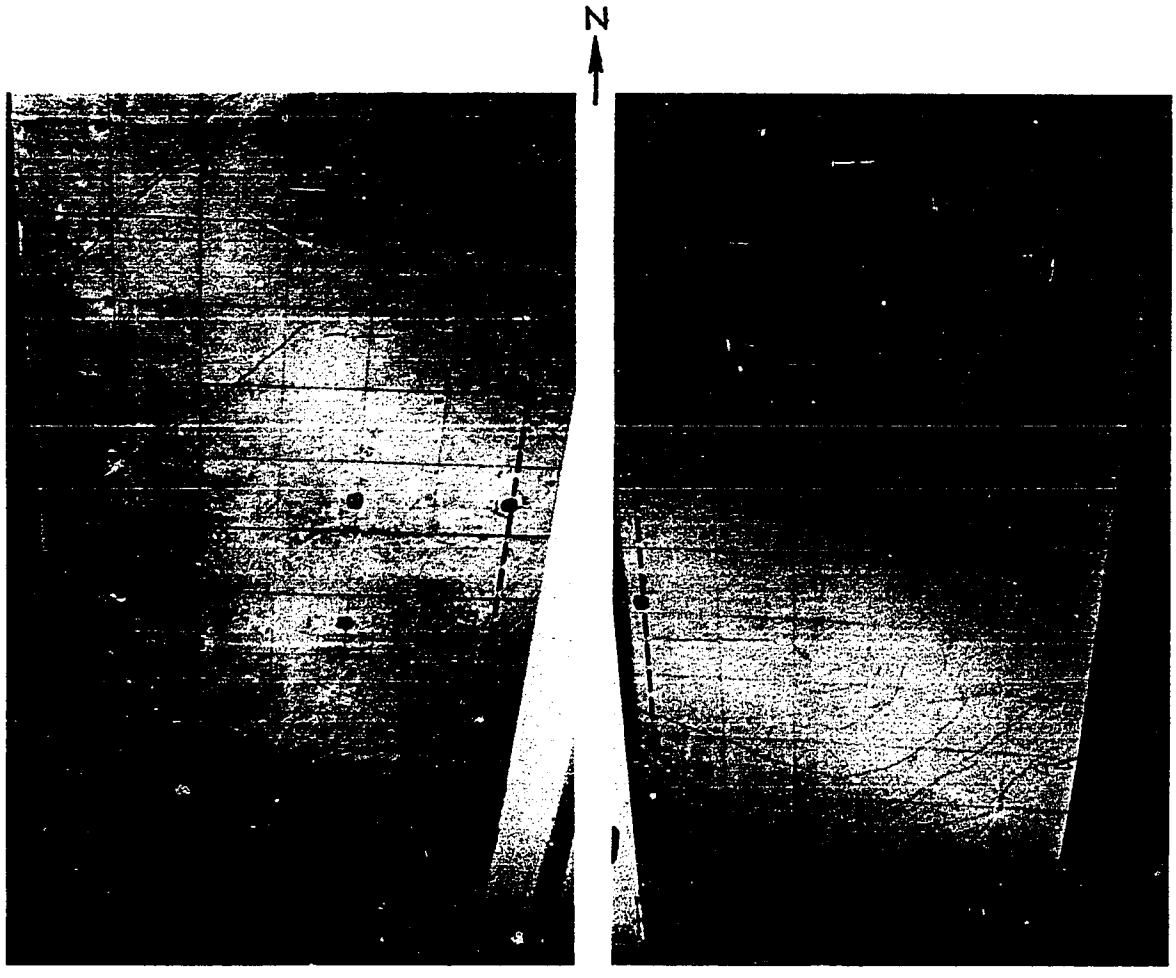

Figure 40. Composite of top surface views of east and west halves of Slab 4

across Slab 3, with the major portion of the deformed surface occuring between these cracks. This type of top surface cracking confirms the establishment of the effective width for the analysis of the slabs as shown by L" in Figure 6.

A close-up view of the diagonal edge cracking and end slip that

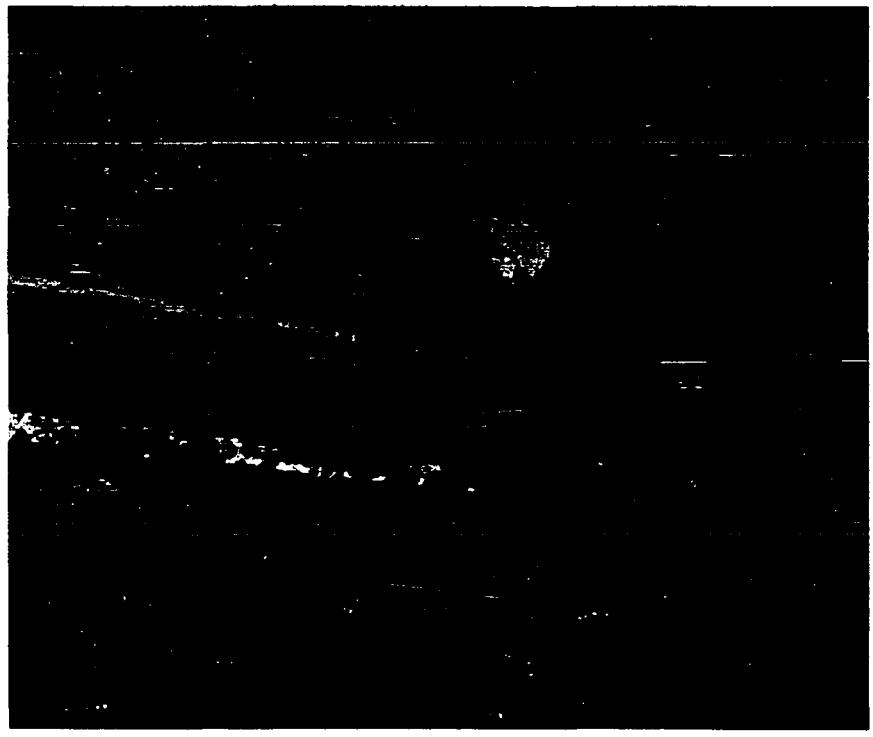

Figure 41. Close-up view of diagonal edge cracking and differential end slip that occurred on Slab 4

occurred for Slab 4 is shown in Figure 41. This cracking and end slip was typical of all five slabs tested. Note the significant difference in the amount of end slip that occurred to the left of the main diagonal crack between B and C in Figure 41 and to the right of this same crack. This indicates that the observed end slip occurred mainly over the central effective load-carrying element of the slab.

Slab 4 contained T-wires spot welded to the top corrugations. These T-wires served as the shear-transferring devices for the deck used in Slab 4. When ultimate shear-bond failure occurred, these spot welds pulled through the decking. The damaged areas where the welds failed can be seen in Figure 42 which shows the underside of Slab 4.

The top surface cracking of Slab 5 is shown in Figure 43. The cracking

Figure 42. Underside of Slab 4 showing locations where spot welds pulled through decking upon ultimate shear-bond failure

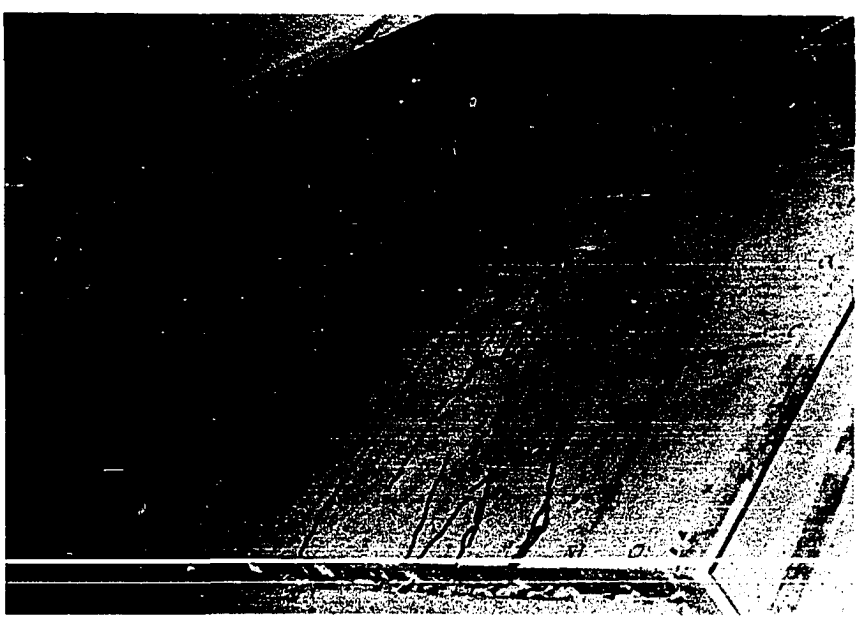

Figure 43. Top surface cracking of Slab 5

of this slab is quite similar to that which occurred for Slab 3 shown in Figure 39. Again, the cracking was peripheral in nature about the loaded area and essentially defines an effective width of the load-carrying portion of the slab.

A close-up view of one of the major edge shear failure cracks for Slab 5 is shown in 44. This figure highlights the typical vertical separation which accompanied the major shear cracks which propagated across all the slabs establishing the main load-carrying elements of the slabs. The vertical separation was only pronounced near the edge of the slab and dissipated as the cracking progressed inward as shown in Figure 44.

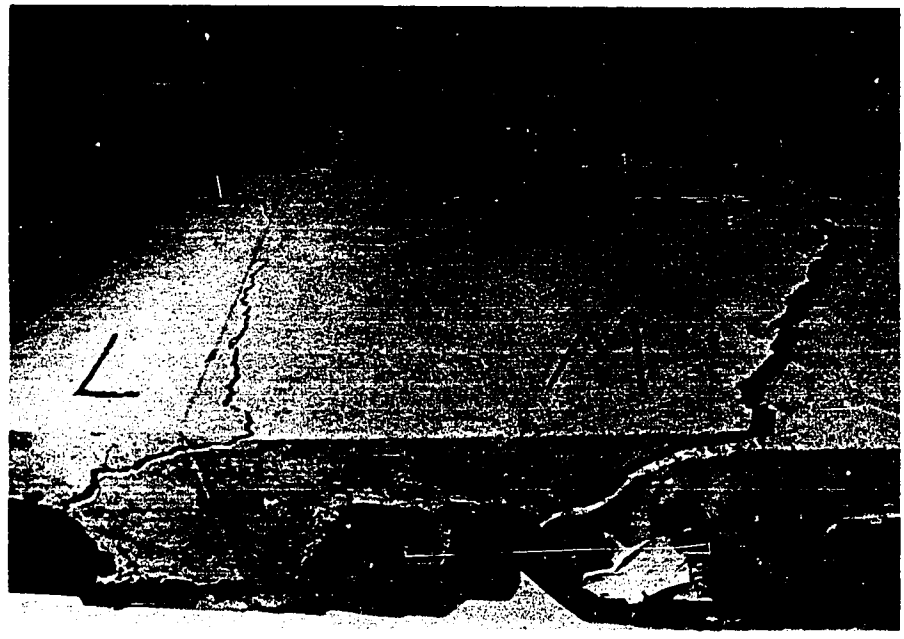

Figure 44. A major diagonal shear crack on Slab 5 indicating the vertical separation accompanying the major failure cracks of the slabs

Behavior as Observed by End Slippage

Failure of all five slabs was accompanied by end slip along most of the east and west edges. The end slip was characterized by a horizontal slippage between the steel deck and the concrete resulting in the concrete extending beyond the deck in a direction parallel to the deck corrugations. A close-up view of end slippage is shown by the photograph in Figure 41. This end slip was the primary characteristic of failure of the slabs and longitudinal slab element specimens.

The end slip that occurred along the east and west edges of the five two-way slab specimens was not uniform along each edge. In fact, no end slip was observed along the last two feet of these east and west edges, and there was no end slip along the north and south edges.

The variation of end slip that occurred along the east and west edges of four slabs is shown in Figure 45 based on measurements after test completion. The side of each slab demonstrating the larger slip values was the side on which primary shear-bond failure was observed to occur.

Of particular importance in Figure 45 is the distance over which most end slip occurred. Most slip occurred over the central region with a width about equal to the L"-length, representing the effective width of the slab as shown in Figure 6.

The interior or central slab sections demonstrated more horizontal movement than the exterior sections. This differential slip occurred at the diagonal cracking along the edge of the slab. This differential concrete movement in connection with the diagonal edge cracking is shown in Figure 41.

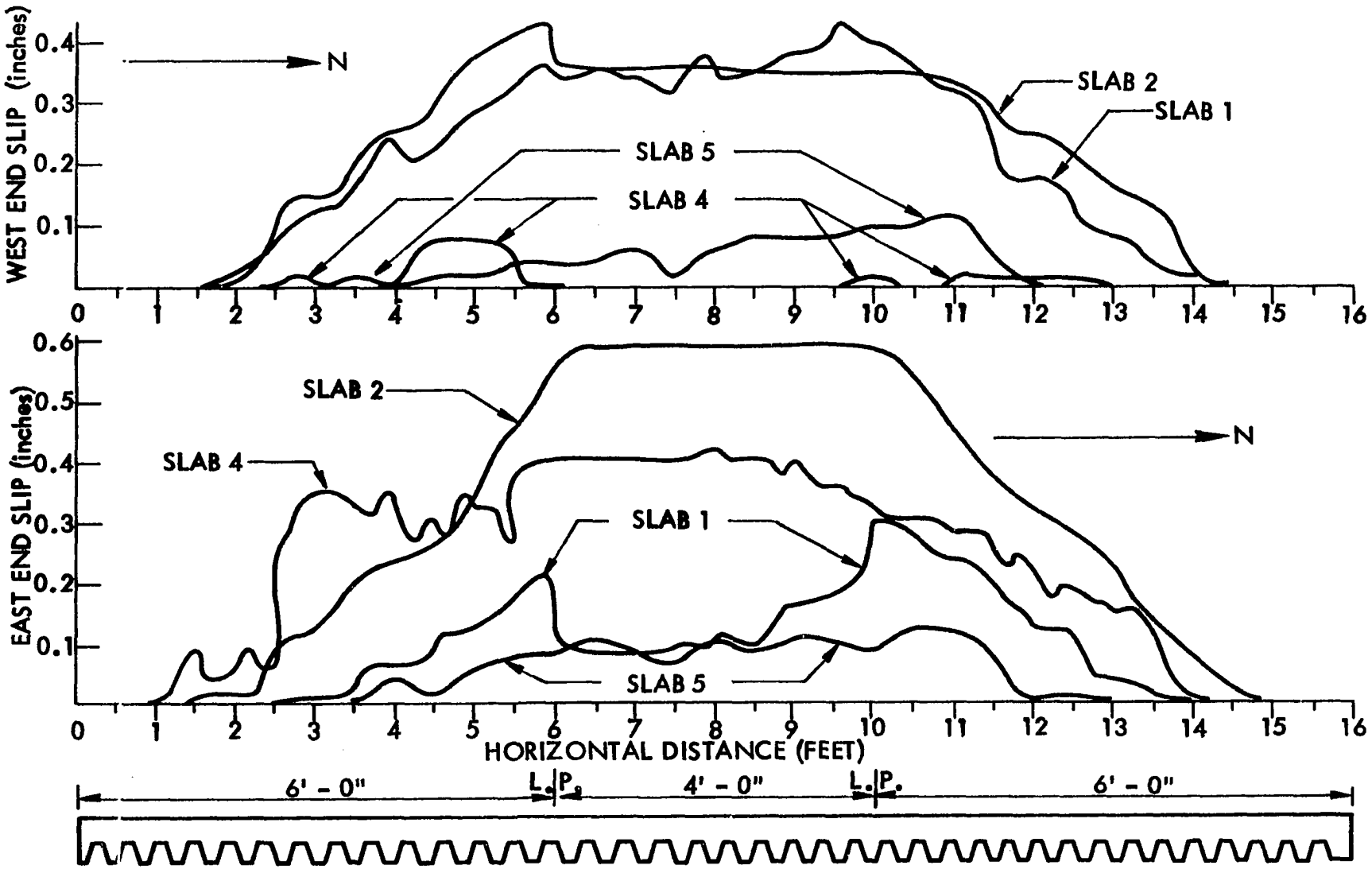

Figure 45. Distribution of final end slip along the east and west edges of slab specimens

Significant magnitudes of end slip at periodic stages during testing are noted in Table 14. First observable end slip occurred prior to the ultimate load in all five slab tests. The approximate loads at which first observable slip occurred were 11.4, 9.4, 7.9, 7.4, and 8.8 kips per load point for Slabs 1-5, respectively. Apparently, the addition of the WWF and, in the case of Slab 1, the corner tie-downs contributed to end-slip restraint.

It is of particular interest to compare end-slip behavior for the one-way longitudinal elements with end-slip behavior for the slab specimens. The first slip of the one-way longitudinal specimens occurred at ultimate load, whereas the slip for the slabs occurred prior to ultimate. This can be attributed to the neighboring elements of the slab in two-way action helping to restrain the slab from complete failure.

An interesting feature of the first observable slip is the state of stress of the steel-deck reinforcement. The longitudinal strains revealed that no strains in excess of the strain corresponding to the yield stress of the deck were observed prior to the first observable slip. This was true for all five slabs tested. Thus, the behavior of the deck at the time of first slip was elastic in all cases.

Reaction Distribution Along Supports

The distribution of the applied concentrated loading in the two-way slab tests is indicated by the vertical reaction measurements taken along the south and west supports of each slab. The reaction measurements were made with the ball-bearing-ball caster and roller transducers located as shown in Figures 23-27 for each slab. The measured reaction values

obtained for each transducer for the load levels of 1/4, 1/2, and 3/4 of ultimate and just prior to ultimate are shown in Figure 46.

The reaction values are plotted in Figure 46 for all slabs except Slab 4 (which exhibited erroneous readings). Only values due to applied loading are indicated. Reaction measurements were taken due to the slab weight at casting, shrinkage and creep changes, and shore removal effects, but these measurements were somewhat erratic and consequently were not included. The reliability of the reaction measurement at all stages of loading was checked by summing all load components, utilizing symmetry where no transducers existed, to compare with the total downward force. These summations checked equilibrium with a maximum error of only 6 percent except one loading case of Slab 5 which had a 10 percent error.

The plotted points in Figure 46 include only the actual measured locations along the south and west supports for each slab. The furthest left measured reaction along the west side of Slab 1 is the corner tie-down force which was plotted as the average of the three instrumented tie-down assemblies. The tie-down force is plotted as a negative value since it acted downward, whereas the upward reactions were plotted as positive values. The other negative values in Figure 46 occurred on the south side at a load just prior to ultimate and indicate a lifting off of the previously applied deadload force on these particular transducers. In fact, complete lift off of Slab 3 occurred along the south edge as noted in Table 14 and is is reflected by the corresponding negative reaction values in Figure 46.

Note in Figure 46 that at the lower levels prior to cracking at 3.4, 5.4, and 7.4 kip levels the west reaction distributions are generally trapezoidal with small peaks in line with the concentrated load points. These

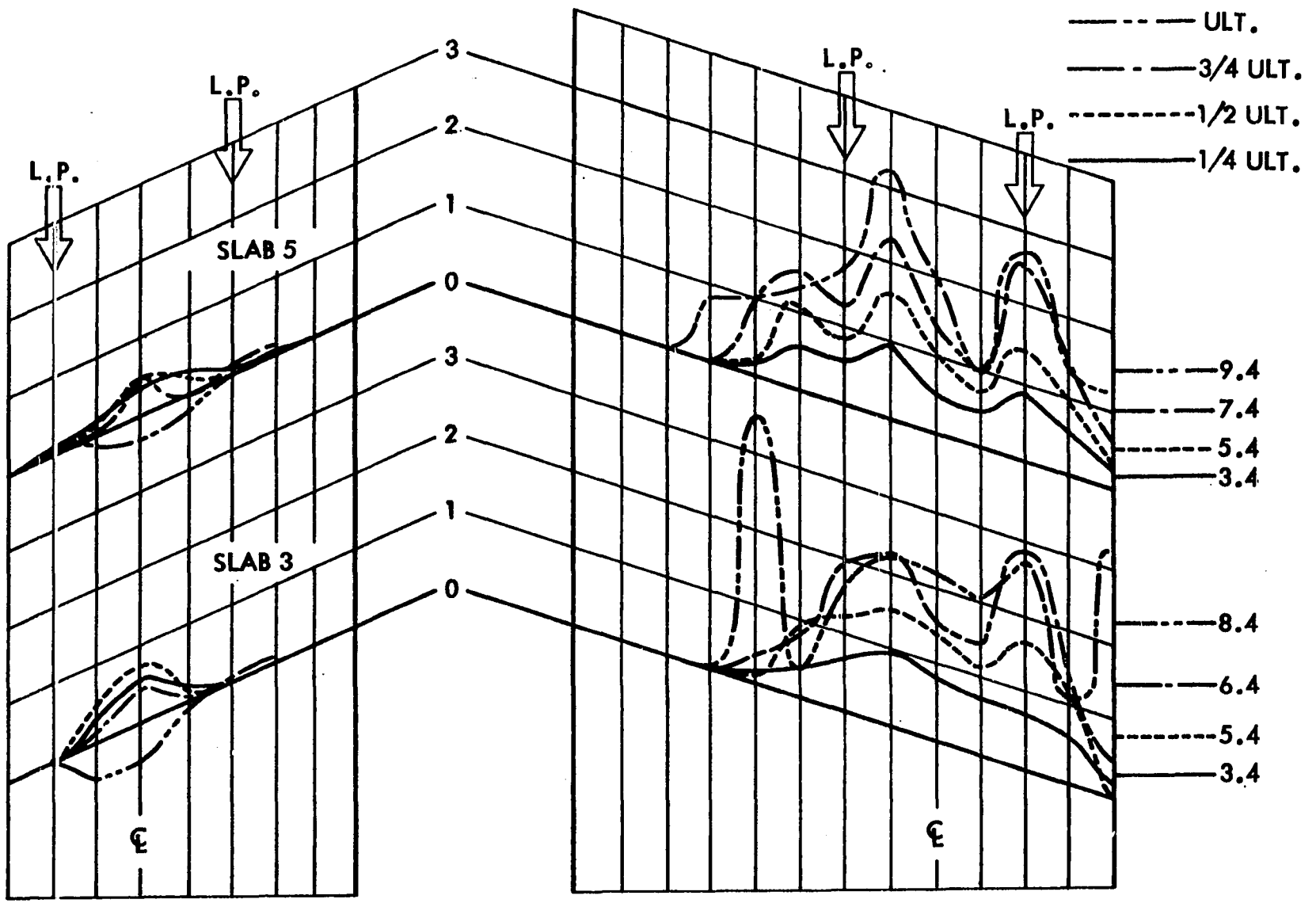
L.P.
L.P.
L.P.
SLAB 5
SLAB 3
℄
℄
3
2
1
0
3
2
1
0
ULT.
3/4 ULT.
1/2 ULT.
1/4 ULT.
9.4
7.4
5.4
3.4
8.4
6.4
5.4
3.4

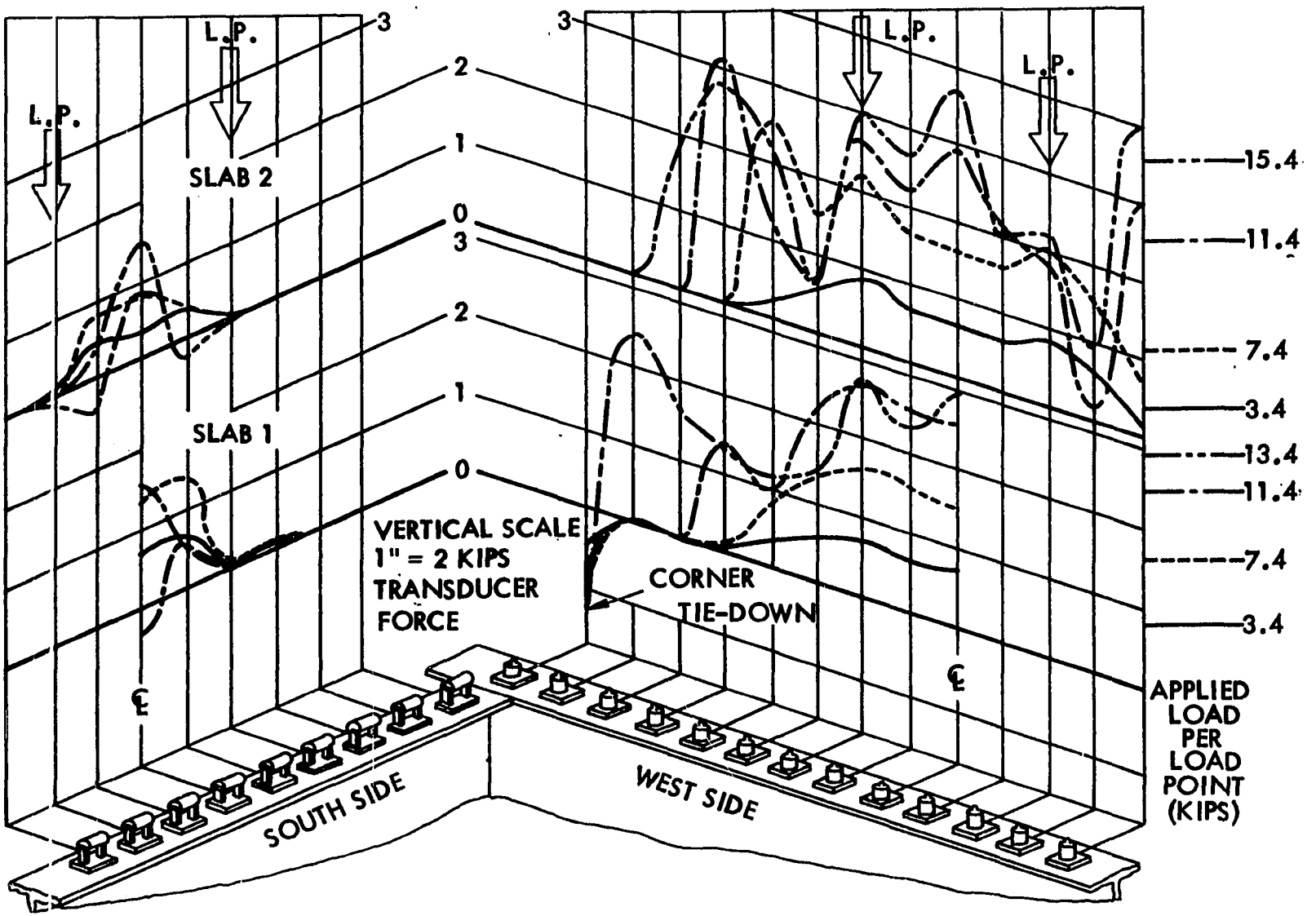

Figure 46. Distribution of reactive forces along the south and west supports for Slabs 1, 2, 3, and 5

lower level distributions agree with the behavior of a normal orthotropic slab subjected to concentrated loading.

The shape of the reaction distribution curve along the west edge becomes somewhat erratic at 3/4 of ultimate load and above, due to excessive cracking of the slabs. The distribution of the reactive forces for these higher load levels generally demonstrated a higher degree of slab efficiency since the curves shift their peak points toward the north and south directions. This change can be attributed to each slab being capable of transmitting shear forces laterally in the north-south directions once the central regions have undergone a considerable load.

The west reaction distributions near ultimate generally indicate an effective width of the central main load carrying element of the slabs in agreement with the L" distance shown in Figure 6. The reaction values along the south support indicate the ability of the slabs to transmit shear in the direction transverse to the corrugations or the so-called "weak" direction. These reaction values occur only between load points due to corner uplift (except Slab 1 where corner uplift was due only to extension of tie-down assemblies). Note that generally the reaction values at or near ultimate were significantly less than the initial loading ranges. This is in line with the slab behavior of tending to dish downward causing a lift-off at the corners inward along each side so that the shorter south side tended to have less reaction near ultimate. Slab 2 had significantly more transverse reinforcing steel, and thus was able to sustain a higher ultimate load and allow more force distribution to the south support at ultimate.

The relationship between applied load on the slab and percent of load distributed to the south and west edges is shown in Figure 47. Note

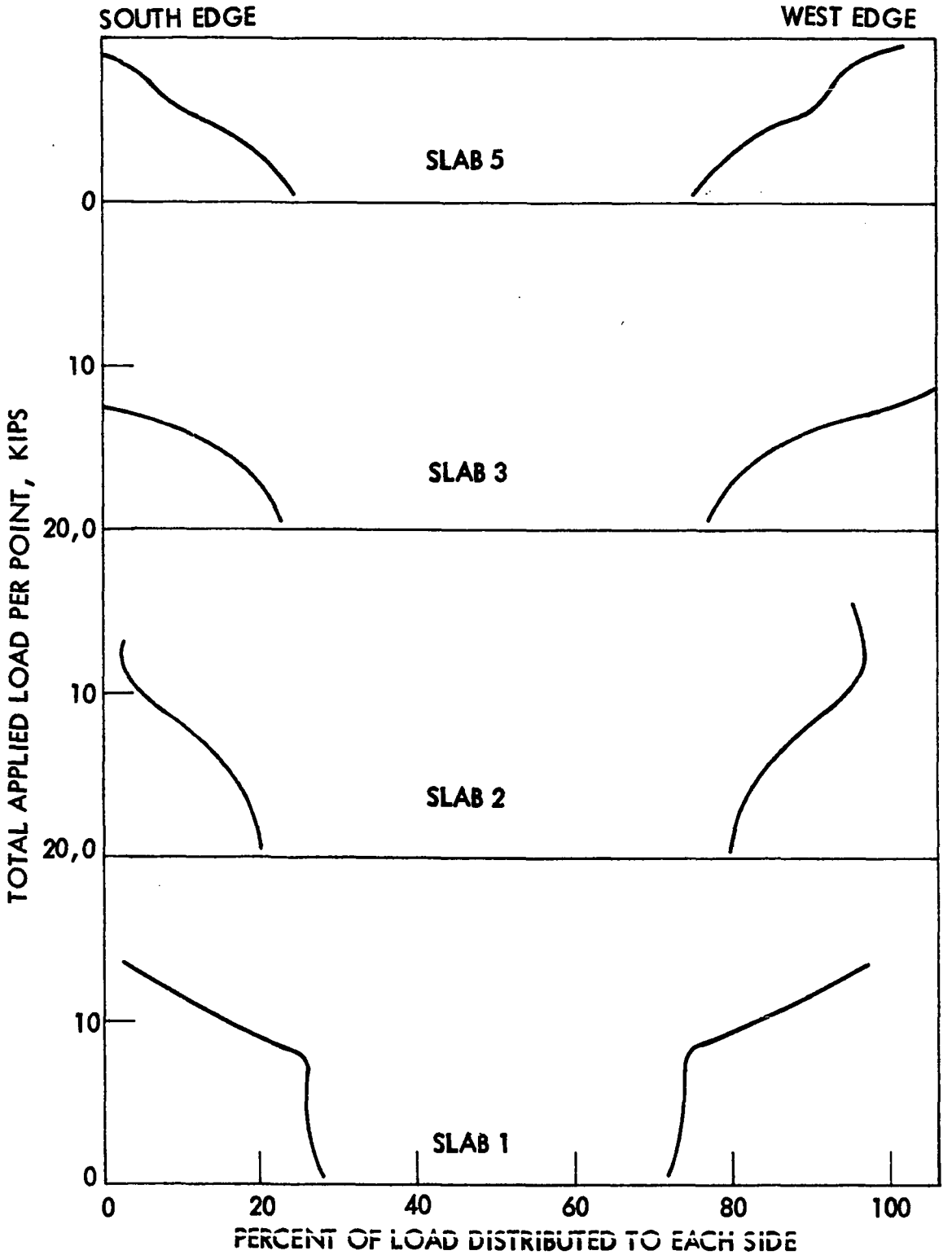

Figure 47. Percentage of applied load transmitted to each reaction support as loading increases for Slabs 1, 2, 3, and 5

that at the very beginning of load application all slabs showed about 78 percent of the load transmitted to the west side in the so-called "strong" direction, except Slab 1 which indicated about 72 percent due to corner tie-downs. The sharp bend in the curves for Slab 1 can be attributed to the corner cracking across the top surface of the slab thus reducing the effectiveness of the corner tie-downs on the reaction distribution. It is noteworthy that all slabs near ultimate had a west edge force summation of at least 97 percent of the total force being carried in one-way action in the direction parallel to the corrugations. The west edge values of over 100 percent and the south edge values less than zero is due to the negative reaction value summation for the south edge resulting from the relieving of the initial slab dead load on this edge. Figure 47 shows that the maximum load on the south support beam does not occur at ultimate as one might expect, but actually occurs somewhere around the design load for all slabs, except possibly Slab 2.

Strain and Deflection Behavior

Various strains and deflections for each of the full-scale, two-way slabs were plotted at intervals to show the deflection contour and strain field distributions at certain intervals of loading. Figures 48-52 show these strain and deflection distributions. Each figure is divided into four quadrants. The northwest, southwest, southeast, and northeast quadrants show, respectively, the following quantities:

1. longitudinal steel strain parallel to steel-deck corrugations (y direction) taken at bottom corrugation,
2. longitudinal concrete strain parallel to steel-deck corrugations

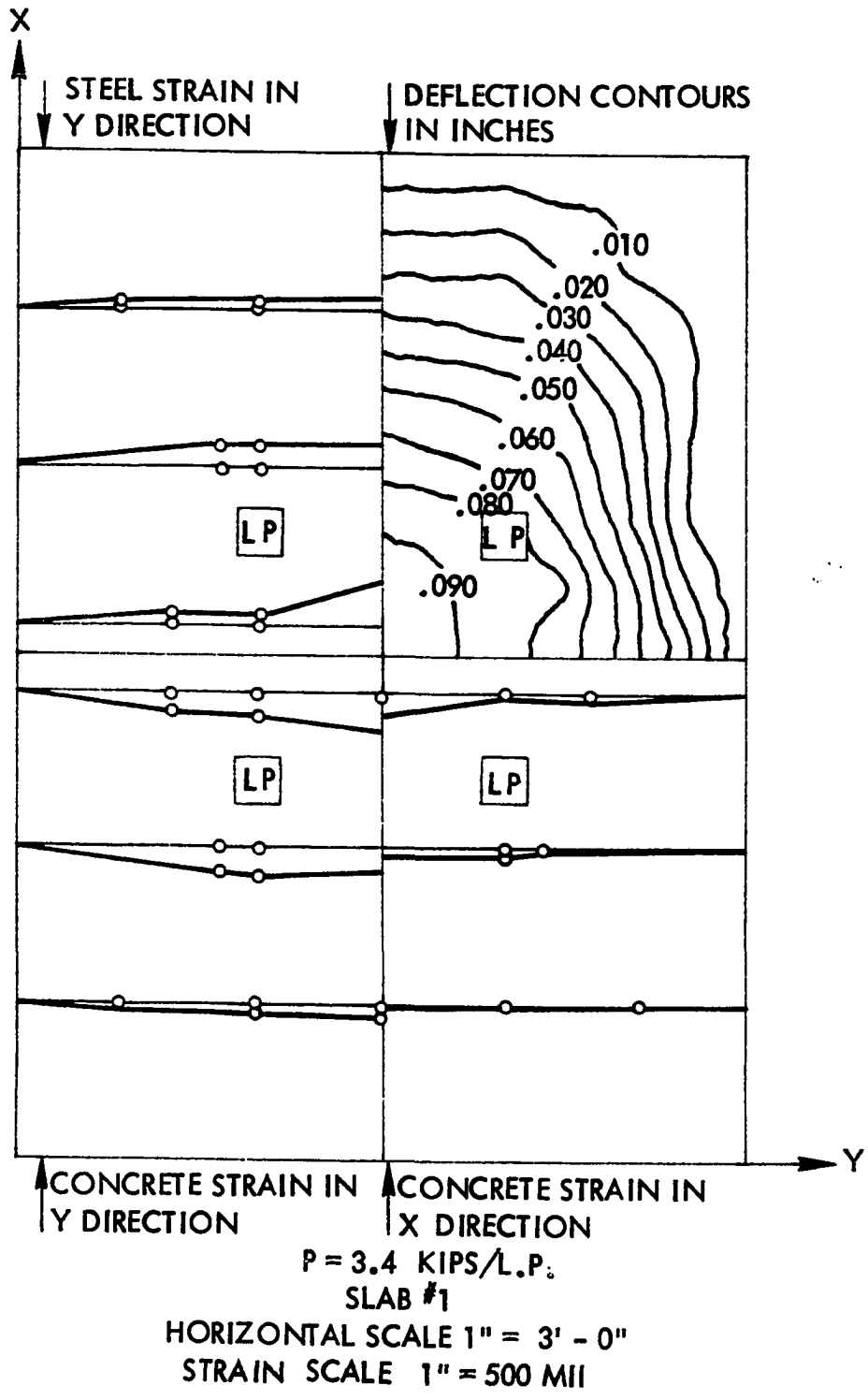

Figure 48. Measured strain and deflection distributions for Slab 1

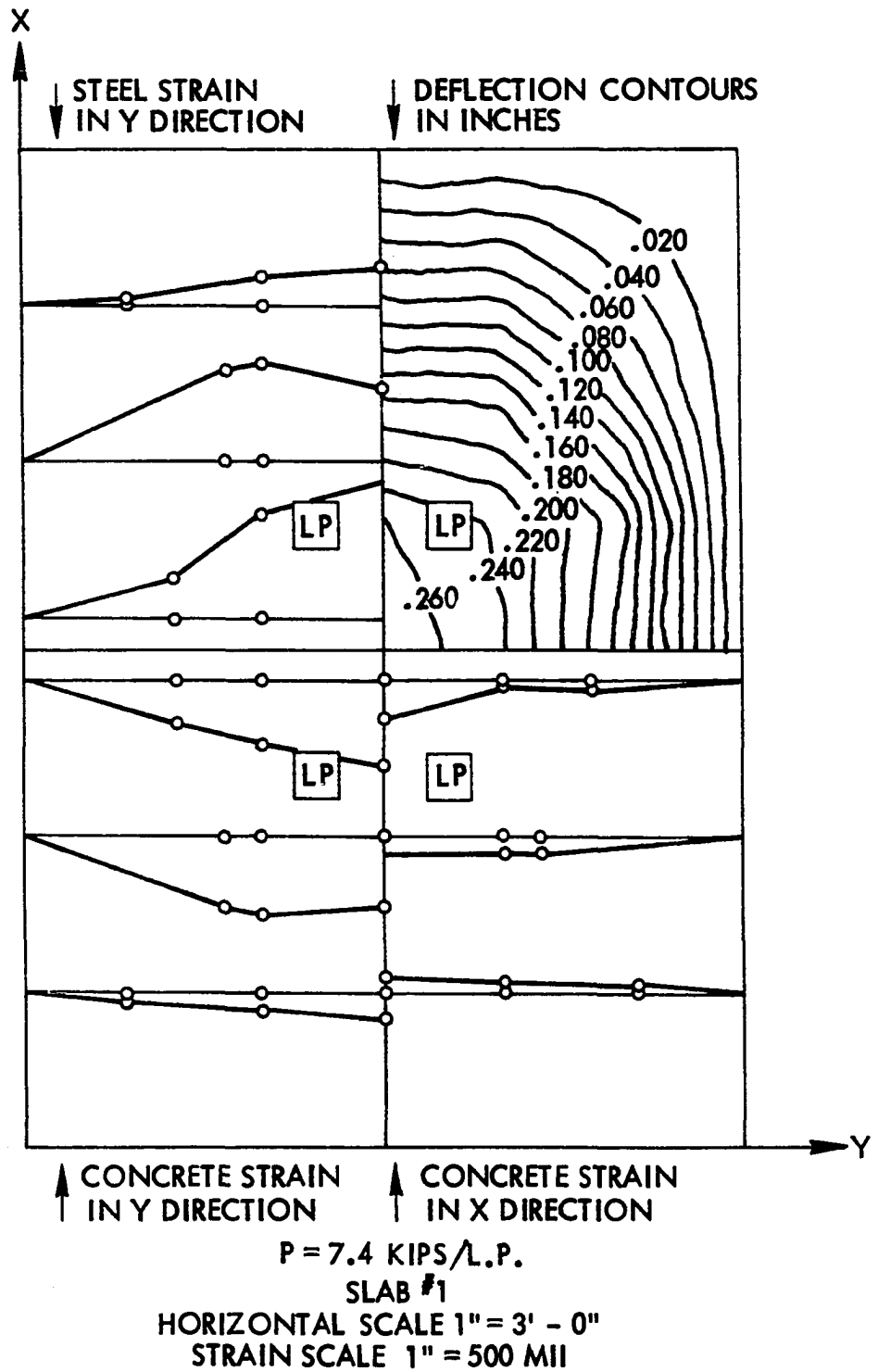

Figure 48. Continued

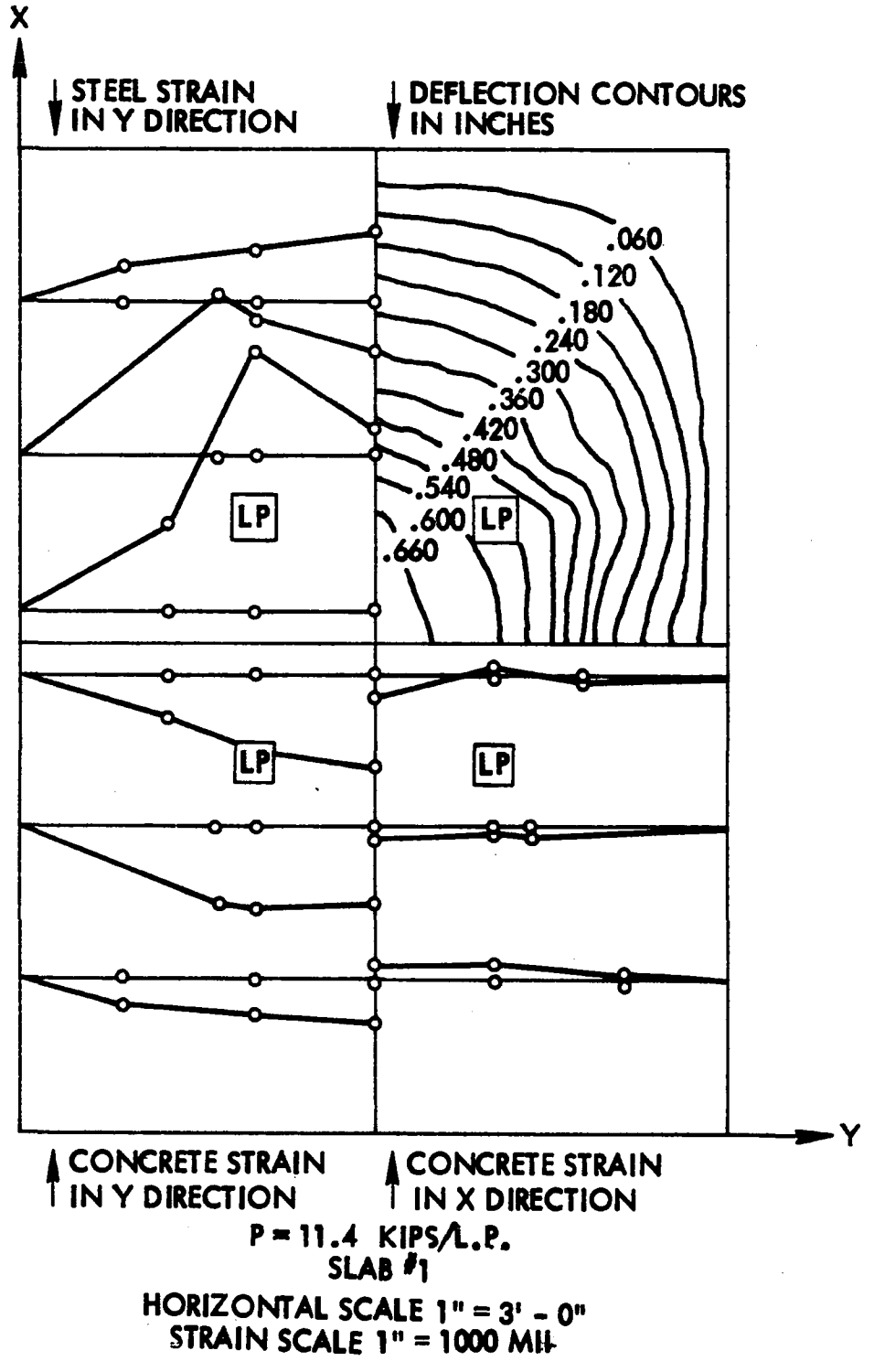

Figure 48. Continued

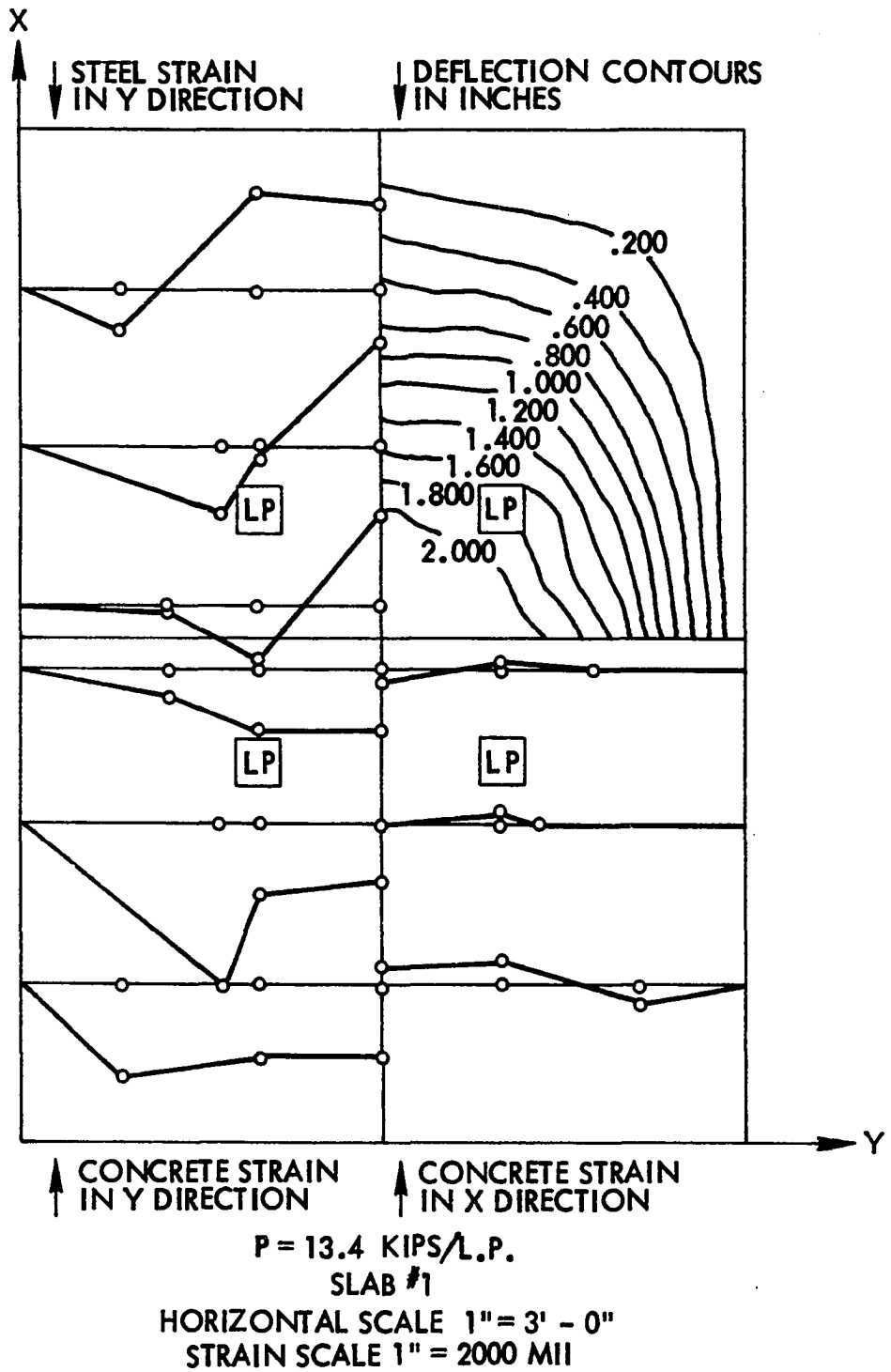

Figure 48. Continued

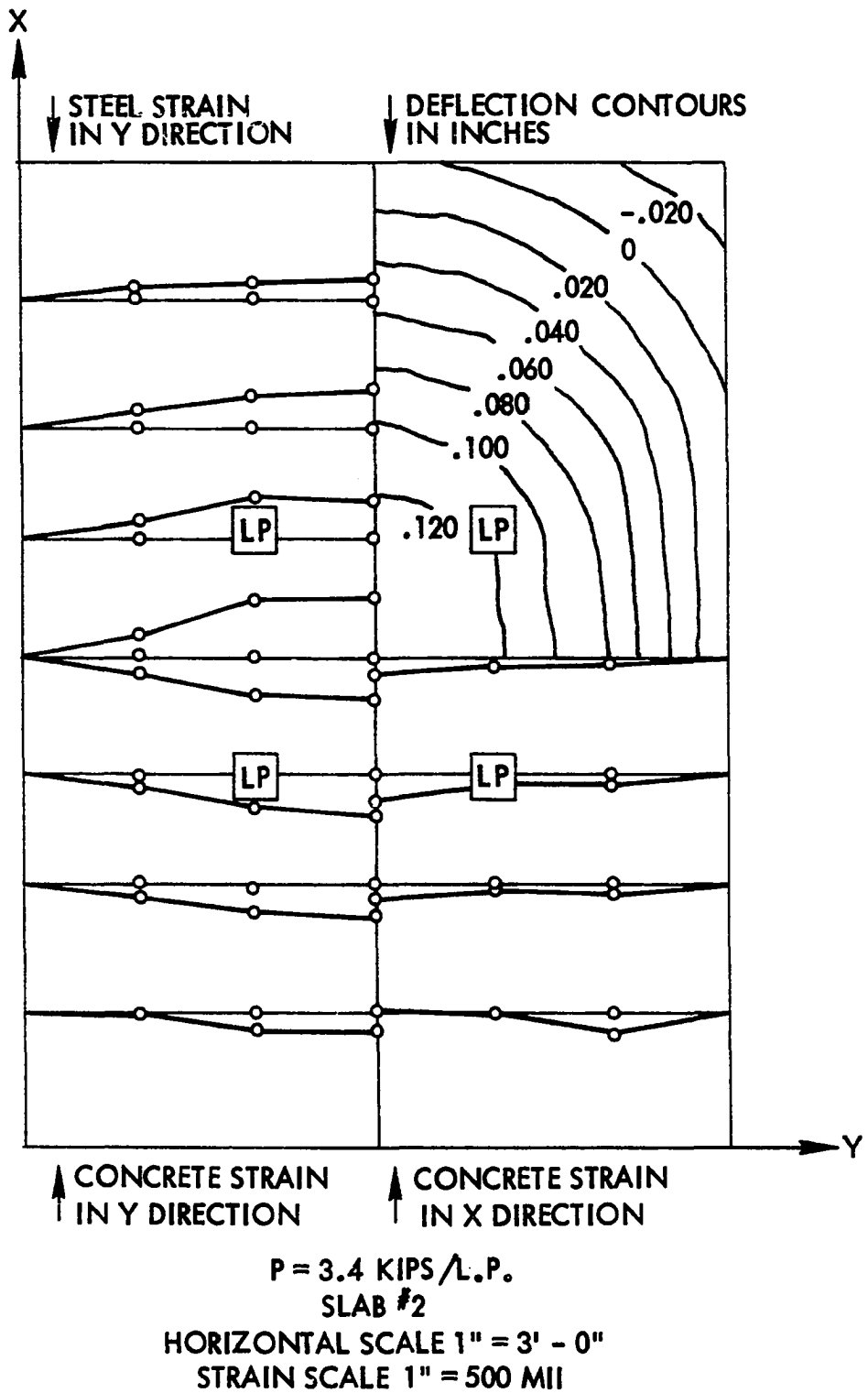

Figure 49. Measured strain and deflection distributions for Slab 2

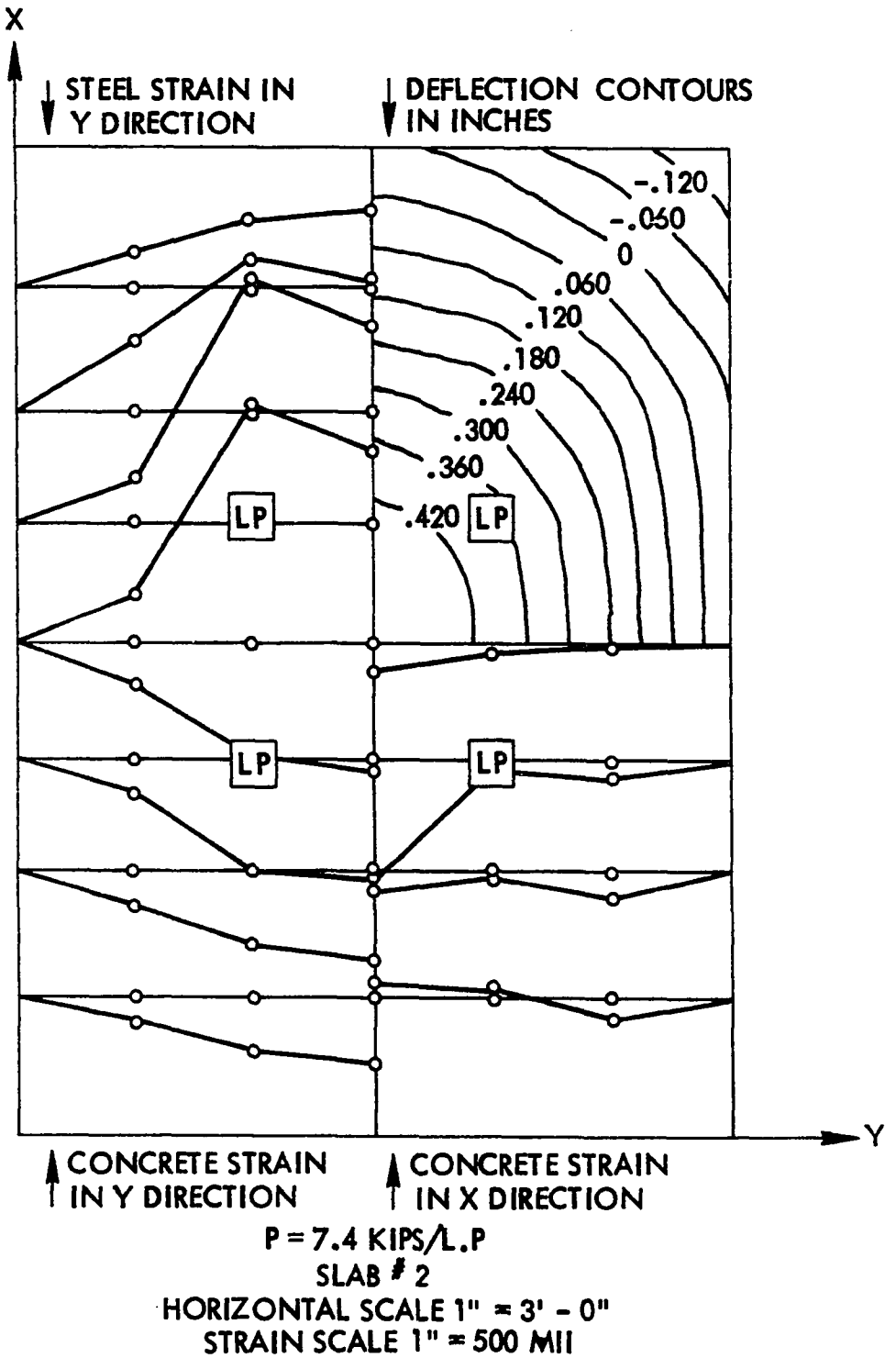

Figure 49. Continued

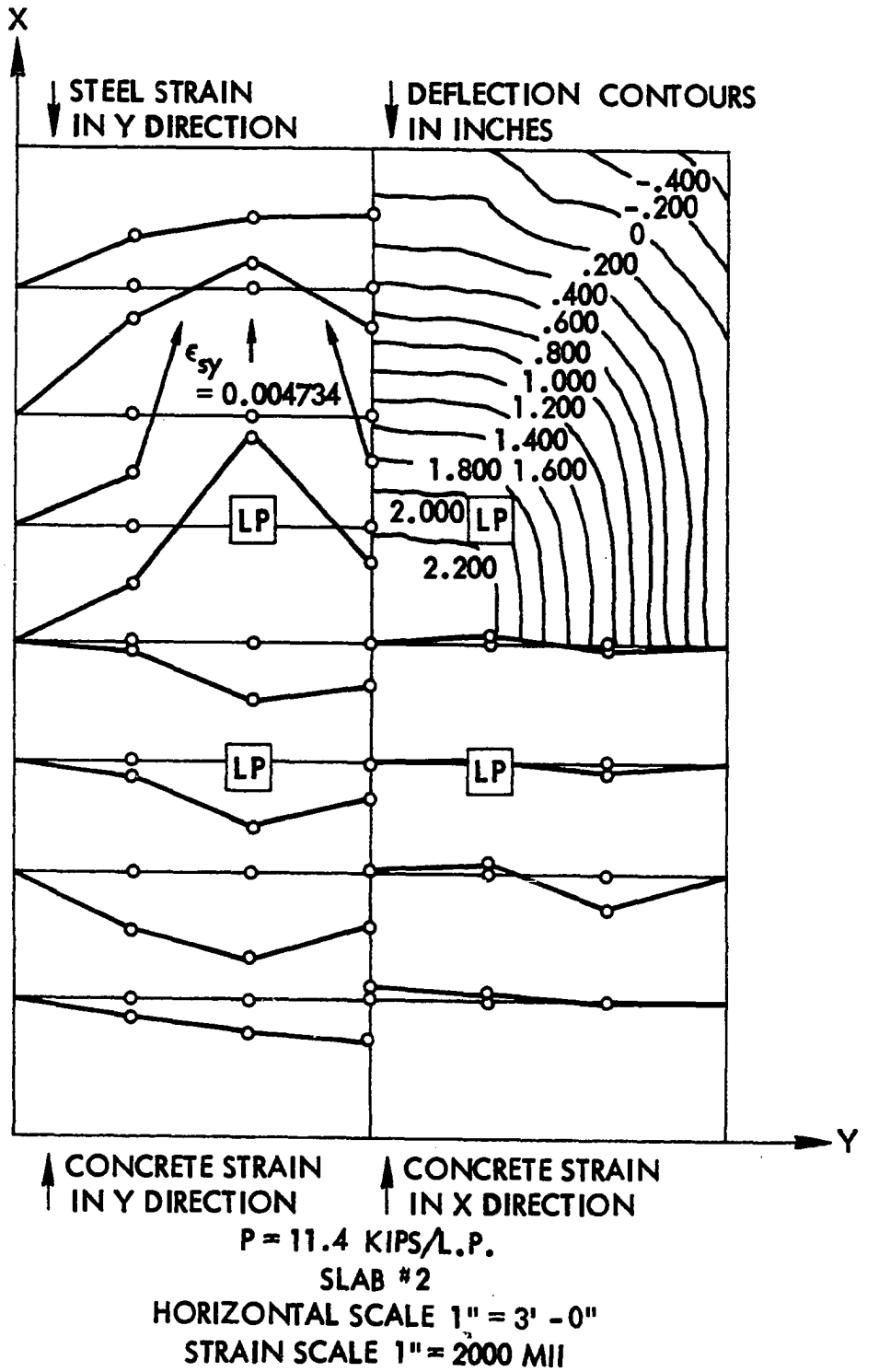

Figure 49. Continued

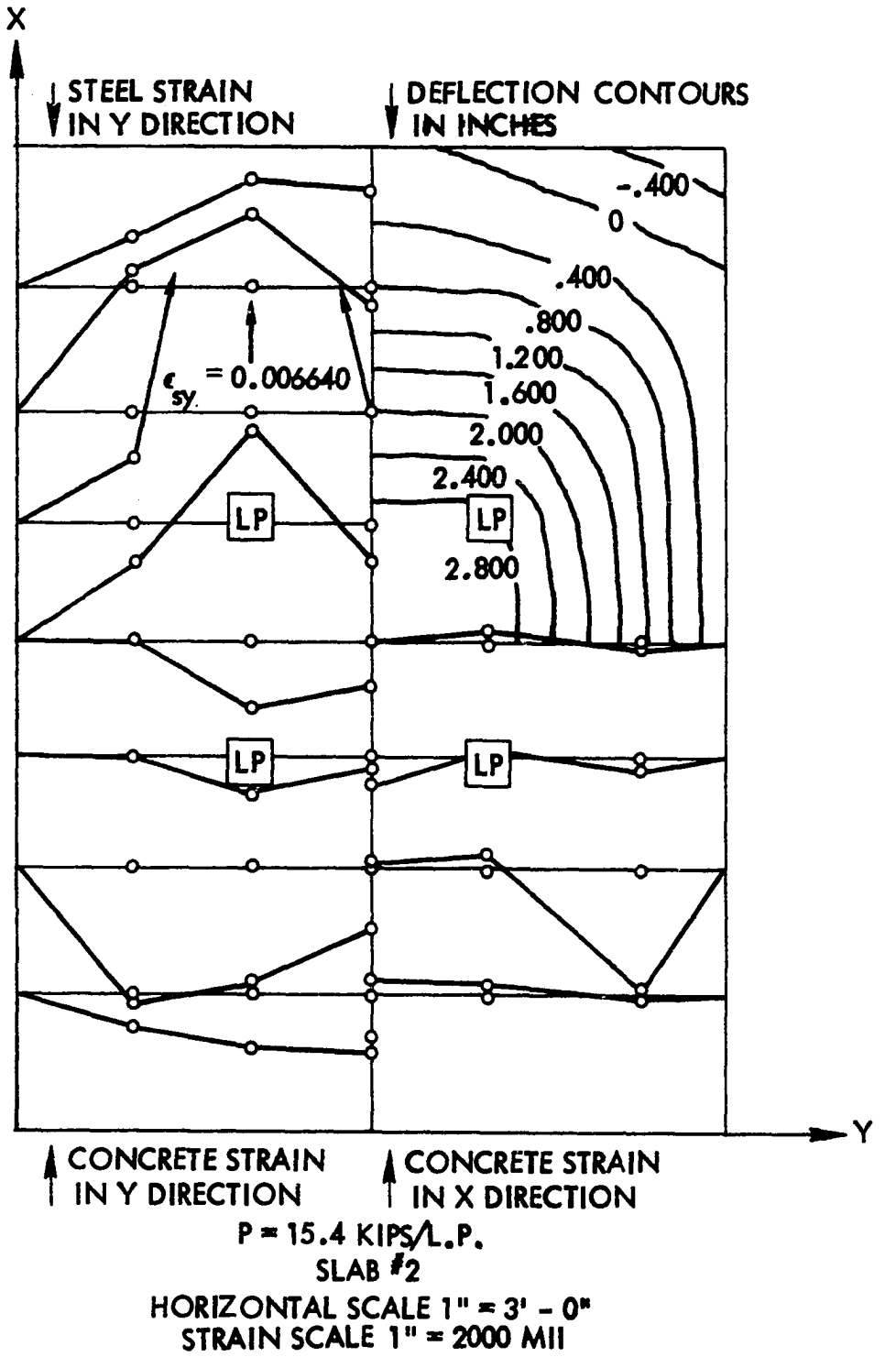

Figure 49. Continued

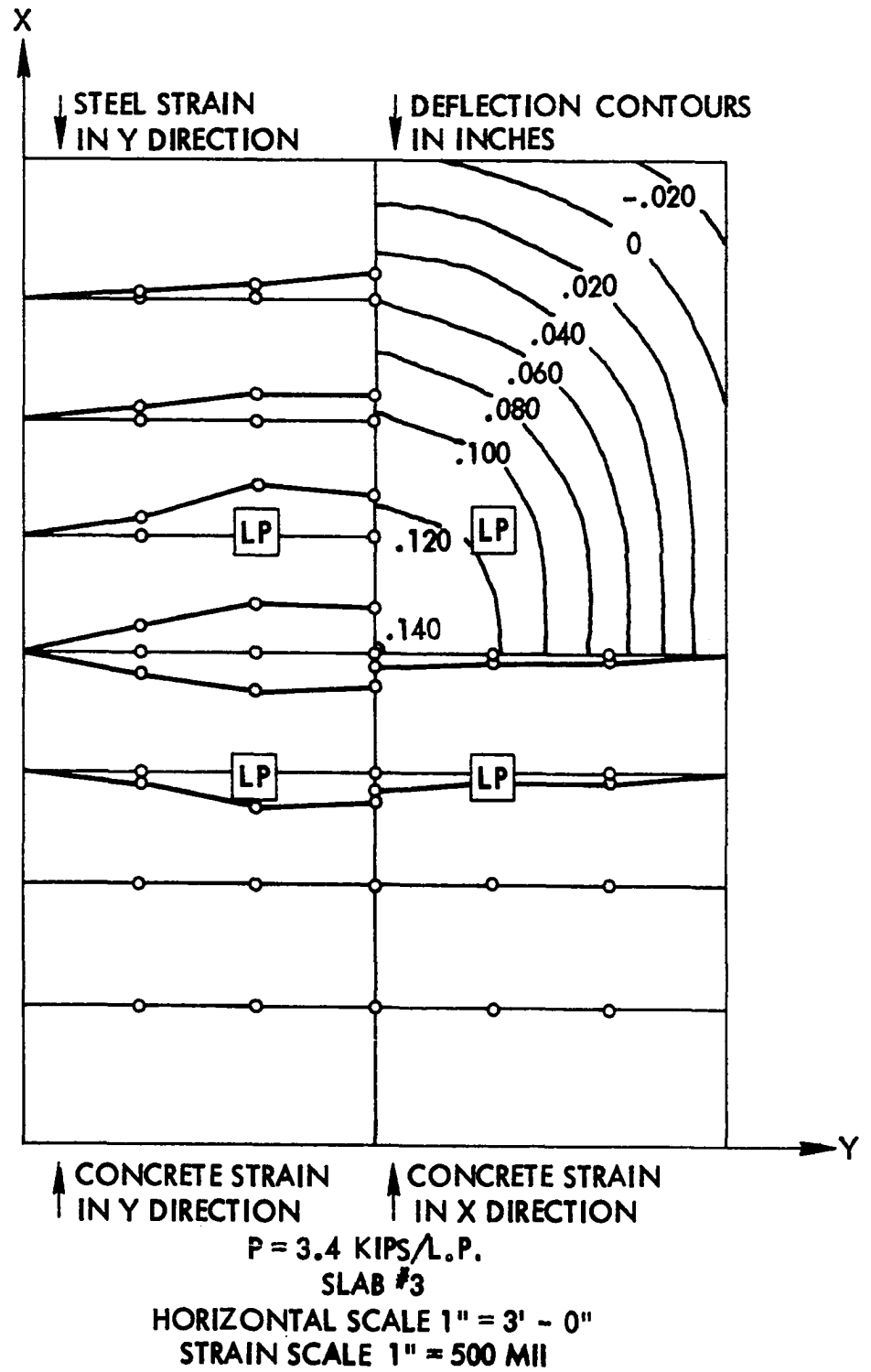

Figure 50. Measured strain and deflection distributions for Slab 3

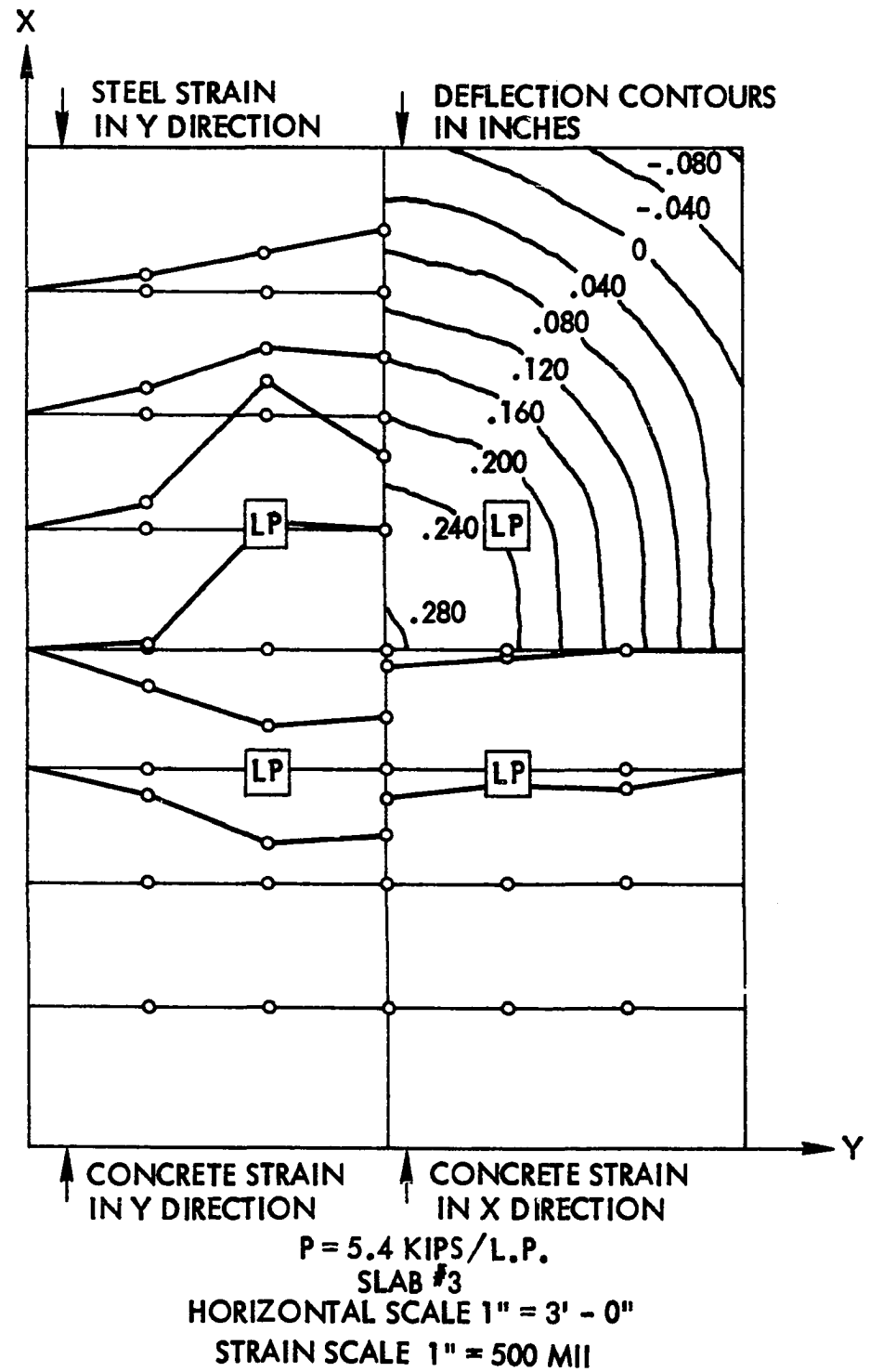

Figure 50. Continued

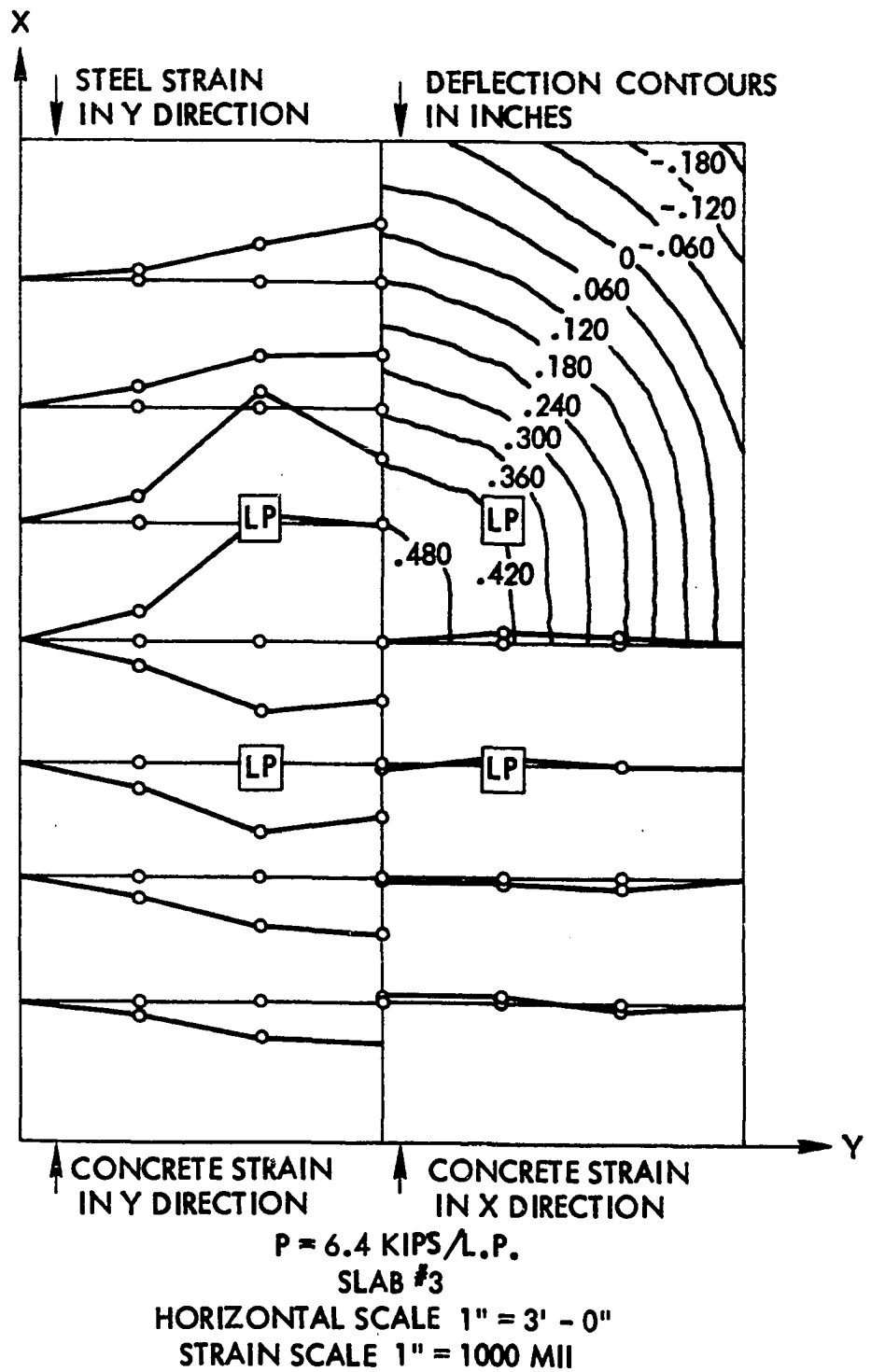

Figure 50. Continued

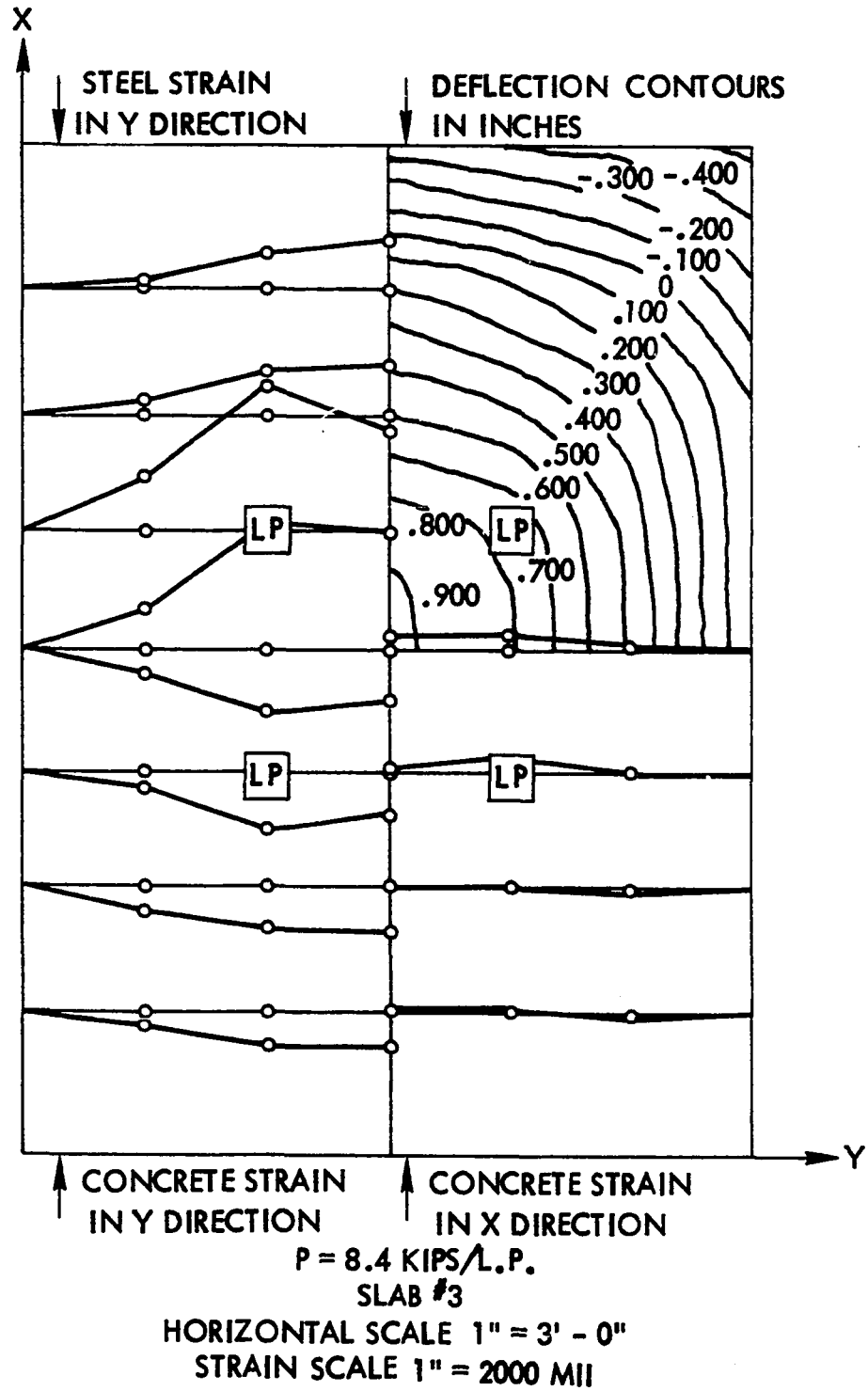

Figure 50. Continued

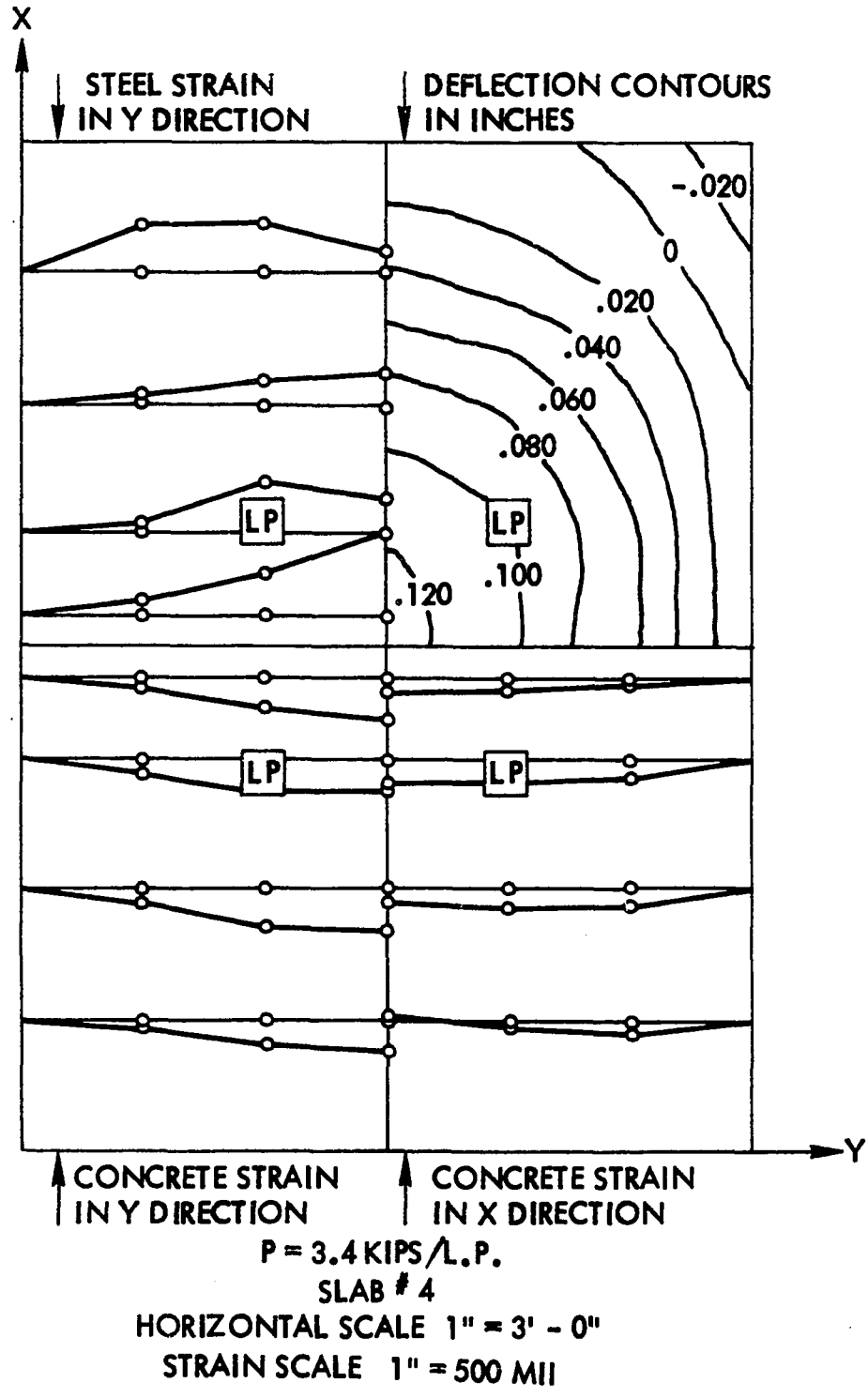

Figure 51. Measured strain and deflection distribution for Slab 4

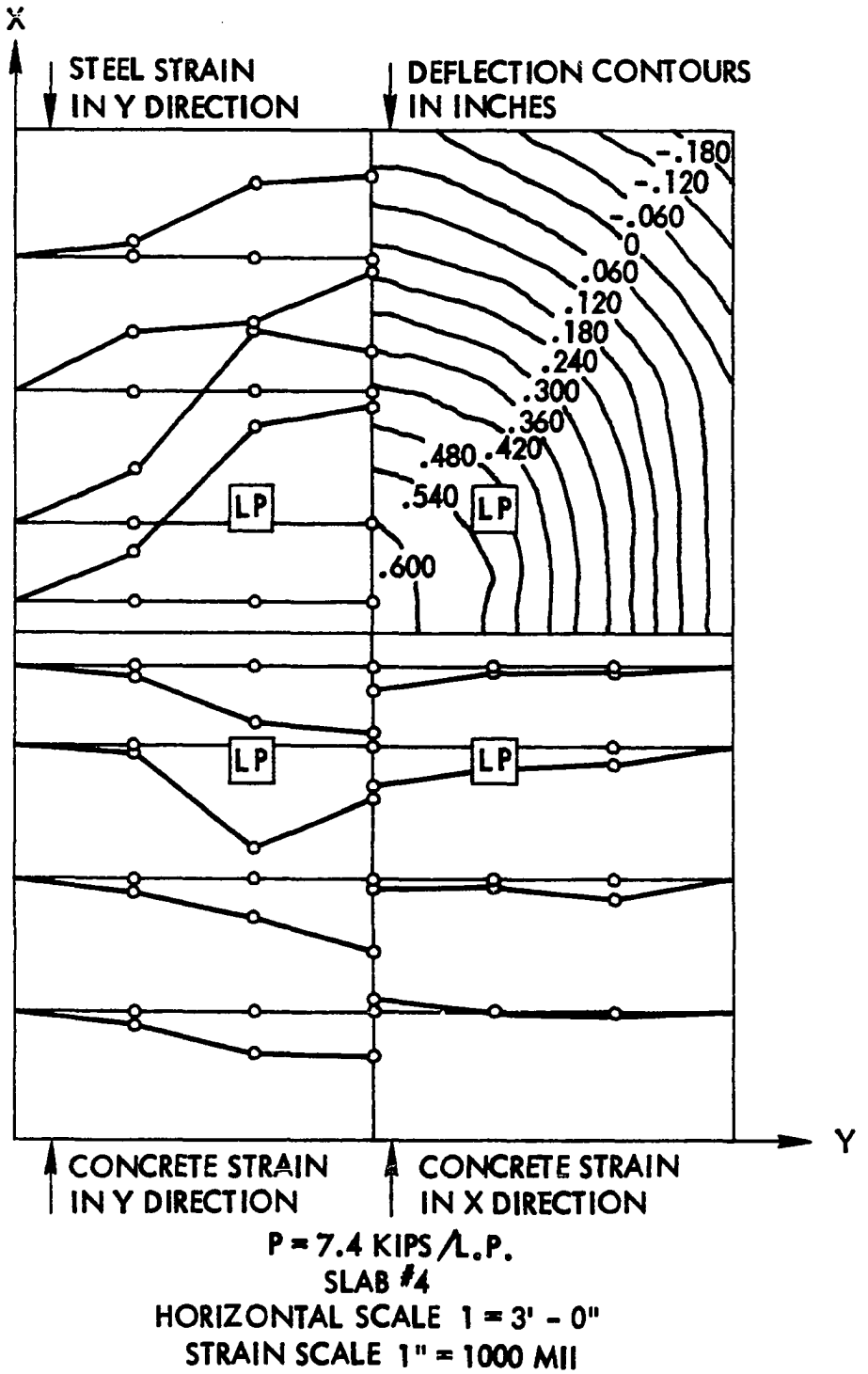

Figure 51. Continued

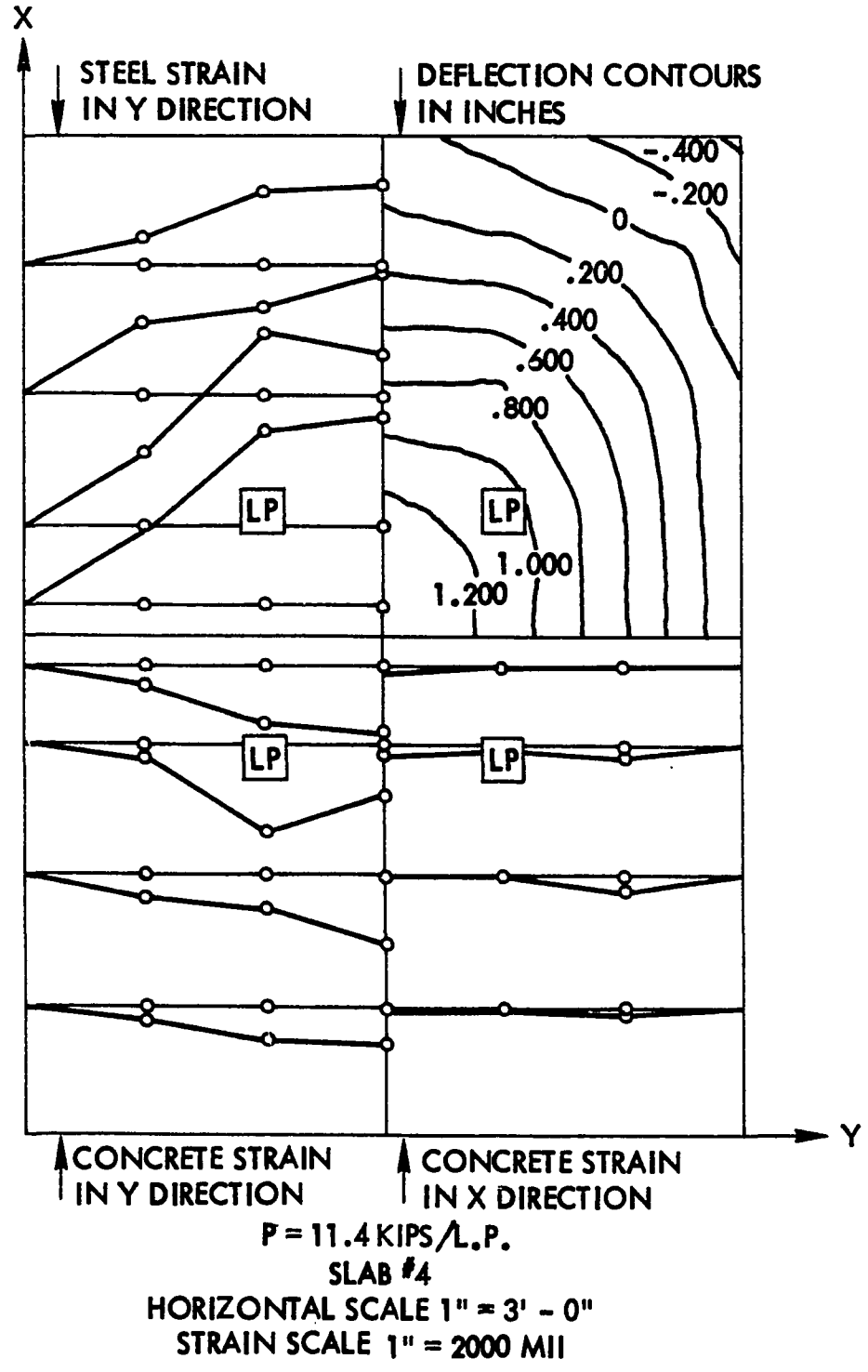

Figure 51. Continued

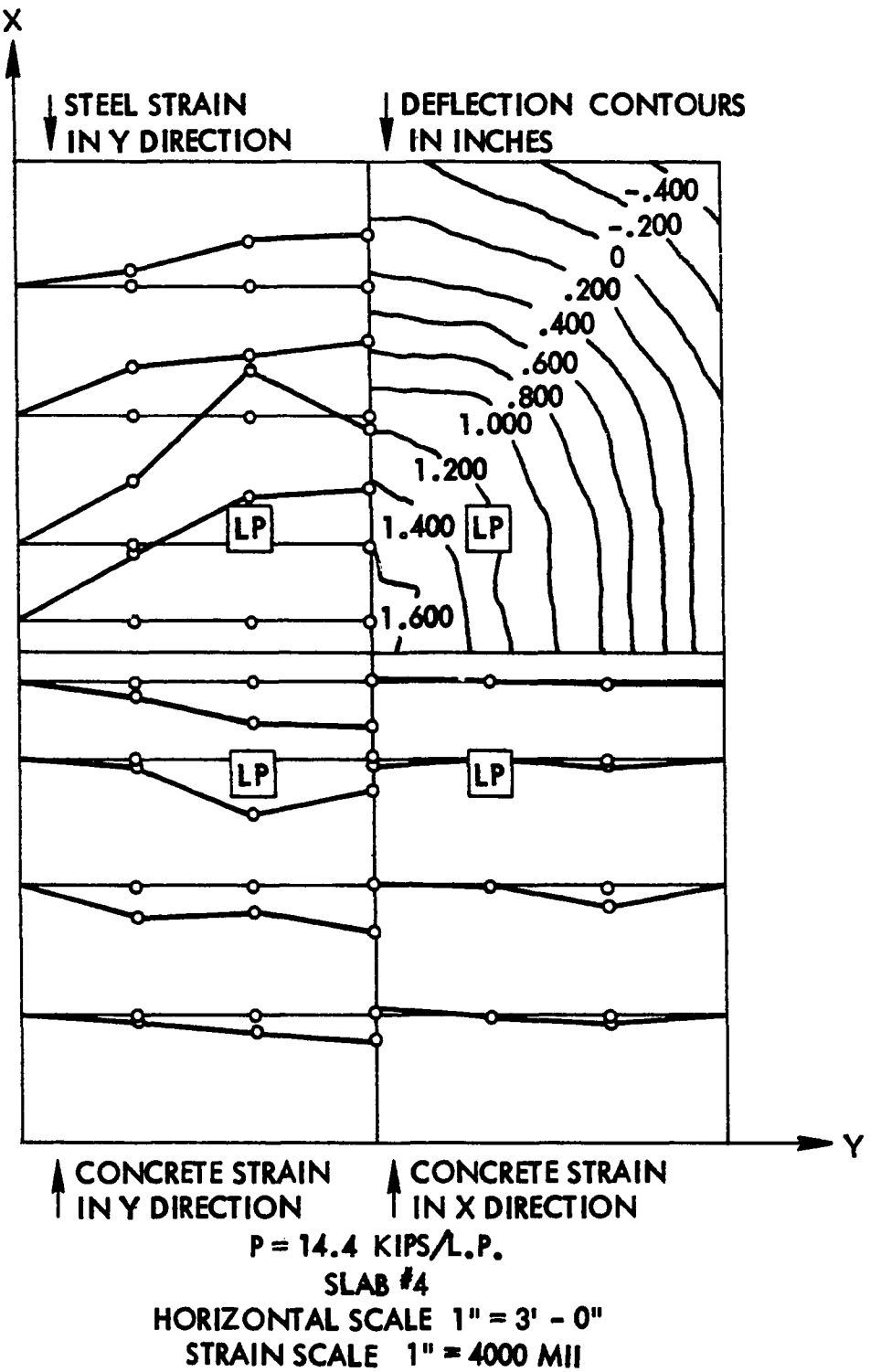

Figure 51. Continued

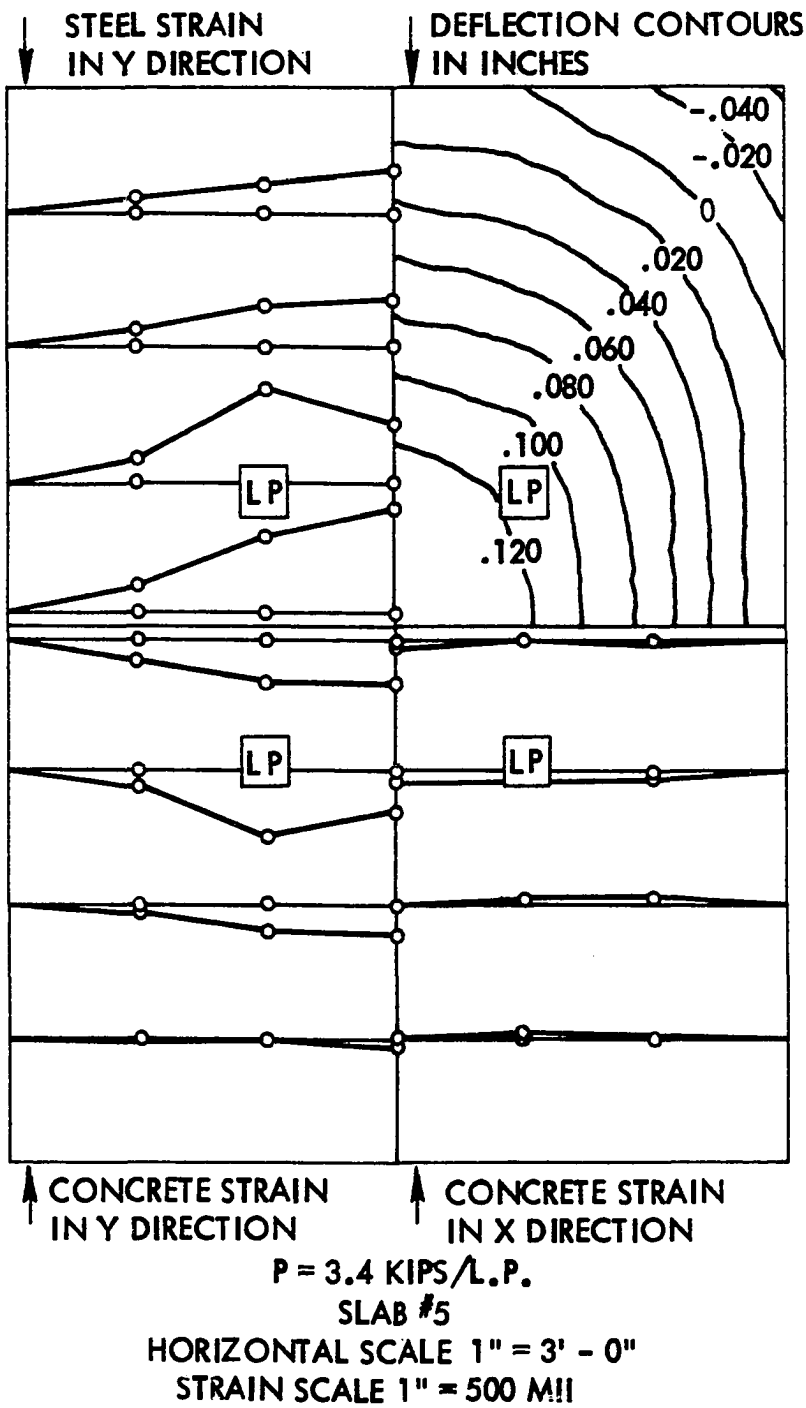

Figure 52. Measured strain and deflection distribution for Slab 5

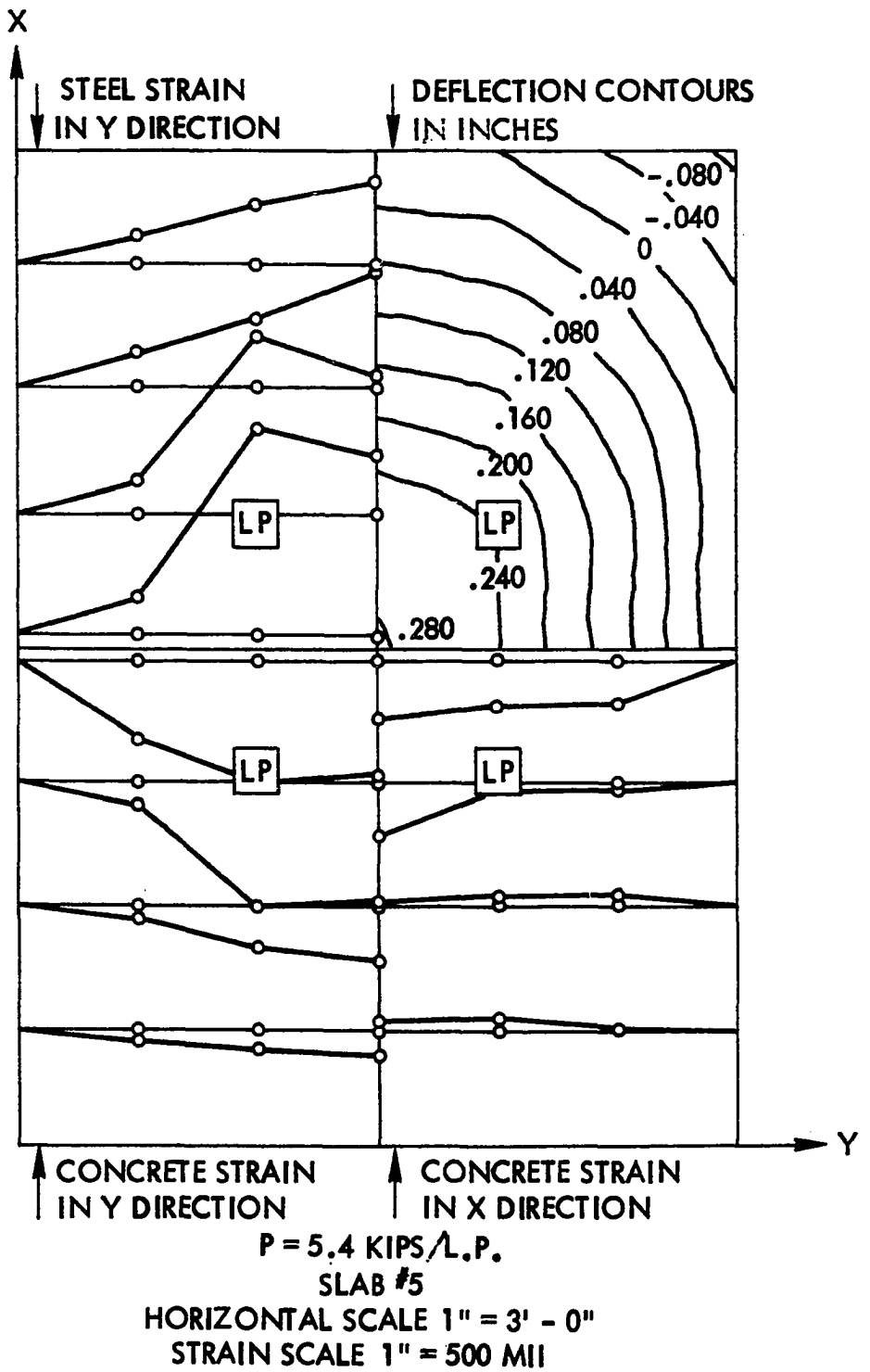

Figure 52. Continued

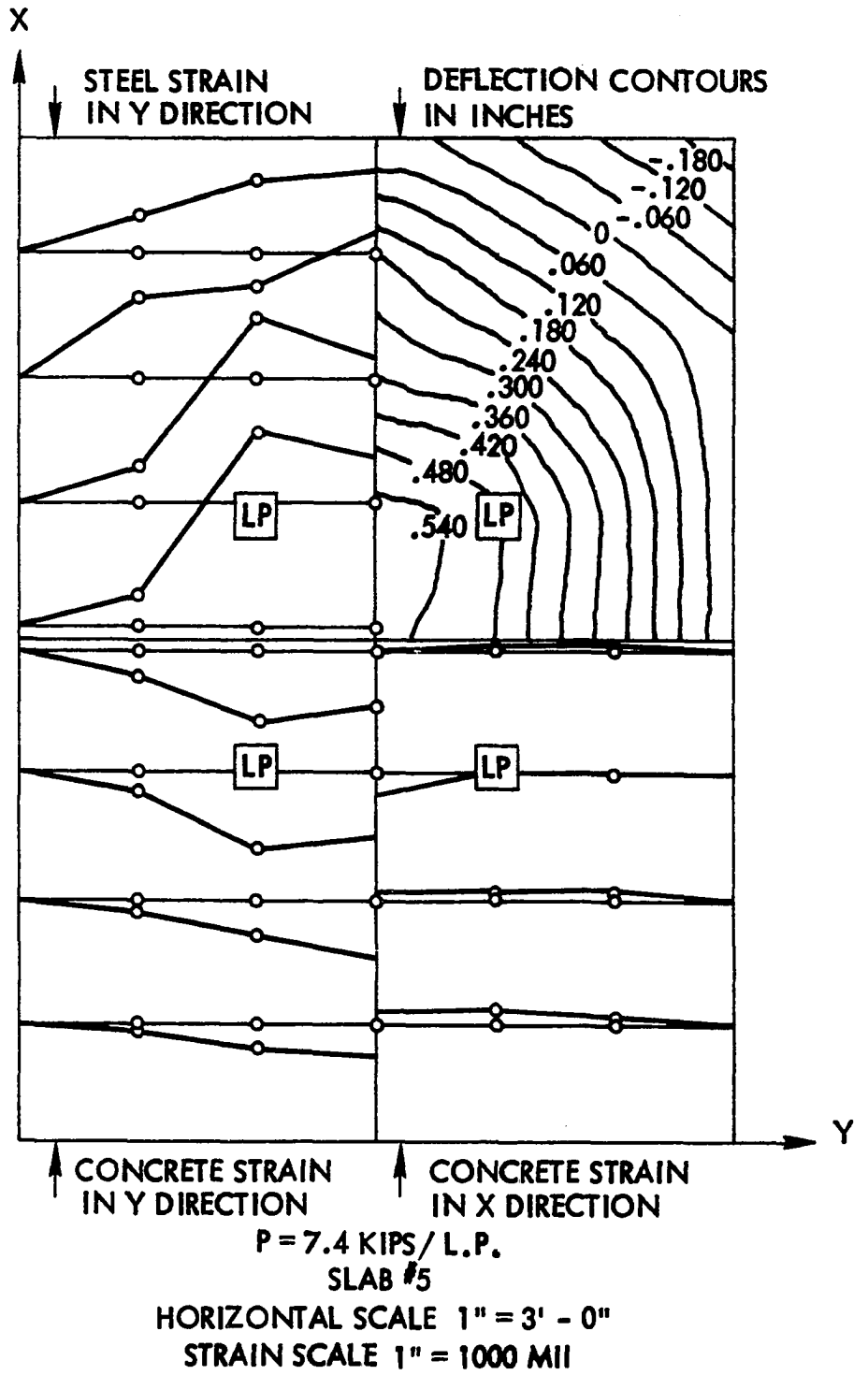

Figure 52. Continued

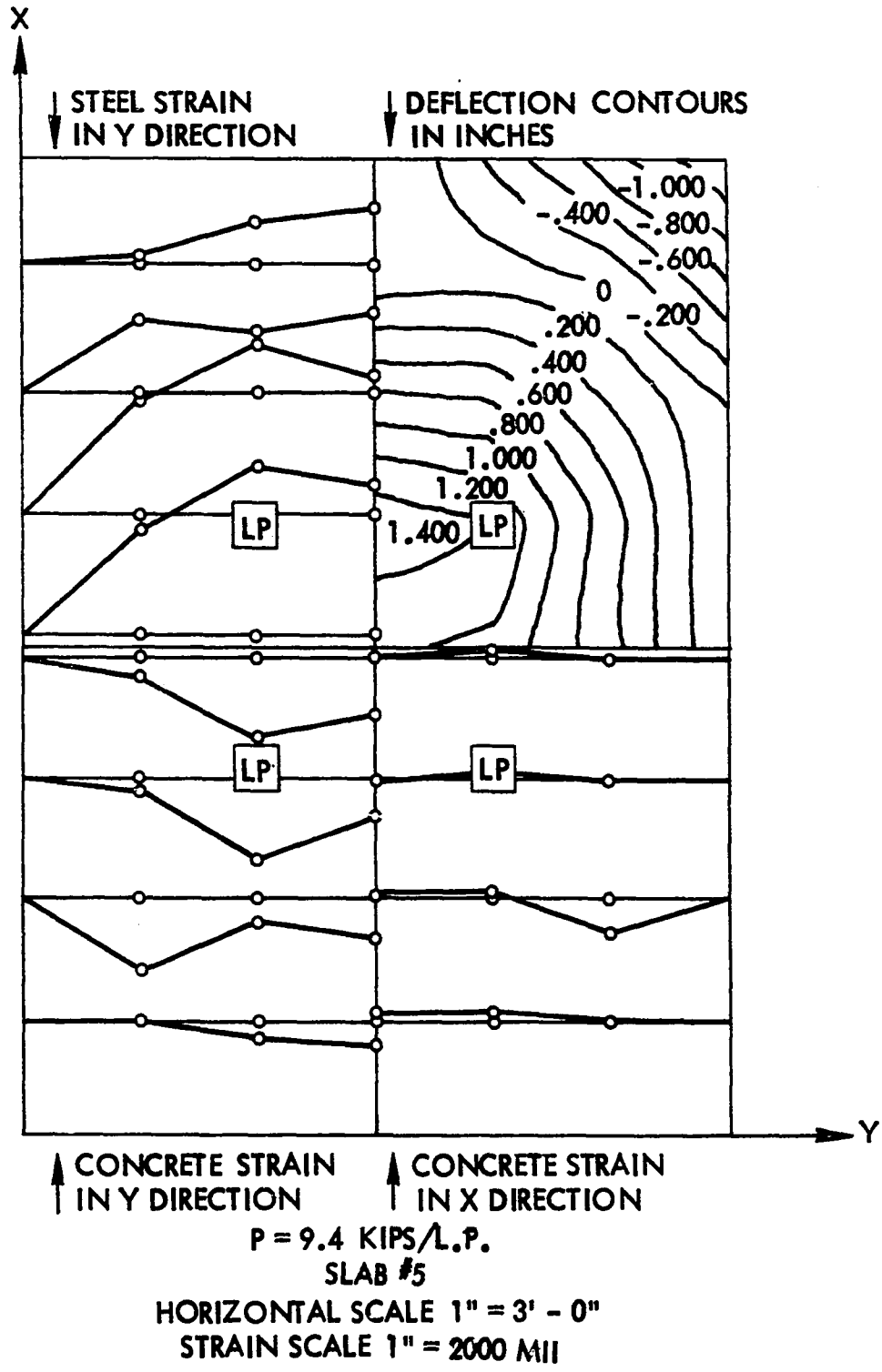

Figure 52. Continued

(y direction) taken on top surface of concrete,

3. transverse concrete strain perpendicular to steel-deck corrugations (x direction) taken on top surface of concrete, and
4. deflection contours.

Locations of deflection and strain gages for each slab were presented previously in Figures 23-27. Each strain gage location in Figures 48-52 is represented by a small dot.

Note that the strain quantities listed above do not include all those measured. The diagonal gage of the rosettes is omitted since these readings were used in determining principal strains which are discussed later. The transverse steel strain readings which were taken from gages positioned at right angles to the deck corrugations, are not included. The transverse steel strains were not included in any of the slab analysis because the readings from these gages revealed a lack of composite action in the transverse direction. The erratic transverse steel strain readings were attributed to independent bending of the deck corrugations on a cross-section transverse to the deck corrugations. Since the gages were located on the bottom fiber of the decking, any bending action of the deck which was independent of the composite action greatly influenced the strain readings. This phenomenon was substantiated on the strain-gaged transverse one-way slab element tests. On the other hand, the steel-deck strains measured parallel to the deck corrugations appear to give correct readings for the composite section. This, too, was substantiated by the strain gaged one-way slab element tests.

The deflection contours in Figures 48-52 were obtained by utilizing a computer program which plotted contours obtained from the deflection data. The deflection contour labels are for inches of deflection downward,

unless preceded by a minus sign indicating an upward displacement. The upward displacements occurred in the corner regions of Slabs 2-5 since those slabs did not have corner tie-downs.

Not all of the strain gage data are shown in Figures 48-52. Only those locations which fall close to the distribution lines located every three feet in the x-direction were used. The reference axis for each distribution section is represented by a light horizontal line at each interval with tensile strains plotted above and compressive strains plotted below the reference line.

The plots in Figures 48-52 indicate the strain and deflection distributions at four discrete load levels for each of the five full-scale two-way slabs. The levels chosen were approximately 1/4, 1/2, 3/4, and full ultimate load. The corresponding load values for each slab are given in Table 17. The cycling load (for Slabs 2-5) and the ultimate load are

Table 17. Loads used for strain and deflection distributions

Slab No.	Actual load values used at various stages of loading (kips/L.P.)				Cycling Load (kips/L.P.)	Ultimate Load (kips/L.P.)
	$P_u/4$	$P_u/2$	$3P_u/4$	Prior to Ultimate		
1	3.4	7.4	11.4	13.4 (2nd one)	None	13.7
2	3.4	7.4	11.4[a]	15.4[a]	9.4	15.5
3	3.4	5.4	6.4[b]	8.4[a] (2nd one)	6.4	8.8
4	3.4	7.4	11.4[a]	14.4[a]	9.4	14.4
5	3.4	5.4	7.4[a]	9.4[a]	5.4	9.4

[a]Load values occur after the 10 cycles of repeated loading.

[b]Load value occurs at the 10th cycle of repeated loading.

given for each slab in Table 17.

The strain and deflection distributions for Slab 1 are shown in Figure 48 and are contained on four plots as the load changes from 3.4 to 7.4 to 11.4 to 13.4 kips per load point. Even though most of the steel strains for Slab 1 were measured on the top corrugation, the values plotted represent bottom corrugation strains. The bottom strains were obtained by extrapolating a linear function from the concrete strain to the top corrugation steel strain. The bottom strains were obtained and plotted for all slabs so as to allow comparison of strain behavior for all slabs at the various load levels.

The strain distributions in Figures 48-52 give rise to several important behavioral observations regarding each slab. These are first discussed for all five slabs and are then followed by comparisons in changes in behavioral characteristics as they occur from slab to slab.

The transverse concrete strains are tensile over the entire section, taken about three feet from the south edge for Slab 1 and taken about three to six feet inward for Slabs 2-5. These tensile concrete strains indicate the negative M_x bending moment that occurred as predicted by the yield-line collapse mechanism shown in Figure 6. The tensile transverse concrete strains continued to increase for each load increment shown except the last when cracking of the slab had occurred. The top surface cracking, shown in Figure 32, that occurred across the slab was generally near this section of tensile strains. The other concrete transverse strains were generally compressive except for a point midway between the load points for the two higher loads where a tensile strain was observed. Thus, after significant slab deformation the concentrated loads caused the negative bending action to occur between their points of application. The concrete

transverse and longitudinal strains for the two south distributions lines for Slab 3 in Figure 50 were omitted for the first two load plots due to an error in data collection that occurred for the furthest southwest six location points. The data appeared reasonable after cycling and thus is included, but this too could be in some error.

The longitudinal steel and concrete bending strains indicate a progressively increasing magnitude of strain from the first section three feet in from the edge towards the central part of the slab. The longitudinal strains (parallel to deck corrugations) increased near the load points, especially the steel strains at 3/4 of ultimate. The erratic strains indicated for the ultimate load level can probably be attributed to the prior cracking that had taken place in the slab.

As can be seen in Figures 48-52, most of the strains increased uniformly from the slab edge to the centerline. Those sections where the trend did not hold were either near the concentrated load points or where there was some influence due to cracking. The higher magnitudes of strains at extreme fibers of steel and concrete generally occurred near the predicted collapse mechanism yield lines given in Figure 6.

The deflection contours, or lines of equal deflections, shown in Figures 48-52 indicate a fairly uniform deflection gradient, or slab slope, for those regions outside the loaded central 4-ft X 4-ft area. These uniformly spaced contours existed for each of the load levels shown for the five slabs. The negative deflection contour lines in Figures 49-52 represent uplift deformations which occurred in the corner regions of all but the first slab. The deflection due to extension of the tie-down rod assemblies was not considered in these contour plots since this extension was quite small.

The centrally loaded region had a fairly constant deflection for each of the load increments, as can be seen from each of the contour plots.

The location of the zero contour line for Slabs 2-5 in Figures 49-52 is significant. The intersection of the zero deflection contour with the 16 foot side occurs at about the same location as the intersection of the yield-lines for the collapse mechanism. Thus, the contact made with the reactions along the east and west slab edges defines an effective width of the main load-carrying portion of the slab. Generally, the zero contour intersection with the east or west edges tended to move inward as the load increased during the initial loading stages up to about one-fourth of ultimate, then remained fairly constant until significant cracking near ultimate caused some changes. Generally, the intersection of the zero contour with the east or west edges occurred at about the same points for all load levels for Slabs 2-5.

The intersection of the zero contour with the north or south side was usually quite close to the center, indicating that not much of the slab was in contact with the support. In fact, Figure 50 shows how Slab 3 completely lifted off its north and south reactive supports prior to its ultimate load (shown at the 8.4 kips level in Figure 50). Slab 3 without supplementary reinforcing did not have sufficient ductility to permit its north and south edges to maintain contact with the supports.

A comparison of Slabs 1-3, which had the same decking but different amounts of supplementary reinforcing indicates that Slab 2 with the most supplementary reinforcing

1. exhibited the greatest deformations,
2. exhibited the highest ultimate load,

3. sustained the highest cycling load, and
4. exhibited more favorable distribution of bending strains, as well as withstanding the largest strains.

An indication of the overall load versus deflection behavior of the five slabs is shown in Figure 53. The deflections shown in Figure 53 are the centerpoint deflections taken during the final cycle of loading. The initial starting point for the curve for Slab 1 is zero since this slab was not cycled. The initial cycle deflections and deflections after the ultimate load are omitted for clarity. As can be seen in Figure 53, Slabs 1, 3, and 5 had about the same stiffness over the initial straight-line portion. Slabs 2 and 4 show slightly less stiffness in Figure 53, but this is probably due to the high cycling load for these two slabs. Points along the abscissa indicate the amount of slab distortion remaining after removal of load upon completion of the test. It is observed that all slabs, except 3 and 5, exhibited fairly linear load-deflection relationships below the level defined by a deflection of L/180. Slabs 3 and 5, without effective supplementary reinforcing, did show some nonlinear behavior at the L/180 level and, did not undergo as much ultimate deflection as did the other slabs.

An indication of deflection behavior corresponding to initial slab cracking can also be seen in Figure 53. Shown for each slab is the load for the first observed crack. As can be seen, the slabs exhibited a stable behavior well beyond the first observable crack.

A detailed load-deflection behavior before repeated loading is shown in Figure 54. Shown here are plots of the initial cycle of loading. As can be seen there is a linear relationship for all slabs up to about 3.4

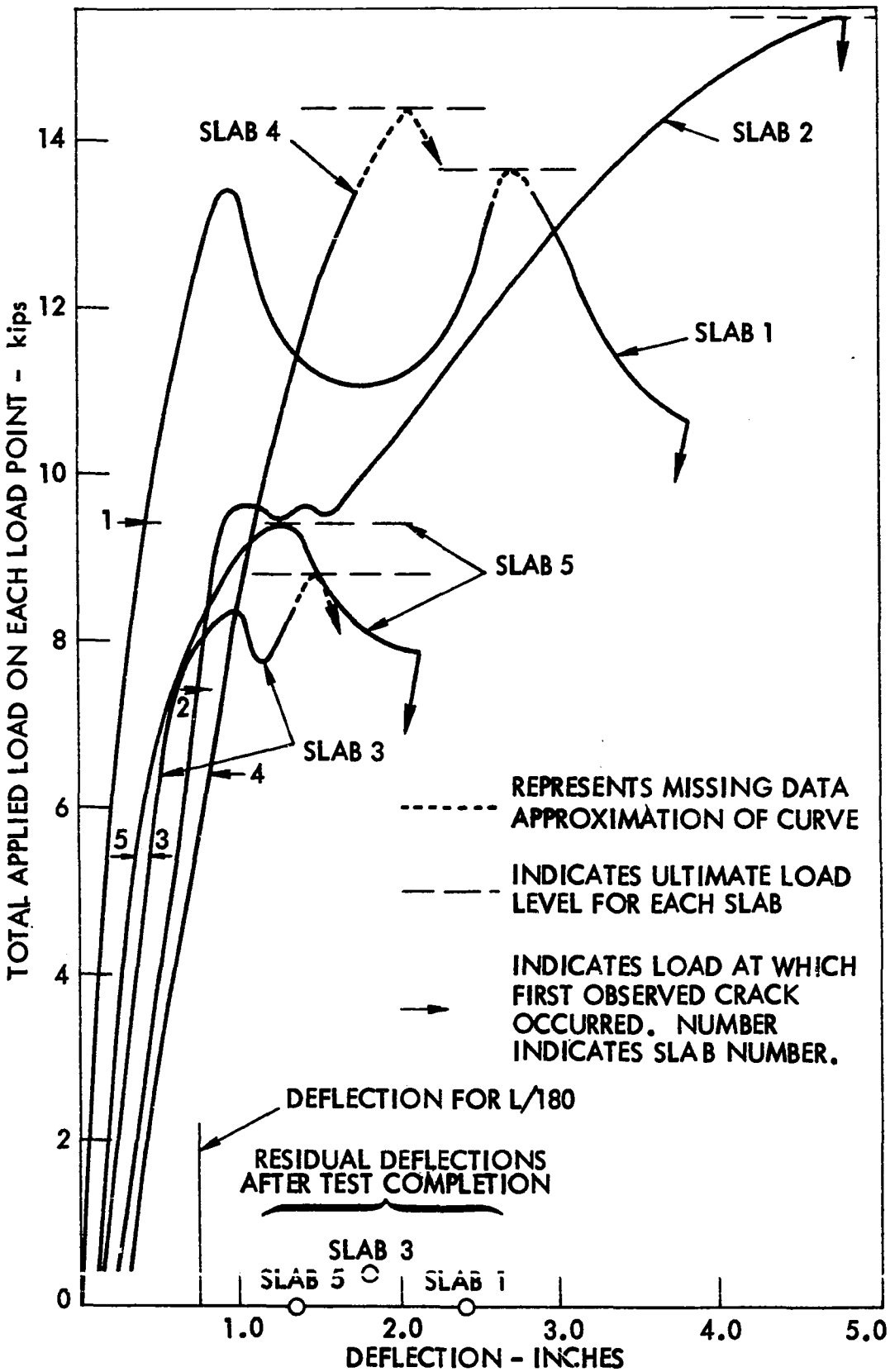

Figure 53. Load versus centerpoint deflection for entire final load cycle

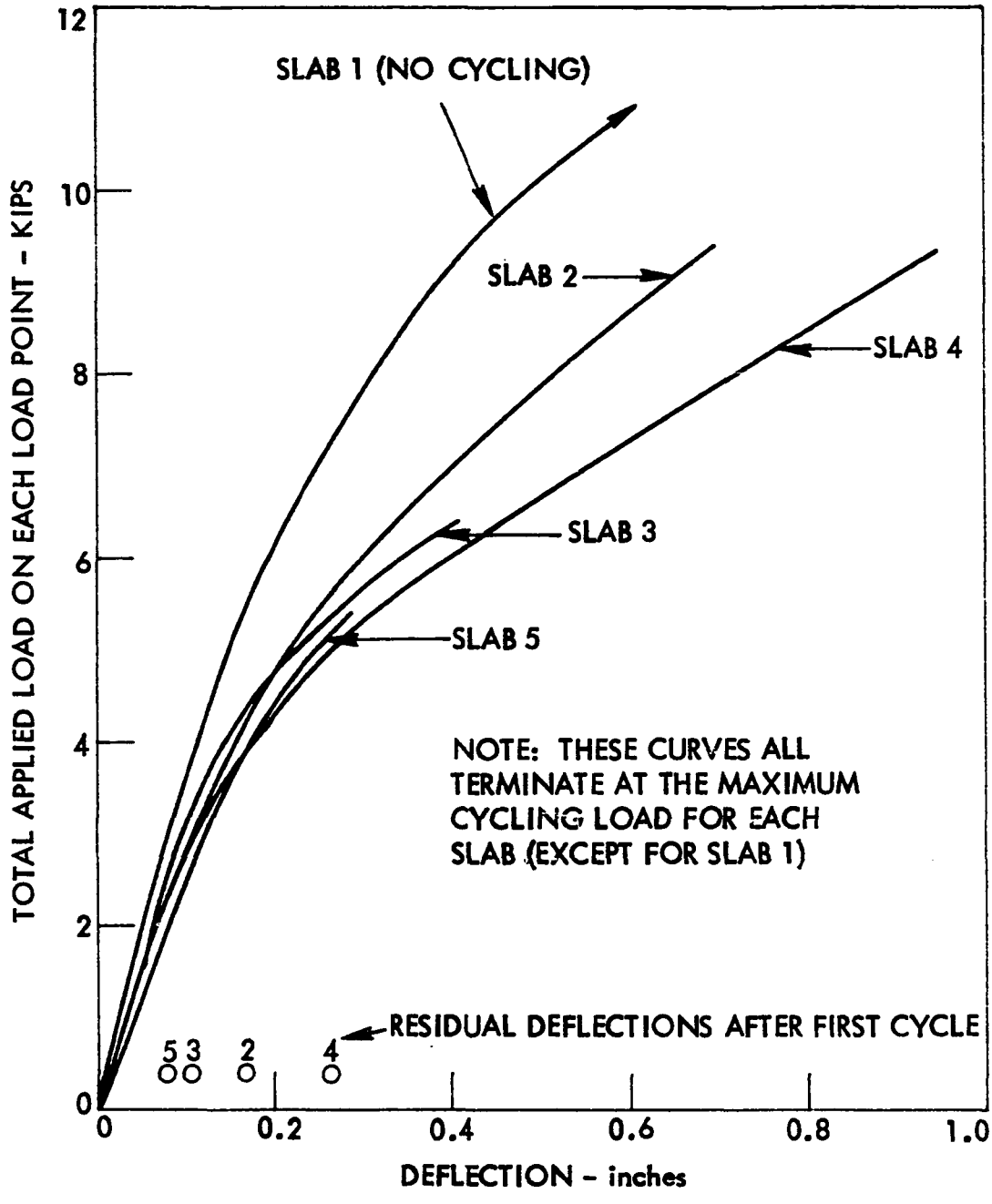

Figure 54. Load versus centerpoint deflection for initial cycle of loading for the five slab tests

kips per load point followed by another fairly linear trend up to the maximum load. Also indicated on Figure 54 is the amount of permanent deformation occurring in the slabs after the first cycle of loading (except Slab 1). The magnitude of this deflection was somewhat dependent upon the maximum load subjected to each slab. Slabs 2 and 4 had the highest loads, and their permanent deformations were the largest. Slab 2, with a large amount of supplementary reinforcement, had slightly less residual deflection than Slab 4.

Figure 55 shows a more detailed illustration of the load-deflection behavior for Slabs 2, 3, and 4 due to cycling. This figure includes all slabs subjected to repeated loading except Slab 5 which was very similar to Slab 3. Slab 5 was omitted from Figure 55 for clarity. The repeated load portions for each slab are grouped and labeled, along with the initial load cycles. The load repetition groupings for each slab were probably curves, but straight-line representations were shown since readings were only taken at minimum and maximum loads.

Of particular importance in Figure 55 is the amount of residual deflection after each cycle. Slab 3 attained most of its residual deflection at the end of the first cycle with only a very slight increase on each subsequent cycle. Slabs 2 and 4 also had most of their residual deflection occurring at the end of the first cycle; with Slab 4 exhibiting the greatest magnitude of final permanent deformation. The amount of permanent deformation for Slab 2 versus Slab 3 is probably due to the higher magnitude of cycling load. The supplementary reinforcement in Slab 2 was primarily responsible for this slab having the capability to develop the increasing cycling load over that of Slab 3 and still maintain a stable

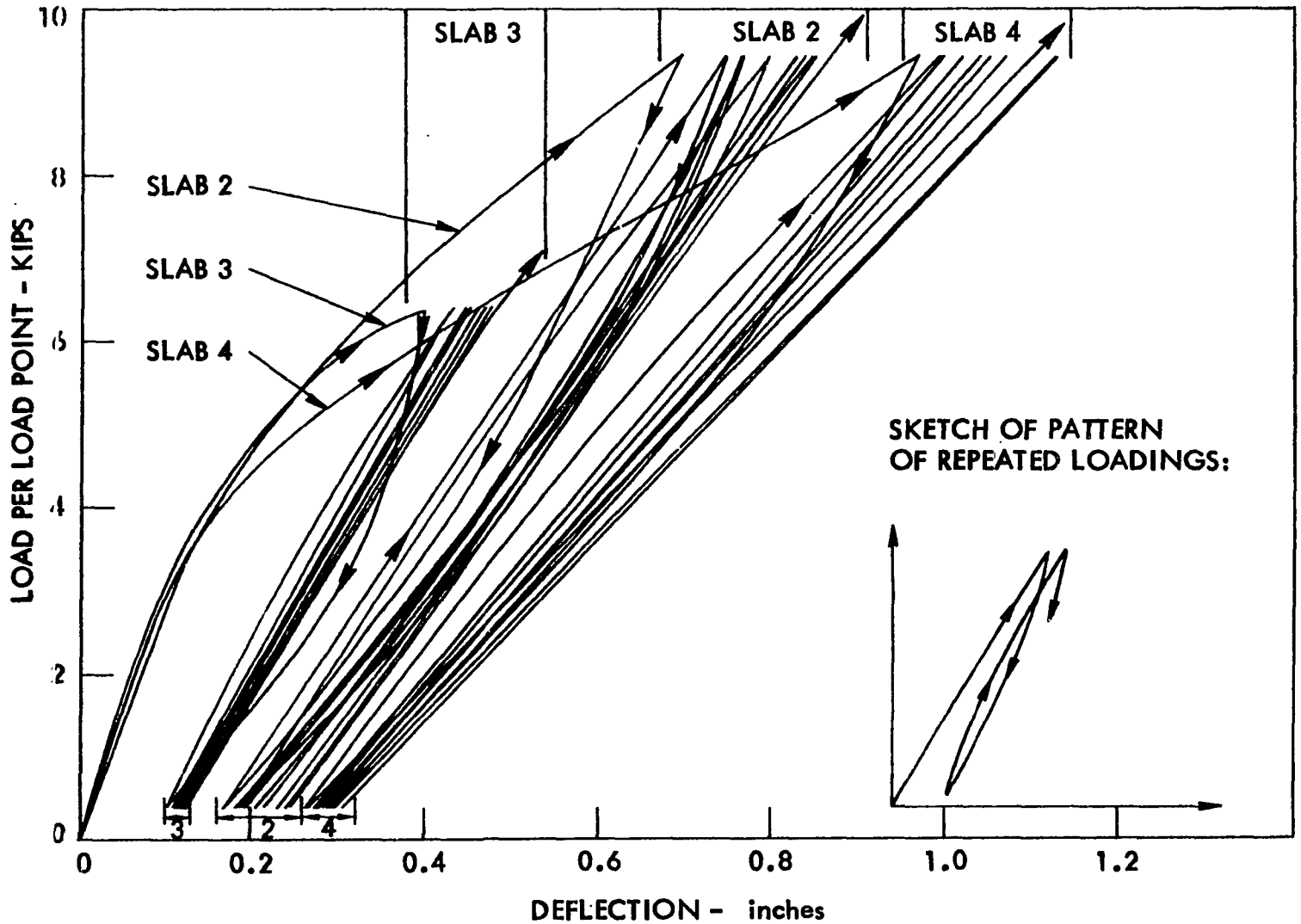

Figure 55. Effect of load cycling on load-deflection behavior for Slabs 2, 3, and 4

repeated load cycle. The difference in magnitudes of Slabs 2 and 4 can be attributed to the difference in deck reinforcement in the two slabs.

It is significant that the cycling loads applied to the slabs were quite high. In terms of percentage of ultimate load, they were 60.6, 72.7, 65.3, and 57.4 for Slabs 2-5, respectively. Each test was intended to be cycled at 60 percent of ultimate, but the cycling load was estimated from behavioral characteristics during loading which explains some of the variances in percentage of cycling load. Slab 3 tended to develop cracks more rapidly during cycling, and was most affected by the repeated loading. This result can probably be attributed to the lack of supplementary reinforcement to help keep the slab intact and to help in the distribution of forces throughout the slab.

The corners of Slabs 2, 3, 4, and 5 were not secured and were free to lift off the supports. Figure 56 shows the vertical uplift deflection that occurred at the southwest load point of each slab, and are indicative of the uplift at the other three corners. The curves shown in Figure 56 represent the final load cycle to ultimate. The beginning point of each curve indicates the residual deformation of the corners after 10 cycles of loading.

As can be seen in Figure 56, the corner deflection behavior remained linear for almost the entire loading for Slabs 2 and 4 (excluding possibly the last load increment of Slab 4, for which the ultimate corner deflection was not recorded). The load-deflection curve for Slab 2 became nonlinear at about 83 percent of the ultimate load, and Slabs 3 and 5 exhibited a linear behavior of corner uplift up to 68 and 60 percent of ultimate, respectively. The major variable contributing to these significant changes

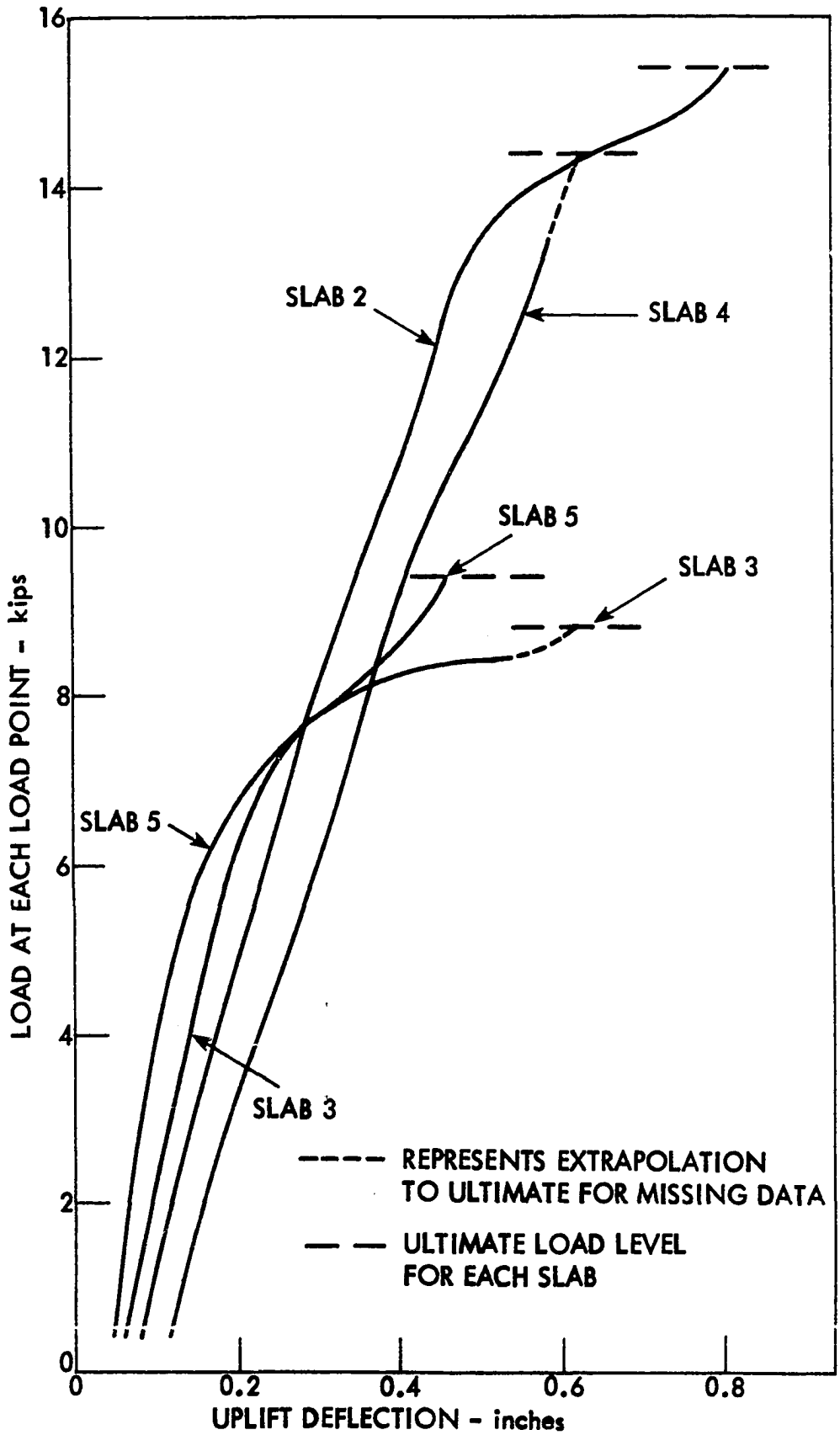

Figure 56. Vertical uplift deflection of the southwest corner of the slabs.

in nonlinearity is probably the amount of supplementary reinforcing. Slabs 2 and 4 had significant amounts of supplementary reinforcing transverse to the decking, whereas Slabs 3 and 5 did not.

Principal Strain Analysis

A principal strain analysis was performed on the three-element rectangular rosette strain gages placed on the concrete surface of the slab specimens. The principal strains, ϵ_1 and ϵ_2, were computed from the following equations as given by Dally and Riley (6):

$$\epsilon_1 = 1/2(\epsilon_x + \epsilon_y) + 1/2(\epsilon_x - \epsilon_y)^2 + (2\epsilon_{45} - \epsilon_x - \epsilon_y)^2 \qquad (38)$$

$$\epsilon_2 = 1/2(\epsilon_x - \epsilon_y) - 1/2(\epsilon_x - \epsilon_y)^2 + (2\epsilon_{45} - \epsilon_x - \epsilon_y)^2 \qquad (39)$$

where ϵ_x, ϵ_y, and ϵ_{45} are the strains in the x, y, and 45-degree angle directions. The x-axis was taken as transverse to the deck corrugations with the y-axis parallel to the corrugations. The directions of the principal strains were obtained from the following equation for the principal angle, ϕ:

$$\tan 2\phi = \frac{2\epsilon_{45} - \epsilon_x - \epsilon_y}{\epsilon_x - \epsilon_y} \qquad (40)$$

where the one principal angle from Equation (40) refers to the angle between the x-axis and the direction of the maximum principal strain, ϵ_1, and the other principal angle refers to the angle between the x-axis and the direction of the minimum principal strain, ϵ_2.

The principal strain analysis was performed on all rosettes placed at the locations shown in Figures 23-27. However, only those principal strains

for those rosettes mounted in the southwest quadrant on the top fiber of concrete are presented. The other gage locations on the concrete surface were primarily for a check on symmetry. The principal strain analysis for those rosette gages mounted on the steel decking is not presented due to the invalid ϵ_x strains transverse to the corrugations. The invalidness of the ϵ_x strains was discussed previously under strain distributions.

The results of the principal strain analysis are shown in Figures 57-61 for each of the five slab tests. Each rosette location in the five figures is depicted by a small square oriented in the direction of the principal angle as given by Equation (40). The magnitudes of the maximum and minimum principal strains are represented by the length of an arrow drawn from each respective face of the squares. The length of the arrow is measured from the face of the square to the end of the arrow. An arrowhead pointing away from the square indicates a tensile strain and an arrowhead pointing toward the square indicates a compressive strain.

The arrow lengths plotted in Figures 57-61 were plotted to consistent scales at each one-fourth of the ultimate load. Due to the large range in magnitude, it was necessary to change scale size as the load values increased. However, the scales were kept consistent at each quarter of ultimate to allow comparisons amongst the slabs. A missing arrow indicates that the principal strain was of very low magnitude. Low values of less than 20 microinches per inch on the lower loads and less than 40 microinches per inch on the loads just prior to ultimate were omitted.

The principal strain analysis was performed for all load increments before and after cycling, however only the results at 1/4, 1/2, and 3/4 of ultimate, and just prior to ultimate load are presented. The load values

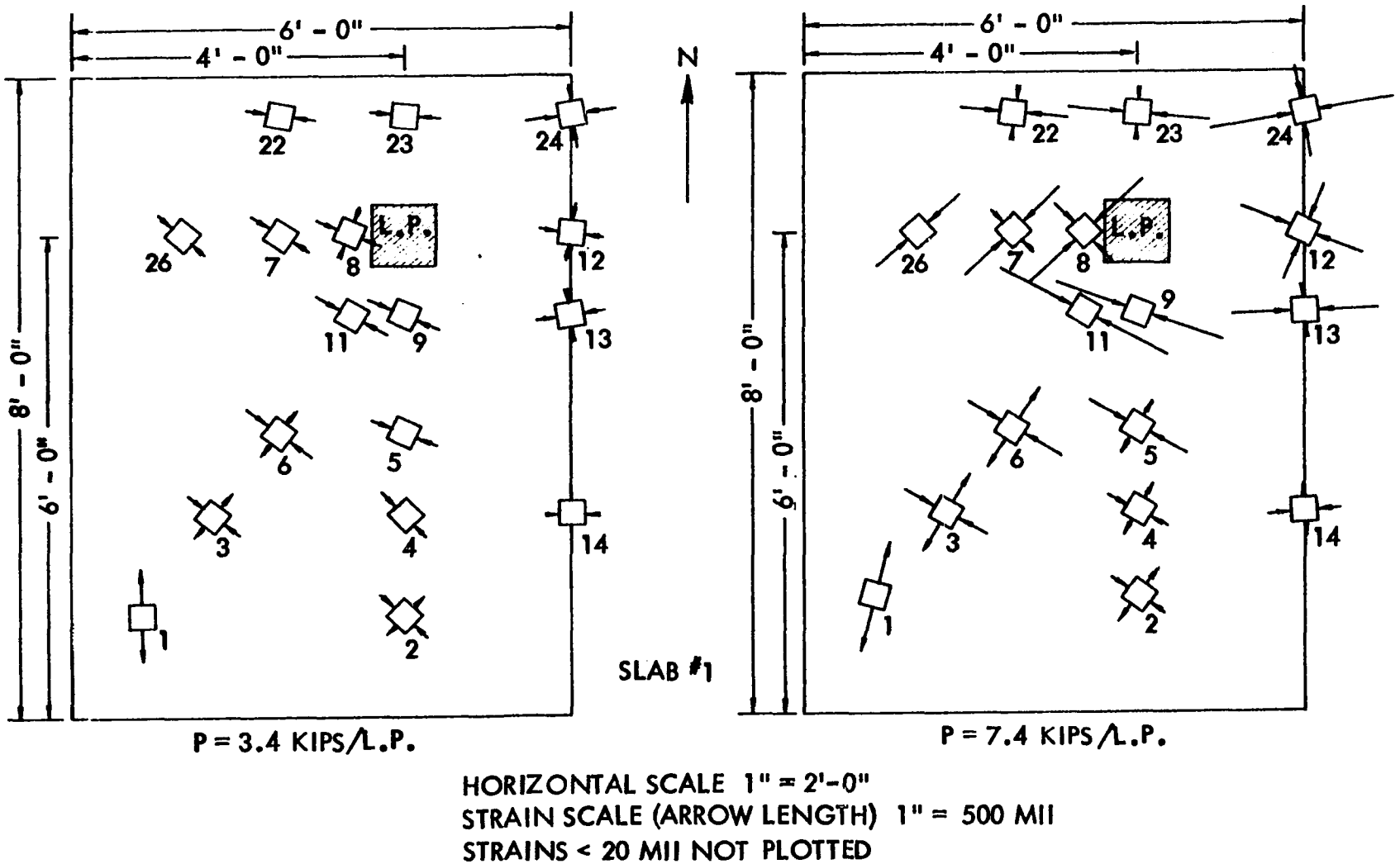

Figure 57. Principal strain analysis results for Slab 1

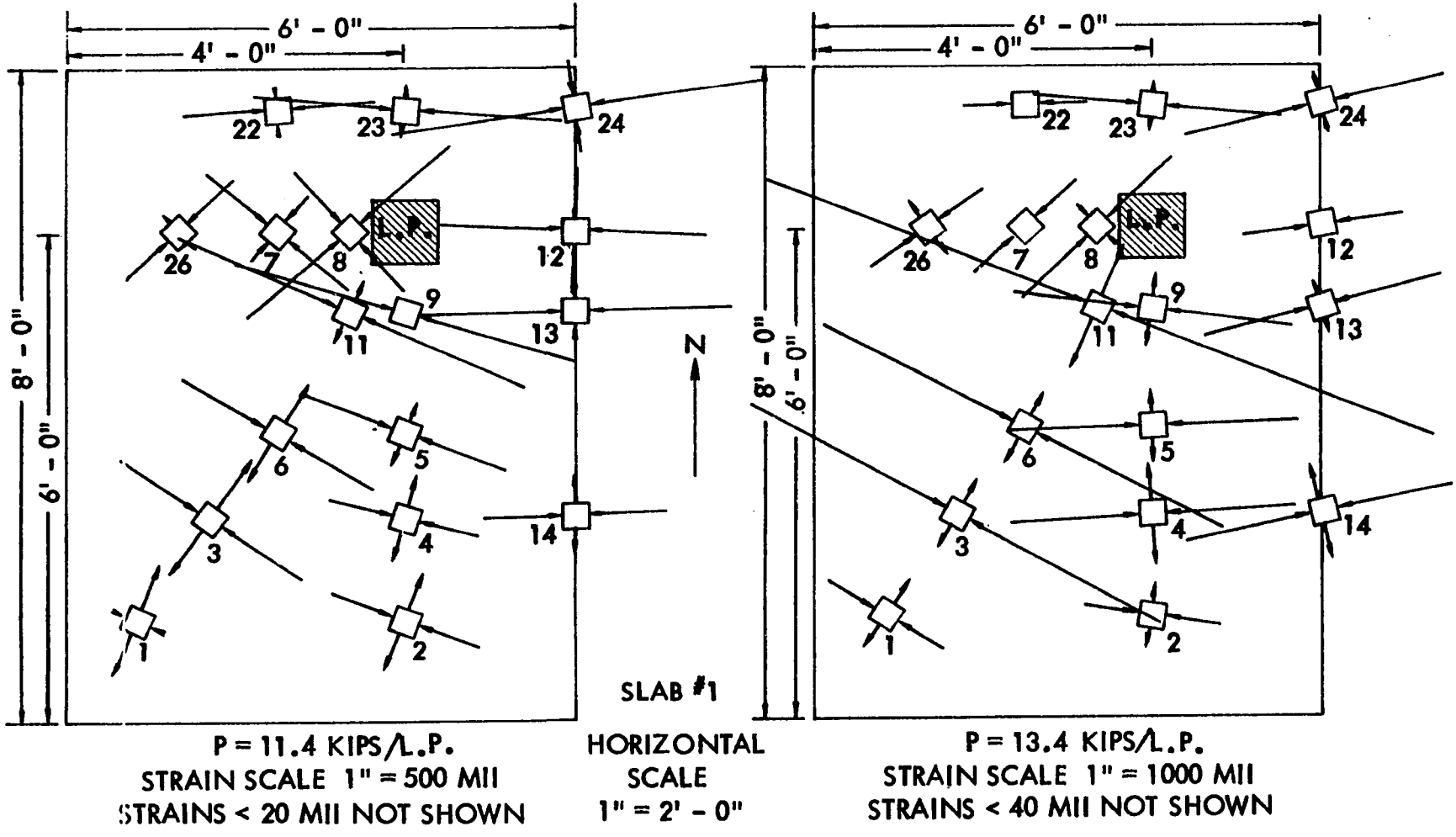

Figure 57. Continued

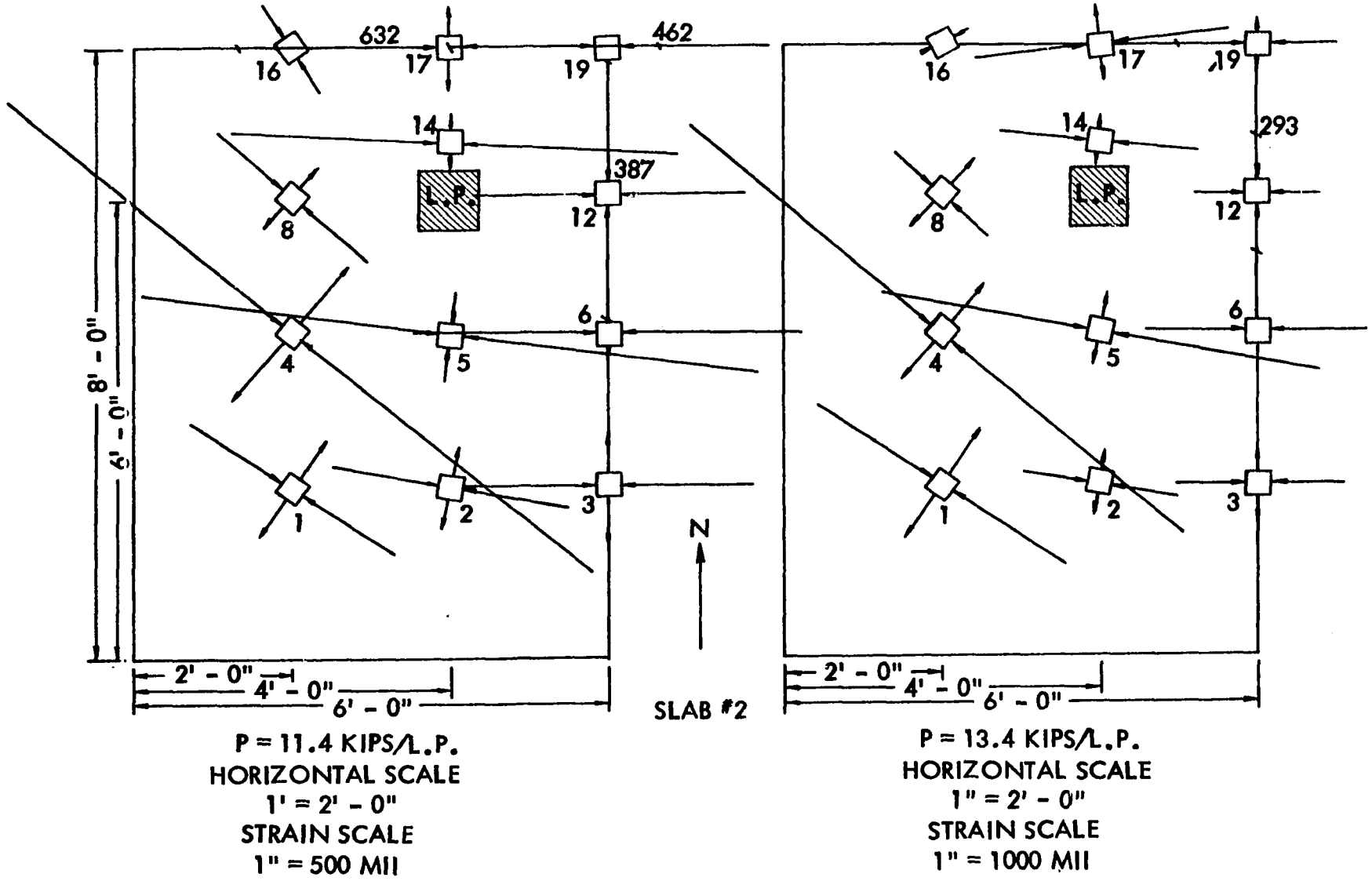

Figure 58. Principal strain analysis results for Slab 2

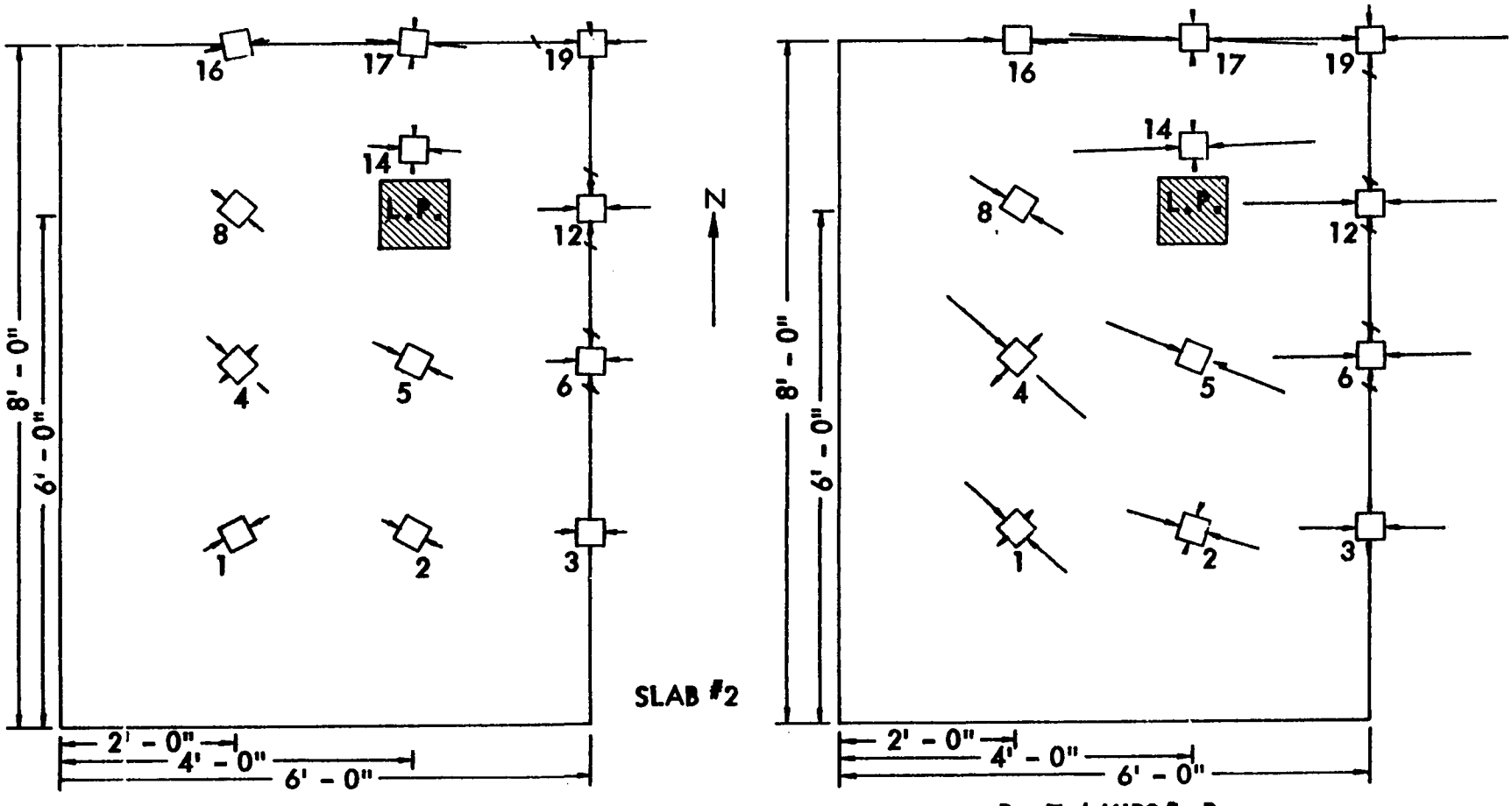

Figure 58. Continued

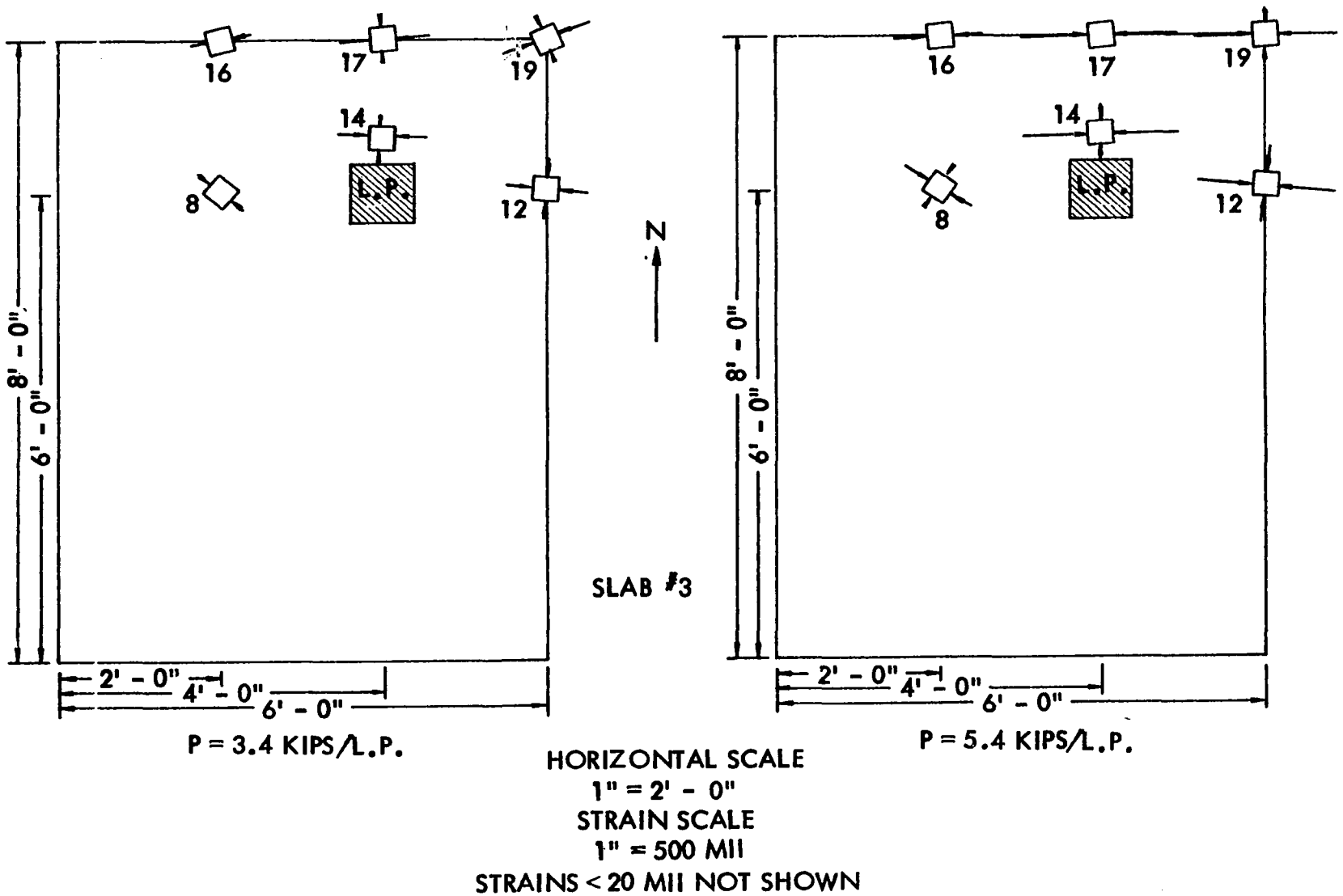

Figure 59. Principal strain analysis results for Slab 3

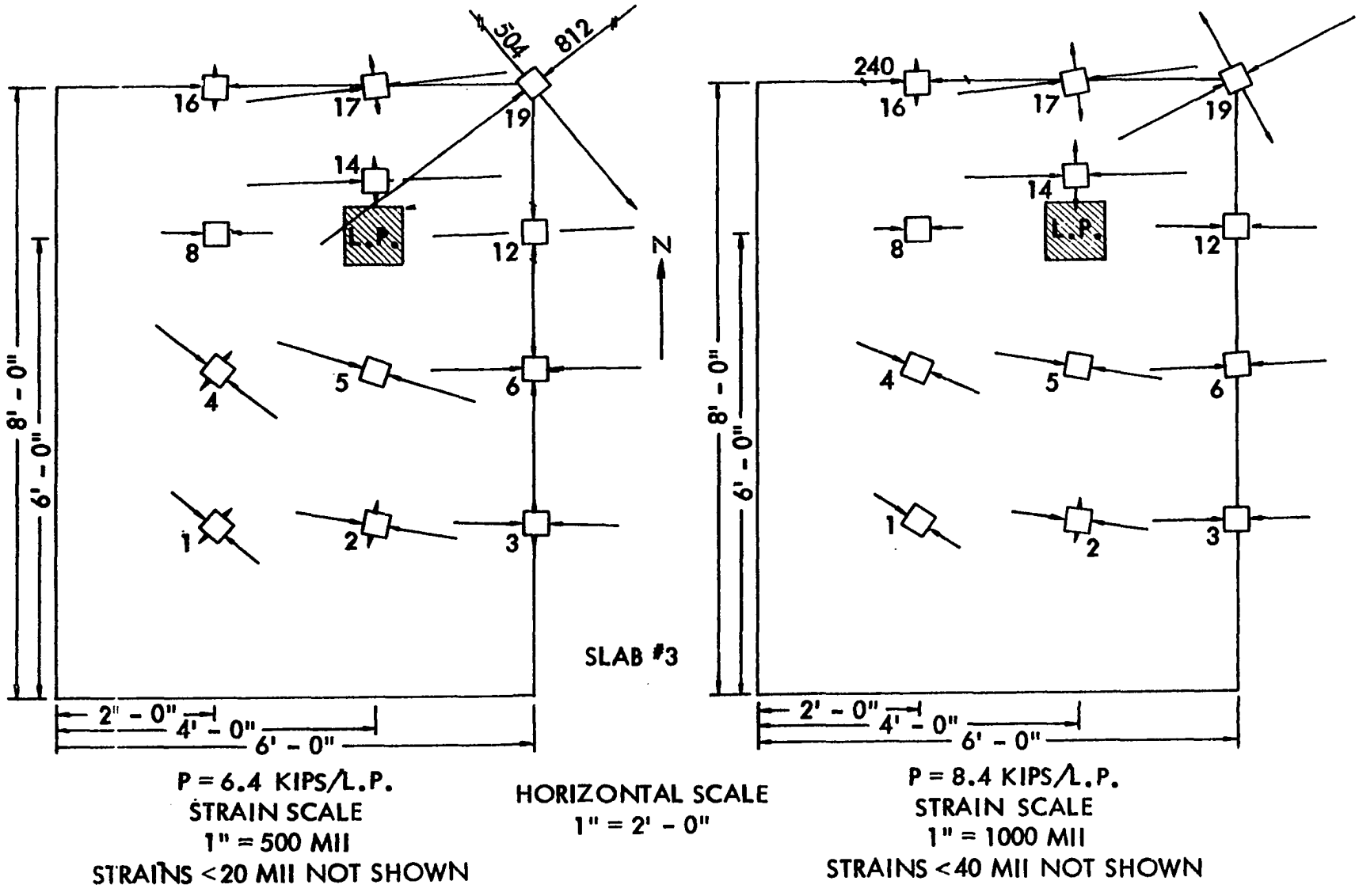

Figure 59. Continued

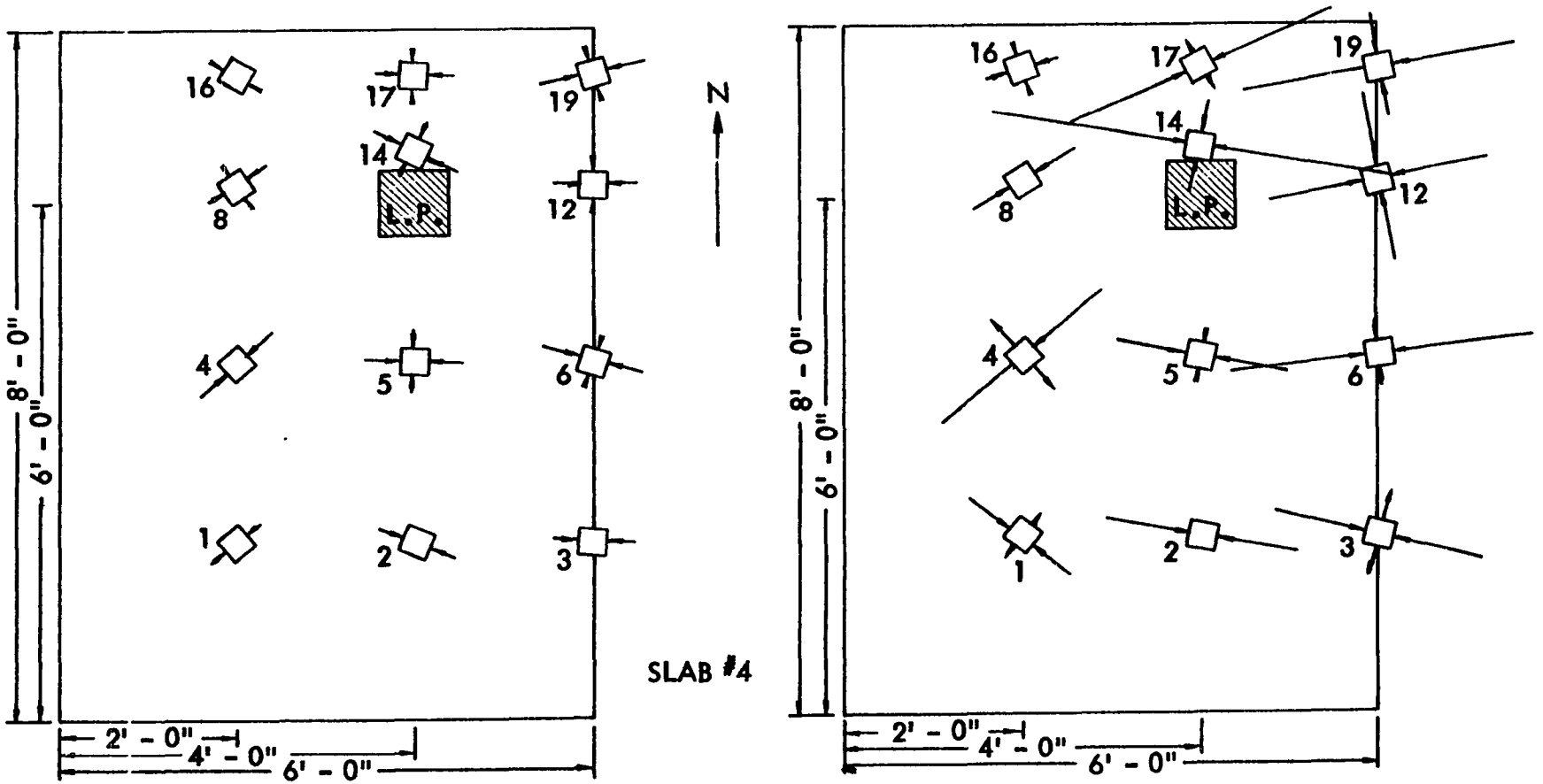

Figure 60. Principal strain analysis results for Slab 4

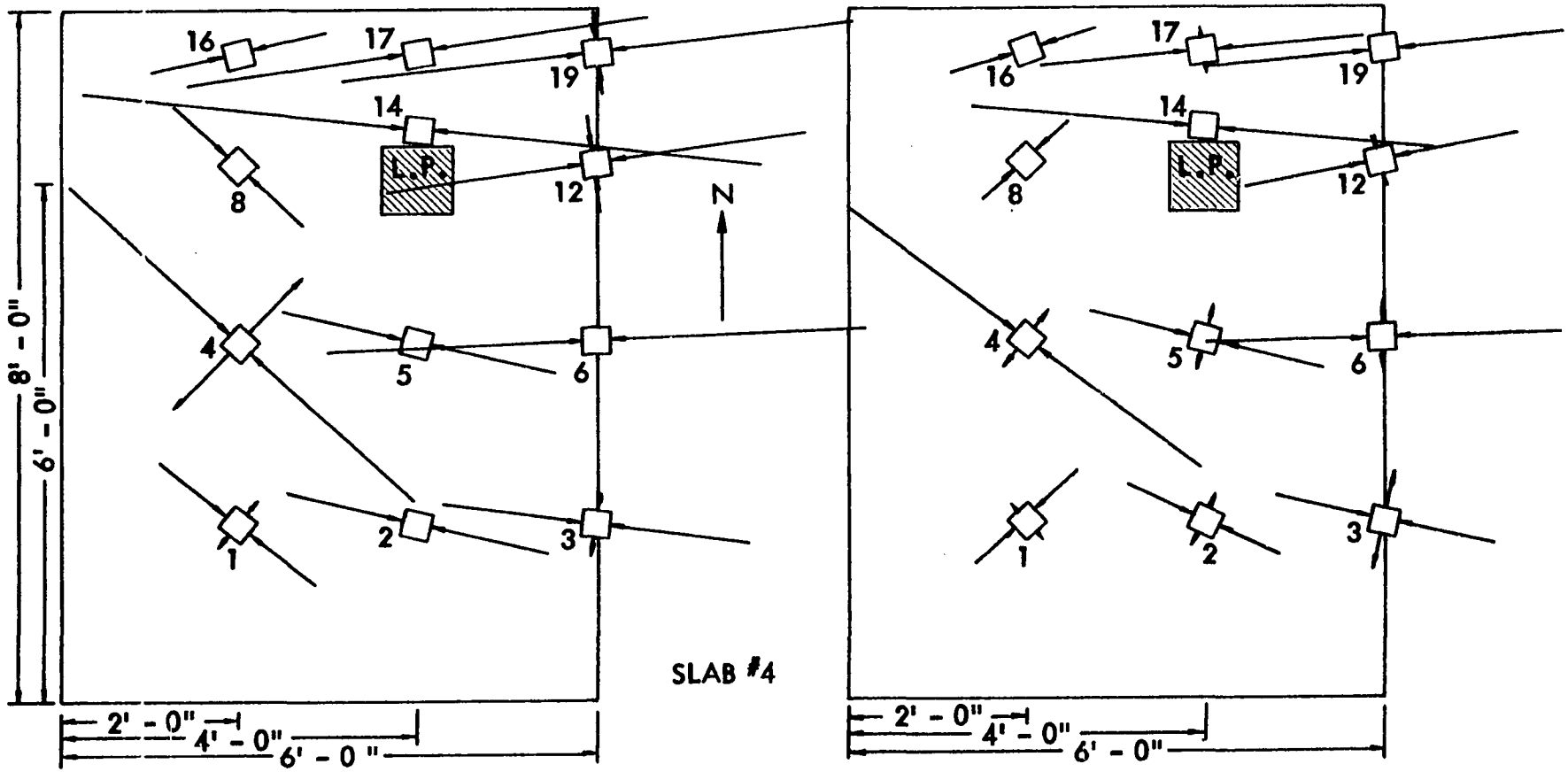

Figure 60. Continued

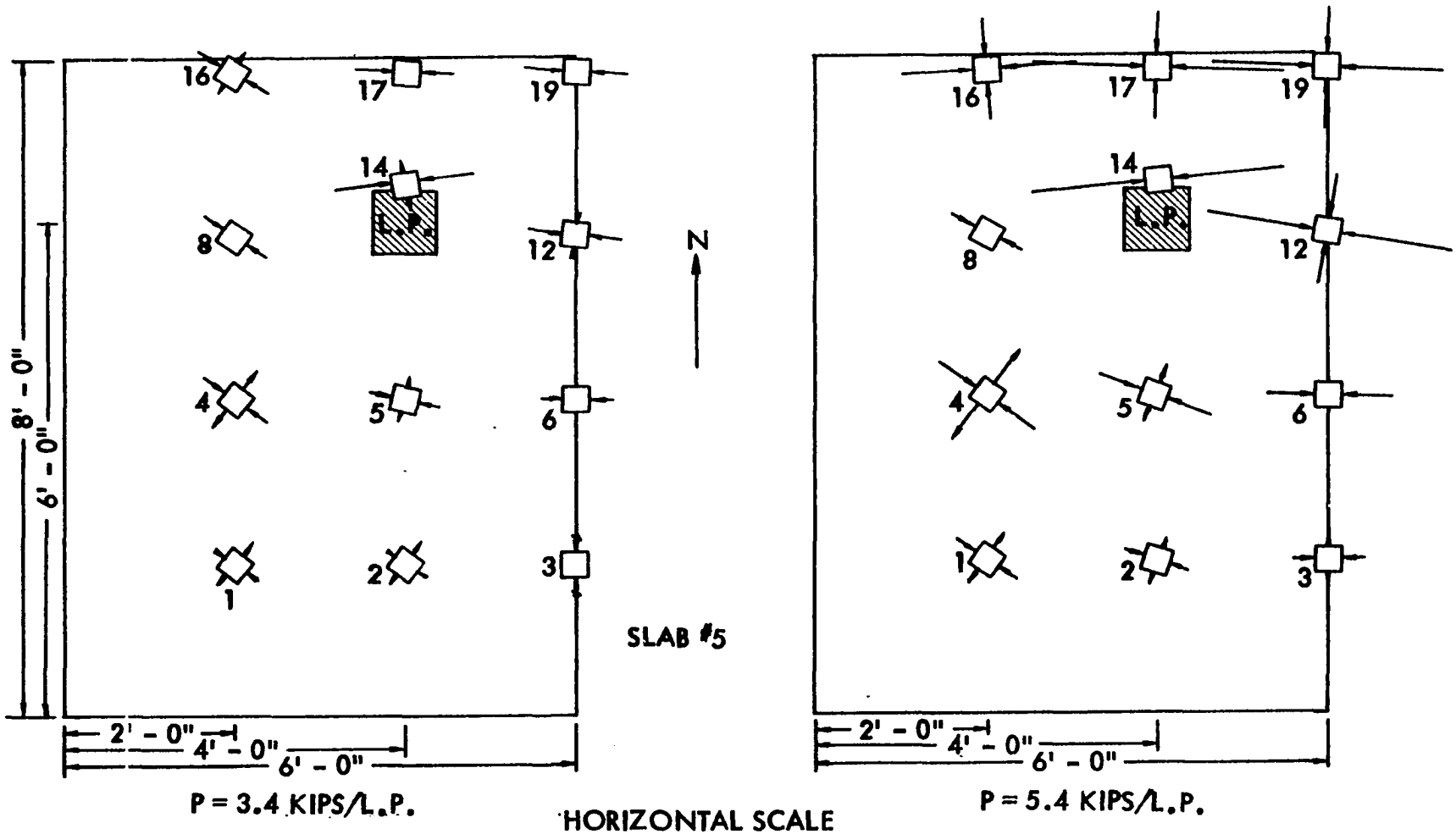

Figure 61. Principal strain analysis results for Slab 5

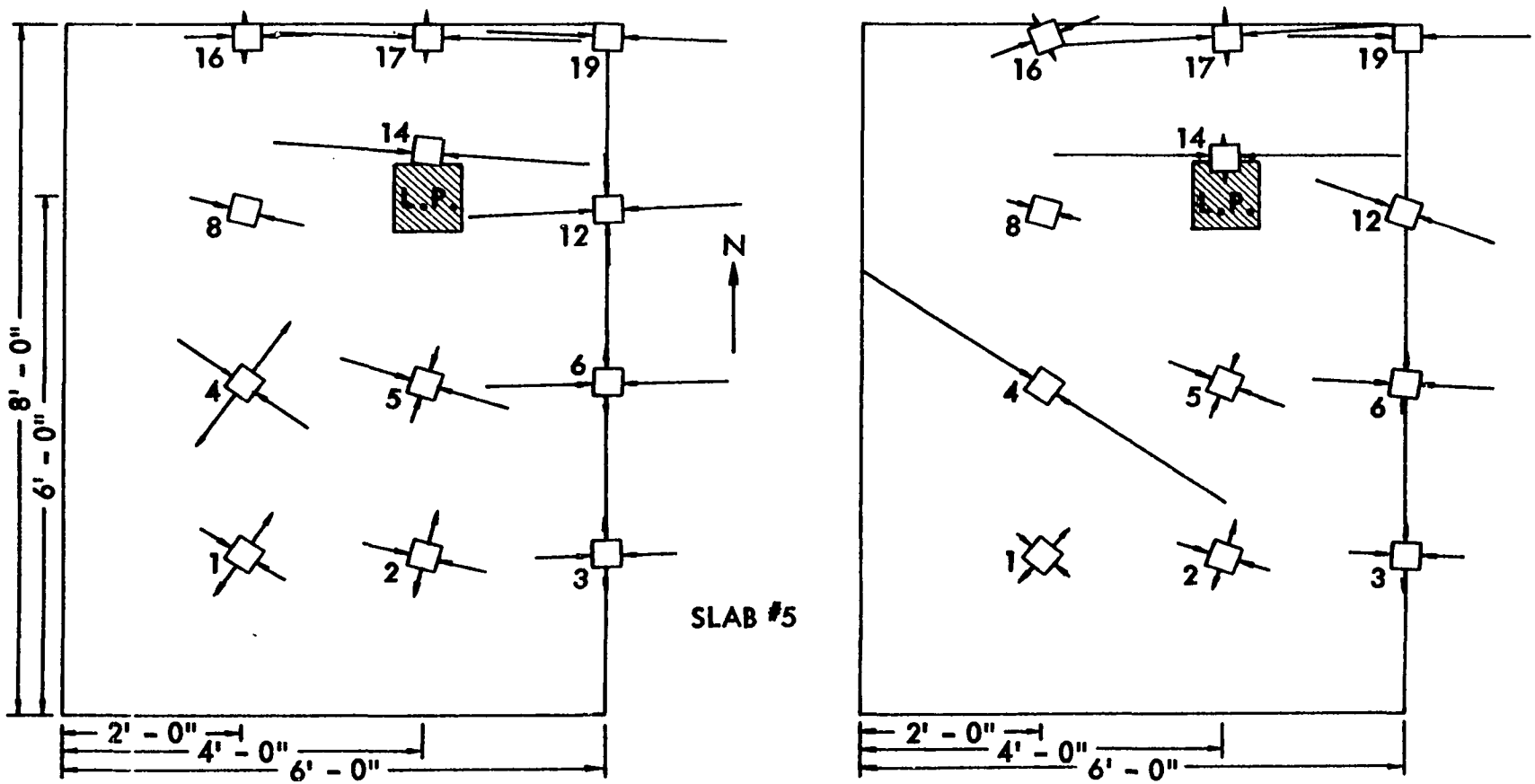

Figure 61. Continued

presented are the same as those presented in Table 17. Six gage locations in the southwest corner of Slab 3 were omitted for the first two load values before cycling due to an apparent error in data collection for those strains. The data for these six locations after cycling appeared okay, and is included, but this data too could be in some error.

The principal strain analysis yields several important behavioral observations regarding the force distributions in the slabs. A look at the general locations of where the largest principal tensile strains occurred substantiates where the top surface cracking occurred as was shown in Figure 32. A study of Figure 32 and the directions of principal tensile strains reveals that those strains are generally perpendicular to the top surface cracking. Note that as the top surface cracking across the slabs in the east-west direction curves towards the east and west edges, so does the direction of the principal angle. The locations of these high principal tensile strain regions further substantiates the location of the top surface cracking of the negative yield line pattern as given in Figure 6.

The high tensile strain at the furthermost southwest gage location on Slab 1 is due to the corner tie-down force. The direction of tensile strain also is nearly perpendicular to the diagonal corner cracking that occurred on Slab 1 at a load value just prior to 11.4 kips per load point.

A rough indication of the cracking occurrances from the tensile strain magnitude can be seen by looking at the magnitude of strain necessary to cause cracking of concrete as indicated by the modulus of rupture stress. The values of the uniaxial strain corresponding to modulus of rupture cracking are 132, 139, 142, 142, and 148 microinches per inch, respectively for Slabs 1-5. The actual value of tensile strain to cause cracking of the

slabs is dependent on the state of the biaxial stress field. However, uniaxial strains give an indication as whether cracking was possible. As can be seen the magnitudes of the tensile strains do generally predict the cracking locations across the slab surfaces, including the corner cracking of Slab 1.

The principal strains were not converted into corresponding stresses due to the time necessary to determine the complex biaxial stress-strain relations for concrete. However, a method presented by Liu, Nilson, and Slate (20) does give the appropriate stress-strain relations for concrete to account for microcracking and the biaxial effects. A method such as presented by Reference (20) should be used if stresses are desired from the given strain fields.

The locations of the larger compressive principal strains generally follow a diagonal pattern extending outward from the concentrated load point application location to the edge of the slab. These diagonal lines coincide with the locations of the expected positive moment yield line patterns as given in Figure 6. These large compressive principal strains are generally perpendicular to those yield lines. These principal strains further substantiate the locations and directions of the expected yield pattern for the areas of the slabs subjected to the higher moment forces.

Actual moment field distributions in the slabs can be computed from the strain fields. These moment computations should take into account the biaxial relations of concrete strength; however, as can be seen by the strain distributions previously presented and the principal strains, the compressive strain is much larger in magnitude than the other principal strain. Thus, approximate moments very close to the two experimental

ones at each gage location may be computed based on the uniaxial strains. These moments were computed for all strain locations for all loads before and after cycling for the five slab tests. These moment distributions follow the strain distributions and thus, will not be repeated here. However, sample moment computation behavior is presented in connection with the equivalent orthotropic plate analysis performed on the five slab tests.

CHAPTER 6. RESULTS AND ANALYSIS OF SLAB ELEMENT TESTS

Slab Elements with Steel-Deck Corrugations Transverse to Specimen Length

The 12 slab elements constructed with the deck corrugations transverse to the specimen length gave results for the determination of the flexural capacity transverse to the deck corrugations. These 6 X 2-foot specimens were tested as was shown in Figure 18. The description of these specimens was given in Table 6.

Various behavioral characteristics of these transverse specimens were observed. These include deflections, strains, and mode of failure. The instrumentation was presented previously in Table 12. The primary mode of failure for those specimens containing no supplementary reinforcement was that of sudden flexural failure like that of a plain concrete beam. For those specimens containing supplementary reinforcement, the failure was characterized by yielding of the reinforcement or by failure of the splices of the supplementary steel. The added supplementary steel resulted in a somewhat more ductile behavior near failure load.

Failure of all transverse sections was initiated by a vertical crack propagating from one of the top corrugations in the central region between the two line loads. A typical principal failure crack is shown in Figure 62 for transverse Specimen 2. Those specimens containing more substantial amounts of supplementary reinforcing had several vertical cracks in the central region between the load points, however, the orientation and location of the principal failure crack was essentially the same in all cases.

The test results for the 12 slab element specimens are presented in Table 18. In addition to ultimate loads, the table gives the cross-sectional

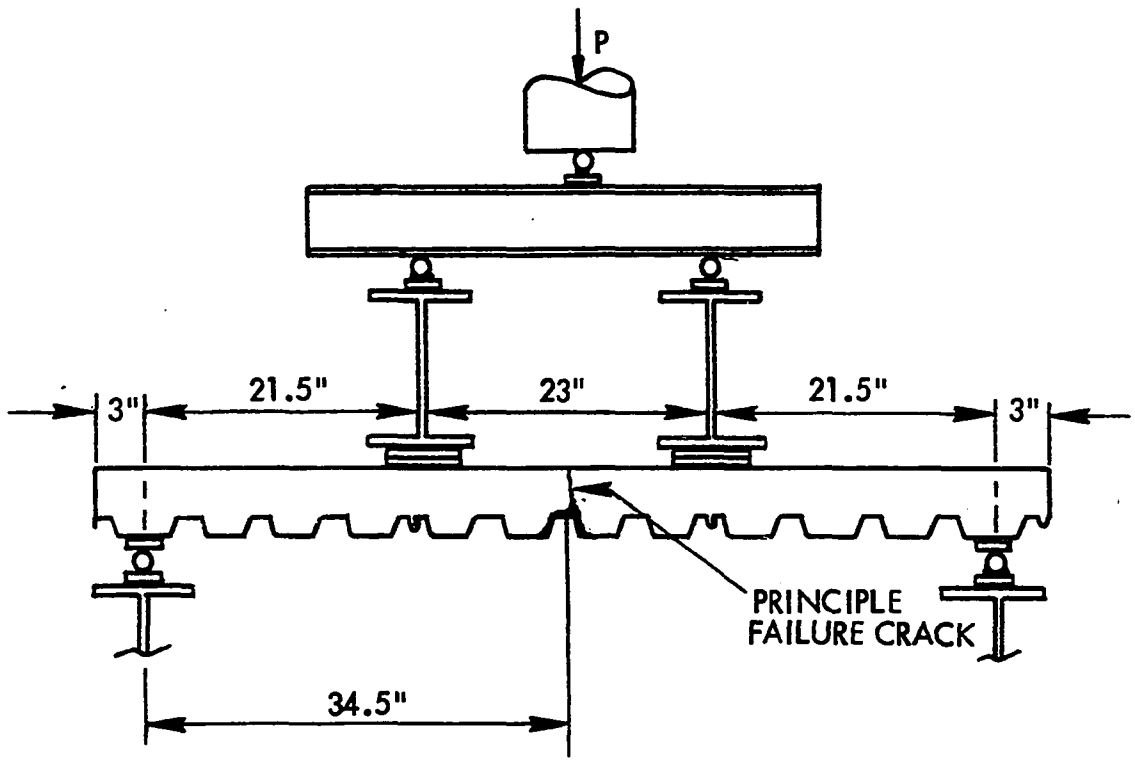

Figure 62. Principal failure crack for transverse specimens

area of supplementary steel reinforcing parallel to the specimen length and its depth location. Also shown is the applied load at which first cracking was observed. For those specimens containing no supplementary reinforcing, first cracking occurred at the same instant the ultimate load was reached. The loads do not include the self-weight of the specimens. The unit dead loads are presented in a separate column.

Several interesting computations were made regarding the predicted ultimate load capacity of these transverse members. The information of depths and steel areas in Table 18 was used to arrive at various computed flexural quantities which are summarized in Table 19. The total ultimate moment capacity in Table 19 includes the specimen dead weight. Since the transverse specimens had to span only a distance of two feet with their lengths basically uniformly supported during casting, the moment due to dead

Table 18. Ultimate experimental test results for slab elements with deck corrugations transverse to length. (see Table 6 for description.)

Transverse Specimen No.	Total Applied Load At First Observable Crack, (kips)	Specimen Unit Dead Weight, w (psf)	Total Ultimate Applied Load, P_{ue} (kips)	Ultimate Applied Shear, V_{ue} (kips/ft)	Shear Span, L' (in.)
1	1.55	56.0	1.55	0.39	24
2	1.95	56.0	1.95	0.49	21.5
3	1.55	50.0	5.25	1.31	21
4	1.45	50.0	1.85	0.46	21
5	3.55	50.0	6.25	1.56	21
6	unknown	50.0	1.95	0.49	21
7	1.25	50.0	1.25	0.31	21
8	2.2	48.0	4.3	1.08	24
9	2.1	48.0	3.5	0.88	24
10	2.1	48.0	3.9	0.98	24
11	0.36	50.9	0.36	0.09	24
12	0.55	50.9	0.55	0.14	24

Table 18. Continued

Transverse Specimen No.	Ultimate Applied Moment, M_{ue} (ft-kips/ft)	Out-to-out Depth, D (in.)	Depth Above Corrugations, $D-d_d$ (in.)	Span Length, L (in.)	Area of Supplementary Steel Parallel to Length, A_{s2} ($in.^2/ft$)	Depth to Centroid of Supplementary Steel (in.)
1	0.78	5.0	3.45	66	0.	0.
2	0.87	5.0	3.45	66	0.	0.
3	2.30	4.5	2.95	66	0.144	2.80
4	0.81	4.5	2.95	66	0.0575	2.85
5	2.73	4.5	2.95	66	0.144	2.80
6	0.85	4.5	2.95	66	0.0575	2.85
7	0.55	4.5	2.95	66	0.	0.
8	2.15	4.5	3.18	65	0.150	3.07
9	1.75	4.5	3.18	65	0.150	3.07
10	1.95	4.5	3.18	65	0.150	3.07
11	0.18	5.5	2.50	67	0.0282	1.0
12	0.28	5.5	2.50	67	0.0282	1.0

Table 19. Results of computed flexural properties of transverse specimens

Transverse Specimen No.	Total Ultimate Moment, Including Dead Weight, (ft-kips/ft)	Gross Moment of Inertia, $in.^4/ft$			Depth to Weighted Average of Depths, d_3, (in.)	Modulus Rupture, f_r (psi)
		To deck c.g.s. I_{g_1}	Above deck I_{g_2}	To weighted depth I_{g_3}		
1	0.99	83.5	41.1	53.6	3.77	466
2	1.08	82.9	41.1	53.6	3.77	466
3	2.49	58.0	25.7	36.3	3.31	455
4	1.00	58.0	25.7	36.3	3.31	455
5	2.92	58.0	25.7	36.3	3.31	455
6	1.04	58.0	25.7	36.3	3.31	455
7	0.74	58.0	25.7	36.3	3.31	455
8	2.33	56.8	32.2	42.1	3.48	541[a]
9	1.93	56.8	32.2	42.1	3.48	541[a]
10	2.13	56.8	32.2	42.1	3.48	541[a]
11	0.38	60.7	15.6	53.6	3.77	483
12	0.48	60.7	15.6	53.6	3.77	483

[a] $f_r = 521 \sqrt{\frac{4142}{3835}} = \frac{\sqrt{f'_c} \text{ @ 16 days}}{\sqrt{f'_c} \text{ @ 21 days}}$.

[b] Computed from splice length using ultimate bond strength. See text.

Table 19. Continued

Transverse Specimen No.	Computed Moment, (ft-kips/ft)			Computed Ultimate Moment, M_u, (ft-kips/ft)	
	Using I_{g_1}	Using I_{g_2}	Using I_{g_3}	By ACI	By General Strain Analysis
1	1.48	0.93	1.10	–	–
2	1.48	0.93	1.10	–	–
3	1.14	0.66	0.83	2.61	2.55
4	1.14	0.66	0.83	1.05	1.03
5	1.14	0.66	0.83	2.61	2.55
6	1.14	0.66	0.83	1.05	1.03
7	1.14	0.66	0.83	–	–
8	1.33	0.91	1.09	3.35 (2.26)[b]	3.24
9	1.33	0.91	1.09	3.35 (2.26)[b]	3.24
10	1.33	0.91	1.09	3.35 (2.26)[b]	3.24
11	1.19	0.50	1.14	–	–
12	1.19	0.50	1.14	–	–

weight was taken as simply $(1/8)(w)L^2$. This dead weight moment was then added to the live load experimental moment obtained from Table 18. This total experimental capacity is then used as a comparison to various computed moment capacities.

Since those specimens not containing supplementary reinforcement failed like that of a gross concrete section, a question arises as to the effective depth of this section. Three computed moment capacities were arrived at by using three different depths resulting in three corresponding moments of inertia to be used in the following ordinary flexure formula:

$$M = \frac{(f_r)(I_g)}{12c} \tag{41}$$

where

f_r = modulus of rupture strength of concrete,

I_g = the gross moment at inertia of the section, and

c = depth to extreme tension fiber.

The two moment of inertias, I_{g_1} and I_{g_2} in Table 19, are computed by considering a rectangular section whose depth is to the steel deck c.g.s. for I_{g_1}, and whose depth is to the top of the steel deck for I_{g_2}.

The third moment of inertia, I_{g_3}, was computed using a weighted depth. The weighted depth was obtained from the following expression:

$$d_3 = \frac{A_1 d_1 + A_2(d_1 + d_2)}{A_1 + A_2}$$

where

A_1 = area above the corrugations,

A_2 = area within the corrugations,

d_1 = depth of A_1,

d_2 = depth of A_2 = depth of deck, d_d, and

d_3 = weighted depth of concrete area.

As can be seen in Table 19, comparing the resulting three computed moment capacities to the experimental capacity indicates that the depth to the top of the corrugations gives the best conservative result for those specimens containing no supplementary steel, i.e. Numbers 1, 2, 7, 11 and 12 (neglecting the area of steel for 11 and 12 since steel was in the top part of specimen). Thus, the flexural capacity transverse to the corrugations can be adequately determined from Equation (41) using the gross moment inertia of a section above the corrugations. This result is for those cases involving no supplementary reinforcing.

For those cases when supplementary steel existed, the flexural capacity was computed utilizing the following standard ACI (2) and (4) formula:

$$M_u = \frac{A_s F_y}{12} (d - a_u/2) \qquad (42)$$

where

$$a_u = \frac{A_s F_y}{.85 f'_c (12)},$$

A_s = area of supplementary steel,

F_y = yields strength (see Table 2), and

f'_c = concrete strength (see Table 3).

The resulting ultimate moment computations based on Equation (42) are tabulated in Table 19. However, the use of Equation (42) assumes an ultimate concrete strain of 0.003 in the top fiber. A check was performed and it was found that the supplementary reinforcing had insufficient strain ductility to allow the concrete strain to reach its ultimate assumed value. Also shown in Table 19 are ultimate moments as computed by general strain analysis.

The assumptions of this general strain analysis are based on the steel reaching yield strain (near ultimate for this high-strength steel) as the limiting criteria and letting the resulting equilibrium of tensile and compressive forces determine the predicted ultimate moment. The method of this general strain analysis is discussed later in this chapter. Note that the invalid ACI Equation (42) and the general strain analysis still give predicted moments which are very close to each other.

The predicted moments by these computations compare fairly well with the experimental results for Specimens 3, 4, 5, and 6 but do not compare very favorably for Numbers 8, 9, and 10. Specimens 8, 9, and 10 contained deformed wire spot-welded to the top corrugations. This wire came in segments of roughly one panel width of the decking and, when placed, had splices of about 4½ inches. As discussed below, the actual moment capacity for Specimens 8, 9, and 10 was limited by the splice.

The number in parenthesis for Specimens 8, 9, and 10 in Table 19 under the column giving the computed ultimate moment, M_u, was found by determining the maximum force the splice would withstand. The ultimate bond stress for D4 deformed wire based on pullout tests was given by Lloyd and Kesler (21) as 800 psi. Equating this ultimate bond force to the force of the reinforcing steel results in the following expressions (for 4 wires per foot):

$$4U_u \pi t_w \ell = A_{s_2} f_s$$

where

U_u = ultimate bond stress = 800 psi (21),

t_w = diameter = 0.212 inches,

ℓ = length of splice = 4½ inches,

A_{s_2} = area of deformed wire steel per foot = 0.150 square inches, and

f_s = stress in supplementary steel reinforcement in psi.

Thus,

$$f_s = \frac{4U_u \pi t_w \ell}{A_{s_2}} = 64{,}019 \text{ psi} \qquad (43)$$

Using the stress given by the bond Equation (43), the moment capacity was then computed using the strain and force diagrams given in Figure 63. Note that a linear stress-strain relationship for the concrete was used in this case in that the computed concrete strain necessary for equilibrium was about one-fourth that at f'_c. Thus for low concrete strains, the concrete stress-strain diagram is essentially linear. Equating the C and T forces in Figure 63 gives the resulting strain in the concrete, ϵ_c. This is accomplished by substituting for f_c the following relationship:

$$f_c = \epsilon_c E_c$$

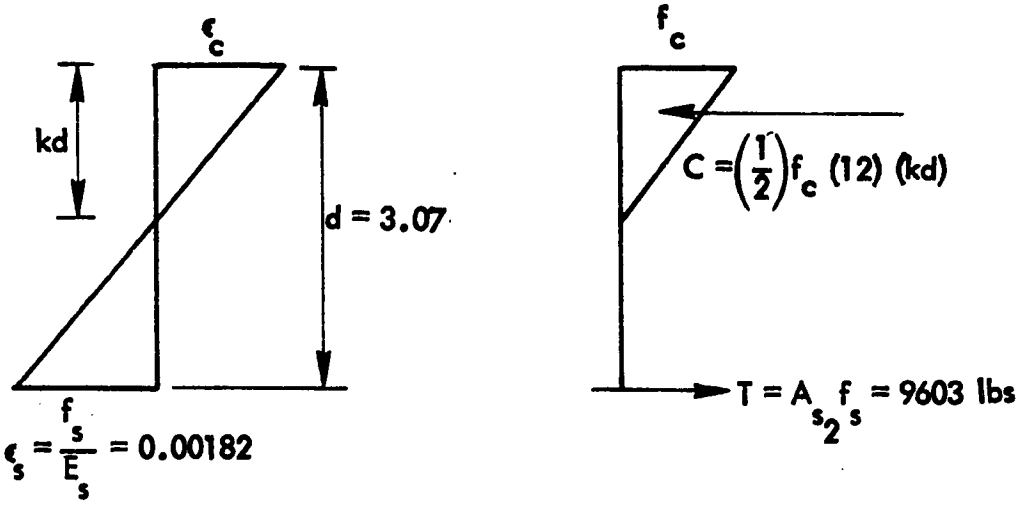

Figure 63. Strain and force relations for Transverse Specimens 8, 9, and 10

where

E_c = modulus of elasticity of concrete, taken as 57,000 $\sqrt{f'_c}$ as given by ACI code (2).

Once ϵ_c was known, then the location of the C force was known, as given in Figure 63. The resulting moment of the section of 2.26 ft-kips per ft was then found by summing moments about the C force. This moment is given in parenthesis for M_u in Table 19 for Specimens 8, 9, and 10.

It is important to note that the M_u for Specimens 8, 9, and 10 was based on a limiting stress as determined by the splice of the supplementary steel, and thus, the steel did not reach yield. However, for Specimens 3, 4, 5, and 6, the capacity, M_u, was adequately predicted by assuming a yielding of the supplementary steel.

Thus, the ultimate flexural strength of sections containing supplementary reinforcement transverse to the deck corrugations may be obtained by general strain analysis, ultimate strength computations, neglecting any beneficial effect of the presence of the steel decking, except for those cases controlled by splices of the supplementary steel. For those cases where yielding of supplementary steel is preceded by a bond failure of the splice, the flexural capacity transverse to the deck corrugations may be obtained by considering the ultimate bond strength of the splice. This in turn gives the steel stress in the supplementary steel which then can be used to determine the moment capacity.

A summary of the behavioral characteristics of the transverse slab element tests can be shown by looking at the load-deflection characteristics. These load versus deflection relationships are shown in Figure 64. Note that the specimens were grouped and the average load-deflection curve

is shown for the centerpoint only of each group. Each group comprises all specimens that were identical in size and reinforcing as indicated on the figure. As would be expected, those specimens containing the larger amounts of supplementary reinforcing exhibited the greatest ductility, whereas those containing no additional supplementary steel exhibited a load-deflection curve like that of a plain concrete beam. The usual L/360 criteria is shown on the figure as a measure of the relative amount of deflection sustained by each type of specimen.

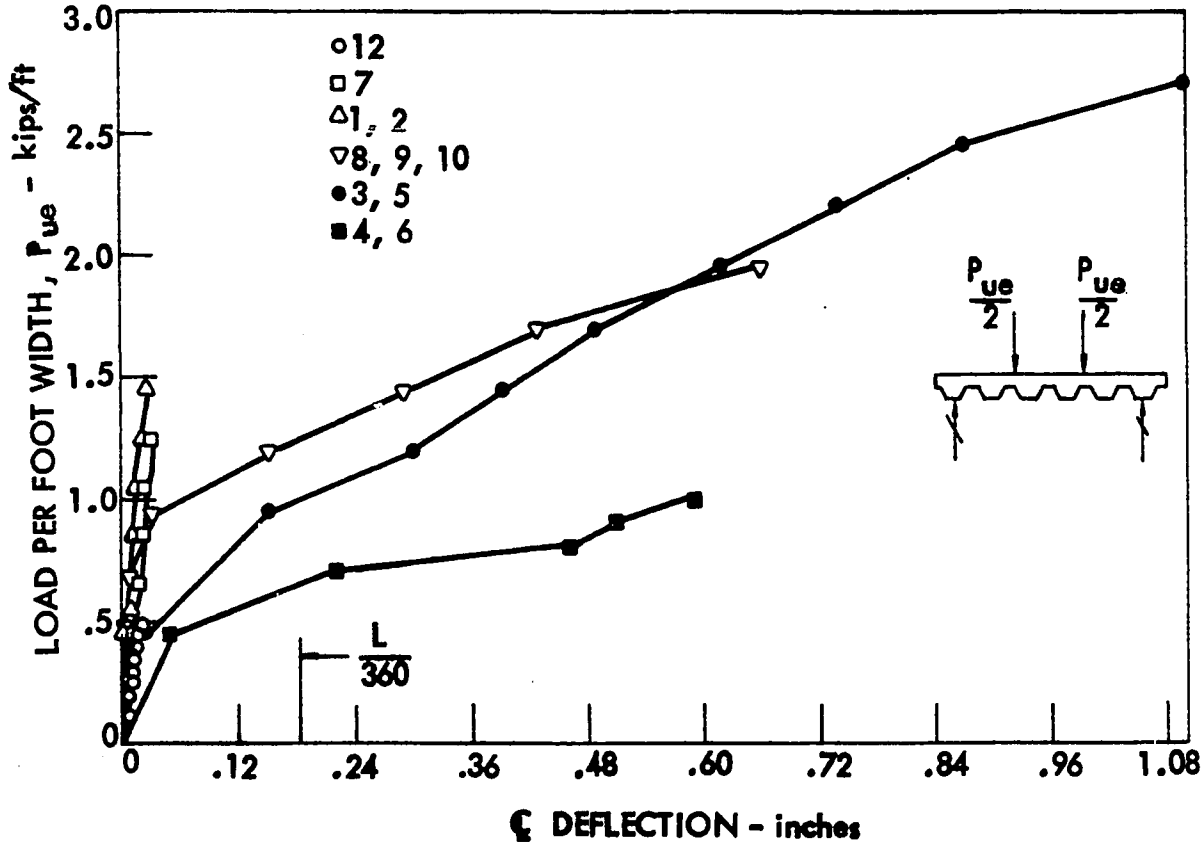

Figure 64. Load-deflection relationships of the transverse slab element tests

Slab Elements with Deck Corrugations Parallel to Specimen Length

General results

As discussed previously, testing of slab elements with the deck corrugations parallel to the specimen length was done primarily for four purposes. These purposes are as follows:

1. To determine shear-bond regression coefficients for use in predicting one-way ultimate shear capacity for the 3-inch-deep decking used in Slab 5,
2. to determine the one-way characteristics of slab tests by testing companion specimens exactly like the two-way slabs,
3. to test the effect of light supplementary reinforcing on shear-bond strength, and
4. to determine behavioral characteristics of failure of one-way elements reinforced with 3-inch-deep steel decking.

A complete summary of experimental results of these one-way longitudinal slab element tests is shown in Table 20. Included in Table 20 are the ultimate applied loads, shears, and moments exclusive of the specimen's own weight which is listed separately. The specimen dead weight was taken as an approximate average weight over the length of the member. Other pertinent information in the table includes the area of steel reinforcing, depths to the reinforcing, and the applied load at which the first major crack was observed. All specimens were tested with either a single concentrated-line load or two single concentrated-line loads as shown in Figure 4. The description of specimen purpose, size, and material properties is given in Table 9.

Table 20. Loads, shears, and moments for longitudinal specimens

Specimen No.	Span Length, L (in.)	Shear Span, L' (in.)	Applied Load At First Crack (kips)	Total Applied Load, P_{ue} (kips)	Total Applied Shear, V_{ue} (kips/ft)	Total Applied Moment (ft-kips/ft)
1	68.	24.	9.7	10.9	2.73	5.45
2	68.	24.	10.3	10.3	2.58	5.15
3	68.	24.	11.3	12.1	3.03	6.05
4	68.	24.	10.3	10.3	2.58	5.15
5	68.	24.	11.8	11.8	2.95	5.90
6	68.	24.	10.8	10.8	2.70	5.40
7	140.	45.5	5.0	13.5	2.38	9.02
8	140.	45.5	3.3	15.0	2.65	10.04
9	140.	70.	2.44	6.84	1.14	6.63
10	140.	48.	4.2	8.8	1.48	5.93
11	140.	70.	1.84	7.24	1.22	7.09
12	140.	48.	2.7	8.3	1.39	5.55
13	68.	24.	7.33	13.03	2.18	4.36
14	68.	24.	8.13	13.63	2.26	4.51
15	68.	24.	8.13	13.53	2.24	4.48
16	140.	48.	3.5	8.5	1.44	5.75
17	140.	70.	2.44	7.14	1.18	6.91
18	188.	86.	1.23	5.93	0.99	7.11
19	140.	45.5	3.5	9.5	1.57	5.96
20	140.	45.5	3.3	9.3	1.54	5.86
21	188.	86.	1.01	3.81	0.64	4.55
22	188.	86.	2.55	7.66	1.28	9.15
23	140.	70.	unknown	10.28	1.71	9.99
24	140.	70.	4.22	10.30	1.72	10.01
25	116.	48.	6.94	14.70	2.45	9.80
26	116.	48.	5.82	13.59	2.27	9.06
27	116.	48.	4.02	12.34	2.06	8.23
28	68.	24.	15.94	18.75	3.10	6.21
29	68.	24.	11.89	18.87	3.15	6.29
30	68.	24.	10.77	17.63	2.92	5.84
31	68.	24.	8.52	15.60	2.58	5.16
32	68.	24.	8.52	15.94	2.64	5.28
33	68.	24.	7.39	15.72	2.60	5.20
34	116.	48.	5.14	11.78	1.98	7.91
35	116.	48.	5.14	11.89	1.98	7.93
36	116.	48.	1.77	10.91	1.82	7.27
37	140.	70.	2.35	8.60	1.43	8.36
38	140.	70.	2.32	8.77	1.46	8.53
39	188.	86.	1.77	7.62	1.27	9.10

Specimen Dead Weight (psf)	Area of Steel Decking, A_s (in./ft)	Area of Supplementary Steel Parallel to Length A_s, ($in.^2$/ft)	Out-to-Out Depth Near Load Point (in.)	Deck to c.g.s. of Deck (in.)	Depth to Supplementary Steel Parallel to Length (in.)
51.6	0.625	0.039	4.69	4.07	3.66
52.8	0.625	0.	4.78	4.15	–
51.7	0.625	0.057	4.70	4.07	3.78
52.9	0.625	0.	4.90	4.27	–
52.0	0.625	0.039	4.80	4.17	3.76
51.8	0.625	0.057	4.77	4.14	3.85
48.9	0.376	0.	4.50	3.85	–
52.6	0.376	0.	4.87	4.22	–
52.4	0.575	0.	5.63	4.12	–
52.1	0.575	0.	5.69	4.12	–
51.7	0.575	0.	5.56	4.05	–
51.4	0.575	0.	5.56	4.05	–
50.1	0.575	0.	5.44	3.93	–
51.9	0.575	0.	5.63	4.12	–
51.1	0.575	0.	5.56	4.05	–
51.7	0.575	0.	5.56	4.05	–
48.6	0.575	0.	5.31	4.05	–
52.4	0.575	0.	5.63	4.12	–
55.5	0.575	0.0282	5.87	4.36	1.0
52.0	0.575	0.0282	5.56	4.12	1.0
51.5	0.452	0.	5.69	4.18	–
53.1	0.979	0.	5.62	3.99	–
53.2	0.979	0.	5.56	4.05	–
53.2	0.979	0.	5.50	3.99	–
54.8	0.979	0.	5.81	4.30	–
53.1	0.979	0.	5.56	4.05	–
53.9	0.979	0.	5.56	4.05	–
52.5	0.979	0.	5.50	3.99	–
51.3	0.979	0.	5.38	3.99	–
52.4	0.979	0.	5.50	3.99	–
52.1	0.745	0.	5.56	4.18	–
52.7	0.745	0.	5.56	4.05	–
52.9	0.745	0.	5.63	4.12	–
53.3	0.745	0.	5.69	4.18	–
54.6	0.745	0.	5.81	4.30	–
52.1	0.745	0.	5.50	3.99	–
53.7	0.745	0.	5.75	4.24	–
53.4	0.745	0.	5.75	4.24	–
53.0	0.745	0.	5.69	4.18	–

All longitudinal specimens tested ultimately failed by a shear-bond mode of failure except one, that being Specimen 7 which failed by a flexural mode of failure. All specimens reinforced with decking containing embossments as their shear transferring device (i.e., Specimens 1-6 and 9-39) failed by a shear and bond action consisting of the concrete portion between a load point and the end reaction over-riding the embossments. This shear-bond mode of failure was characterized by a major failure crack (usually diagonal) near the load point allowing the separation of the concrete portion to occur resulting in a slippage at the ends of the specimens. The shear-bond failure and end slippage was catastropic and occurred at the ultimate load of the specimens. No end slippage was evident until the ultimate load was reached for all 38 longitudinal slab elements failing by shear-bond.

The addition of supplementary reinforcing did not alter the mode of failure. In other words, the addition of WWF was not sufficient to prevent the horizontal slippage between the concrete and steel interface. In some instances the steel decking yielded prior to the shear-bond failure. Nevertheless the load at which shear-bond failure occurred was always the ultimate load unless a flexural failure by rupture of the deck took place as for Specimen 7.

Shear-bond analysis of longitudinal specimens

Previous tests conducted at Iowa State University (References 24 and 40) have verified the shear-bond regression analysis for steel-deck reinforced slab elements constructed from steel deck sections like these in Slabs 1-4. However, shear-bond verification was needed for the deeper (3-inch) type of deck utilized in Slab 5. Longitudinal Specimens 9-18 and

21-39 in Table 20 were conducted primarily to ascertain the validity of the shear-bond regression approach for the 3-inch-deep steel deck cross sections. A complete discussion of the behavioral characteristics and analysis of these 3-inch-deep slab element specimens is contained in Reference (32). Also included in Reference (32) is a discussion of the computation of theoretical deflections. Additional discussion in Reference (32) concerns the computation of design loads obtained from the shear-bond regression formulations of the experimental data. An example of the shear-bond regression of the experimental results is illustrated in this section for the longitudinal specimens containing the 3-inch-deep embossed deck employed in Slab 5.

The shear-bond regression analysis of the relationship between $V_{ue}s/b_d dp$ and $d\sqrt{f'_c}/L'p$ is shown in Figure 65 for longitudinal Specimens 9-18, which were reinforced with the 20-gage Type O decking, the same gage as Slab 5. Since Type O deck has embossments in a fixed pattern, then s in the regression relations is taken as unity. As can be seen, the regression of the two relationships exhibits good linearity, with all data within $\pm$ 8% of the regression fit. Thus, the shear-bond analysis is reasonably valid for deeper deck cross-sections of the type tested.

The same regression was run for Specimens 22-30 for 16-gage Type O deck and for Specimens 31-39 for 18-gage Type O deck. The 16- and 18-gage deck shear-bond regression analysis had the same linear relationship as the 20-gage did in Figure 65. Only the constants, k_1 and k_2 (slope and intercept, respectively), changed. A summary of these constants obtained for Type O deck for the various gages and these constants for Types I and G decks used in Slabs 1-4 is given in Table 21.

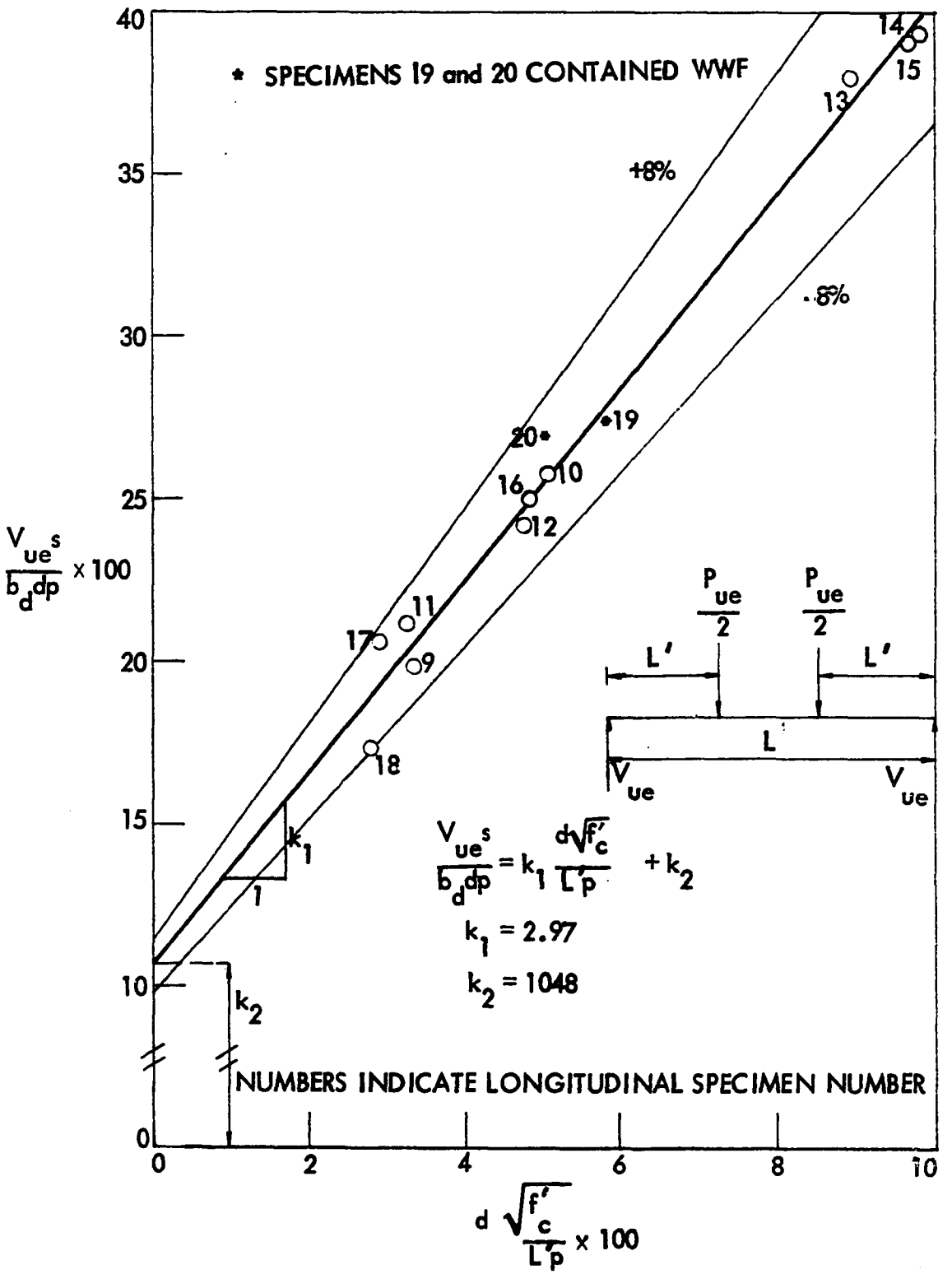

Figure 65. Relationship between $V_{ue}s/b_d dp$ and $\sqrt{f'_c}d/L'p$ for longitudinal slab elements with 20-gage Type O decking

Table 21. Summary of k_1 and k_2 constants for $V_{ue}s/b_d dp$ vs. $d\sqrt{f'_c}/L'p$ and constants k_3 and k_4 for $V_{ue}s/b_d dt$ vs. $d\sqrt{f'_c}/L't^2$

Deck Type	Nominal Gage	Steel Thickness, in.	k_1	k_2	Deck Used For Slab No.
0	20	0.0347	2.97	1,048	5
0	18	0.0453	3.45	1,202	none
0	16	0.0595	4.30	1,007	none
I[a]	20	0.0369	3.18[b]	648[b]	1, 2, & 3
G[a]	24	0.0252	11.68	12,539	4[c]

		k_3	k_4
I[a]	All thicknesses tested	3.10	8,340
0	All thicknesses tested	3.29	8,292

[a]Obtained from reference (40).

[b]These values were based on 22-gage deck regression analysis in reference (40).

[c]s in the regression relationship equals the T-wire spacing of 3 inches for this slab.

Taking the dowel shear as a function of the square of the thickness of steel, as done in Reference (40), gives a regression of $V_{ue}s/b_d dt^2$ vs $d\sqrt{f'_c}/L't^2$. Performing this regression on all gages tested, i.e. 22, 20, 18 and 16, also gives a linear relationship. This composite regression of all gages involving Type 0 deck using Specimens 9-18 and 21-39 is shown in Figure 66. As can be seen in the figure, the composite regression based upon the thickness squared gives a good linear relationship for shear-bond analysis.

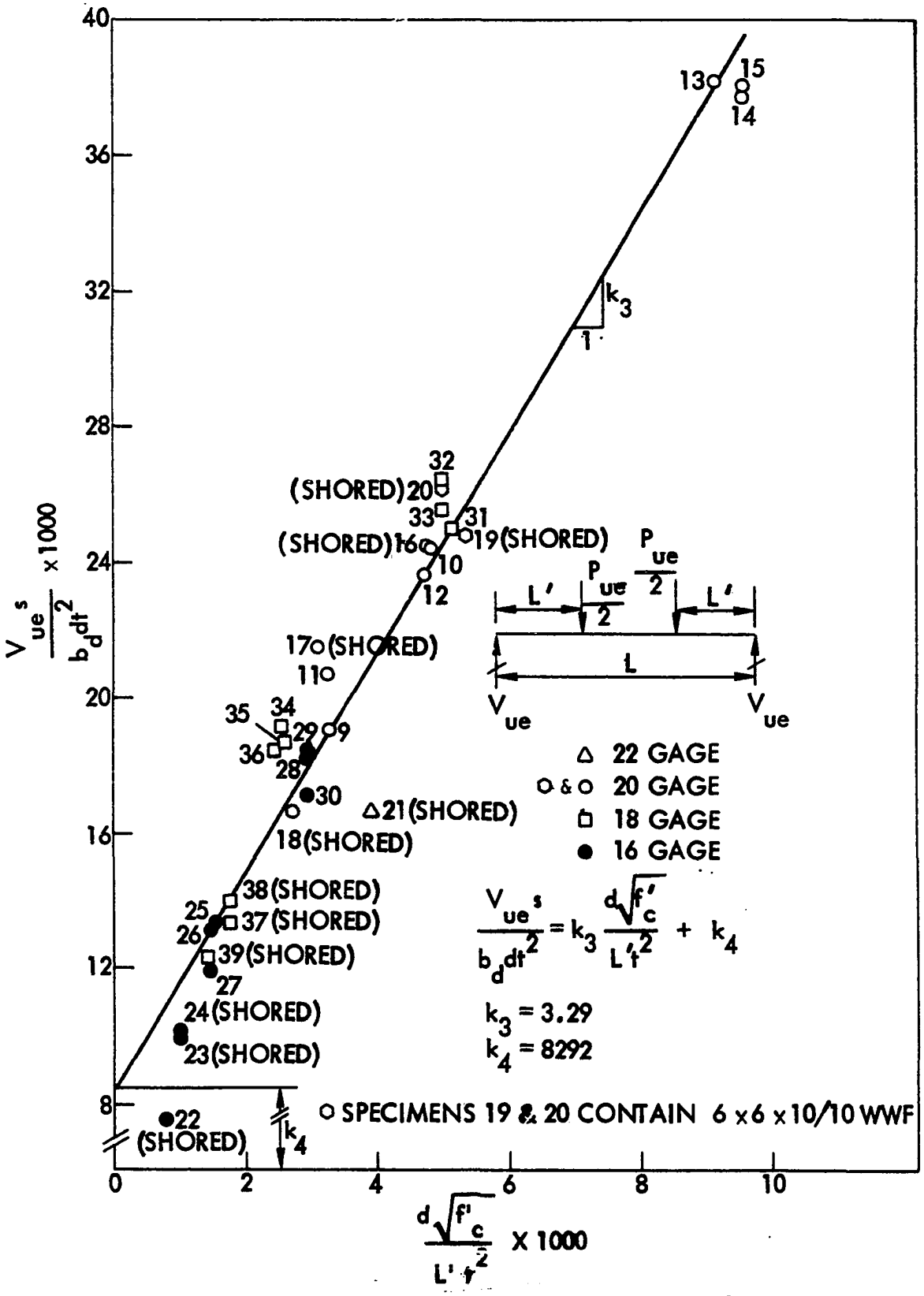

Figure 66. Relationship between $V_{ue}s/b_d t^2$ and $\sqrt{f'_c}d/L't^2$ for all longitudinal slab elements tested containing Type O decking

Flexural analysis of slab elements

General strain analysis A general strain compatibility analysis was utilized to compute the flexural capacity of the longitudinal one-way slab elements. The general strain analysis approach was particularly useful for the deeper 3-inch deck specimens and the specimens reinforced with Type G deck. The Type G deck was of very high strength (F_y = 101.6 ksi) and did not have the stress-strain ductility (see Figure 14) necessary for the usual ACI flexural equation as given by Equation (42). The general strain analysis has the advantage of also being able to take into account locked-in strains due to casting and shoring conditions.

Figure 67 summarizes the strain diagrams that were superimposed to obtain the flexural capacity for the general flexural strain analysis. The first strain diagram in Figure 67 represents the strains in the steel deck due to casting. Note this diagram has compressive strains at top fibers of deck and tensile strains at the bottom fiber, representing the case for a single shore at centerline. The centerline strains are superimposed for all cases illustrated in Figure 67, but the critical location occurs near

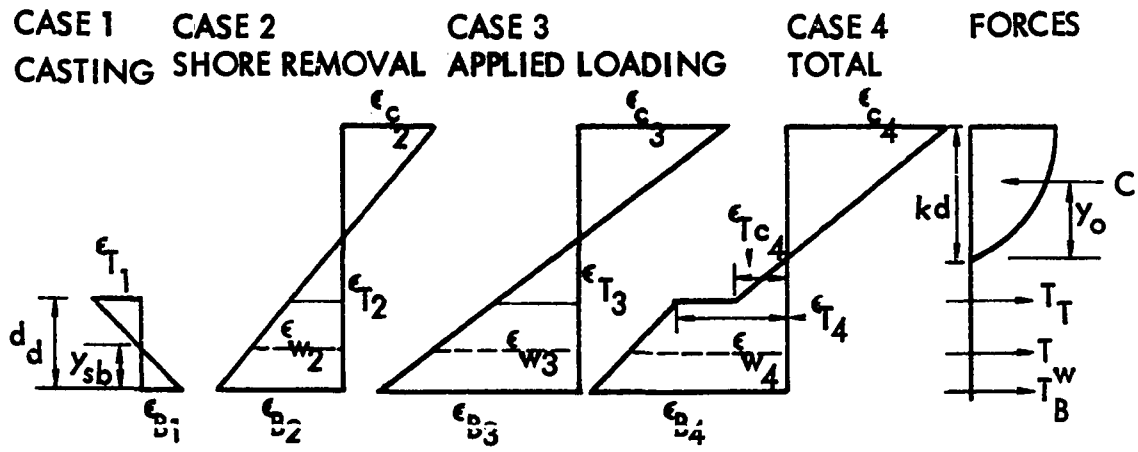

Figure 67. Strain diagrams used to obtain general strain-computed flexural capacity of slab elements

the location of the applied loading. The second strain diagram in Figure 67 represents strains due to shore removal, assuming that the force exerted on the shore is applied to the composite section. The uncracked transformed moment of inertia values were used to determine the strains for Case 2 from the expression Mc/E_cI. The third case in Figure 67 represents strains due to applied loading. If one of the total strains, say the bottom strain of deck at rupture, is known then the bottom strain for Case 3 is known by arithmetic. The strain diagram for live loading (Case 3) is then found by iteration to give equilibrium of the internal compressive force and the tensile forces, i.e. until $C = T_T + T_w + T_B$.

The compressive force, C, was found from a theoretical stress-strain equation of the concrete. The theoretical equation selected was obtained by Smith and Young (47) and is given by:

$$f = f'_c \left(\frac{\epsilon_c}{\epsilon_o}\right) e^{1-\epsilon_c/\epsilon_o} \qquad (44)$$

where

f'_c = compressive cylinder strength,

ϵ_o = strain of concrete @ f'_c, taken as 0.002,

ϵ_c = strain at top fiber of concrete, and

f = stress corresponding to strain, ϵ_c.

Evaluating the total compressive force, C, then results in the following equation:

$$C = b(kd) f'_c \left(\frac{\epsilon_o}{\epsilon_c}\right) e \left[e^{-\epsilon_c/\epsilon_o}\left(-\frac{\epsilon_c}{\epsilon_o} - 1\right) + 1\right] \qquad (45)$$

The subsequent location of this C-force from the neutral axis is given by

$$y_o = \frac{kd\left[e^{-\epsilon_c/\epsilon_o}\left[-1-2\left(\frac{\epsilon_o}{\epsilon_c}\right)-2\left(\frac{\epsilon_o}{\epsilon_c}\right)^2\right]+2\left(\frac{\epsilon_o}{\epsilon_c}\right)^2\right]}{\frac{\epsilon_o}{\epsilon_c}\left[e^{-\epsilon_c/\epsilon_o}\left(-\frac{\epsilon_c}{\epsilon_o}-1\right)+1\right]} \qquad (46)$$

In order to complete the general strain flexural analysis, one quantity on the total strain diagram in Figure 67 is needed. That one quantity could be any one of the strains indicated in the figure, i.e. ϵ_{C_4}, ϵ_{T_4}, ϵ_{W_4}, or ϵ_{B_4} or somewhere in between. For those decks having a steel stress-strain curve of small ductility, such as Deck G, the controlling strain was selected as the strain at ultimate stress for the bottom fiber of deck (ϵ_{B_4}). If enough ductility is capable of being developed, the controlling strain should be taken as $\epsilon_{C_4} = 0.003$ as limited by the ultimate strain of the concrete. In between cases depend upon the definition of the design ultimate moment. For example, if the design is based upon initial yielding of the bottom fibers of deck, then ϵ_{B_4} should be equal to the strain at the yield strength of the steel. Likewise, the design could be based upon initial yielding of the top fiber of deck, in which case ϵ_{T_4} would be the yield strain. If any other criteria other than choosing ϵ_{B_4} is used, then the strain determined for ϵ_{B_4} from the general analysis should be inspected to see if this strain development is possible as indicated by the steel coupon stress-strain relationship.

Three-inch-deep deck slab elements Since some of the slab elements with 3-inch-deep decking yielded prior to shear failure, the general analysis was performed on the longer elements that were given in Table 20. The ultimate moments computed by initial yielding of the bottom fibers of deck

are shown in Table 22. Also shown for a comparison are the moments based on yielding of the top fiber of deck. These moments are then compared to the ACI Code moment as given by Equation 42.

As can be seen in Table 22, a significant difference in the predicted flexural capacity exists depending on the method of computations. All specimens in Table 22 failed ultimately by a shear-bond mode of failure, so the experimental values do not necessarily compare with the computed ones. Specimen 21 in Table 22 is of particular significance because it exhibited yielding across the entire deck cross section prior to failure. The reserve strength in Specimen 21, as indicated by the 1.09 ratio of Column 3 to Column 2 in Table 22, can probably be attributed to the strain-hardening strength and some redistribution of forces in the steel decking. All specimens in Table 22 which contained strain gages demonstrated yielding of the bottom fibers of decking prior to ultimate shear-bond failure. A report of the experimental strain results for these specimens is given in Reference (32).

Longitudinal specimens companion to two-way slab tests The one-way slab element specimens tested in this investigation with exactly the same span length and shear span as the two-way slab tests were considered as companion test specimens. These longitudinal elements were cast companion to Slabs 4 and 5. Separate companion slab elements for the steel deck used in the first three two-way slabs were not constructed since numerous previous tests (40) had been conducted. The particular companion slab elements presented in this discussion are Specimens 7 and 8 for Slab 4 and Specimens 19 and 20 for Slab 5. (See Table 20 for particulars regarding experimental load results.) All companion specimens were tested as shown

Table 22. Computed ultimate moments by general strain analysis

Slab Element No.	[1] Ultimate Moment By Yielding of Bottom Fiber (ft-k/ft)	[2] Ultimate Moment By Yielding of Top Fiber (ft-k/ft)	[3] Experimental Ultimate Moment (ft-k/ft)	Ratio 3/1	Ratio 3/2	Ratio 3/ACI Moment
21	5.55	6.41	6.13	1.10	0.96	0.95
22	9.46	12.57	10.76	1.14	0.86	0.90
39	7.74	9.87	10.72	1.38	1.09	1.09
18	7.47	9.15	8.70	1.16	0.95	0.96
9	7.15	9.16	7.51	1.05	0.82	0.83
11	7.00	9.01	7.96	1.14	0.88	0.90
17	7.00	9.01	7.78	1.11	0.86	0.88
23	9.41	12.81	10.89	1.16	0.85	0.89
24	9.23	12.60	10.90	1.18	0.87	0.91
37	7.61	10.03	9.27	1.22	0.92	0.93
38	7.61	10.04	9.44	1.24	0.94	0.95
10	7.15	9.17	6.81	0.95	0.74	0.76
12	7.00	9.01	6.42	0.92	0.71	0.73
16	7.03	9.03	6.62	0.94	0.73	0.75

in Figure 4 with a span length of 140 in. and a shear span of 45½ in.

Specimens 8, 19, and 20 failed by the shear-bond mode of failure. Specimen 7 failed by flexure resulting in an ultimate rupturing of the steel deck reinforcement by first tearing the bottom corrugations and then tearing of the complete deck cross section. End slip was noted at the time of failure for the shear-bond failures. No end slip was observed for the one specimen failing in flexure. One significant difference between Specimens 7 and 8 was that the depth of Specimen 8 was larger at the failure location resulting in an increased moment capacity which allowed the shear capacity of the spot-welds to be exceeded causing a shear-bond failure to occur first.

Specimens 19 and 20 contained supplementary 6 x 6 x 10/10 WWF placed about one inch from the top fiber. The addition of the WWF did not apparently affect the shear-bond behavior. In fact, the results of the shear-bond calculations for Members 19 and 20 indicate they fall in line with the other specimens. This is indicated by looking at where Specimens 19 and 20 fall on the shear-bond regression curves in Figures 65 and 66.

A comparison of computed ultimate moment capacities by Equation (42) and experimental capacities is shown for the four longitudinal companion specimens in Table 23. As can be seen, Specimens 19 and 20 companion to Slab 5 reached only an average of 73.5 % of ultimate moment capacity. However, Elements 7 and 8 sustained about 91.5% of the computed ACI flexural capacity. This is, of course, unconservative. Specimens 8, 19, and 20 have a value less than computed due to the premature shear-bond failure.

The computed ultimate moment for Slab Element 7 warrants further discussion. The steel deck in Specimen 7 was of high strength steel with

Table 23. Computed and experimental moment capacities of companion longitudinal slab elements (See Table 20 for load values, depths, and areas of reinforcement)

Slab Element No.	Applied Dead Load Moment = $wL^2/8$ (ft-k/ft)	Total Ultimate Experimental Moment = $M_{DL} + M_{LL}$ (ft-k/ft)	Computed Ultimate Moment from Eq. (42) (ft-kips/ft)	Experimental M_u / Computed M_u
7	.82	9.84	10.75	0.92
8	.855	10.87	11.99	0.91
19	.91	6.87	9.57	0.72
20	.88	6.74	9.01	0.75

smaller strain capability. In fact, the ACI code equation (42) is not valid for the computed ultimate moment capacity of this type of specimen. The ACI code assumes a 0.003 strain reached in the concrete due to the steel not having sufficient strain ductility to give a normal ductile beam type behavior. Specimen 7 failed quite suddenly.

The general strain analysis as given by Figure 67 and Equations (44), (45) and (46) was used to compute the ultimate moment capacity for the slab elements in Table 23. The controlling strain for Specimens 7 and 8 was taken as the strain corresponding to the ultimate steel stress (F_u) of the steel. The results of these computations are shown in Table 24. An additional calculation was performed assuming a yield strain at the bottom fiber of deck and is included in Table 24. As can be seen, not much difference exists between the two controlling criteria. This is due to the yield strain being very close to the ultimate strain for this steel deck. The significance of the general strain ultimate moment analysis is shown by the closeness of the computed value to the experimental value in Table 24. Thus, a general strain analysis should be performed for the ultimate

Table 24. Results of general strain moment analysis for Slab Elements 7 and 8

	Slab Element 7	Slab Element 8	1G24[a]	2G24[a]
1. Experimental moment capacity (ft-k/ft)	9.84	10.89	8.53[a]	10.36[a]
2. Ultimate computed moment assuming ultimate strain at bottom fiber	10.43	10.53	6.77	9.63
3. Ultimate computed moment assuming yield strain at bottom fiber	10.06	10.16	5.89	9.20
Ratio 1/2	0.94	1.03	1.26	1.07
Ratio 1/3	0.98	1.07	1.45	1.12

[a] From Reference (40).

moment computation of slab elements reinforced with a very high strength non-ductile type of steel deck. The general analysis may also be necessary for those deeper steel deck configurations which cannot develop overall yielding. However, more experimental work is needed to ascertain the correct flexural characteristics and definition of failure.

The general behavior of the slab elements companion to the slab specimens can be summarized by the load-deflection characteristics. See Figure 68. Since the specimens had different widths, the load is in terms of kips per foot of width. Included in Figure 68 is Specimen 40I22 from Reference (40) which was very similar to the slab Specimens 1, 2, and 3 and had a length, depth, and shear span of 140, 4½, and 46 inches, respectively.

As can be seen from Figure 68, there is a significant difference in the

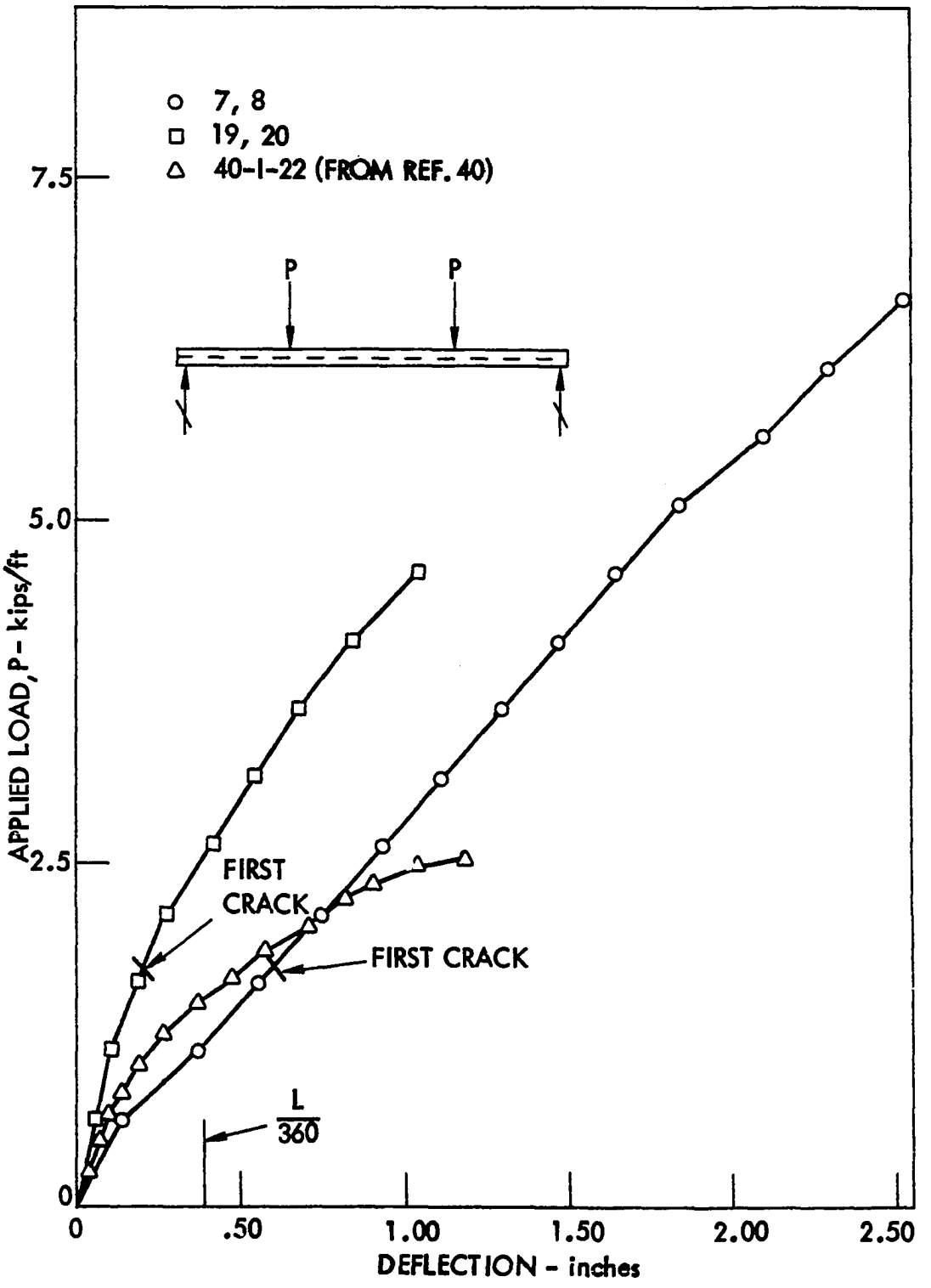

Figure 68. Load-deflection characteristics for slab elements companion to the slab specimens

experimental load-deflection behavior. Slab Elements 7 and 8 exhibited an almost straight line load-deflection curve, whereas the other specimens exhibited some ductility. Specimens 19 and 20 were somewhat stiffer with little ductility, whereas Specimen 40I22 was much more ductile. The load at which first cracking was observed is shown for those cases when obtained. As an indication of the amount of deflection, the L/360 limitation is indicated in Figure 68.

Specimens with variable amounts of supplementary reinforcing

As a preliminary attempt to ascertain the effect of the supplementary reinforcement (WWF) on shear-bond failure behavior, six specimens were cast. These specimens contained the same WWF as used in Slabs 1 and 2. The basic experimental results of these specimens were presented in Table 20. A comparison of the average results of each pair of identical specimens containing WWF to those containing no WWF is summarized below in Table 25. Since the area of supplementary steel was not appreciably different for those four specimens containing the WWF, an average of all four specimens containing WWF was compared to those not containing the WWF. As can be seen in Table 25, the load capacity was apparently increased by 10.7%.

Table 25. Experimental effects of elements containing WWF

Average of Specimen	Area of WWF Parallel to length, A_{s_1}, ($in.^2/ft$)	Average Total Applied Load (kips)	% increase of lines 2 and 3 over line 1
2 and 4	0.	10.3	—
1 and 5	0.039	11.35	10.7
3 and 6	0.057	11.45	

The influence on the shear-bond regression analysis can be observed by comparing these load values with the previously obtained shear-bond regression data (obtained from Reference 40). This is done in Figure 69. The values shown were computed neglecting the area of WWF (which is small compared to deck area) in the computation of the reinforcement ratio, p. As can be seen, the slab element specimens containing the WWF fall reasonably close to the previously plotted regression fit, but reflect about the same increase as shown in Table 25. Thus, the addition of the supplementary reinforcing did not appreciably affect the shear-bond strength by more than about 11 %.

The strain gages placed on the six slab elements showed reasonably good linear characteristics across the cross section of the slab elements at most stages of loading. No yielding of the fibers of any part of the steel cross section were observed. The maximum strain near ultimate for any of the observed strains was only 770 microinches on the bottom fiber of steel deck.

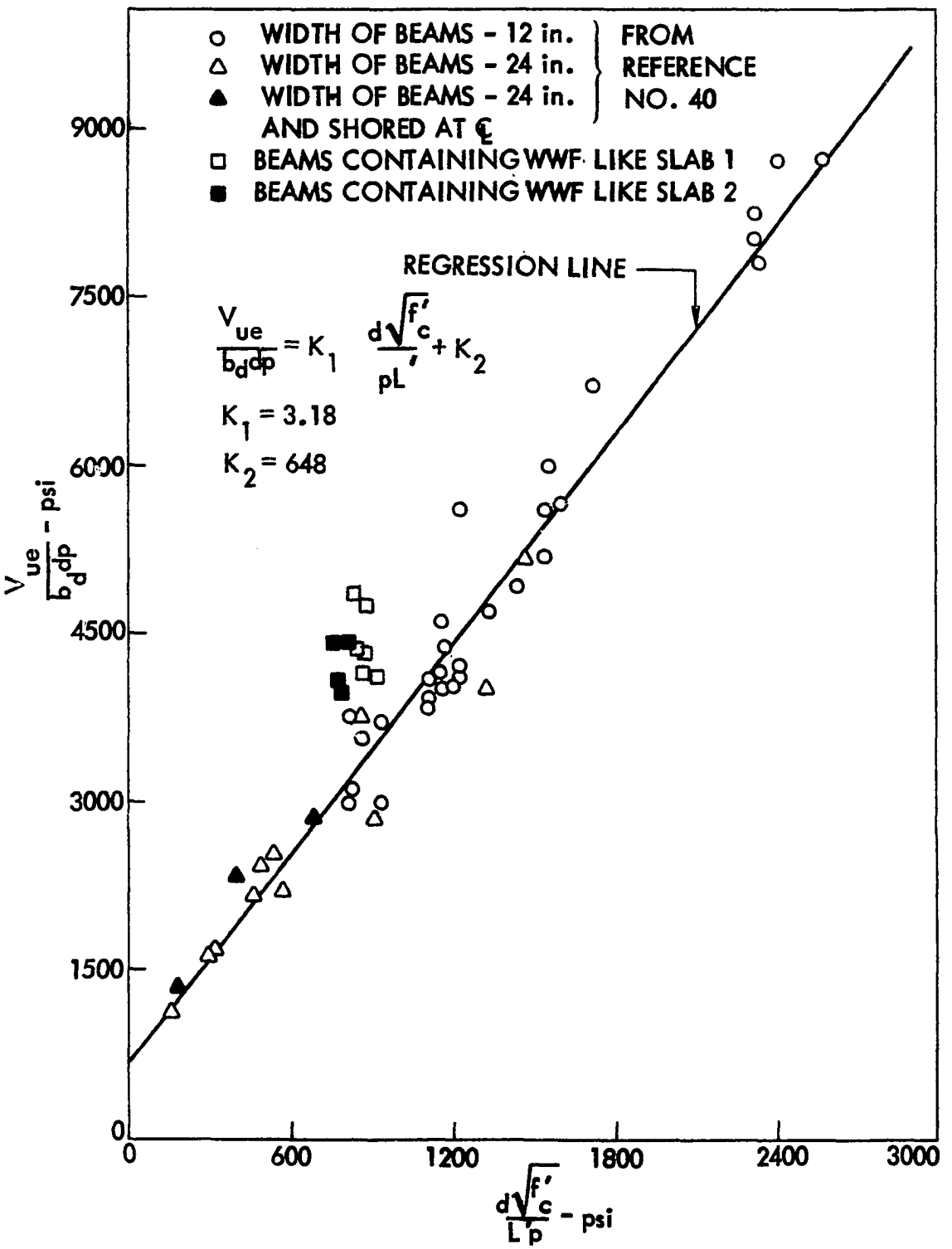

Figure 69. Illustration of shear-bond strength of slab elements containing WWF compared to previously obtained shear-bond analysis

CHAPTER 7. THEORETICAL ANALYSIS OF STEEL-DECK-REINFORCED SLABS

General Remarks

Four methods of analysis were employed to investigate the ultimate strength and behavioral characteristics of the full-scale two-way slab tests. These methods were discussed in detail in Chapter 2 and include the following:

1. Yield-line theory,
2. Shear-bond regression analysis,
3. Orthotropic plate theory, and
4. Curve fitting of the deflected surfaces as applied to orthotropic theory.

The yield-line theory and shear-bond analysis methods were used as a means of ultimate strength determination, whereas the orthotropic theory and curve fitting techniques were employed as a means of predicting and investigating the behavioral characteristics of deflections and force distributions throughout each of the slabs. The quantitative results of these theoretical means of analyses compared to the experimental results are presented in this chapter.

Application of Yield-Line Analysis to Test Slabs

Mechanisms considered

The procedure for yield-line analysis was discussed previously in Chapter 2. The discussion in this section is concerned with the application of the yield-line analysis to the experimental test slabs and with the comparison of the computed results to the experimental results.

The application of yield-line analysis involved primarily four collapse

mechanisms. These collapse mechanisms are shown in Figure 70. The mechanism indicated in Figure 70a was found to be the controlling mechanism for all five test slabs. This result was substantiated by the observed crack patterns on both top and bottom surfaces of all slabs tested. See crack patterns and discussion in Chapter 5.

The ultimate applied load, P, at each of the four concentrated load points was computed using each of the collapse mechanisms shown in Figure 70. The computed P value for Figure 70a was found from the following expression: [See also Equation (8)]

$$m = \frac{w\alpha\beta^2(L'')^2[-3\alpha + 4\alpha\gamma - 3\gamma + 3]}{6\left[\mu\beta^2 + i\beta^2 + \left(\frac{L''}{L}\right)^2\left(\frac{\alpha}{\gamma}\right)\right]} + \frac{2P\alpha\beta L''}{L\left[\mu\beta^2 + i\beta^2 + \left(\frac{L''}{L}\right)^2\left(\frac{\alpha}{\gamma}\right)\right]} \tag{47}$$

Likewise, the P value for Figure 70b was found from

$$m = \frac{L^2 w\left(\frac{1}{2} - \frac{\alpha}{3}\right)}{2\left(\frac{1}{\alpha\beta^2} + 2\mu\right)} + \frac{4Px}{2L\sqrt{\alpha^2\beta^2 + \frac{1}{4}}\left(\frac{1}{\alpha\beta} + 2\mu\beta\right)}, \tag{48}$$

the P value for Figure 70c was found from [See also Equation (5)]

$$m = \frac{w\alpha\beta^2\gamma L^2(-3\alpha + 4\alpha\gamma - 3\gamma + 3)}{6(\mu\beta^2\gamma + \alpha)} + \frac{2P\alpha\beta\gamma}{(\mu\beta^2\gamma + \alpha)}, \text{ and} \tag{49}$$

the P value for Figure 70d was found from [see also Equation (11)]

$$P_u = 2\pi m(1 + i)\sqrt{\mu}. \tag{50}$$

Note that the uniform load, w, is considered to be negligible in Figure 70d. A detailed development of Equations (47), (49) and (50) is contained in Chapter 2.

A summary of the computed ultimate loads, P_u, for each of the four

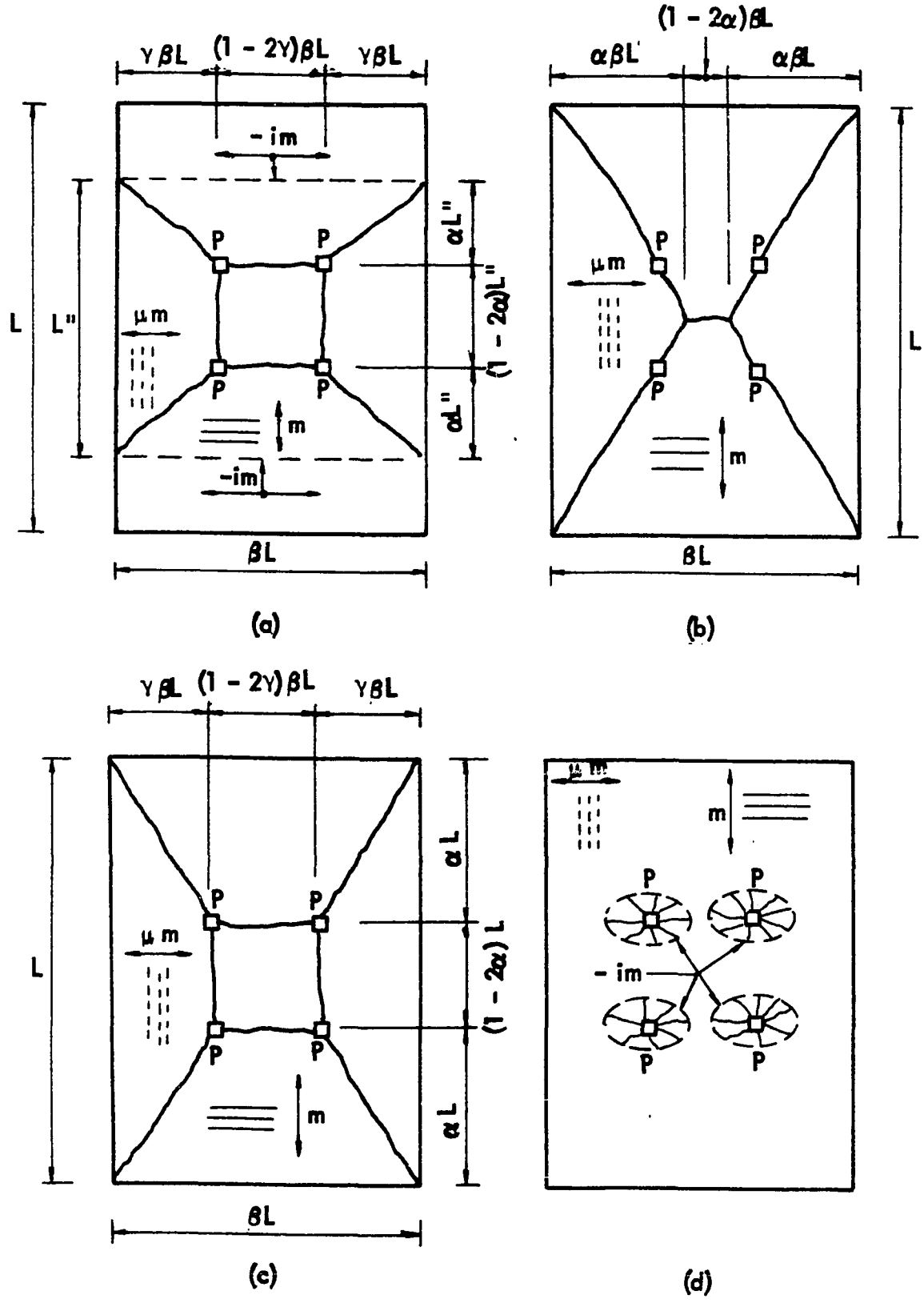

Figure 70. Collapse mechanisms utilized in ultimate strength determination by yield-line analysis

primary collapse mechanisms is shown in Table 26. As can be seen, the lowest computed ultimate load values were obtained from the mechanism shown in Figure 70a. These computed values can be compared to the experimental ones which are also contained in Table 26.

Table 26. Computed ultimate concentrated loads for the various collapse mechanisms shown in Figure 70

Slab No.	Exper. P_u (kips/load pt.)	Computed P_u (kips/load pt.) by mechanism in: P_u in Fig. 70a	L'' in Fig. 70a (ft)	P_u in Fig. 70b	P_u in Fig. 70c	P_u in Fig. 70d
1	13.7	15.26	8.4	19.5	19.6	22.8
2	15.5	17.32	10.1	19.3	19.3	33.0
3	8.8	12.64	8.3	16.4	16.5	17.7
4	14.4	19.83	9.4	23.2	23.2	34.8
5	9.4	11.66	7.4	17.2	17.3	14.6

The experimental values compare very closely to the computed values for all slabs except Slab 4 which had a very high strength steel deck (F_y = 101.6 ksi) which was not stressed to its ultimate flexural yielding capacity along the yield lines. It should be emphasized that none of the five slabs actually failed by the flexural mode as would be predicted by the yield-line theory. All five slabs failed by the shear-bond failure mode.

However, the computed values in Table 26, when compared with the experimental values, demonstrate the possible validity of the yield-line theory as a design tool. The yield-line theory might be particularly useful for floor systems constructed with multiple panels since the adjacent floor panels would provide restraint against end-slip and

subsequent shear-bond failure. This might have delayed shear-bond failure until overall yielding along the yield-lines of the collapse mechanism took place. Thus, it is concluded from the close correspondence of the theoretical yield-line calculations with the experimental load tests that the yield-line theory provides a good potential for predicting the flexural capacity of two-way slabs reinforced with corrugated cold-formed steel decking.

The effective width as defined by the distance, L'', in Figure 70a compares favorably with the effective width as observed from the top and bottom surface cracking. See Figures 32 and 34. This width also compares favorably with that obtained from the reaction measurements as given in Chapter 5.

Methods of computation of m, μm, and im and assumptions

The significance of the computed flexural collapse values, as given in Table 26, warrants further discussion as to the methods of obtaining the flexural moment capacities of m, μm, and im for the longitudinal, transverse, and negative moments, respectively. The detailed discussion of the means of obtaining each of these flexural capacities was provided in connection with the companion longitudinal and transverse slab elements in Chapter 6. The final basis for the computations used to arrive at the computed values in Table 26 will be discussed.

A complete summary of the computed flexural values used for Table 26 is presented in Table 27. The longitudinal moment, m, refers to that moment capacity on a cross-section perpendicular to the steel deck corrugations, i.e. the strong direction moment. The transverse moment, μm, is the moment capacity on a cross-section parallel to the corrugations, i.e.

Table 27. Computed flexural capacities m, μm, and im for the five two-way slab specimens

Slab No.	Longitudinal Moment, m (ft-k/ft)	Transverse Moment, μm (ft-k/ft)	Negative Moment, im (ft-k/ft)	Coefficient of Orthotropy, μ	Coefficient i
1	9.55	1.16	0.870	0.122	0.091
2	8.62	2.73	0.738	0.316	0.086
3	8.18	0.80	0.802	0.098	0.098
4	10.68	2.40	0.986	0.225	0.092
5	8.69	0.55	0.55	0.063	0.063

the weak direction moment. As can be seen in Table 27, the relative strengths between these two moments, given as the coefficient of orthotropy, μ, varies from 0.063 to 0.316.

The longitudinal moment capacity, m, was computed using the general strain analysis presented in Figure 67 of Chapter 6. This ultimate flexural capacity was obtained by establishing the maximum compressive concrete strain as 0.003 for Slabs 1, 2, 3, and 5. The corresponding strain at each steel layer was then found so as to create equilibrium of the internal tensile and compressive forces. After equilibrium was established, summation of moments was taken about the compressive force. The tensile forces consisted of the steel decking and the supplementary steel reinforcements and the strength of the concrete when the strain was less than that to cause normal modulus of rupture stress (considering a uniaxial case). In addition, the steel deck tensile force was divided into three layers consisting of the top plate elements, web plate elements, and bottom plate elements. See the accompanying discussion to Figure 67 contained in Chapter 6.

The use of the maximum concrete compressive strain of 0.003 was found to give satisfactory moment capacities for Slabs 1, 2, 3, and 5,

particularly since the steel deck reinforcement in these slabs had sufficient ductility to develop such a strain compatibility. However, the steel deck in Slab 4 had insufficient ductility to develop a concrete strain of 0.003. Thus, for Slab 4, the longitudinal moment capacity, m, was based on equating the strain at the bottom steel deck plate elements to the strain to cause yielding of 101.6 ksi. Consideration was also given to assuming that the bottom plate elements had reached the strain corresponding to the ultimate stress of the steel. Doing this changed the moment capacity from 10.68 to 11.06 ft-kips/ft. Further consideration of the Slab 4 longitudinal moment capacity was given to letting the top plate elements of the deck reach the yield strain. However, this resulted in a strain at the bottom plate elements greater than the ultimate strain.

Based upon the above analysis of the longitudinal moment capacity studies, it is recommended that the general strain analysis be used. A maximum concrete compressive strain of 0.003 should be assumed, except for cases when the strain in the bottom fiber of the steel exceeds ultimate (such as exists for the high strength, low ductility steels). For such cases involving high strength steels, it is recommended that the general strain analysis be used with the requirement that the strain at the bottom plate elements be equal to the yield strain. Another possibility is that the strain of the top plate elements be limited to the yield strain, providing that in this instance the strain compatibility condition does not indicate a strain at the bottom greater than ultimate. For those cases involving only steel decking as the tension reinforcement, and the steel is of sufficient ductility for the 0.003 criteria, then the equation

$$M_u = A_s f_y (d - a_u/2)/12.0$$

is adequate. Here the steel-deck cross section is considered as centered at the c.g.s. of the deck.

The transverse moment capacity, μm, was also computed using the general strain analysis procedure as described above and in Chapter 6. However, the criteria of 0.003 was not valid for any of the transverse moment capacities. The transverse capacity of Slabs 1 and 2, with the welded wire fabric supplementary reinforcement, was based upon the general strain analysis letting the strain reach a level corresponding to the ultimate strain of the welded wire fabric. This was compared with the case where the strain was assumed to reach yield, and about the same computed ultimate load was obtained for the slab. This was because little difference exists between the two μm's due to the high strength steel with a small amount of ductility. (See Figure 14.)

The transverse moment capacity, μm, of Slab 4 was based on the strain at the limiting bond stress of the splices existing between the sections of the transverse deformed wires which were connected to the steel decking. The general strain analysis was used letting the strain at the splice of the transverse wires prevail as discussed in connection with transverse slab elements in Chapter 6.

The transverse moment capacity for Slabs 3 and 5 containing no supplementary reinforcement in the tension zone was determined on the basis of the strength of the concrete alone. The depth considered as effective was that as found from the transverse slab element analysis discussed in Chapter 6. Thus, the transverse capacity for Slabs 3 and 5 was determined by using a gross moment of inertia for a depth from the top of slab to the top of deck together with the modulus of rupture strength of the concrete as given

by the following expression:

$$\mu m = \frac{f_r I_g}{12c} \tag{51}$$

The negative moment capacities, im, of all the slabs were found the same way as μm for Slabs 3 and 5. That is, the negative moment capacity was based only upon the strength of concrete employing Equation (51). Two depths were considered in computing I_g in Equation (51). One depth was from the top of slab to the top of the decking, whereas the other depth was taken from the top of slab to the c.g.s. of the decking. The latter was thought to be closer to the true im when the added benefits of the torsional resistance and the added transverse moment increase due to bi-axial compressive stress in the perpendicular direction were considered. However, as a conservative estimate of im, the depth of the top of the corrugations was chosen and used for the computations in Table 26.

Ultimate loads, P_u, were computed using several values of im and it was found that the particular controlling mechanism was somewhat sensitive to the strength of im. The difference in P values and widths, L'', for the controlling mechanism for the two different im-computational methods is demonstrated in Table 28. As can be seen, the values using im for a depth to the top of the deck result in computed values closer to the experimental ones. However, the slabs in this investigation did not reach the full flexure capacity. Slabs which fail by flexure may be better predicted using a computed im for a depth to the deck c.g.s., but in lieu of such experimental results, the more conservative im for a depth to the top of the deck is recommended.

Also shown in Table 28 are values of P_u and L'' if im were considered as

having a value of zero. As can be seen, the negative moment capacity, im, could also be considered conservatively as having a strength equal to zero. However, since no complete flexural failures were achieved, a proper im verification was not found.

Table 28. Effect of change in negative moment capacity, im, on the mechanism in Figure 70a

	im by depth above deck		im by depth above c.g.s.		im = 0	
Slab No.	P_u (kips/load pt.)	L" (ft)	P_u (kips/load pt.)	L" (ft)	P_u (kips/load pt.)	L" (ft)
1	15.26	8.4	16.62	9.0	12.67	7.3
2	17.32	10.1	18.26	10.5	15.84	9.4
3	12.64	8.3	14.02	9.0	10.09	7.0
4	19.83	9.4	20.71	9.7	17.53	8.5
5	11.66	7.4	14.2	8.6	9.48	6.4

Analysis of Test Slabs Using One-Way Shear-Bond Computations

Each test slab was analyzed as a one-way slab subjected to an equivalent uniform load. The one-way shear-bond regression method of analysis as discussed in Chapter 2 was employed to give approximate ultimate uniform loads. These computations give an indication of the effectiveness of approximating the concentrated loads by a uniform load for the five full-scale slabs tested. This served as a preliminary means of analysis to that contained in the next section.

The experimental ultimate load at the four concentrated load points

was converted into an equivalent uniform load distributed over an area between the slab supports (i.e., 15.5 ft by 11.6 ft). This equivalent uniform load is indicated in Table 29. As can be seen from the different uniform load values, the slabs with more transverse supplementary steel withstood a larger load, except for Slab 4. See Table 13 in Chapter 5 for the amount of supplementary steel and other pertinent slab variables.

Table 29. Equivalent ultimate uniform and predicted one-way shear-bond loads

Slab No.	Ultimate experimental load per load point (kips/L.P.)	Equivalent ultimate uniform load (psf)	Calculated shear-bond uniform load, W_u, (psf)
1	13.7	305	235
2	15.5	345	207
3	8.8	196	215
4	14.4	321	450
5	9.4	209	241

The calculated uniform load shear-bond values given in Table 29 were obtained from the following equation contained in Reference (40):

$$W_u = \frac{24d}{L}\left[k_1\sqrt{f'_c}\left(\frac{d}{L'}\right) + k_2 p\right] \qquad (52)$$

The notation of this equation is the same as that presented previously for Equation (1) in Chapter 2. The effective depth, d, in Equation (52) was taken as the overall slab average depth to the c.g.s. of the deck. The constants k_1 and k_2 are tabulated in Table 21 in Chapter 6.

The calculated values for Slabs 3 and 5 in Table 29 are significant since they are very close to the experimental ultimate loads. Thus, the one-way shear-bond method appears to adequately predict the load for slabs

without supplementary reinforcing. Slab 5 had 6 X 6 X 10/10 WWF, but the fabric was located in the top part of slab, negating its benefit for positive reinforcing. However, it is felt that this close prediction of load for Slabs 3 and 5 is somewhat coincidental with the pattern of loading and span length used. Other concentrated load patterns may or may not give the same results. Nevertheless, the predicted values for Slabs 3 and 5 are quite adequate. The over prediction is due probably to the effects of cycling for these two slabs.

The equivalent uniform load shear-bond calculation did not give adequate results for Slabs 1 and 2. (See Table 29.) This is attributed to the supplementary reinforcing used in these two slabs. The failure of Slab 4 to reach even its one-way shear-bond predicted load is attributed to the shear on a beam strip transverse to the corrugations. This transverse shear placed additional shear on the spot welds holding the T-wires in place, thus weakening the longitudinal shear capacity. This reduction is discussed later in this chapter.

An approximation for the predicted shear-bond value can be made for slabs containing supplementary reinforcing through the use of the yield-line analysis. That is, the predicted values for Slabs 1 and 2 multiplied times the ratio of the predicted load of Slab 1 or 2 to that of Slab 3 gives a fairly close approximation. This is based on the supposition that the yield-line theory calculations take into account the flexural transverse force distribution benefits due to the supplementary reinforcing transverse to the corrugations. Table 30 contains the results of this proportioning.

The proportioned results in Table 30 are quite conservative and serve only as an approximation due to the addition of the supplementary

Table 30. Proportioned (by yield-line calculations) shear-bond predicted uniform loads

Slab No.	Equivalent Experimental Uniform Load, (psf)	Calculated Shear-bond Uniform Load, W_u (psf)	Yield-Line Predicted Load, (kips/L.P.)	Proportional Multiplication Used	Predicted Value of Uniform Load (by Proportioning) (psf)
1	305	235	15.26	$\frac{15.26}{12.64}$ (235) =	284
2	345	207	17.32	$\frac{17.32}{12.64}$ (207) =	284
3	196	215	12.64		

reinforcing. The approximations presented in Tables 29 and 30 serve only as one-way approximations for a concentrated loaded system converted into equivalent load. It should be emphasized that these types of calculations may not be sufficient for all the more common cases of concentrated loads encountered in practice. The method in the next section utilizing a shear-bond approach based on an established yield-line collapse mechanism is believed to be much more general and applicable to a wide range of loading configurations and shapes of slabs.

Application of Shear-Bond Analysis in Conjunction with the Yield-Line Analysis

Concept of application

A method of analysis which combines the shear-bond approach and the yield-line theory approach provides a means of predicting the ultimate strength of two-way slabs. Each method of analysis was described separately in Chapter 2. However, the concept of applying the two together as a means

of arriving at the ultimate slab strength for concentrated loads is discussed in this section followed by calculated results and recommendations for design. This application of shear-bond analysis in conjunction with the yield-line analysis was considered the primary theoretical means of analysis used in this investigation.

The concept involves first establishing the proper yield-line mechanism and then applying the principles of the shear-bond approach to the effective load-carrying segment established by the mechanism. Figure 71 shows the collapse mechanism and the effective load-carrying segment used for analysis of the five two-way slab tests.

The collapse mechanism shown in the top of Figure 71 was established by conventional yield-line theory formulation and is also the same controlling yield-line mechanism shown in Figure 70a. Ordinarily, this yield-line mechanism would be used to predict a flexural type of slab failure. However, for this combined analysis the yield-line theory was used only to establish the collapse mechanism. Even though the five test slabs failed ultimately by shear-bond, the observed crack patterns (presented in Chapter 5) still conformed with the yield-line collapse mechanism. Therefore, the yield-line theory was used to define the crack pattern for the collapse mechanism and subsequently establish the effective load-carrying segment of width L'' in Figure 71.

Determination of the effective width, L'', of the load-carrying segment permitted computation of the vertical shear forces resisting the downward applied loads for the load-carrying segment. The two shear forces computed were V_T and V_L, shown in Figure 71. The V_L shear force was computed using the shear-bond regression analysis applied to a one-way slab

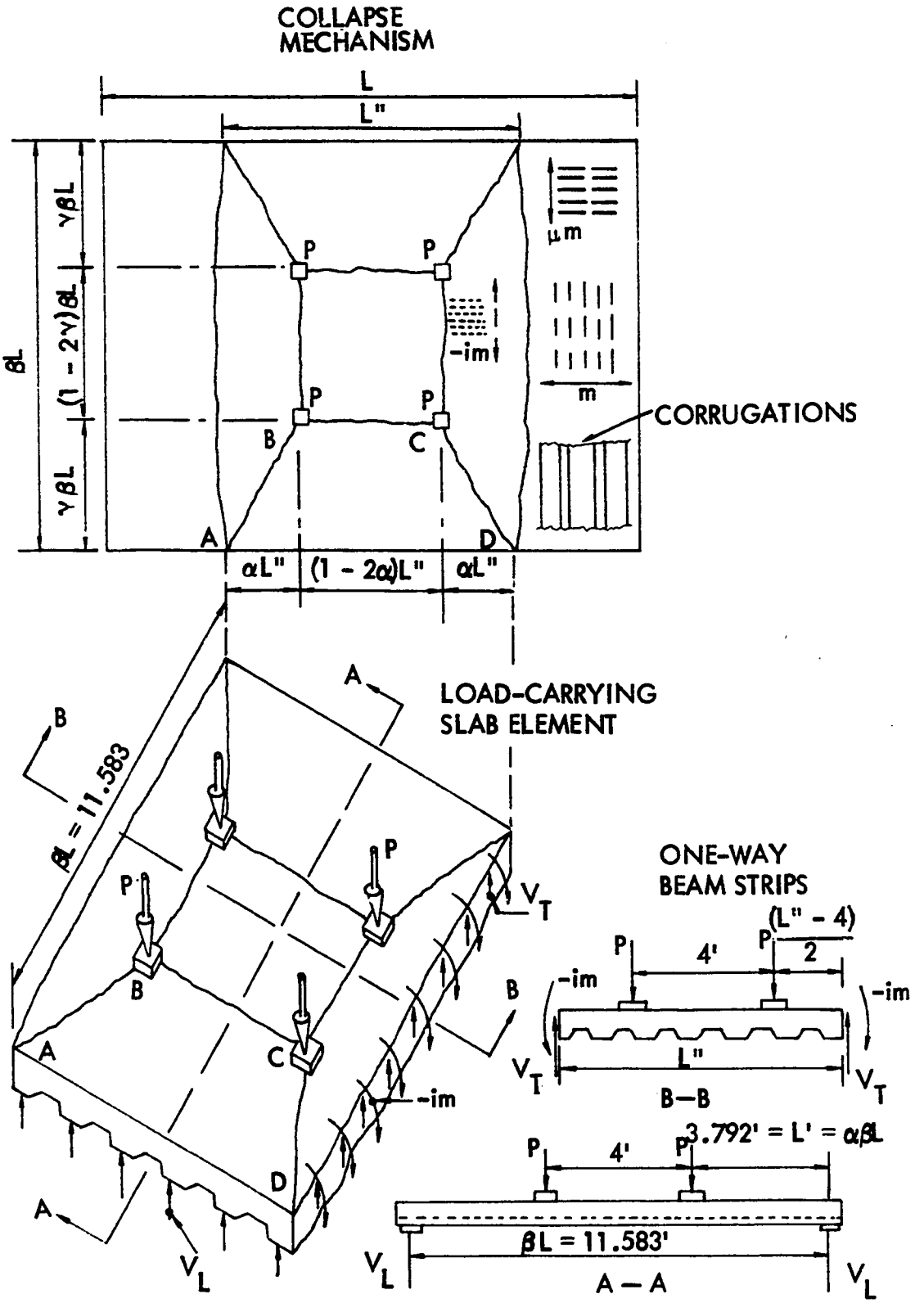

Figure 71. Collapse mechanism and effective load-carrying segment used for analysis of five full-scale slab elements

element parallel to the deck corrugations as shown by section A-A in Figure 71. This longitudinal shear, V_L, was computed using a modified version of the shear-bond Equation (1) to account for the average shear span over the shear-bond failure region of the L" width. The trapezoidal section over which shear-bond failure was assumed to occur is designated in Figure 71 by region marked ABCD. The modified version of Equation (1) for computing V_L is presented in the next section.

The V_T shear force was obtained from using a one-way slab element transverse to the steel deck corrugations, as shown by Section B-B in Figure 71. This transverse shear force, V_T, was obtained by two different criteria and the lower value of the two was taken as the controlling V_T force. One V_T criteria was based on the shear strength of the concrete above the neutral axis, assuming a cracked section not contributing shear below the neutral axis.

The second V_T criteria was based on the statical shear reaction of a transverse slab element of length, L". This shear reaction was obtained by simple one-way beam statics as that reaction existing on the end of the element when subjected to its flexural capacity.

The controlling V_T shear force was the smaller of the concrete shear strength or the statical shear at maximum transverse flexural capacity. Additional shear contributions from aggregate interlocking and shear friction in a cracked section are neglected.

The predicted ultimate concentrated load at each load point was obtained by adding V_T and V_L. The calculations of V_T and V_L were thus based on a per load point computation to compare to the experimental load at each load point. The results of the computations and the corresponding details

are presented next.

Methods for computations and results

The results of the computations and some of the other pertinent items for the application of the shear-bond analysis in conjunction with the yield-line collapse mechanisms are presented in Table 31. The L'' length values in the table are the same ones as given previously in Table 26 for the collapse mechanism in Figure 70a. Thus, the computation of L'' is based on those values and methods indicated in the previous section "Application of Yield-Line Analysis to Test Slabs."

The third and fourth columns in Table 31 give two average depths that were used in the computations. The average overall depth of the slab was used in the yield-line analysis to establish L'', the width of the effective load-carrying slab element. The computations of V_T and V_L were based on the effective load-carrying element of the slab, and thus the average depth of this element was used to compute the vertical transverse and longitudinal shears. Likewise, the μm transverse moment capacity, given in the fifth column of the table, is based on an average depth for the slab element of width, L''. Thus, this μm is slightly different than that given in Table 27 which was used for the yield-line analysis of the full slab.

The two criteria for computing the transverse element shear, V_T, are given by columns six and seven in Table 31. The V_T force in column six was based on assuming a concrete shear strength of $2\sqrt{f'_c}$ for a depth above the neutral axis neglecting any shear contribution below the neutral axis. The neutral axis was determined from conventional cracked transformed section concepts. The transformed area of steel utilized in these neutral axis

Table 31. Computed values for the application of the shear-bond analysis in conjunction with the yield-line collapse mechanism

1 Slab No.	2 L", See Fig. 71 (ft)	3 Average overall slab depth (in.)	4 Avg. depth of load-carrying slab element (in.)	5 μm for load-carrying slab element (ft-k/ft)	6 $V_T = \frac{12\ \beta L d_n \sqrt{f'_c}}{1000}$ (kips/L.P.)	7 $V_T = \frac{\beta L \mu m}{L'' - 4}$ (kips/L.P.)	8 V_L Eq. 56 (kips/L.P.)	9 CALC P_u $V_T + V_L$ (kips/L.P.)	10 EXP P_{ue} (kips/L.P.)	11 Ratio of $\frac{\text{CALC}}{\text{EXP}}$
1	8.4	4.83	5.04	1.24	4.12	3.26	8.52 (9.37)[a]	11.78 (12.37)[a]	13.7	0.86 (0.90)[a]
2	10.1	4.62	4.75	2.86	5.65	5.42	8.97 (9.87)[a]	14.39 (15.29)[a]	15.5	0.93 (0.99)[a]
3	8.3	4.63	4.73	0.86	0.0	2.30	7.31	7.31	8.8	0.83
4	9.4	4.68	4.90	2.56	7.01	5.49[b] 3.88	16.29[b] 11.52	21.78[b] 15.40	14.4	1.51[b] 1.07
5	7.4	5.44	5.46	0.56	1.90	1.90	6.57	8.47	9.4	0.90

[a]Based on a 10 percent increase in V_L to account for increased shear-bond resistance of WWF.

[b]Based on an elliptical interaction of V_T and V_L on T-wire spot weld strength.

computations was only that of the supplementary reinforcing consisting of either WWF or T-wires in all slabs except Slab 3. The corresponding neutral axis depths, d_n, were 0.459, 0.683, 0.0, 0.814, and 0.208 inches, respectively, for Slabs 1-5. A value of zero for the depth to the neutral axis was conservatively assigned to Slab 3, since no transverse supplemental reinforcement existed for this slab.

The resulting computation for V_T in column six in Table 31 was based on the ultimate shear of a concrete beam as recommended by the ACI Building Code (2). This is given by the term $2bd\sqrt{f'_c}$ where the ϕ factor was not included. In this case, the beam width per load point was $\beta L/2$ (Figure 71). With βL in feet, $\sqrt{f'_c}$ in psi, d_n (in place of d) in inches, and V_T in kips per load point, the resulting expression for values in column six is given by Equation (53).

$$V_T = \frac{12\ \beta L d_n \sqrt{f'_c}}{1000} \tag{53}$$

The other criteria for V_T as given in column seven of Table 31 was based on the shear developed in a beam strip at the time the beam element reached its flexural capacity. Section B-B of Figure 71 illustrates a transverse beam segment with a resulting shear span $(L'' - 4)/2$ where L'' is in feet and the four represents the distance between load points. Taking V_T times the shear span and equating this to the transverse moment capacity, μm, results in the following expression per foot of width for V_T:

$$V_T = \frac{2\mu m}{L'' - 4} \tag{54}$$

For a beam width per load point of $\beta L/2$, the resulting equation from which values in column seven were computed is

$$V_T = \frac{\beta L \mu m}{L'' - 4} \tag{55}$$

where L'' and βL are in feet, and μm is in ft-kips/ft. The computation of V_T in Equations (54) and (55) conservatively neglects the negative moment, - im, on the end of the transverse strip.

The computation of V_L in column eight of Table 31 is based on the one-way shear-bond strength of a beam segment parallel to the deck corrugations. This beam segment is shown by section A-A in Figure 71. The shear-bond failure for the five slab tests was assumed to occur over the trapezoidal region marked ABCD in Figure 71. This was verified by the experimental results since end slip occurred over the region of L''. Equation (1) for shear-bond was modified to account for an L' shear span over a beam width of 4 ft (distance between load points) and to account for a $L'/2$ shear span in the triangular regions bordering AB and CD in Figure 71.

Taking the shear-bond expression [Equation (1)] for each of the two triangular regions (see Figure 71) with a shear span of $L'/2$, and for the rectangular region with a shear span of L', and rearranging terms and combining for the three regions results in the following equation which was used in computing column eight:

$$V_L = \frac{dL''}{2000s}\left[\frac{k_1 d\sqrt{f'_c}}{L'}(1 + 2\alpha) + k_2 p\right] \tag{56}$$

where the notation is the same as for Equation (1) except that L'' is the effective width in inches and α is a non-dimensional length parameter as shown in Figure 71. The regression constants used in Equation (56) were obtained from the one-way slab element tests and were presented previously in Table 21 in Chapter 6. The term "s" in Equation (56) was unity for all

slabs except Slab 4, where s was 3, since the T-wires in Slab 4 were spaced on 3-inch centers. The units on the V_L quantity given by Equation (56) are kips per load point of applied load.

Dead load of the slab was considered in the above computations for L'', V_T, and V_L. The yield-line calculations for L'' included the effect of the uniform dead load as can be seen from Equation (47) where w is the slab dead weight. In computing the shear capacities V_T and V_L, the dead load was assumed to be carried by the longitudinal beam element. Equation (56) for V_L is for live load only without the dead weight added. The constants k_1 and k_2 were determined on the basis of applied load only. The live load capacities for V_T were not reduced by the dead load since the longitudinal strip was assumed to carry the dead weight. Thus, all computed values are for the amount of applied load.

Once V_T and V_L shear forces were determined, the predicted ultimate live load at each load point was found by adding the lower of the two V_T forces to the V_L forces. This predicted load is shown in the ninth column of Table 31. The actual experimental ultimate load per load point is shown in column ten followed in column eleven by the ratio of calculated to experimental, representing the degree of closeness of the computed to actual values.

As can be seen by the eleventh column, the computed values compare quite closely to the experimental ones, except for Slab 4 which is subsequently discussed. Slab 3 is the next furthest from predicting the correct failure load. A more correct predicted load for Slab 3 would probably be achieved by adding a V_T of 2.30 using Equation (55) to the V_L of 7.31, thus giving a predicted ultimate of 9.61 kips per load point. The zero value

of V_T from Equation (54) for Slab 3 is obviously incorrect, since some shear contribution of the concrete must exist. However, since no shear failures were obtained from any of the transverse one-way slab specimens, only a conservative approximation of V_T by column six was made as discussed with Equation (54). The 9.61 kip-per-load-point value is nine percent over the actual experimental value of 8.8. Undoubtedly, the high cycling load that was used (72.7 percent of the ultimate) weakened the slab severely. However, due to lack of actual test data to substantiate the 9.61 figure, the more conservative value is used for the predicted ultimate load of Slab 3.

The numbers in parenthesis in columns eight, nine, and eleven for Slabs 1 and 2 represent the predicted values if the effect of the supplemental reinforcing is considered for the shear-bond strength, V_L. Chapter 6 indicated that for the slab elements containing supplementary reinforcing placed on the steel decking, the benefit in shear-bond strength was a little over ten percent. The values in parenthesis in column eight for Slabs 1 and 2 represent a ten percent increase due to the additional reinforcing. Thus, the ratios in column eleven of 0.90 and 0.99 are a better indicator of the predicted strength.

The ratio values of 0.90, 0.99, 0.83, and 0.90 for Slabs 1, 2, 3, and 5 are considered very good and within normal concrete experimental variation. These values are on the conservative side due to strength benefits such as torsional resistance between the longitudinal and transverse elements, aggregate interlocking, dowel shear in the V_T force (dowel shear in V_L is taken into account), and deck stiffness.

The ratio of 1.51 for Slab 4 in column eleven is considered as

incorrect. This is due to the shear forces V_T and V_L both acting on the spot welds connecting the T-wires to the steel decking. The values in columns seven, eight, nine, and eleven (denoted by a superscript b for Slab 4) represent approximate reduced values to account for the interaction of V_T and V_L on the spot welds. The reduction in V_T and V_L values was accomplished by reducing the resultant as given by the expression $\sqrt{(V_T)^2 + (V_L)^2}$. Figure 72 graphically shows how this reduction for Slab 4 was made. Figure 72a indicates the vertical shear forces on the spot weld which connects the T-wire to the steel deck. The reduction as shown in Figure 72b was based on the use of an elliptical curve to represent the interaction strength of V_L and V_T on the spot weld strength. As can be seen in column eleven in Table 31, this method predicted the true ultimate load with an error of only seven percent.

The procedure shown in Figure 72 involved the following steps:

1. Plot V_T and V_L on x- and y-axis, which forms a rectangle having diagonal equal to $\sqrt{(V_T)^2 + (V_L)^2}$. Construct an ellipse with V_T as one-half the minor axis and V_L as one-half the major axis.
2. Define $\theta = \tan^{-1} V_T/V_L$ which establishes the reduced resultant strength, R_s, on the elliptical interaction curve.
3. The reduced resultant strength, R_s, can then be computed from Equation (57) using the

$$R_s^2 = \frac{V_L^2 V_T^2}{V_L^2 \sin^2 \theta + V_T^2 \cos^2 \theta} \qquad (57)$$

standard proportion of an ellipse.

4. The values V_T' and V_L' can be obtained as

$$V_T' = R_s \sin \theta$$

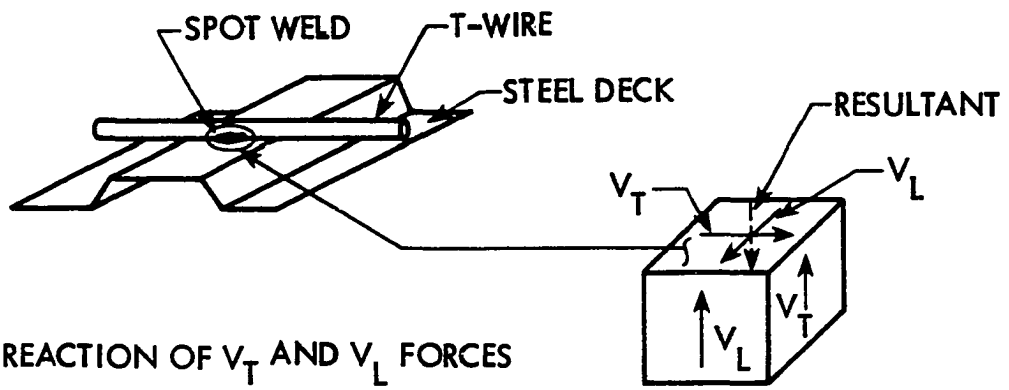

A) REACTION OF V_T AND V_L FORCES ON T-WIRE SPOT WELD

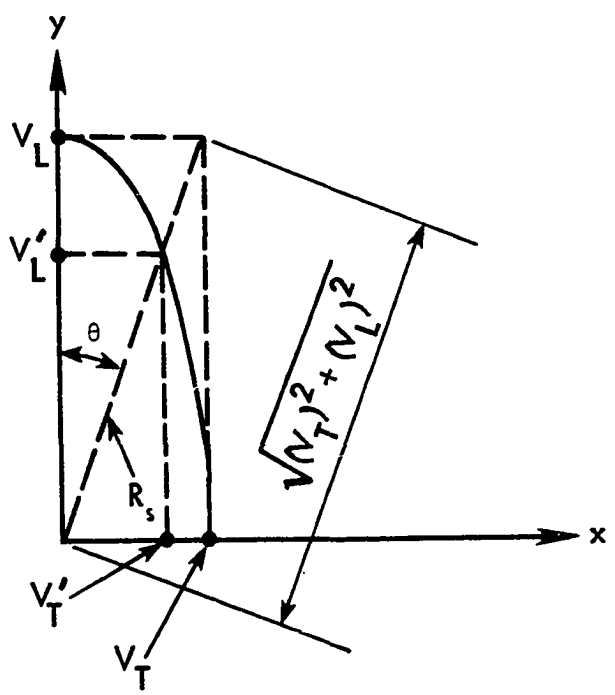

B) ELLIPTICAL INTERACTION APPROXIMATION OF REDUCED V'_T AND V'_L SHEAR CAPACITIES.

Figure 72. Elliptical interaction used for reduction of V_T and V_L shear forces for Slab 4

$V_L' = R_s \cos \theta$

5. The new ultimate predicted live load-carrying capacity of Slab 4 is then $V_T' + V_L'$. These reduced values are indicated by the superscript b for Slab 4 in Table 31.

The computation of the ultimate load by this method is recommended for such slabs where the V_T and V_L forces are concentrated on a single spot shear transferring device. It should be recognized, however, that the method is based on only one test result and needs further verification.

Recommendations for design

The application of the shear-bond analysis in conjunction with the yield-line method resulted in good agreement between predicted ultimate loads and corresponding experimental values. See Table 31. It is possible that the method can be used for a variety of loading configurations and slab sizes.

The overall design procedure relative to steel-deck reinforced slab systems can be summarized by the following steps:

1. Compute the ultimate load for flexural failure by conventional yield-line procedures,
2. Using the collapse mechanism of Item 1, compute the vertical shear forces V_T and V_L on the effective load-carrying element of the collapse mechanism,
3. Obtain the ultimate load based on shear and shear-bond by simply adding the V_T and V_L components,
4. Compute punching shear failure for concentrated loads by recommendations contained in ACI Building Code (2),

5. The computed ultimate load is taken as the smallest value obtained from Items 1, 3, and 4 above. Apply appropriate load factors (2) to obtain design live loads, and
6. Compute deflections and check against limiting values.

The above procedure should prove to be a conservative approach for most building floor systems reinforced with steel decking, especially continuous floor slab systems. The yield-line analysis can take into account the development of negative moments over continuous supports. However, the shear-bond analysis used for V_L does not take into account the blocking action of the neighboring slab panel. Blocking action can conceivably help to prevent shear-bond failures from occurring. However, further research is needed to actually determine the benefits that can be achieved.

Comparison of Test Slabs to Orthotropic Plate Theory and Behavior

Deflection comparisons

Theoretical deflections and force distributions for each of the five two-way slab tests were obtained from the orthotropic plate theory as described in Chapter 2. The orthotropic computations were all performed by use of computer programs adapted to an IBM 360/70 computer. These calculations were based on the following three methods of obtaining the elastic constants:

1. Normal transformed cracked section concepts,
2. Normal transformed uncracked section concepts, and
3. Average cracked and uncracked concepts summed for several slab locations.

The transformed cracked and uncracked concepts were based on conventional procedure as applied to reinforced concrete. The steel deck area was assumed to be concentrated at its c.g.s. for the moment of inertia of a cross-section perpendicular to the deck corrugations (for the y-direction). Since the deck itself has very little stiffness transverse to its corrugations, the steel deck area was neglected for the moment of inertia of a cross-section parallel to the deck corrugations (for the x-direction). The supplementary reinforcement contained in each slab (except Slab 3) was considered in computing the transformed section properties in both the x- and y-directions. Since there was no supplementary reinforcement in Slab 3, no cracked-section computations for the direction transverse to the corrugations were performed.

A third type of orthotropic calculation was performed utilizing average cracked and uncracked concepts. This was done by an iterative process by having the computer perform a stress check at each selected slab location to ascertain if the section was cracked or uncracked. The criteria for cracking was approximated by assuming the maximum tensile stress equal to that obtained by the uniaxial modulus of rupture stress. This approximation neglects biaxial cracking criteria for the concrete, but nevertheless should give fairly good results. Once the computer program determined whether a section was cracked or uncracked, the applicable elastic constants were computed. The average of all the applicable constants for each direction at each location was then found and used to determine deflections and force distributions throughout the slab.

In general the orthotropic deflection calculations predicted the slab deflections quite adequately, depending on the particular slab stiffness and

selection of elastic constants. Comparisons between experimental and computed deflection behavior is shown in Figures 73-77. These figures show the relationship between applied load and vertical deflection at the approximate center of each slab. The offset curves in Figures 74-77, inclusive, are due to the permanent set caused by the cyclic loading of Slabs 2-5. The theoretical curves for the final cycle were drawn from a new zero point taking into account the permanent set for the final cycle of loading.

As can be seen from Figures 73-77, the computations using the average slab properties give the best prediction of deflection for load ranges up to 50 % of ultimate. The next best prediction for deflection was obtained by the normal uncracked concepts. The cracked computations for deflection gave results only indicative of the slab deflection at the time when noticeable cracking had occurred and overestimated considerably the deflection in the design range.

The orthotropic plate theory for computing deflections worked very well up to about 50 % of ultimate load, with the average method of cracked and uncracked comcepts giving the best results. As expected, the orthotropic plate theory does not adequately predict deflections in the range near the ultimate load. For those slabs containing little or no transverse reinforcement (Slabs 1, 3, and 5), the approximate average method of orthotropic theory predicted the deflections reasonably well up to about 90% of the ultimate load. The uncracked orthotropic theory gave satisfactory deflection predictions for Slabs 1, 3, and 5 up to roughly two-thirds of the ultimate load, but underestimates the deflections to a greater degree than does the average section approach.

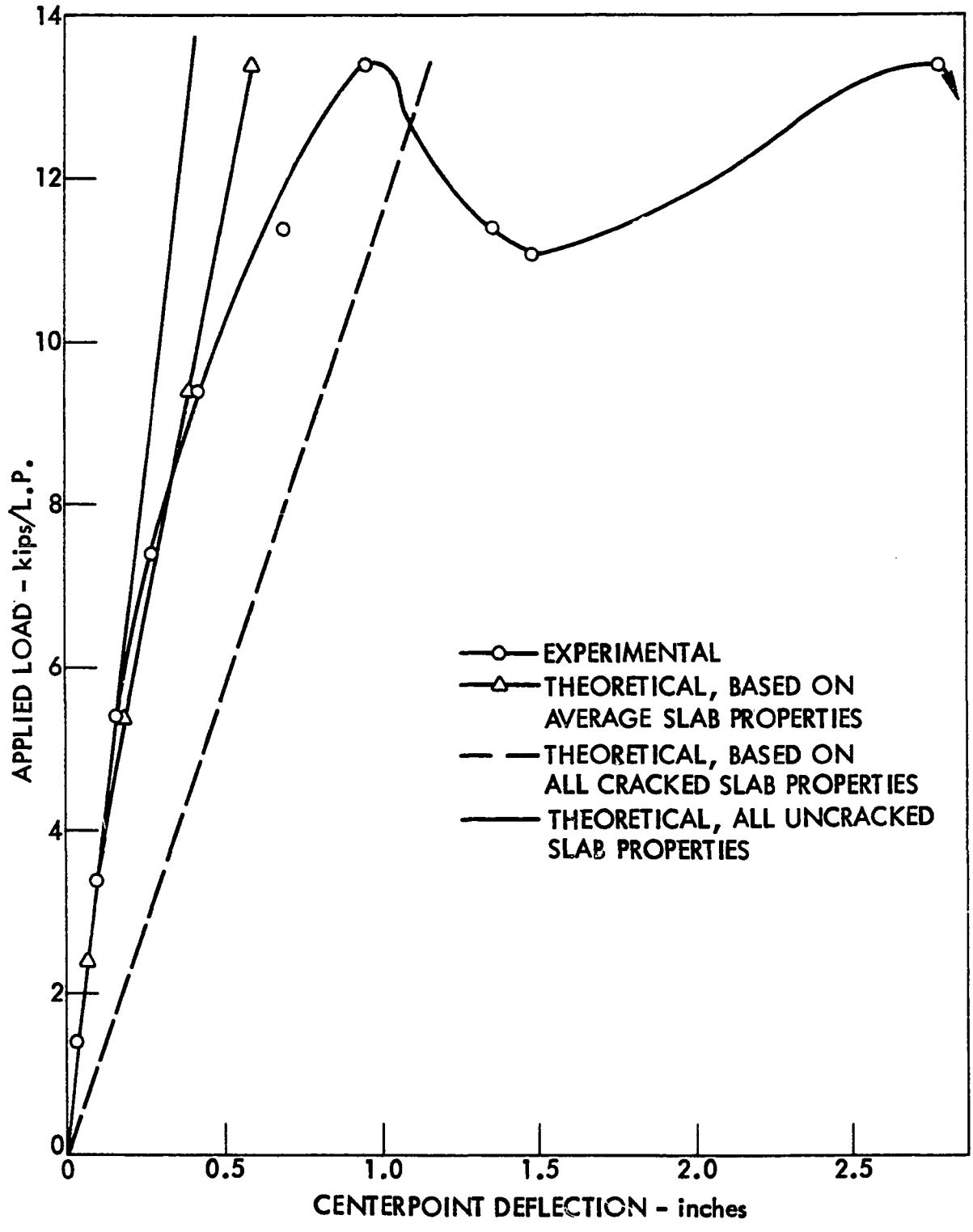

Figure 73. Experimental versus theoretical load-deflection for centerpoint of Slab 1

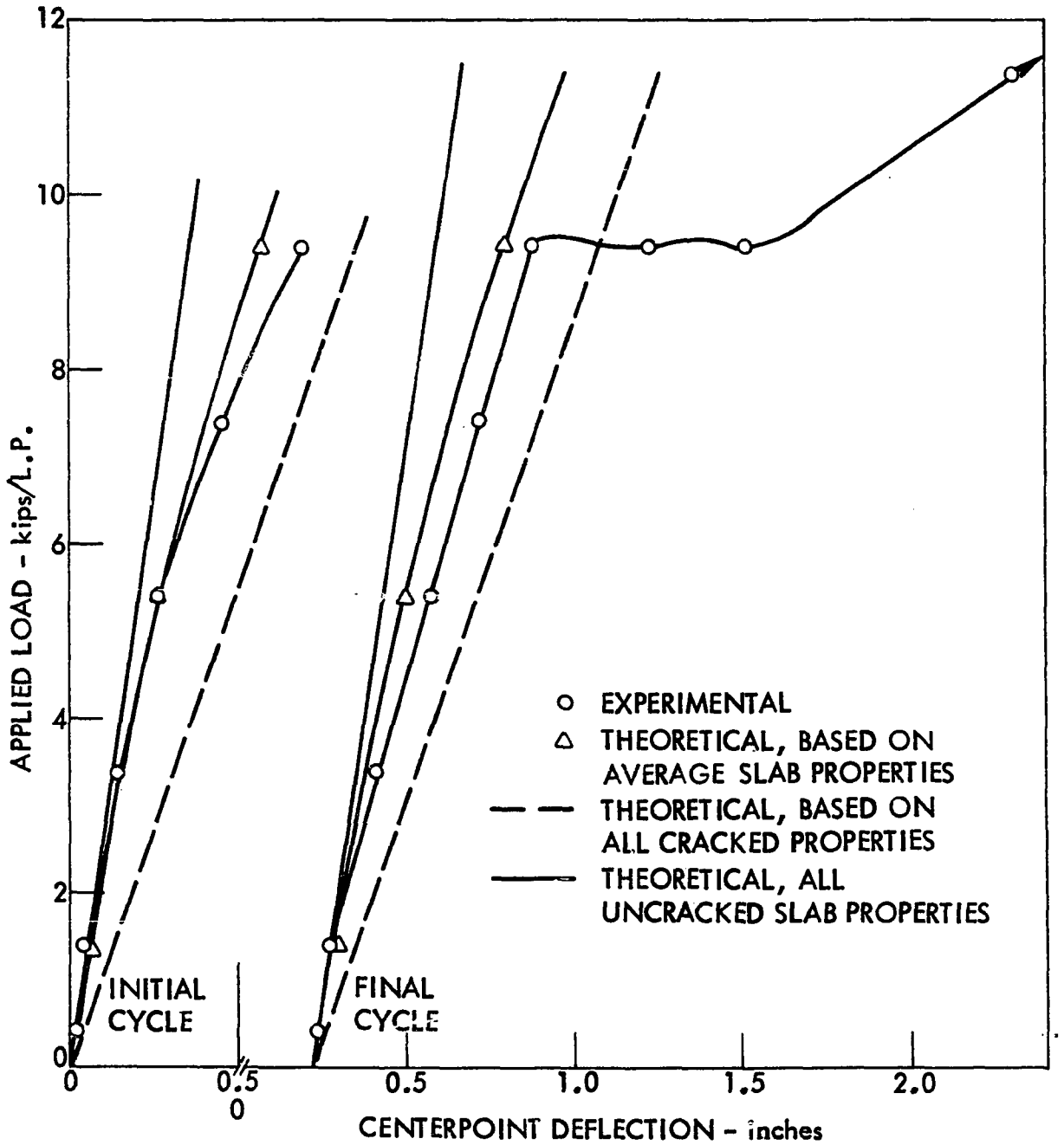

Figure 74. Experimental versus theoretical load-deflection for centerpoint of Slab 2

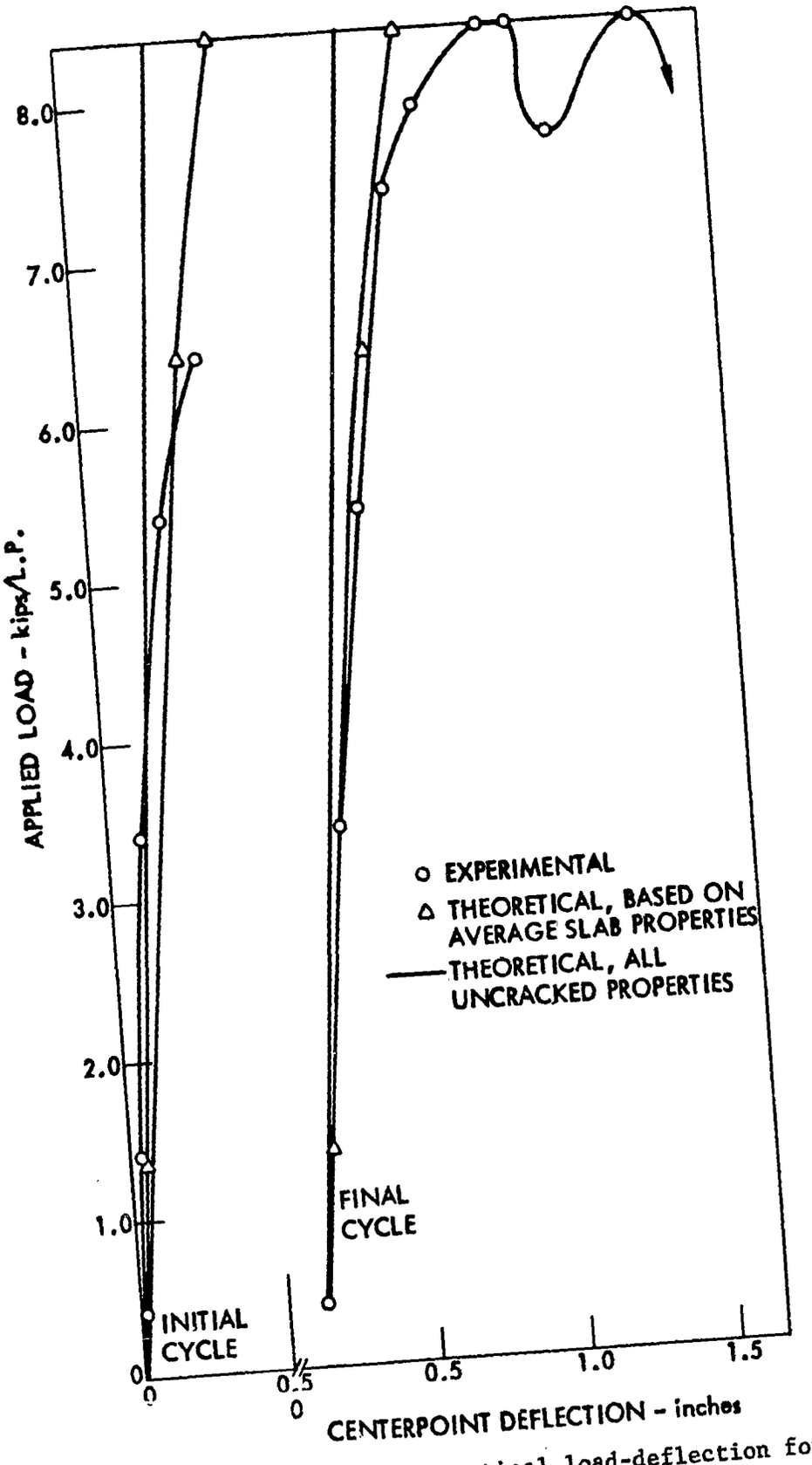

Figure 75. Experimental versus theoretical load-deflection for centerpoint of Slab 3

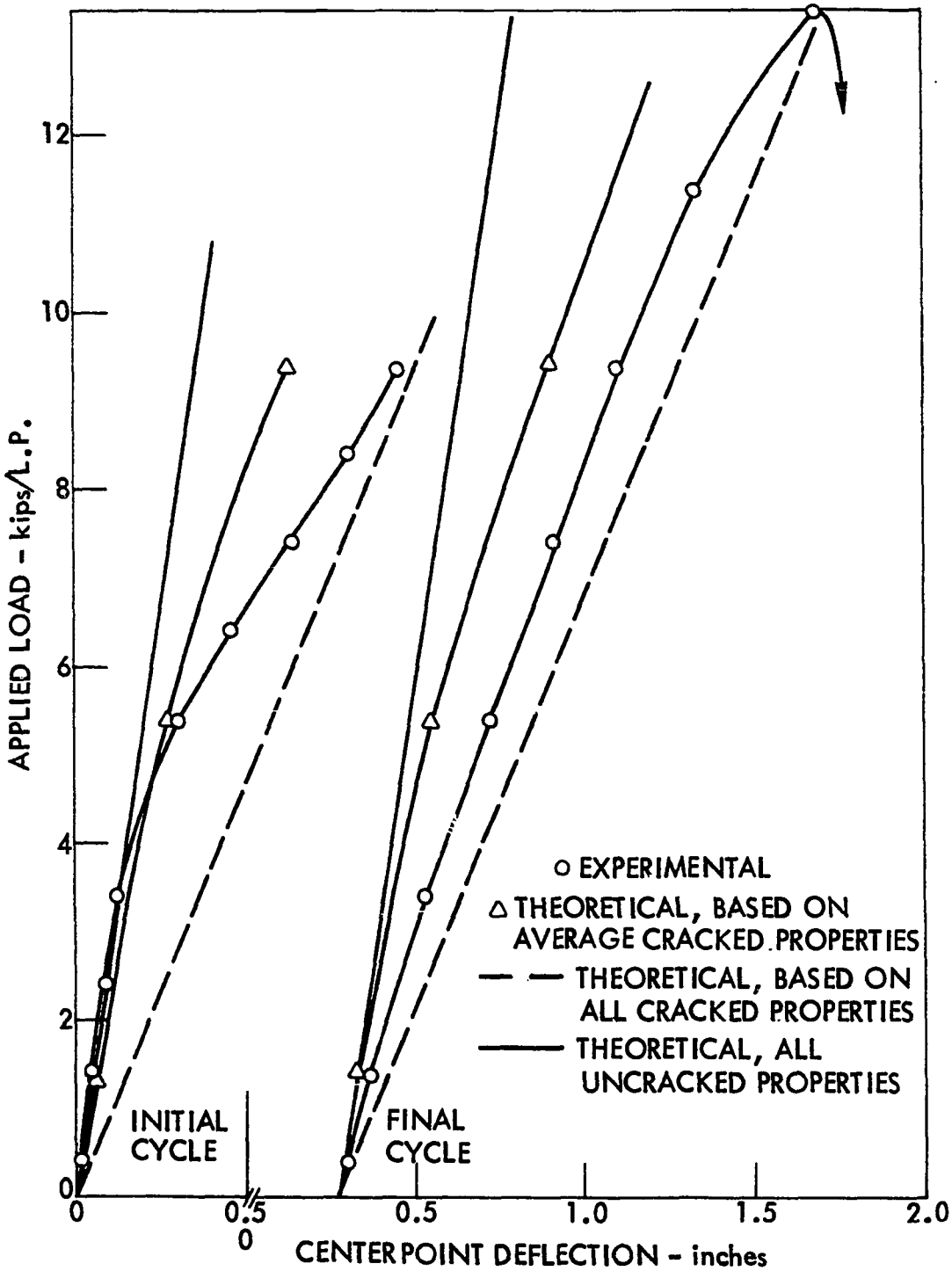

Figure 76. Experimental versus theoretical load-deflection for centerpoint of Slab 4

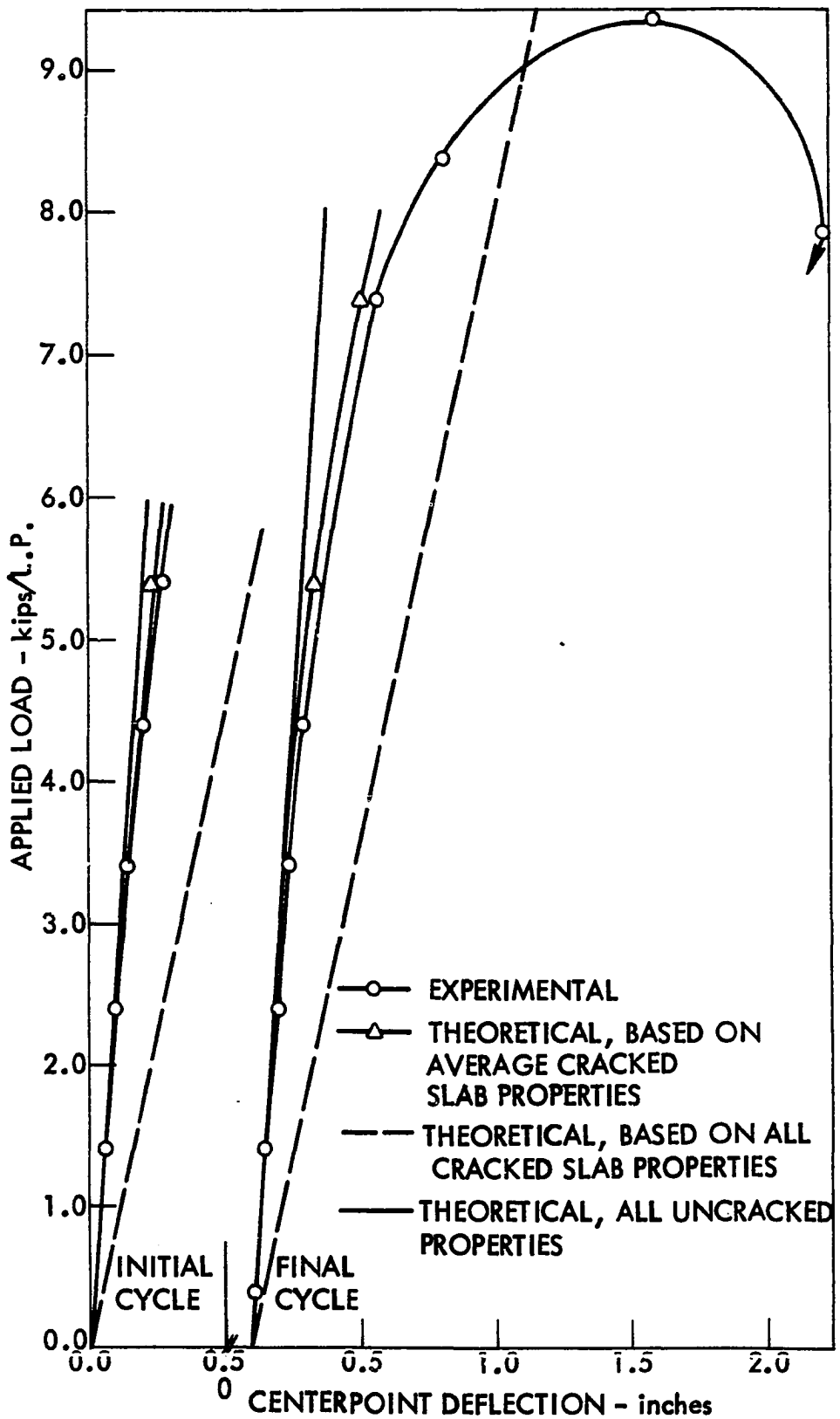

Figur 77. Experimental versus theoretical load-deflection for centerpoint of Slab 5

Moment distributions

Force distributions for the five two-way slabs were computed by the orthotropic plate theory as described in Chapter 2. As an example of how the forces varied throughout the slab, the most significant of these, M_y, was chosen to illustrate the distribution. M_y is that moment in ft-kips/ft acting on a plane transverse to the deck corrugations and having a moment vector transverse to the corrugations. As described in the previous section, three types of orthotropic theory calculations were performed. Only those M_y-distributions using the average method of computing elastic properties are shown as examples.

The theoretical M_y-moment distributions were compared to experimental values which were computed from the measured concrete and steel strains. The experimental M_y moments were determined from the uniaxial strains, neglecting the biaxial effects of strain on stress. This approximation was satisfactory for most load ranges since the measured strains transverse to the deck corrugations were fairly small in comparison to the strains parallel to the deck corrugations. See Figures 48-52.

The experimental moments, M_y, were computed two ways. The first method for obtaining M_y was based on the measured strain at the extreme fiber of the concrete. The second method was based on the measured strain on the steel dekcing. The two methods employed the general strain analysis technique as described previously in conjunction with the one-way slab elements utilizing Figure 67 and Equations (44), (45), and (46). The effects of shore removal and casting strains were not taken into account; consideration was given only to the applied loading conditions.

The experimental moments based on the general strain analysis concepts

were obtained by a computer program written to iterate the strain distribution across the depth until the resultant compressive force equaled the resultant tensile force (as divided into top, web, and bottom deck elements) at any given section. This procedure then utilizes one of the measured strains as the true strain and finds a compatible equilibrium force distribution to give M_y. Equating the resultant compressive and tensile forces assumed that no membrane forces were present at the cross section. This was considered valid since the slab was simply supported on casters or rollers with essentially little horizontal restraint. The two methods of computing the experimental M_y gave two answers for M_y which in most instances were fairly close indicating little or no membrane forces present. The experimental M_y was taken as the average of the two results, except where one of the two values was obviously in error. In this case, only the more reasonable result was used.

A more refined experimental moment, M_y, could be obtained using the biaxial effects of the stress-strain relations for concrete such as those discussed previously in the principal strain section and given by Reference (20). Once the appropriate biaxial stress-strain relations have been established, then a more correct magnitude of the compressive resultant force and its appropriate location can be found. However, since the magnitude of the concrete strain parallel to the corrugations was much larger than that transverse to the corrugations, the approximate experimental moments should be quite close to the two experimental moments.

Sample results of the theoretical orthotropic and experimental moment, M_y, distributions are shown in Figures 78-82 for Slabs 1-5, respectively. These figures give the distribution of M_y at the center section of the slab

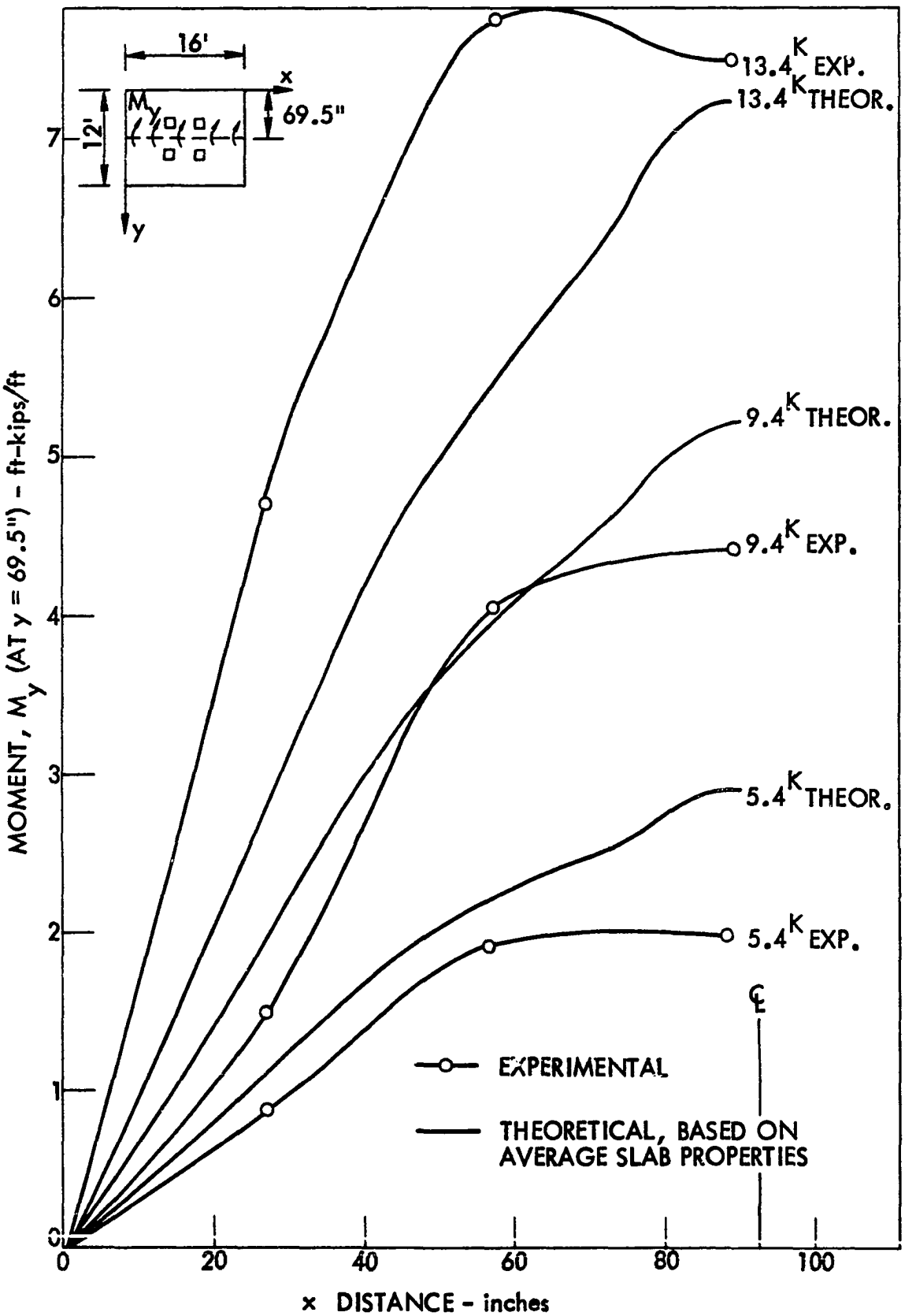

Figure 78. Theoretical versus experimental moments, M_y, at a section y = 69.5 inches for Slab 1

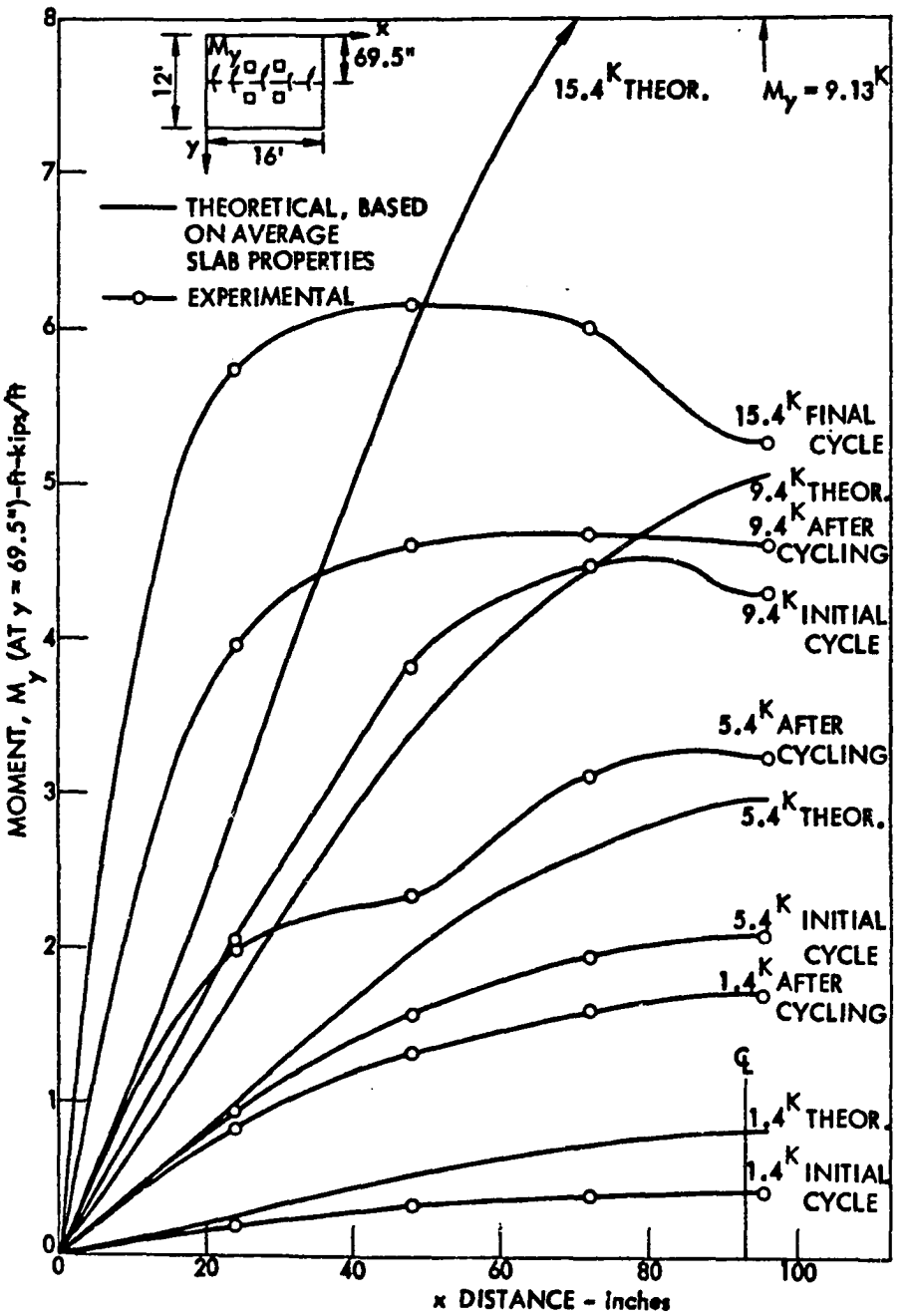

Figure 79. Theoretical versus experimental moments, M_y, at a section y = 69.5 inches for Slab 2

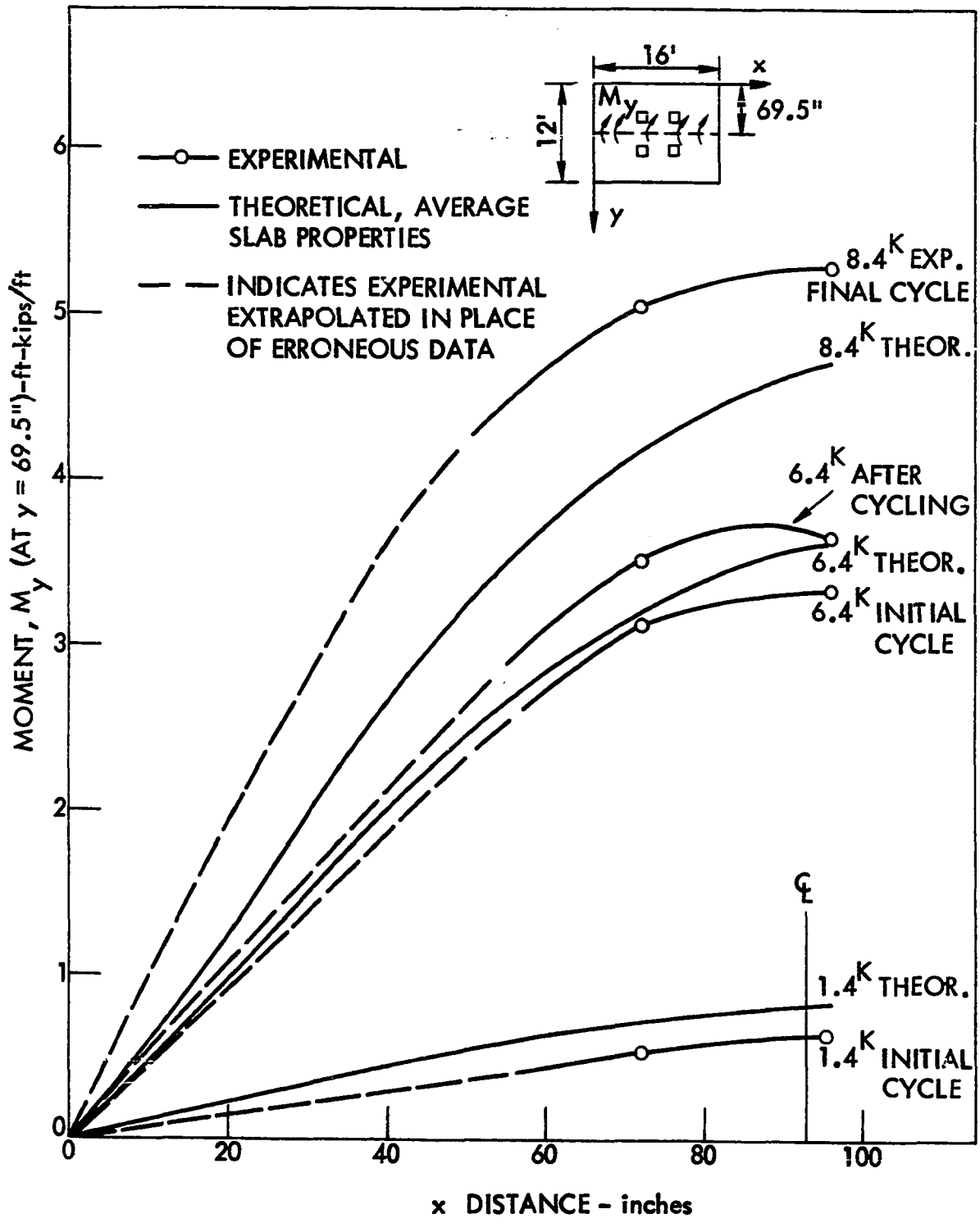

Figure 80. Theoretical versus experimental moments, M_y, at a section y = 69.5 inches for Slab 3

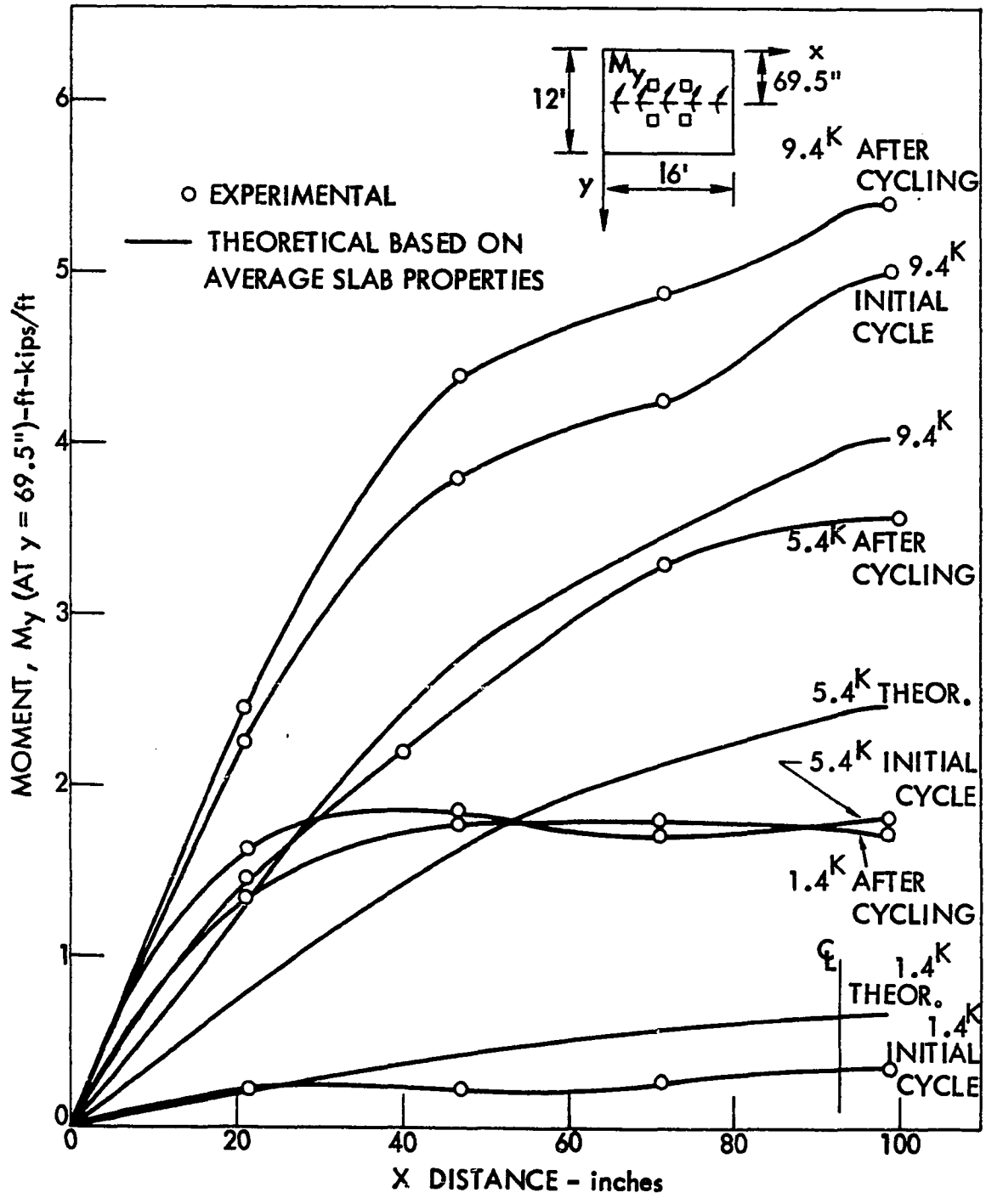

Figure 81. Theoretical versus experimental moments, M_y, at a section y = 69.5 inches for Slab 4

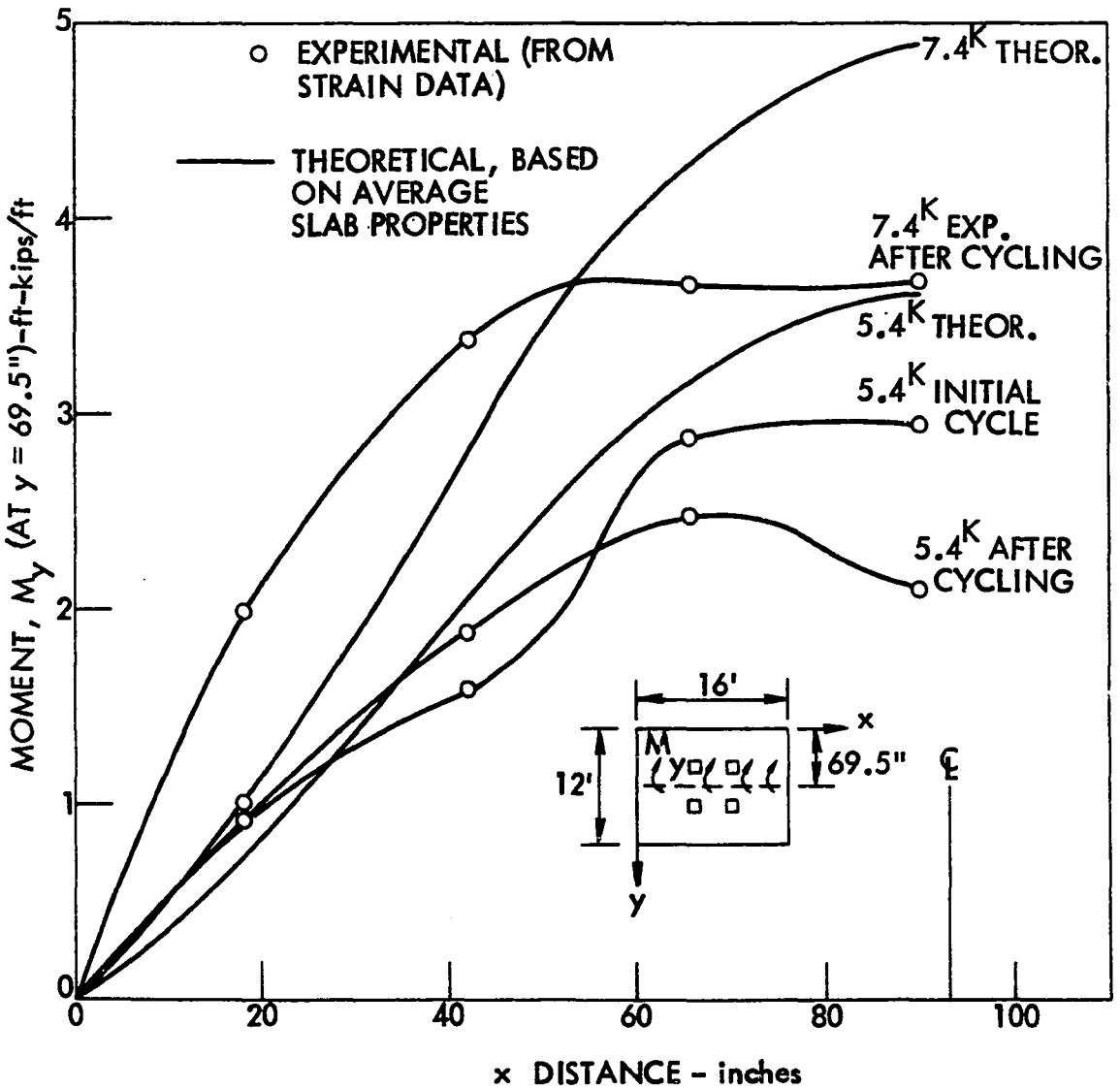

Figure 82. Theoretical versus experimental moments, M_y, at a section y = 69.5 inches for Slab 5

in the y direction and at various x-distances across the slab to the centerpoint. The M_y-curves in these figures are plotted for several increments of applied loading. For Slabs 2-5, the lower increments of loading include the experimental moment determination after cycling as well as before. The moments after cycling were computed using the strain data commencing at the application of the applied loading and thus include the permanent deformations due to the cycling.

As can be seen in Figure 78, for Slab 1, the M_y-distribution obtained from the experimental strains is somewhat lower for the lower load stages such as at 5.4 kips per load point. This lower distribution is also true for the initial cycle of loading on the other slabs as well. The slightly lower moment for lower load increments is probably due to several factors influencing the computation of the experimental and theoretical moments. One important difference is due to the difference in depths. The experimental moments were computed using the actual measured depth at each slab strain gage location, whereas the theoretical orthotropic moments assumed an average slab depth. Thus, the experimental moments should be more correct as far as the depth of slab variation is concerned. For the M_y-distributions shown, the corresponding locations generally had a greater depth, particularly in the central slab regions. Thus, the assumed depths for the orthotropic computations were less than the actual depths and resulted in a higher moment to resist the same load.

Other factors probably influenced the differences in moment distributions. One of these is the assumption regarding biaxial effects as discussed previously. Still another factor concerns the assumptions used in computing the elastic constants, and the assumptions regarding the

stiffness of the deck in the transverse direction. These factors need further study.

The general trend of agreement between the experimental and theoretical curves in Figures 78-82 shows the validity of using the equivalent orthotropic plate analysis of predicting the variation in bending moments. Of particular significance is that the theoretical and experimental curves showing the best agreement correspond to applied loading near 50 % of ultimate. See particularly 9.4 kips/L.P. for Slab 1 in Figure 78. Likewise, see 9.4 kips/L.P. for Slab 2, 6.4 kips/L.P. for Slab 3, and 5.4 kips/L.P. for Slab 5 for the initial cycle in each instance in Figures 79, 80, and 82, respectively. These loads might be considered approximately comparable to the design load for each slab.

In Figure 79, the curves corresponding to 1.4, 5.4, and 9.4 kips/L.P. show an experimental moment distribution for the initial cycle and also for the final cycle of loading. Note that the theoretical curve for 1.4 and 5.4 kips lies between the two experimental curves. The experimental curve for the final cycle of loading would be quite close to the theoretical curve if the permanent deformation moment at the beginning of the final cycle were subtracted from the total moments shown.

Before-and-after cycling curves for Slabs 2-5 appear in each respective figure for those loads prior to the cycling load. Slab 3 in Figure 80 has no 1.4 kips/L.P. level for the final cycle since no data readings were taken at this level.

The advantage of the heavier supplemenatry reinforcement used in Slab 2 is clearly indicated in Figure 79. The horizontal appearance of the experimental curve corresponding to an applied load of 15.4 kips shows that

there is a fairly uniform distribution of resisting moment across the section. This is of importance since this indicates essentially the main load-carrying segments of the slabs for the major moments, M_y, for one-way action.

In comparing the common loading distributions from slab to slab in Figures 78-82, inclusive, the influence of the variations in stiffness can be seen. See, for example, the 5.4 kips/L.P. level for Slabs 1, 2, 4, and 5, where the theoretical 5.4 kip-level moments for Slab 5 are higher for the same level due to the decrease in stiffness for Slab 5. Slab 5 had less depth of concrete over the deck corrugations than did the other slabs.

A second set of M_y-distributions is shown in Figures 83-87 for a section at a y distance of 45.5 inches from the edge of slab. These M_y-moments are shown as a function of the x-distance across each slab for various load increments. These section distributions are significant since they pass through the concentrated load point locations.

Figures 83-87 reveal that the orthotropic and experimental moments give good correlation for all five slabs. The same factors previously discussed for the variation of bending moments at a section achieved by a y-distance of 69.5 in. also apply to bending moments at a y-distance of 45.5 in. Again, the midrange values for the initial cycle of loading agree quite closely to the orthotropic plate method using the average elastic properties. See particularly the 9.4, 9.4, 6.4, 9.4, and 7.4 kips/L.P. levels for Slabs 1-5, respectively.

Note the closeness of the theoretical and experimental curves for near ultimate for Slab 2 in Figure 84. This is probably due to the beneficial effect of the supplementary reinforcement. The large amount of supplementary

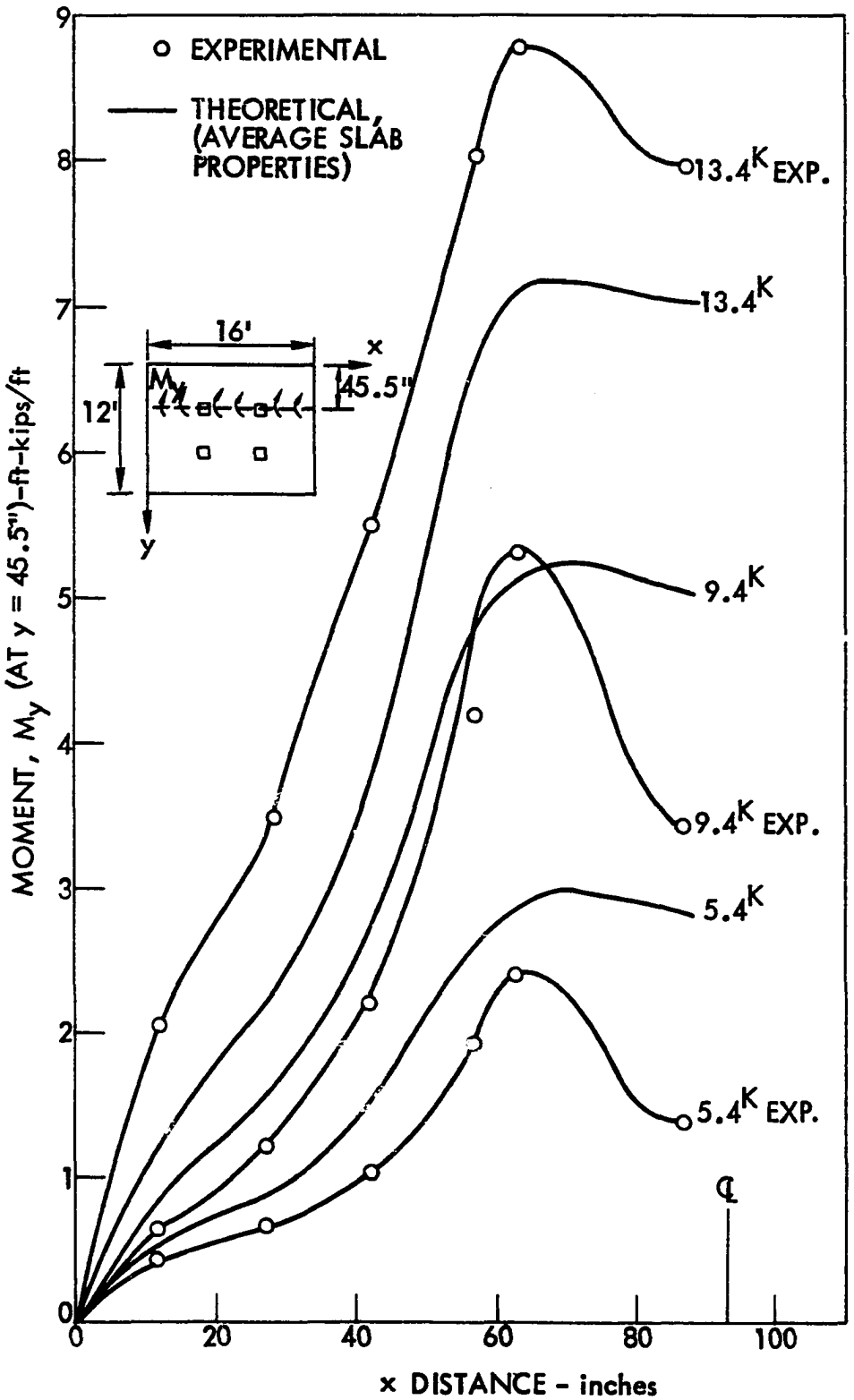

Figure 83. Theoretical versus experimental moments, M_y, at a section y = 45.5 inches for Slab 1

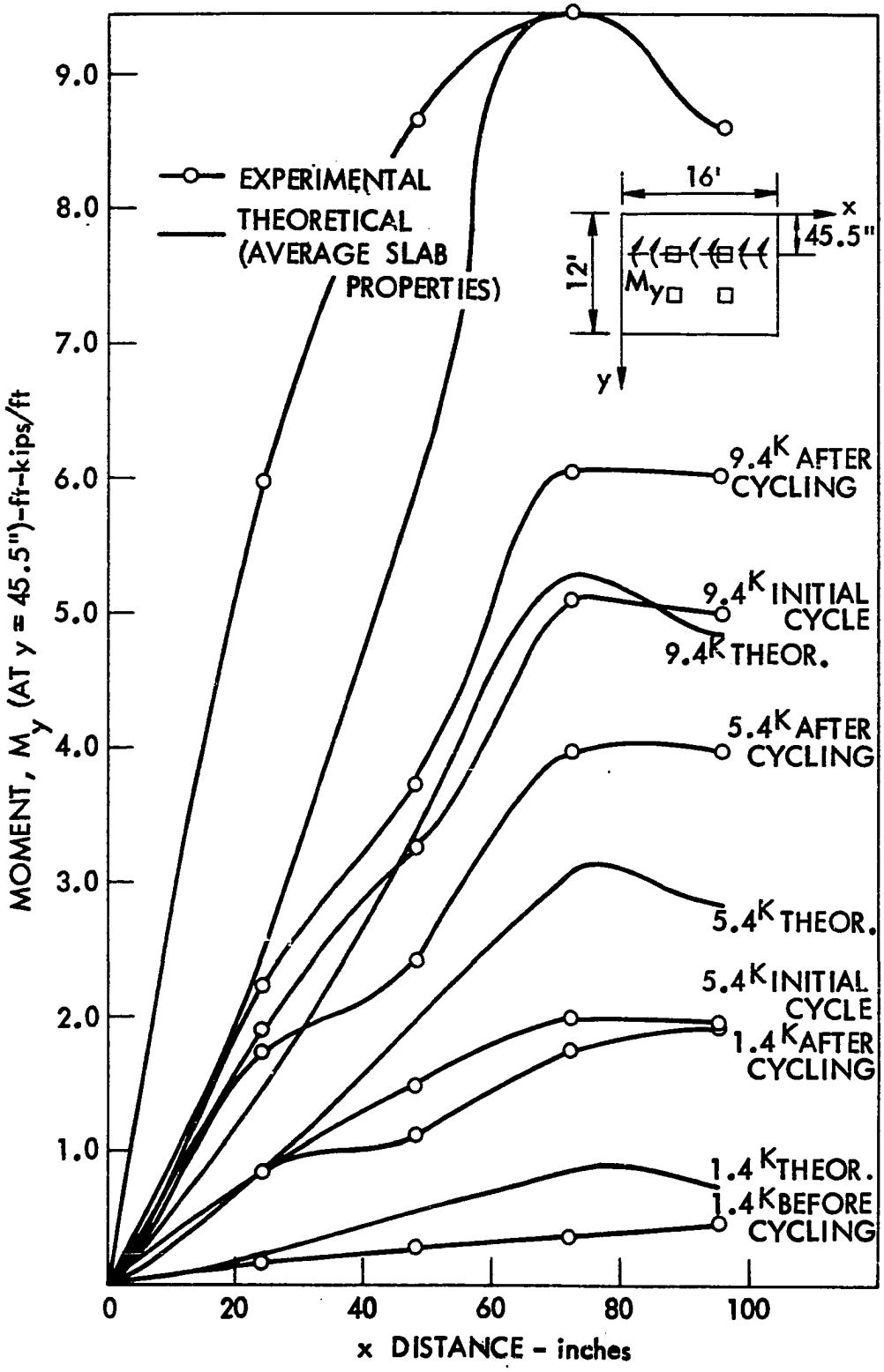

Figure 84. Theoretical versus experimental moments, M_y, at a section y = 45.5 inches for Slab 2

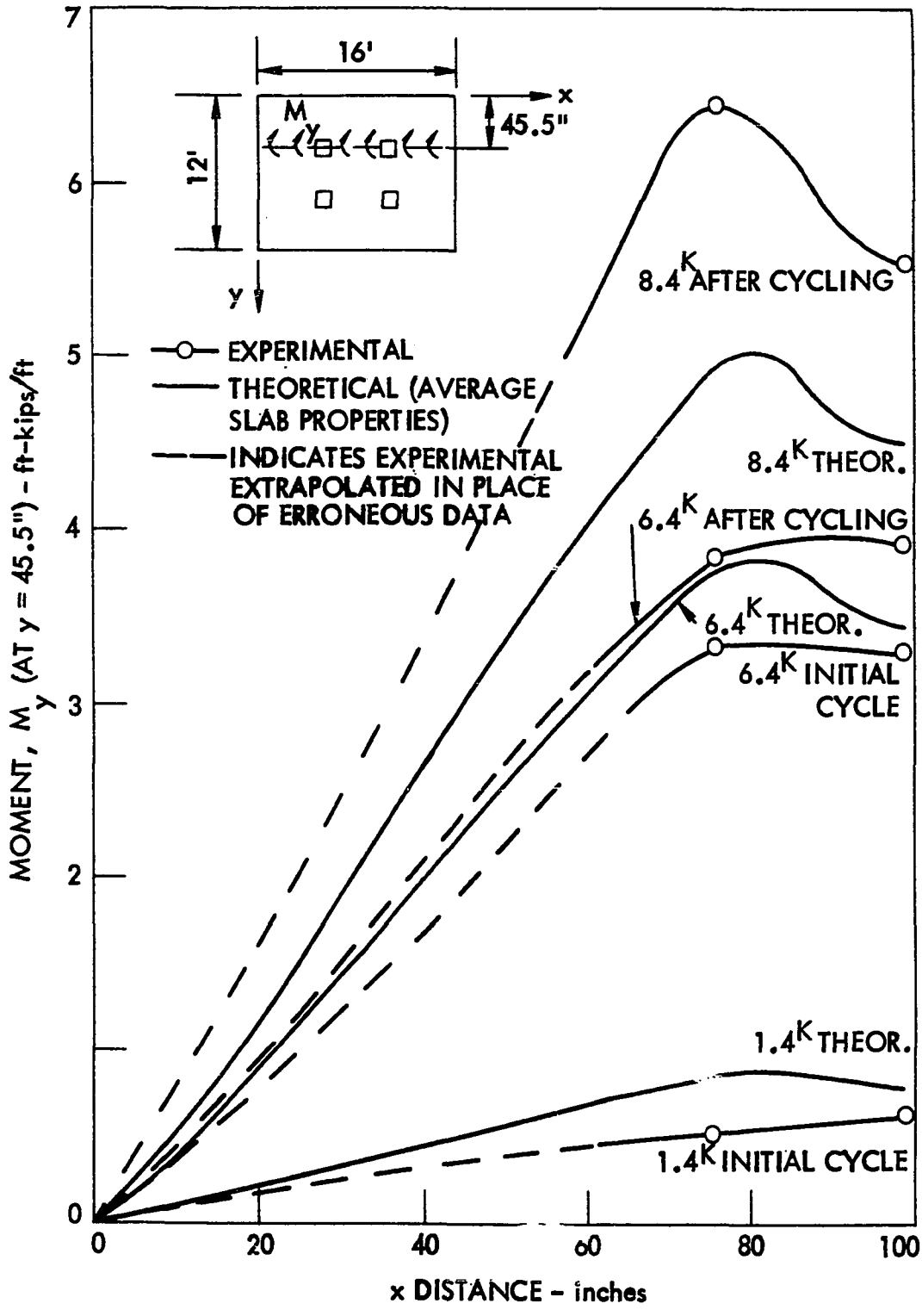

Figure 85. Theoretical versus experimental moments, M_y, at a section y = 45.5 inches for Slab 3

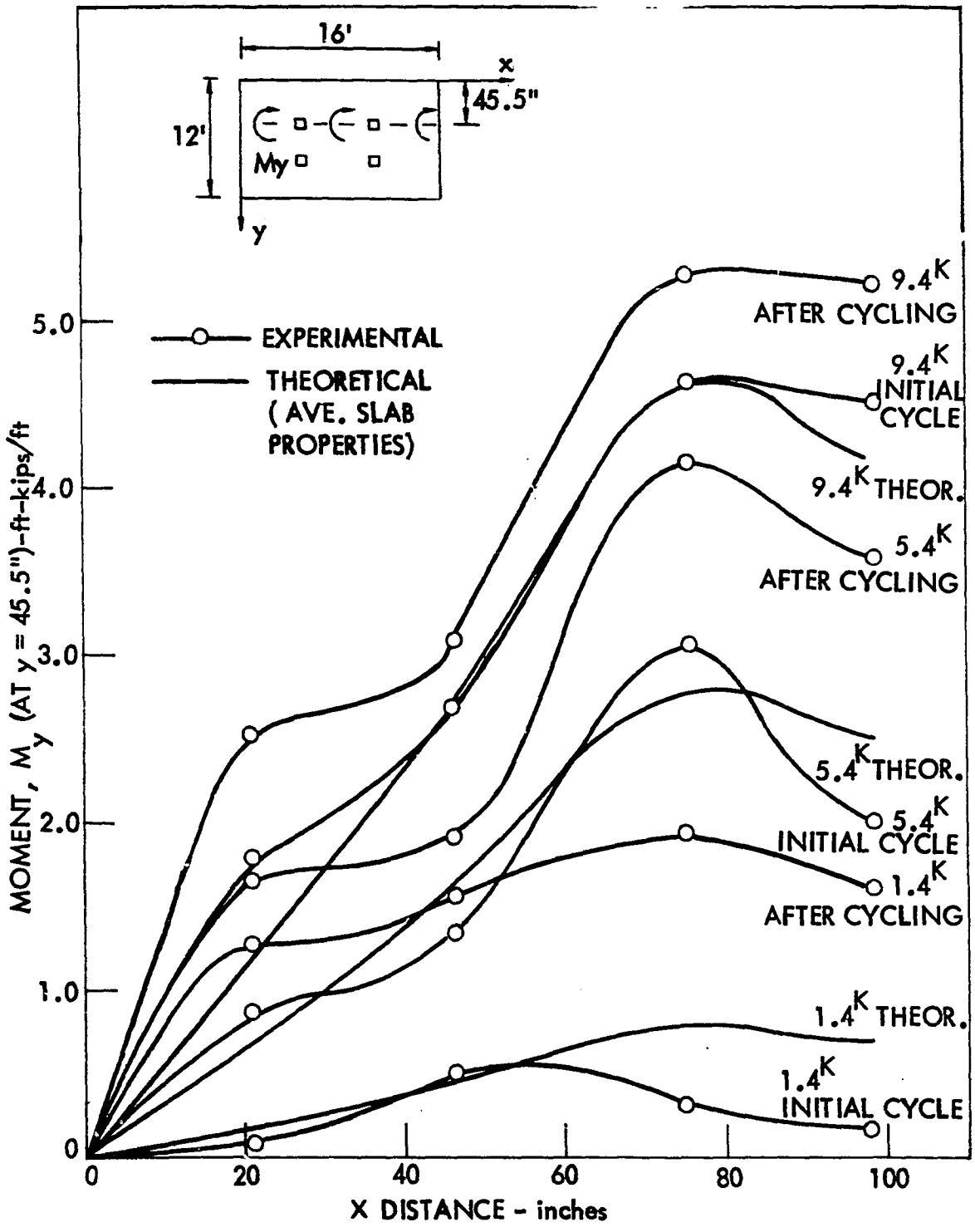

Figure 86. Theoretical versus experimental moments, M_y, at a section y = 45.5 inches for Slab 4

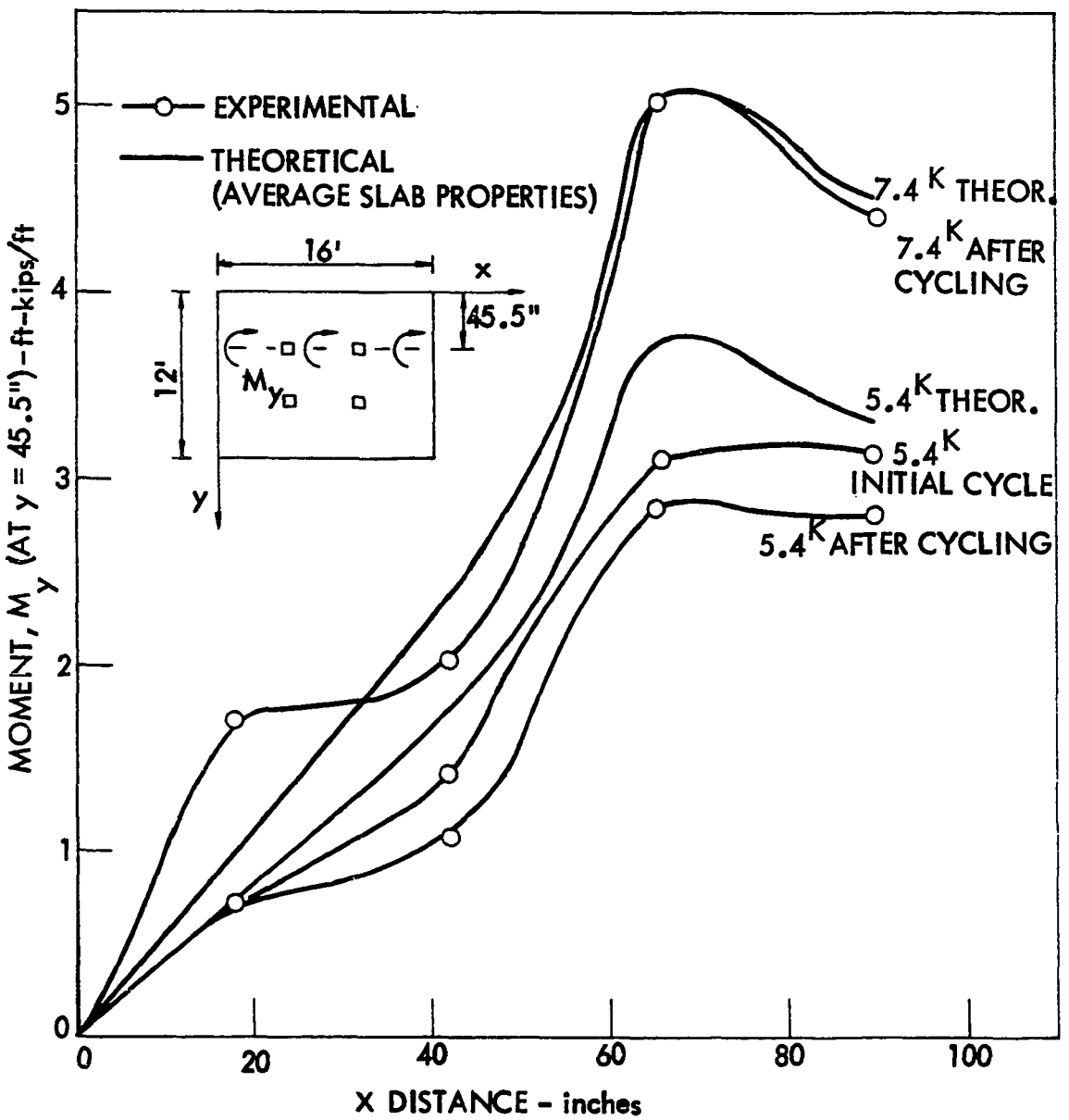

Figure 87. Theoretical versus experimental moments, M_y, at a section y = 45.5 inches for Slab 5

reinforcement in this slab helped to distribute the load quite uniformly across the width of the slab, and thus the average sectional properties used to obtain the theoretical moments provided good results.

The method of treating the steel-deck reinforced slabs as equivalent orthotropic plates, using sectional constants based on average slab properties, proved valid. Factors such as depth variation, biaxial effects, and elastic constant computations need more refinement in the analysis. However, the analysis in its present form is a reliable means of predicting general trends and slab behavior.

Curve fitting for deflected surfaces

The deflected surfaces of the five full-scale slab tests were fitted to a sixth-order polynomial function. The deflected surface for this polynomial is given in Chapter 2 as Equation (30). The results of the curve-fitting procedure indicate that a close fit was obtained using Equation (30). An example of this fit is shown in Figure 88, where two cross sections of measured deflections are compared with the fitted curve for Slab 5. In fitting the curves, symmetry of deflections was taken advantage of wherever possible. The two sample cross-sections are in two different directions. One section is for varying of distance along a constant x distance of 114 inches. The other section is for a varying x distance along a constant y distance of 93.5 inches. As can be seen in Figure 88, the deflections based on the polynomial curves show a close correspondence to the actual measured deflections. The applied load on Slab 5 at this stage was 5.4 kips per load point.

A complete listing of the 28 coefficients, consisting of C_1, C_2,

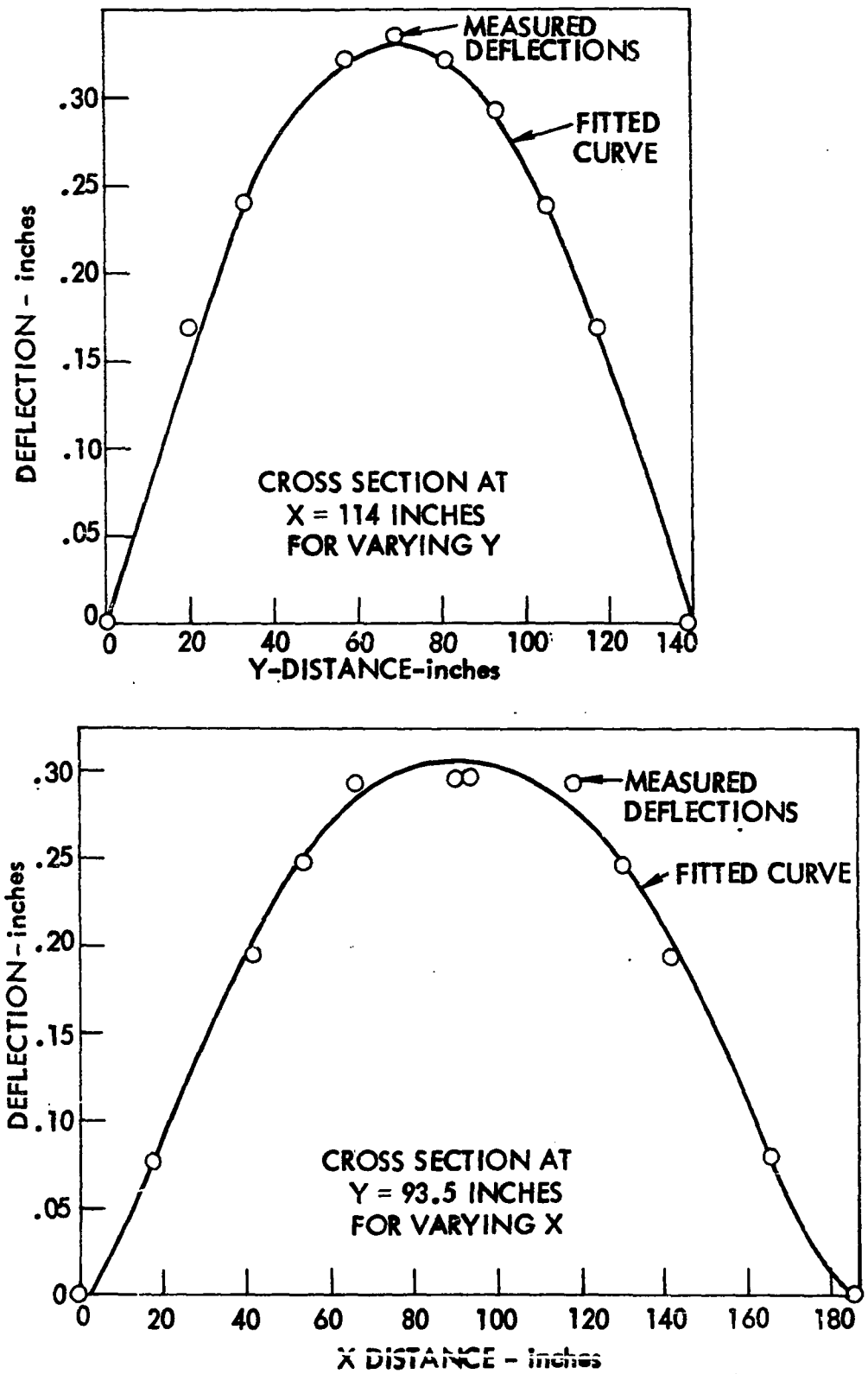

Figure 38. Two sample cross-sections showing the agreement of the polynomial fitted curve with the measured deflections for Slab 5 at 5.4 kips/L.P.

C_3, ..., and C_{28} in Equation (30) is given in Table 32 for a load of 5.4 kips/L.P. for each slab. These coefficients can be used in Equations (31-37) to obtain the force distributions throughout each of the slabs. The distribution of the moment and shear forces for all five slabs at various load increments was not completed due to lack of computer funding and time.

Table 32. Coefficients C_1, C_2, ..., and C_{28} for Equation (30) for a polynomial deflection fit at a load of 5.4 kips/L.P.

Coefficient	Slab No. 1	2	3	4	5
	Data Set 1	Data Set 2	Data Set 3	Data Set 4	Data Set 5
C_1	-0.2407566E-02	0.6423748E-01	0.1679031E 00	0.9269792E-01	0.1045502E 00
C_2	0.3620794E-03	-0.4053306E-02	-0.4573554E-02	-0.2190814E-02	-0.1587792E-02
C_3	0.6233496E-03	0.1129949E-02	-0.2589967E-02	-0.3744976E-02	-0.5583525E-02
C_4	-0.6546287E-05	0.1011273E-03	-0.6206808E-04	-0.4883741E-04	-0.1041977E-03
C_5	-0.3235288E-04	-0.1860890E-03	-0.8687492E-04	0.7090824E-04	0.8489547E-04
C_6	-0.1295329E-03	-0.3016298E-04	0.8148811E-04	0.8846050E-04	0.8245297E-04
C_7	-0.3061798E-07	-0.1325392E-05	0.3260871E-05	0.2060296E-05	0.3306831E-05
C_8	0.7180377E-06	0.5043829E-05	0.2772055E-05	-0.1189229E-05	0.1916356E-06
C_9	0.9713822E-06	-0.2506014E-05	-0.5737751E-05	-0.4055657E-05	-0.2765049E-05
C_{10}	0.1319968E-05	0.1540232E-05	-0.2366903E-06	-0.2188807E-05	-0.3001828E-05
C_{11}	0.1157726E-08	0.9924065E-08	-0.4001938E-07	-0.2449171E-07	-0.3653056E-07
C_{12}	-0.8285156E-08	-0.6230345E-07	-0.3374775E-07	0.1481739E-07	-0.1674318E-07
C_{13}	-0.9093106E-08	0.1142908E-07	0.3841091E-07	0.3790825E-07	0.3356405E-07
C_{14}	-0.2938444E-08	0.2855493E-07	0.5646826E-07	0.3864806E-07	0.2322895E-07
C_{15}	-0.5574108E-08	-0.2001003E-07	-0.2270143E-08	0.2138512E-07	0.3567548E-07
C_{16}	-0.6934067E-11	-0.4107283E-10	0.2015228E-09	0.1223475E-09	0.1749951E-09
C_{17}	0.4921921E-10	0.3798595E-09	0.2096565E-09	-0.9260018E-10	0.1494570E-09
C_{18}	0.7744957E-11	-0.7564495E-10	-0.1479819E-09	-0.1052393E-09	-0.3879481E-10
C_{19}	0.2144888E-10	-0.2121800E-09	-0.3994962E-09	-0.2802467E-09	-0.2171212E-09

Table 32. Continued

Coefficient	Slab No. 1	2	3	4	5
	Data Set 1	Data Set 2	Data Set 3	Data Set 4	Data Set 5
C_{20}	0.2992352E-10	0.1085421E-09	0.1737573E-10	-0.1167374E-09	-0.1436818E-09
C_{21}	0.2007246E-10	0.7356370E-10	-0.4877067E-11	-0.7407908E-10	-0.1623035E-09
C_{22}	0.1241747E-13	0.7358149E-13	-0.3609861E-12	-0.2192374E-12	-0.3048944E-12
C_{23}	-0.3825817E-15	0.3014207E-15	0.4405677E-13	0.1492600E-14	0.1937757E-12
C_{24}	-0.1068351E-12	-0.3976549E-12	-0.3335664E-13	0.4009045E-12	0.4741622E-12
C_{25}	-0.7349809E-15	-0.3012725E-14	-0.6578844E-14	0.4048513E-14	0.4416451E-13
C_{26}	-0.5726772E-13	0.5696336E-12	0.1074937E-11	0.7549288E-12	0.5592533E-12
C_{27}	0.5263486E-15	-0.3524303E-14	-0.1410409E-13	0.3811428E-14	-0.8746915E-13
C_{28}	-0.1179864E-12	-0.9082026E-12	-0.5133453E-12	0.2239613E-12	-0.3998466E-12

CHAPTER 8. CONCLUSIONS

Important conclusions regarding the analysis and behavioral results of the full-scale slab and slab element experimental tests are enumerated as follows:

1. An ultimate strength procedure for two-way concrete slabs reinforced with cold-formed steel decking was formulated. The procedure was founded on the principles of yield-line theory and of shear-bond regression analysis. A collapse mechanism established by yield-line procedures was utilized to establish the effective load-carrying-segment width of the slabs. After the width of this segment was established, a shear-bond regression analysis was used to predict the total shear force distributed to the reactive edges perpendicular to the deck corrugations. The total shear existing along the sides of the effective load-carrying segment was subsequently added to the shear-bond components to give the predicted ultimate load for each slab.
2. Theoretical deflections and moment distributions were computed by treating the corrugated steel-deck reinforced slabs as equivalent orthotropic plates and applying conventional plate equations. An iterative procedure was used to establish elastic plate constants. Good agreement between the computed and experimental moments and deflections was found.
3. Ultimate failure of the test slabs was initiated by slippage between the steel deck and the concrete with the concrete moving outward parallel to the deck corrugations in the central regions

of the slabs. The observed slippage extended for a width approximately equal to that of the main load-carrying element of the slab. Small amounts of slippage occurred prior to ultimate; however, the major portion of slip occurred at ultimate. Yielding of the steel did not appear to contribute to failure, however some local yielding in the vicinity of the load points was observed prior to ultimate.

4. Welded wire fabric influenced the behavioral characteristics of the slabs. Slab 2, with the largest amount of supplementary steel, sustained the largest ultimate load and also sustained the largest ultimate deflection. Slab 3, without any supplementary reinforcing, could carry an ultimate load which was only 57 percent that of Slab 2. Likewise, the ultimate deflection of Slab 3 was much less than that of Slab 2. The addition of supplementary steel also had a beneficial effect on the lateral distribution of resisting moments.

5. The use of corner tie-down reactions on Slab 1 resulted in this slab exhibiting stiffer behavioral characteristics than any of the other slabs.

6. The measured edge reactions for the slab tests indicated that about 78 percent of the total load at the beginning of load application was transmitted in the so-called "strong" direction to the east and west reactions. An exception was Slab 1, which had corner tie-downs and indicated about 72 percent. All slabs, near ultimate, had a load distribution to the east and west edges of at least 97 percent of the total force, indicating the significance

of the one-way action of the main load-carrying element of the slabs. The lateral distribution of live load in the so-called weak direction varied over a considerable range. The maximum edge reactions in the weak direction usually occurred when the live load was about 50% of ultimate, or roughly equivalent to the design load.

7. The one-way slab element tests revealed the following conclusions:
   a. Ultimate failure of the one-way slab element specimens with the deck corrugations parallel to the span length was initiated by a shear-bond failure consisting of a horizontal slippage of the concrete with respect to the steel deck. The shear-bond regression analysis approach gave very good linear predictions of the ultimate load for these one-way elements reinforced with three-inch-deep steel deck as well as 1½-inch deck.
   b. The addition of welded wire fabric appeared to increase the one-way shear-bond capacity for elements with the deck corrugations parallel to the length by about 11 percent.
   c. A general strain analysis was used to predict the flexural capacity of the slab elements with deck corrugations parallel to specimen length. This analysis was found particularly useful for those specimens reinforced with steel deck having a yield stress of 101.6 ksi since this steel did not have sufficient ductility to assume yield across the entire deck cross section. The addition of the supplementary reinforcing and the effects of casting and shore removal were

also analyzed by the general strain analysis procedure.

d. Ultimate failure of the one-way slab element specimens with the deck corrugations transverse to the specimen length was by a flexural failure of the concrete section above the deck corrugations. Those specimens without supplementary steel transverse to the deck corrugations had an ultimate strength predicted by considering the flexural capacity using the gross concrete section above the corrugations based on the modulus of rupture strength. Those transverse specimens with the supplementary steel parallel to the specimen length had an ultimate strength predicted by flexural concepts by considering only the supplementary steel as taking the tensile force in a section above the corrugations.

LITERATURE CITED

1. American Concrete Institute. Building Code Requirements for Reinforced Concrete (ACI 318-63). Detroit, Michigan: American Concrete Institute, 1963.

2. American Concrete Institute. Building Code Requirements for Reinforced Concrete (ACI 318-71). Detroit, Michigan: American Concrete Institute, 1971.

3. American Concrete Institute. Commentary on Building Code Requirements for Reinforced Concrete (ACI 318-63). Detroit, Michigan: American Concrete Institute, 1965.

4. American Concrete Institute. Commentary on Building Code Requirements for Reinforced Concrete (ACI 318-71). Detroit, Michigan: American Concrete Institute, 1971.

5. American Iron and Steel Institute. Specification for the Design of Cold-Formed Steel Structural Members. New York: American Iron and Steel Institute, 1968.

6. Dally, J. W., and Riley, W. F. Experimental Stress Analysis. New York: McGraw-Hill Book Co., 1965.

7. Ekberg, C. E., Jr., and Porter, M. L. "Full-Scale Laboratory Tests of a Concrete Slab Reinforced with Cold-Formed Steel Decking." Iowa State Engineering Research Institute Progress Report No. 10, ERI-98100, Ames, Iowa, February 1971.

8. Ekberg, C. E., Jr., and Schuster, R. M. "Floor Systems with Composite Form-Reinforced Concrete Slabs." Eighth Congress of the International Association for Bridge and Structural Engineering, Final Report, Zurich (1968): 385-394.

9. Ekberg, C. E., Jr., Porter, M. L., and Boettcher, L. A. "A Preliminary Investigation for the Use of Cold-Formed Steel Decking As Reinforcement for Continuous One-Way Concrete Slabs." Unpublished Progress Report No. 11 (rough draft), Dept. of Civil Engineering, Iowa State University, Ames, Iowa, February 1971.

10. Ekberg, C. E., Jr., Schuster, R. M., and Porter, M. L. "Further Investigation of Light Gage Steel Forms as Reinforcement for Concrete Slabs." Iowa State Engineering Research Institute Progress Report No. 5, ERI-395, Ames, Iowa, 1969.

11. Ekberg, C. E., Jr., Schuster, R. M., and Porter, M. L. "Further Testing of Light Gage Steel Forms as Reinforcement for Concrete Slabs." Iowa State Engineering Research Institute Progress Report ERI-201, Ames, Iowa, 1968.

12. Fisher, J. W. "Design of Composite Beams with Formed Metal Deck." Paper presented at AISC National Engineering Conference, Pittsburgh, Pa., May 1970.

13. Fisher, J. W., Kim, S. W., and Slutter, R. G. "Tests of Lightweight Concrete Composite Beams and Pushout Specimens with Cellular Steel Deck." Report No. 200.67.438.1. Bethlehem, Pa.: Fritz Engineering Laboratory, Lehigh University, July 1967.

14. Friberg, Bengt F. "Combined Form and Reinforcement for Concrete Slabs." American Concrete Institute Journal, Proceedings, 25 (1954), 697-716.

15. Hondros, G. "Application of Electrical Resistance Strain (S.R.4) Gages in the Measurement of Surface and Internal Strains in Plain and Reinforced Concrete." Preprint No. 20.1.63, 18th Annual Instrument Society of America Conference and Exhibit, Chicago, Sept. 1963.

16. Iowa State University Computation Center Library, ULSQ Subroutine of Math Library package, Ames, Iowa, 1972.

17. Jones, L. L., and Wood, R. H. Yield-Line Analysis of Slabs. New York: American Elsevier Publishing Company, Inc., 1967.

18. Larson, T. D. Portland Cement and Asphalt Concretes. New York: McGraw-Hill Book Co., Inc., 1963.

19. Lekhnitskii, S. G. Anisotropic Plates (translated from Russian edition by Tsai, S. W., and Cheron, T.). 2nd edition, New York: Gordon and Breach Science Publishers, 1968.

20. Liu, T. C. Y., Nilson, A. H., and Slate, F. O. "Biaxial Stress-Strain Relations for Concrete." Journal of the Structural Division, American Society of Civil Engineers, Proceedings, 98, No. ST5 (May 1972), 1025-1034.

21. Lloyd, J. P., and Kesler, C. E. "Splices and Anchorages in One-Way Slabs Reinforced with Deformed Wire Fabric." American Concrete Institute Journal, Proceedings, 67, No. 8 (August 1970), 636-642.

22. Love, J. S., Barnoff, R. M., and Larson, T. D. "Composite Action From Corrugated Bridge Deck Forms." Materials and Structural Research Report, Dept. of Civil Engineering, The Pennsylvania State University, University Park, Pa., March 1967.

23. Mouw, K. W., and Ekberg, C. E., Jr. "Fatigue Testing of Light Gage Metal Forms." Engineering Research Institute, Special Report, ERI-348, Ames, Iowa, 1969.

24. Porter, M. L. "Investigation of Light Gage Steel Forms as Reinforcement for Concrete Slabs." Unpublished MS Thesis, Library, Iowa State University, Ames, Iowa, 1968.

25. Porter, M. L. and Ekberg, C. E., Jr. "Behavior of Concrete Slabs Reinforced with Three-Inch Deep Cold-Formed Steel Decking." Oral Presentation given at Second Specialty Conference on Cold-Formed Steel Structures, St. Louis, Missouri, October 1973.

26. Porter, M. L., and Ekberg, C. E., Jr. "Data Summary of a Fifth Full-Scale Laboratory Test of a Concrete Slab Reinforced with Cold-Formed Steel Decking." Unpublished progress Report No. 17 (rough draft), Department of Civil Engineering, Iowa State University, Ames, Iowa, June 1972.

27. Porter, M. L., and Ekberg, C. E., Jr. "Data Summary of a Second Full-Scale Laboratory Test of a Concrete Slab Reinforced with Cold-Formed Steel Decking." Unpublished Progress Report No. 13 (rough draft), Department of Civil Engineering, Iowa State University, Ames, Iowa, June 1971.

28. Porter, M. L., and Ekberg, C. E., Jr. "Data Summary of a Third Full-Scale Laboratory Test of a Concrete Slab Reinforced with Cold-Formed Steel Decking." Unpublished Progress Report No. 14 (rough draft), Department of Civil Engineering, Iowa State University, Ames, Iowa, August 1971.

29. Porter, M. L. and Ekberg, C. E., Jr. "Formulation of Yield-Line Theory as Applied to Steel-Deck-Reinforced Concrete Slab." Unpublished Progress Report No. 9 (rough draft), Department of Civil Engineering, Iowa State University, Ames, Iowa, July 1970.

30. Porter, M. L., and Ekberg, C. E., Jr. "Investigation of Cold-Formed Steel-Deck-Reinforced Concrete Floor Slabs." Proceedings of First Specialty Conference on Cold-Formed Steel Structures. Dept. of Civil Engineering, University of Missouri-Rolla, August 19-20, 1971.

31. Porter, M. L. and Ekberg, C. E., Jr. "Summary of Full-Scale Laboratory Tests of Concrete Slabs Reinforced with Cold-Formed Steel Decking." Ninth Congress of the International Association for Bridge and Structural Engineering, Preliminary Report, Zurich (1972): 173-183.

32. Porter, M. L., Boettcher, L. A., and Ekberg, C. E., Jr. "An Investigation of the Behavior of 3-inch Deep, Cold-Formed Steel Decking as Positive Reinforcement for One-way Concrete Slabs." Unpublished Progress Report No. 16 (rough draft), Dept. of Civil Engineering, Iowa State University, Ames, Iowa, May 1972.

33. Porter, M. L., Boettcher, L. A., and Ekberg, C. E., Jr. "Data Summary of a Fourth Full-Scale Laboratory Test of a Concrete Slab Reinforced with Cold-Formed Steel Decking." Unpublished Progress Report No. 14 (rough draft), Dept. of Civil Engineering, Iowa State University, Ames, Iowa, December 1971.

34. Porter, M. L., Boettcher, L. A., and Ekberg, C. E., Jr. "Preliminary Tests on Slab Elements Constructed with V-Grip Steel Decking." Unpublished Progress Report No. 15 (rough draft), Dept. of Civil Engineering, Iowa State University, Ames, Iowa, January 1972.

35. Porter, M. L., Mauser, J. C., and Ekberg, C. E., Jr. "An Investigation of the Behavior of Surface Conditions of Cold-Formed Steel Decking Used as Reinforcement for Concrete Slab Elements." Iowa State Engineering Research Institute Progress Report No. 18, ERI-73060, Ames, Iowa, May 1973.

36. Porter, M. L., Schuster, R. M., and Ekberg, C. E., Jr. "Investigation of Light Gage Steel Forms As Reinforcement for Concrete Slabs." Iowa State Engineering Research Institute Progress Report ERI-276, Ames, Iowa, 1968.

37. Robinson, H. "Composite Beams Incorporating Cellular Steel Decking." American Society of Civil Engineers, Proceedings, 95, No. ST3 (March 1969), 355-380.

38. Robinson, H. "Tests on Composite Beams with Cellular Deck." American Society of Civil Engineers, Proceedings, 93, No. ST4 (August 1967), 139-164.

39. Schuster, R. M. "Composite Steel-Deck-Reinforced Concrete Systems Failing in Shear-Bond." Ninth Congress of the International Association for Bridge and Structural Engineering, Preliminary Report, Zurich (1972), 185-191.

40. Schuster, R. M., and Ekberg, C. E., Jr. "Commentary on the Tentative Recommendations for the Design of Cold-Formed Steel Decking as Reinforcement for Concrete Floor Slabs." Iowa State Engineering Research Institute Progress Report No. 8, ERI-79600, Ames, Iowa, August 1970.

41. Schuster, R. M., and Ekberg, C. E., Jr. "Tentative Recommendations for the Design of Cold-Formed Steel Decking as Reinforcement for Concrete Floor Slabs." Iowa State Engineering Research Institute, Progress Report No. 7, ERI 64500, Ames, Iowa, January 1970.

42. Schuster, R. M., and Ekberg, C. E., Jr. "Tentative Recommendations for the Design of Cold-Formed Steel Decking as Reinforcement for Concrete Floor Slabs." Iowa State Engineering Research Institute Progress Report Number 6, Revised, Ames, Iowa, March 1970.

43. Schuster, R. M., Porter, M. L., and Ekberg, C. E., Jr. "Pilot Test of Light Gage Steel Forms as Reinforcement for Concrete Slabs." Iowa State Engineering Research Institute Progress Report EP068-123, Ames, Iowa, 1968.

44. Slutter, R. G., and Adams, R. G. "Tests of Composite Beams with Holorib Composite Slabs." Report No. 200.63.408.2, Bethlehem, Pa.: Fritz Laboratory, Lehigh University, July 1964.

45. Slutter, R. G. "Test of Cincinnati Center Composite Beam." Report No. 200.67.458.2, Bethlehem, Pa.: Fritz Laboratory, Lehigh University, January 1968.

46. Slutter, R. G. "Tests of Lightweight Concrete Pushout Specimens Containing Stud Shear Connectors and Metal Deck Form." Report No. 200.66.438.1. Bethlehem, Pa.: Fritz Laboratory, Lehigh University, March 1966.

47. Smith, G. M., and Young, L. E. "Ultimate Flexural Analysis Based on Stress-Strain Curves of Cylinders," American Concrete Institute Journal, Proceedings, 28, No. 6 (December 1956), 597-609.

48. Timoshenko, S., and Woinowsky-Krieger, S. Theory of Plates and Shells. 2nd edition. New York: McGraw-Hill Book Company, Inc., 1959.

ACKNOWLEDGMENTS

The research investigation contained herein involving cold-formed steel decking as reinforcement for concrete slabs was conducted under sponsorship of the American Iron and Steel Institute (AISI). The author wishes to express his appreciation to the sponsor for making this investigation possible and to the AISI Task Group on Composite Construction under chairmanship of Mr. A. J. Oudheusden for their guidance, assistance, and understanding. This sponsored work has been conducted at Iowa State University under the auspices of the Engineering Research Institute under the directorship of Dr. P. W. Peterson.

The author wishes to thank most highly Dr. C. E. Ekberg for his leadership, guidance, and contributions rendered while serving as Principal Investigator and Major Professor for this research project. His aid, encouragement, and understanding throughout the duration of the investigation is greatly appreciated.

A special thanks is given to the approximately 45 hourly employees who aided in the gathering of the data. In particular, the work of Mr. Lynn A. Boettcher for his contributions in the Laboratory, in the placement of strain gages, and in the gathering of data is greatly appreciated. Particular thanks are extended to Messrs. Leonard Timm, Peter Manz, and Gordon Port for their aid in the gathering of data and data reduction. Appreciation also goes to Dr. F. W. Klaiber for his aid in the design of the transducers.

The author would like to thank Dr. H. A. Elleby for his valuable discussions concerning the analysis phases of this investigation.

Last, but not least, the author wishes to thank his wife Monica for her patience and understanding throughout this investigation.